.

RADIONUCLIDE MOBILITY AT THE NOPAL I NATURAL ANALOG

Prepared for

U.S. Nuclear Regulatory Commission
Contract No. NRC–02–07–006

Prepared by

David A. Pickett[1]
James D. Prikryl[1]
Bret W. Leslie[2]
English C. Pearcy[1]

[1]Center for Nuclear Waste Regulatory Analyses
San Antonio, Texas

[2]U.S. Nuclear Regulatory Commission
Washington, DC

September 2011

ABSTRACT

During its prelicensing activities to prepare for reviewing a license application for the proposed repository at Yucca Mountain, Nevada, the U.S. Nuclear Regulatory Commission (NRC) sponsored natural analog studies conducted by the Center for Nuclear Waste Regulatory Analyses (CNWRA®) at the Peña Blanca uranium mining district in the state of Chihuahua, Mexico. The purpose of this knowledge management report is to summarize NRC-sponsored Peña Blanca natural analog work, with emphasis on understanding radionuclide mobility—the key focus of the work. Detailed studies focused almost entirely on Nopal I, the site of a former uranium mine excavation that afforded excellent exposure and accessibility to observe a uranium ore body *in situ*. This report discusses the beginnings of NRC-sponsored Peña Blanca work and Nopal I site selection, hydrologic characterization, fracture characterization, uranium mineralogy, radionuclide mobility studies, and performance assessment applications. While published work is summarized briefly, this report emphasizes making available the results of studies that were unpublished and appeared only in posters or presentations. The overriding objective of this report is to provide interested parties access to the information gained through several years of NRC-sponsored activities.

NRC-sponsored natural analog studies at Peña Blanca have provided a great deal of useful information on the uranium mineral evolution, radionuclide release behavior, and radionuclide transport characteristics of a geologic setting analogous to Yucca Mountain. Most significant have been the contributions to understanding specific processes (e.g., oxidative uranium mineral alteration, radionuclide transport in fractured tuff, preferential release, and episodic system behavior)—and how they can help evaluate conceptual models used in performance assessment. More broadly, these efforts enriched staff understanding of processes that can affect repository performance—and related uncertainties and variability.

CONTENTS

Section Page

ABSTRACT ii
FIGURE v
TABLES ix
ACKNOWLEDGMENTS x

1 INTRODUCTION 1-1
1.1 The Role of Natural Analogs in the Licensing Process 1-1
1.2 Objectives of NRC Analogs Program 1-2
1.3 DOE Peña Blanca Work 1-2
1.4 Report Organization 1-2
1.5 References 1-3

2 GENESIS OF THE GEOCHEMICAL NATURAL ANALOG RESEARCH PROJECT AND SITE SELECTION 2-1

3 HYDROLOGIC CHARACTERIZATION 3-1
3.1 Groundwater Hydrology 3-1
3.2 Hydraulic Characterization of Hydrothermally Altered Nopal Tuff 3-2
3.3 Unsaturated Zone Water Chemistry 3-3
3.4 References 3-4

4 FRACTURE CHARACTERIZATION 4-1
4.1 Detailed Mapping 4-1
4.2 Characteristics of Fractures 4-1
4.3 References 4-2

5 NOPAL I MINERALOGY 5-1
5.1 Geologic Setting of the Nopal I Deposit 5-1
5.2 Mineralogic Mapping 5-1
5.3 Mineralogic Studies 5-2
5.3.1 Primary Mineralization 5-2
5.3.2 Secondary Mineralization 5-4
5.3.2.1 Uranyl Minerals 5-4
5.3.2.2 Nonuranium- and Uranium-Bearing Minerals 5-5
5.3.3 Thermodynamic Properties of Uranyl Minerals at Nopal I 5-6
5.4 References 5-77

6 RADIONUCLIDE MOBILITY 6-1
6.1 Gamma and Alpha Radiation Measurements 6-1
6.2 Vegetation Radiation 6-1
6.3 Uranium Measurements in Tuff and Iron-Rich Fracture Filling 6-1
6.4 Other Rock Chemistry Data Relevant to Ore Body Evolution and Radionuclide Mobility 6-2
6.4.1 Context of Analyses 6-2
6.4.2 Mineralogical Data 6-3

CONTENTS (continued)

Section Page

6.4.3 Chemical Data 6-3
6.4.4 Summary 6-4
6.5 Groundwater Radionuclide Data 6-5
6.6 Uranium-Series Systematics in Ore Body, Host Tuff, and Fracture-Filling Minerals 6-5
6.6.1 Setting and Samples 6-6
6.6.2 Methods 6-6
6.6.3 Results 6-7
6.6.3.1 Bulk Rocks 6-7
6.6.3.2 Sequential Extraction of Fracture Infilling 6-8
6.6.4 Discussion 6-9
6.6.4.1 Bulk Rock Uranium Contents 6-9
6.6.4.2 Bulk Rock Uranium-Series Activities 6-10
6.6.4.3 Sequential Extraction Uranium-Series Activities 6-12
6.6.5 Summary 6-13
6.7 Uranium-Series and Stable Isotope Data for Carbonate and Silicate Fracture Deposits at Nopal I 6-13
6.7.1 Introduction 6-14
6.7.2 Setting and Samples 6-14
6.7.3 Methods 6-15
6.7.4 Results 6-15
6.7.4.1 Uranium and Thorium Concentration Data for Calcites and Caliches 6-15
6.7.4.2 Uranium-Series Isotopic Results for Calcites and Caliches 6-17
6.7.4.3 Uranium-Series Isotopic Results for Opals and Uranophane 6-18
6.7.4.4 Oxygen and Carbon Isotopic Analyses of Calcites and Caliches 6-19
6.7.5 Discussion 6-20
6.7.6 Summary 6-21
6.8 References 6-21

7 APPLICATIONS TO PERFORMANCE ASSESSMENT 7-1
7.1 Source Term and Transport 7-1
7.2 Radioisotope Disequilibrium and Preferential Release 7-2
7.3 Episodic Behavior 7-3
7.4 References 7-4

8 SUMMARY 8-1

APPENDIX A — BIBLIOGRAPY OF NRC-FUNDED PEÑA BLANCA-RELATED DOCUMENTS
APPENDIX B — SCIENTIFIC NOTEBOOKS ASSOCIATED WITH CNWRA NATURAL ANALOG WORK AT PEÑA BLANCA

FIGURES

Figure Page

1-1 Location Map of the Nopal I Ore Body Site, Peña Blanca Mining District 1-6
1-2 Overhead View of the Nopal I Exposure From the Northeast 1-6

3-1 Vertical Cross Section of the Nopal I Uranium Deposit Illustrating Its Location Above the Water Table and Within Welded Silicic Tuffs of the Nopal and Coloradas Formation 3-8
3-2 Map of the Level +00 and Level +10 Exposures at Nopal I Showing Nopal Formation Tuff and Water-Sampling Locations. Tuff Samples Were Collected at Locations NRG1, NRG2, NRG3, and NRG5 3-9

4-1 A Photo, Shot Looking to the Northeast, of the Vertical Walls Separating Benches of the Nopal I Uranium Deposit. These Walls as Well as the Wall Separating Levels +10 and +00 Benches Were Mapped at a Scale of 1:25 4-3
4-2 A Photo, Shot Looking to the South From the +40 Level Down to the Level +00, Shows the Cleared Area of the Level +10 Bench and a Portion of Level +00 Bench. The Cleared Areas of Levels +10 and +00 Were Mapped at a Scale of 1:25 4-3
4-3 Summary of Fracture Trends for 11,178 Mapped Fractures on the Cleared Benches .. 4-4
4-4 Mapped Fractures and Calculated Fracture Density on the Wall Between Level +00 and Level +10 4-4
4-5 Mapped Fractures and Calculated Fracture Density on the Wall Between Level +10 and Level +20 4-5
4-6 Calculated Fracture Density by Length on the Level +00 and Level +10 Benches. The Break Between the Upper Left and Lower Right Portions of the Mapped Area Reflects the Wall Area Between the Two Levels (Level +00 is in the Lower Right) 4-6

5-1 Schematic Cross-Section of the Nopal I Uranium Deposit. The Deposit Is Located Above the Water Table and Hosted in Silicic Tuffs of the Nopal and Coloradas Formations 5-12
5-2 Photograph of the Nopal I Uranium Deposit Looking to the Southwest; the Vertical Wall at the Left of the Photo Is About 10 m [33 ft] High and Separates the Level +00 and Level +10 Exposures 5-13
5-3 Photograph of the Nopal I Uranium Deposit Looking Toward the South and Showing the Level +10 Exposure After Clearing of Loose Rock and Soil 5-13
5-4 Plan View Map of the Nopal I Uranium Deposit Showing the Cleared Portions of Level +00 and Level +10 and the Area of Visible U Mineralization on the Cleared Outcrop 5-14
5-5 Plan View Map Showing Results of a Gamma Survey Conducted on the Cleared Areas of the Nopal I Deposit. The Heavy Green Line Indicates the Limit of Visible U Mineralization and Marks the Nominal Edge of the Deposit 5-15
5-6 (a) Photograph of Rock Specimen of Uranium Ore From Nopal I Showing Brecciated Tuff Fragments Cemented by Uraninite-Bearing Fine Crystalline Matrix (Black Material) 5-16
5-7 SEM Photograph of Fine Crystalline Uraninite-Bearing Matrix Cementing Tuff Fragments Composed of Quartz (Q). The Uraninite (U) Within the Matrix is Intimately Intergrown With Kaolinite (K) 5-16

FIGURES (continued)

Figure Page

5-8 Backscattered Electron Photomicrograph of Uranium Phases Filling Open Space Within Brecciated Tuff. Granular Uraninite (G) Composed of Fine Crystalline Uraninite Intergrown With Kaolinite and Quartz Is Followed by Colloform Uraninite (C) 5-17

5-9 Backscattered Electron Photomicrograph of Colloform Uraninite (C) Lining a Fracture in Brecciated Tuff. Note the Radial and Concentric Microfractures Within the Colloform Uraninite Crystals 5-18

5-10 Relative Sequence of Formation and Abundance of Uranium Minerals at the Nopal I Deposit 5-18

5-11 Transmitted Light Photomicrograph of Red-Colored Ianthinite (IA) Filling Open Space in Brecciated Tuff. The Ianthinite Is Being Replaced By Yellow-Colored Schoepite (S) and Uranophane (UR) 5-19

5-12 Backscattered Electron (Top Photo) and Corresponding Plane Light (Bottom Photo) Photomicrographs of Uranium Phases Filling Open Space in Brecciated Tuff 5-20

5-13 Backscattered Electron Photomicrograph of Colloform Uraninite (C) Lining Open Space Between Silicified Breccia Fragments (BF). The Remaining Open Space Is Filled By Dehydrated Schoepite (DS) 5-21

5-14 Transmitted Light Photomicrograph of Schoepite (S) and Uranophane (UR) Filling an Open Void. Schoepite Occurs at the Margin of the Void and Follows Colloform Uraninite (C) 5-21

5-15 Scanning Electron Photomicrograph of Acicular Uranophane Crystals Within Filling a Void at the Nopal I Deposit. Field of View Is 0.1 mm [3.9×10^{-3} in] Across 5-22

5-16 Transmitted Light Photomicrograph of Uranophane and Beta-Uranophane Filling Open Space in Brecciated Tuff. Beta-Uranophane (B-UR) Occurs as Equigranular, Yellow-Colored Crystals, Whereas Uranophane (UR) Is Composed of the Finer, Acicular, Blue-Green Crystals. 5-22

5-17 Backscattered Electron Photomicrograph of a Fracture Containing Predominantly Intergrown Soddyite (SO) and Uranophane (UR) 5-23

5-18 Transmitted Light Photomicrograph of Rhombic-Shaped Soddyite (SO) Crystals in a Fracture With Kaolinite (K) and Smectite (SM). Field of View Is 2.6 mm [0.1 in] Across 5-23

5-19 Transmitted Light Photomicrograph of Clusters of Acicular Weeksite (W) Crystals Within a Fracture In Brecciated Tuff (BF). Field of View Is 1.3 mm [5.1×10^{-2} in] Across 5-24

5-20 Backscattered Electron Photomicrograph of Intergrown Soddyite (SO), Uranophane (UR), and Weeksite (W) Filling a Fracture in Brecciated Tuff. At the Top Left, Original Granular Uraninite Has Been Replaced By Uranophane 5-24

5-21 Reflected Light Photomicrograph of Iron Minerals Filling a Fracture at Nopal I. Hematite (H) Grows Into Open Space From Goethite (G) and Amorphous Iron-Oxyhydroxide (A) Substrates 5-25

5-22 Reflected Light Photomicrograph of Iron Minerals Filling a Fracture at Nopal Showing Goethite (G) Partially Replacing Cubic Pyrite That Was Originally Intergrown With Kaolinite (K) 5-25

5-23 Fields of Uranyl Mineral Stability as a Function of Aqueous Solution Composition and Temperature 5-26

FIGURES (continued)

Figure Page

6-1 Gamma Intensity Map of the Exposed Surface of Level +10 of the Nopal I Uranium Ore Deposit, Showing Locations of Whole-Rock Sampling Traverses A and J and Major East-West Fracture Set B 6-37
6-2 2-Theta Angle Spectra (In Degrees), Measured By X-ray Diffraction, For Samples of Fracture-Filling Material Taken From Progressively Greater Distances From the Edge of the Ore Body in Traverse B 6-38
6-3 The Ratio of XRD Intensities For Characteristic Kaolinite and Alkali Feldspar Peaks in Bulk Tuff Samples Along Traverse J. Also Shown Are Linear Ranges of the Occurrences of Uranophane, Hematite, and Alunite 6-39
6-4 Zinc, Uranium, And Iron as Fe_2O_3 From Traverse A. The Fe_2O_3 Concentration Is Divided by 10 For Convenience of Plotting; the Patterns Are More Important Than the Actual Values 6-39
6-5 Zinc, Uranium, Iron as Fe_2O_3, and Sulfur Concentrations From Traverse J. The Limit of Visible Uranium Mineralization (On the Right) Is at About the 12-m [ ] Mark 6-40
6-6 Trace Element Concentrations Along Traverse J in Matrix and Mineralized Tuff, Including Rubidium, Strontium, Barium, Zirconium, Yttrium, and Vanadium (a) and Copper, Nickel, Chromium, Scandium, and Niobium (b) 6-41
6-7 Major Element Oxide Concentrations Along Traverse J in Matrix and Mineralized Tuff. The Limit of Visible Uranium Mineralization (On the Right) Is at About the 12-m [3.3 ft] Mark 6-42
6-8 Rare-Earth Element Patterns of Selected Samples From Nopal I Level +10. Note that the X Axis Is Not Scaled By Atomic Number; Rather, Only the Measured REE Are Shown, in Order of Increasing Atomic Number 6-43
6-9 Map of the Level +00 and Level +10 Exposures at Nopal I, Showing Sampling Traverses (Heavy Lines A–H). Light Gray Denotes the Area Cleared of Debris For Detailed Study 6-44
6-10 Uranium Concentrations in Bulk Samples Collected Along Traverses on Nopal I Levels +00 and +10 (Locations in Figure 6-9). Distance Is Measured From the Edge of the Uranium Ore Body 6-45
6-11 Uranium-Series Activity Ratios (a) $^{234}U/^{238}U$ and (b) $^{230}Th/^{234}U$ Along the Level +10 Traverses. Included Are Example Conservative Uncertainty Bounds 6-46
6-12 Sequential Extraction U Contents From Traverse B Samples, Represented as Micrograms of U in a Fraction Per Gram of Rock (Rather Than ppm in the Fraction) 6-47
6-13 Uranium-Series Activity Ratio $^{234}U/^{238}U$ in Sequential Extraction Products From Traverse B, Plotted Against Distance From the Ore Body Boundary in Meters 6-48
6-14 $^{234}U/^{238}U$ Versus $^{230}Th/^{238}U$ Plot of Traverse Bulk Rock Samples, With Preferred Model For Evolution (After Pickett and Murphy, 1997). Symbols as in Figure 6-11, With the Addition of Crosses (+) For Traverse D 6-49
6-15 Map of the Nopal I Exposure With Sample Locations and Uranium Concentrations (ppm) for Crystalline Calcite, Caliches, and Opals. The Zone of Visible Uranium Mineralization, or Ore Body, Is in Yellow. Contour Interval Is 2 m [6.6 ft] 6-50
6-16 Field Photograph of Crystalline Calcites From Level +10 of the Nopal I Exposure 6-51
6-17 Typical Fracture-Filling Caliche From Near the Nopal I Ore Body. Location Is Shown in Figure 6-18 6-51

FIGURES (continued)

Figure Page

6-18 View From the Northeast of the Nopal I Uranium Deposit. Dashed Blue Line Is Approximate Outline of the Zone of Visible Uranium Ore on Both Levels +00 (lower) and +10 (upper) 6-52
6-19 Photograph of a Typical Opal Sample, Showing Its Translucent to Transparent Color and Botryoidal Character. The Field of View is 13 mm [0.51 in] Wide 6-52
6-20 Photograph of an Association of Uranium-Rich Opals With Yellow Uranophane Needles. Field of View is 7 mm [0.28 in] Wide. 6-53
6-21 Uranium and Thorium Concentrations of Grain-Size Fraction Pairs of Calcite and Caliche Samples From Nopal I. The Line Connecting Pairs Is Not Visible if the Points Overlap 6-53
6-22 Total-Dissolution Th-230 Dates on Calcite, Caliche, and Opal From the Nopal I Exposure. The Term “Model Age” Means That the Date Is Calculated Directly From the Isotopic Measurements, With No Corrections 6-54
6-23 Isochron Plots Using Total Dissolution (TD) and Leachate Pairs for N99-28 and N99-32, and Two Total Dissolution Fractions From the Same Powder for N99-29 and N99-30 6-55
6-24 (a) Activity Ratios on Pairs of Total Dissolution and Leachate Measurements on One Calcite (Far Right of Plot) and 7 Caliches, Plotted on a Uranium Series Evolution Diagram 6-56
6-25 Uranium-Series Evolution Plots of Data From Opals (Blue), Uranophane (Black), Calcite (Red), and Quartz “Caliche” (Green) From Nopal I 6-57
6-26. $\delta^{18}O$, Plotted as Permil Values Against SMOW, of the Carbonate and Silicate Components of Calcites and Caliches 6-57
6-27 Oxygen Isotope Ratios (In Permil Against SMOW) For Calcites and Caliches Plotted Against the Interpreted ^{230}Th-^{234}U-^{238}U Age. Data For Carbonates and Silicate 6-58
6-28 Uranium Concentrations in Nopal I Calcites and Caliches Plotted Against the Difference Between $\delta^{18}O$ Values in Residues and Carbonates. The Latter Value Is Termed Δ and Can Be Useful For Understanding Temperature Conditions 6-59
6-29 Carbon Isotope Ratios For Calcites and Caliches Around Nopal I 6-59
6-30 Nopal I Caliche Uranium Concentrations Plotted Against Uranium-Series Age. The Points Include Previously Reported Ages of 18 and 54 ka 6-60

TABLES

Table Page

3-1 Gravimetric Porosity of Nopal Tuff Samples 3-6
3-2 Pycnometric Porosity of Nopal Tuff Samples 3-6
3-3 Saturated Hydraulic Conductivity (cm/s) of Nopal Tuff Samples 3-6
3-4 Bulk Permeability K_b (m^2) for Nopal Tuff Samples 3-6
3-5 Nopal I Water Chemistry Data 3-7

5-1 Comparison of Chemical Compositions of the Nopal and Coloradas Formations and the Topopah Spring Member of the Paintbrush Tuff Formation (Values in Weight Percent) 5-9
5-2 Electron Microprobe Analyses of Nopal I Uraninite (Normalized to 100 Atom Percent) 5-10
5-3 Uranium Minerals Identified at the Nopal I Uranium Deposit 5-12

6-1 Major Element Analyses of Rocks Collected From Transect J on Nopal I Level +10 6-25
6-2 Trace Element Analyses of Rocks Collected From Transect J on Nopal I Level +10 6-26
6-3 Major Element Analyses of Rocks Collected From Transect A on Nopal I Level +10 6-27
6-4 Trace Element Analyses of Rocks Collected From Transect A on Nopal I Level +10 6-27
6-5 Rare-Earth Element Concentrations (ppm) in Selected Samples From Nopal I Level +10 6-28
6-7 Nopal I Traverse B Sequential Extraction Scheme 6-28
6-6 Uranium-Series Activity Ratios on Ore Standards 6-28
6-8 Bulk Rock Alpha Spectrometry Results 6-29
6-9 Sequential Extraction Data From Traverse B 6-31
6-10 Uranium and Thorium Concentration of Total-Rock Calcite and Caliche 6-32
6-11 Uranium and Thorium Concentrations and Activity Ratios in Calcites and Caliches 6-33
6-12 Estimated Uranium Concentrations in Carbonate and Silicate Fractions in Nopal I Calcite (N99-11) and Caliches (Others) 6-34
6-13 Uranium and Thorium Concentrations and Activity Ratios in Opals and Uranophane 6-34
6-14 Stable Isotope Data for Calcites and Caliches From Nopal I 6-35

ACKNOWLEDGMENTS

This report describes work performed by the Center for Nuclear Waste Regulatory Analyses (CNWRA®) and its contractors for the U.S. Nuclear Regulatory Commission (USNRC) under Contract No. NRC–02–07–006. The activities reported here were performed on behalf of the USNRC Office of Nuclear Material Safety and Safeguards, Division of High-Level Waste Repository Safety. The report is an independent product of the CNWRA and does not necessarily reflect the view or regulatory position of USNRC. The USNRC staff views expressed herein are preliminary and do not constitute a final judgment or determination of the matters addressed or of the acceptability of any licensing action that may be under consideration at USNRC.

The authors gratefully acknowledge J. Myers for his technical review, E. Pearcy and J. Winterle for their programmatic review, L. Mulverhill for her editorial review, and A. Ramos for his administrative support. We also thank the colleagues with whom we collaborated on much of this work, especially W. Murphy, L. Veblen, I. Reyes, and R. Green.

QUALITY OF DATA, ANALYSES, AND CODE DEVELOPMENT

DATA: All CNWRA-generated data contained in this report meet quality assurance requirements described in the Geosciences and Engineering Division Quality Assurance Manual. Sources of other data should be consulted for determining the level of quality of those data.

ANALYSES AND CODES: None.

1 INTRODUCTION

With respect to evaluating the safety of geologic disposal of high-level nuclear waste, a natural analog can provide useful information on the long-term behavior of materials, systems, and environments at temporal and spatial scales not available in laboratory studies. During its prelicensing activities to prepare for reviewing a license application for the proposed repository at Yucca Mountain, Nevada, the U.S. Nuclear Regulatory Commission (NRC) sponsored natural analog studies the Center for Nuclear Waste Regulatory Analyses (CNWRA®) conducted at the Peña Blanca uranium mining district in the state of Chihuahua, Mexico (Figure 1-1). Recognizing the useful analog properties of the site, the U.S. Department of Energy (DOE) later conducted its own studies there. This knowledge management report documents NRC-sponsored Peña Blanca work by summarizing both published and unpublished studies. The purpose here is not to provide an exhaustive review of the field of natural analogs; rather, it is to summarize, in one location, NRC/CNWRA contributions to the natural analog field based on Peña Blanca studies. Detailed studies focused almost entirely on Nopal I, the site of a former uranium mine excavation that afforded excellent exposure and accessibility to observe a uranium ore body *in situ* (Figure 1-2). Key analogous features of Nopal I include the tectonic setting (Basin and Range), host rocks (fractured, silicic, volcanic tuff), hydrologic setting (unsaturated zone), geochemical conditions (oxidizing, bicarbonate-rich), desert climate, and the occurrence of uraninite (UO_2) as an analog to spent nuclear fuel (Pearcy, et al., 1994).

A website describing CNWRA activities at Peña Blanca will be maintained at http://www.swri.org/4org/d20/ghs/PBlanca/default.htm.

A useful overview may also be found in a draft book chapter (Prikryl, et al., 2002) transmitted to NRC and approved for release; the book was not subsequently published. Some of the material in that chapter was used in this knowledge management report.

1.1 The Role of Natural Analogs in the Licensing Process

The NRC perspective on how natural analogs may contribute to the licensing process for high-level waste disposal has been mentioned in several reports and presentations over the years, but was the primary topic of three talks given between 2003 and 2007 (Pickett, 2003, 2004; Pickett and Leslie, 2007). The regulation governing the proposed Yucca Mountain repository does not specifically require the use of analogs, but natural analog information is mentioned as one potential element of support for analyses and performance assessment models. For example, 10 CFR 63.21(c)(15) states, in part:

> Analyses and models that will be used to assess performance of the geologic repository must be supported by using an appropriate combination of such methods as field tests, *in situ* tests, laboratory tests that are representative of field conditions, monitoring data, and natural analog studies.

Similarly, the Yucca Mountain Review Plan (NRC, 2003) mentions natural analogs as one type of information source that may used by (i) DOE to develop and support models and parameters and (ii) the NRC staff to evaluate DOE models and parameters. Most commonly, analogs are mentioned with respect to support for postclosure performance assessment model abstractions. Analogs are also part of the generic acceptance review checklist recommended in Appendix B of the review plan. Analogs are mentioned among the examples of appropriate methods that should have been used to support models.

1.2 Objectives of NRC Analogs Program

NRC elected to conduct natural analog studies to develop an independent capability for understanding and interpreting natural analogs in the context of repository performance assessment. The purpose of this independent capability, as well as independent capabilities for developing process models and performance assessment, was to directly support prelicensing interactions and license application review. The NRC objectives in carrying out natural analog studies are detailed in Chapter 2.

1.3 DOE Peña Blanca Work

In the late 1990s, DOE began sponsoring Nopal I studies by national laboratory scientists and their associates. This work focused on unsaturated zone water flow, saturated zone flow and transport characteristics, and uranium mineral genesis, with an emphasis on geochemical and isotopic methods. A performance assessment-type model for uranium transport was developed. This knowledge management report, being a record of NRC-sponsored work, will not detail those studies, nor provide comparative analyses of them. A recent paper provides a relatively brief summary of the DOE efforts (Levy, et al., 2011).

1.4 Report Organization

This report begins with a brief discussion of the beginnings of NRC-sponsored Peña Blanca work and a description of the process leading to the selection of Nopal I as a suitable analog site. Subsequent chapters summarize hydrologic, geologic, and mineralogic characterization of Nopal I, analyses aimed at understanding radionuclide mobility, and performance assessment applications. This report relies largely on background information and detailed descriptions already available to the public, either in published papers or in reports and presentations that may be viewed on the NRC's Agencywide Documents Access and Management System (ADAMS) public document site. Information, analyses, and conclusions that have been published in journals, conference proceedings, or other publications are summarized only briefly. Content that is publicly available in ADAMS but has not otherwise been published is treated in more detail and is supplemented, where necessary, by data that are not yet public. (An example of previously nonpublic data presented in this report would be the detailed analytical data supporting a publicly available slide presentation delivered at a conference.) An important objective of this report is to provide access to information gained through several years of NRC-sponsored activities not otherwise easily available to the public. To further address this objective, Appendix A contains a listing of NRC-funded Peña Blanca-related documents, including documents such as field trip reports and conference presentation slides that are available in ADAMS, and Appendix B contains a list of the scientific notebooks, with their ADAMS number, associated with NRC-funded natural analog work at Peña Blanca.

Many of the early results from Nopal I, when the work was sponsored by the NRC Office of Research, were originally presented in periodic and topical reports CNWRA issued (Pearcy, 1994a,b, 1990; Pearcy and Murphy, 1991a,b; Pearcy, et al., 1993a,b, 1991; Leslie, et al., 1993; Pearcy and Leslie, 1993; Green, et al., 1995; Prikryl, et al., 1995; Pickett, et al., 1996). Murphy and Kovach (1993) prepared a more general NRC/CNWRA study of the use of analogs in disposal programs. French investigators (e.g., George-Aniel, et al., 1991; Calas, et al., 2008) conducted extensive early studies of Nopal I. Like the DOE work, these studies are not detailed in the present report.

1.5 References

Calas, G., P. Agrinier, T. Allard, and P. Ildefonse. "Alteration Geochemistry of the Nopal I Uranium Deposit (Sierra Peña Blanca, Mexico), a Natural Analogue for a Radioactive Waste Repository in Volcanic Tuffs." *Terra Nova*. Vol. 20. pp. 206–212. 2008.

George-Aniel, B., J.L. Leroy, and B. Poty. "Volcanogenic Uranium Mineralization in the Sierra Peña Blanca District, Chihuahua, Mexico—Three Genetic Models." *Economic Geology*. Vol. 86. pp. 233–248. 1991.

Green, R.T., G. Rice, and K. Meyer-James. NUREG/CR–6356, CNWRA 94–027, "Hydraulic Characterization of Thermally Altered Nopal Tuff." Washington, DC: NRC. July 1995.

Murphy, W.M. and L.A. Kovach, eds. "The Role of Natural Analogs in Geologic Disposal of High-Level Nuclear Waste." CNWRA 93–020. San Antonio, Texas: Center for Nuclear Waste Regulatory Analyses. 1993.

Leslie, B.W., E.C. Pearcy, and J.D. Prikryl. NUREG/CR–5817, CNWRA 92–01S, "Geochemical Natural Analogs." *NRC High-Level Radioactive Waste Research at CNWRA, January–June 1992.* W. Patrick, ed. Vol. 3, No. 1. May 1993.

Levy, S., S. Goldstein, P.F. Dobson, P. Goodell, T.-L. Ku, A. Abdel-Fattah, G. Saulnier, M. Fayek, and R. de la Garza. "Peña Blanca Natural Analogue Project: Summary of Activities." Proceedings of the 13th International High-Level Radioactive Waste Management Conference, Albuquerque, New Mexico, April 10–14, 2011. La Grange Park, Illinois: American Nuclear Society. pp. 330–341. 2011.

NRC. NUREG–1804, "Yucca Mountain Review Plan—Final Report." Rev. 2. ML032030389. Washington, DC: NRC. July 2003.

Pearcy, E.C. CNWRA 94–011, "Fracture Transport of Uranium at the Nopal I Natural Analog Site." San Antonio, Texas: Center for Nuclear Waste Regulatory Analyses. 1994a.

———. CNWRA 94–01S, "Geochemical Natural Analog Research." *NRC High-Level Radioactive Research at CNWRA, January Through June 1994*. B. Sagar, ed. San Antonio, Texas: Center for Nuclear Waste Regulatory Analyses. 1994b.

———. CNWRA 90–02Q, "Geochemical Natural Analogs." *Report on Research Activities for the Quarter April 1 Through June 30, 1990.* W. Patrick, ed. San Antonio, Texas: Center for Nuclear Waste Regulatory Analyses. 1990.

Pearcy, E.C. and B.W. Leslie. CNWRA 93–01S, "Geochemical Natural Analog Research." *NRC High-Level Radioactive Research at CNWRA, January Through June 1993.* B. Sagar, ed. San Antonio, Texas: Center for Nuclear Waste Regulatory Analyses. 1993.

Pearcy, E.C. and W.M. Murphy. NUREG/CR–5817, CNWRA 90–01A, "Geochemical Natural Analogs." *Report on Research Activities for Calendar Year, 1990.* W. Patrick, ed. Washington, DC: NRC. December 1991a.

———. CNWRA 91–03Q, "Geochemical Natural Analogs." *Report on Research Activities for the Quarter July 1 Through September 30, 1991.* W. Patrick, ed. San Antonio, Texas: Center for Nuclear Waste Regulatory Analyses. 1991b.

Pearcy, E.C., J.D. Prikryl, W.M. Murphy, and B.W. Leslie. "Alteration of Uraninite from the Nopal I Deposit, Peña Blanca District, Chihuahua, Mexico, Compared to Degradation of Spent Nuclear Fuel in the Proposed U.S. High-Level Nuclear Waste Repository at Yucca Mountain, Nevada." *Journal of Applied Geochemistry.* Vol. 9. pp. 713–732. 1994.

Pearcy, E.C., W.M. Murphy, R.T. Green, B.W. Leslie, and J.D. Prikryl. NUREG/CR–5817, CNWRA 91–01A, "Geochemical Natural Analogs." *NRC High-Level Radioactive Waste Research at CNWRA, Calendar Year 1991.* Vol. 2. W. Patrick, ed. Washington, DC: NRC. May 1993a.

Pearcy, E.C., J.D. Prikryl, W.M. Murphy, and B.W. Leslie. CNWRA 93–012, "Uranium Mineralogy of the Nopal I Natural Analog Site, Chihuahua, Mexico." San Antonio, Texas: Center for Nuclear Waste Regulatory Analyses. 1993b.

Pearcy, E.C., W.M. Murphy, and J.D. Prikryl. CNWRA 91–02Q, "Geochemical Natural Analogs." *Report on Research Activities for the Quarter April 1 Through June 30, 1991.* W. Patrick, ed. San Antonio, Texas: Center for Nuclear Waste Regulatory Analyses. 1991.

Pickett, D.A. "Natural Analogs and the Yucca Mountain Review Plan: NRC Perspective." Presentation at the NAnet International Workshop on Natural Analogues: Their Application to Repository Safety Assessment and Stakeholder Communication, Château de Cadarache, France, May 2004. Meeting Summary Published in W. Miller, et al., 2006, "Network to Review Natural Analogue Studies and Their Applications to Repository Safety Assessment and Public Communication (NAnet): Synthesis Report." European Commission Research Report EUR 21919. Brussels, Belgium: European Commission. 2004.

———. "Natural Analogs and the Yucca Mountain Review Plan: NRC Perspective." Presentation at the Electric Power Research Institute (EPRI) Natural Analogues Workshop, October 2003. Meeting Summary Published in J. Kessler, 2003, "Applying Information From Analogue Systems to the Evaluation of Radioactive Waste Repositories." Proceedings of the EPRI Natural Analogues Workshop, Palo Alto, California, October 9–10, 2003. Report 1007897. Palo Alto, California: EPRI. 2003.

Pickett, D.A. and B.W. Leslie. "Use of Natural Analog Information by the Regulator: The U.S. Nuclear Regulatory Commission (NRC) Approach." Presentation at the 10th Natural Analogue Working Group Workshop, Munich, Germany, August 25–26, 2007. ML072060289. 2007.

Pickett, D.A., J.D. Prikryl, and E.C. Pearcy. CNWRA 95–02S, "Geochemical Natural Analog Research." *NRC High-Level Radioactive Research at CNWRA, July Through December 1995.* B. Sagar, ed. San Antonio, Texas: Center for Nuclear Waste Regulatory Analyses. 1996.

Prikryl, J.D., D.A. Pickett, and E.C. Pearcy. "Natural Analog Studies at the Nopal I Uranium Deposit, Peña Blanca District, Chihuahua, Mexico." ML061310294. San Antonio, Texas: Center for Nuclear Waste Regulatory Analyses. 2002.

_____. CNWRA 95–01S, “Geochemical Natural Analog Research.” *NRC High-Level Radioactive Research at CNWRA, January Through June 1995*.” B. Sagar, ed. San Antonio, Texas: Center for Nuclear Waste Regulatory Analyses. 1995.

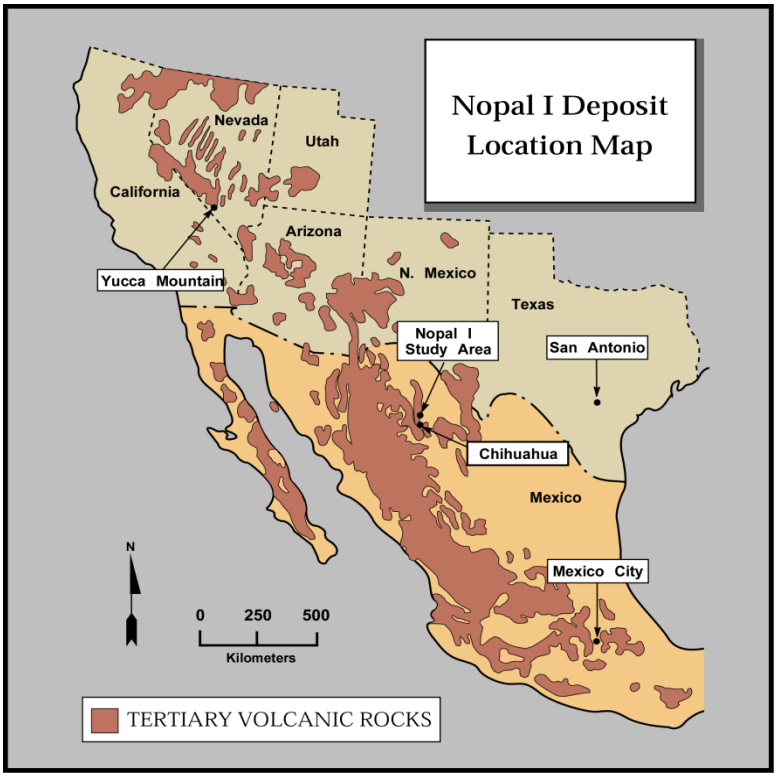

Figure 1-1. Location Map of the Nopal I Ore Body Site, Peña Blanca Mining District

Figure 1-2. Overhead View of the Nopal I Exposure From the Northeast

2 GENESIS OF THE GEOCHEMICAL NATURAL ANALOG RESEARCH PROJECT AND SITE SELECTION

Late in 1987, the U.S. Congress amended the Nuclear Waste Policy Act, designating Yucca Mountain, Nevada, as the sole repository site to be characterized. A repository site in the unsaturated zone at Yucca Mountain raised questions about modeling site hydrology, contaminant transport, and geochemistry. U.S. Nuclear Regulatory Commission (NRC) regulations for disposal of high-level nuclear waste in effect at the time, 10 CFR Part 60, required prediction of the performance of the repository for times from 300 to 10,000 years. NRC recognized that then-current engineering practices allowed performance assessment modeling only for tens of years and saw a need for performance assessment computer codes to be validated for times on the order of 10^2 to 10^5 years and on a spatial scale of kilometers. Because of these temporal and spatial scales, the high-level nuclear waste regulations specified, at 10 CFR Part 60 Sections 60.21(c)(1)(ii)(F) and 60.101(a)(2), that computer codes used to model the performance of the repository be supported using an appropriate combination of field tests, *in-situ* tests, and natural analogs.

During 1989, NRC initiated a natural analog research project to support preparations to evaluate a license application anticipated to be received from U.S. Department of Energy (DOE) for a geologic high-level nuclear waste repository at Yucca Mountain. Laboratory studies had already been initiated, but because of the large temporal and spatial scales required, NRC initiated natural analog studies to address questions “which test the limits of short-term experiments” (NRC, 1989).

NRC recognized that (i) natural analog studies would be most useful to identify potentially significant processes that may not be observed in short-term laboratory experiments, (ii) natural analogs might allow observation of coupled processes that are not easily modeled, and (iii) natural analogs could help determine data needs for site characterization. NRC was aware of the inherent limitations of natural analog studies as uncontrolled natural experiments and planned to conduct an interdisciplinary, multifaceted approach to help mitigate those limitations.

Site selection began with a comprehensive review of the natural analog literature (Pearcy and Murphy, 1991). This review used state-of-the-art information to identify the usefulness and the limitations of natural analog studies applied to investigations of the disposal of high-level nuclear waste. Processes and events likely to be important to waste isolation at a Yucca Mountain repository were identified, and a subset of those processes and events were recognized as potentially amenable to natural analog study. A set of criteria for the successful use of natural analog studies was established, and candidate sites were proposed and described.

Pearcy and Murphy (1991) identified the Nopal I uranium deposit in the Peña Blanca District, Chihuahua, Mexico, as a potentially valuable natural analog to a geologic high-level nuclear waste repository at Yucca Mountain. To the authors’ knowledge, Professor Phillip C. Goodell at the University of Texas at El Paso was the first to recognize the similarities between these two sites. The Nopal I deposit is an unusual example of a substantial mass of uraninite (natural UO_2) that had partially oxidized in a geologic and geochemical environment similar in important respects to Yucca Mountain. Both the Sierra Peña Blanca and Yucca Mountain are Basin and Range horsts composed of rhyolitic tuffs in semiarid to arid climatic regions. The repository horizon envisioned for Yucca Mountain and the uranium deposit at Nopal I are both located in the chemically oxidizing and hydrologically unsaturated zone above the water table. In addition to these similarities, the Nopal I deposit had been partially mined then abandoned, leaving an excellent exposure of much of the ore body accessible for study.

Later, Pearcy and Murphy (1992) documented the selection of the Peña Blanca District—and, in particular, the Nopal I deposit—as a site for detailed study in the NRC-sponsored Geochemical Natural Analog Research Project.

References

NRC. "Geochemical Analog of Contaminant Transport in Unsaturated Rock Statement of Work." Letter (June 22) to J. Latz, CNWRA, from M. Mace, NRC, with attachment. Washington, DC: NRC. 1989.

Pearcy, E.C. and W.M. Murphy. CNWRA 90–008, "Geochemical Natural Analogs Literature Review." San Antonio, Texas: Center for Nuclear Waste Regulatory Analyses. 1991.

_____. CNWRA 92–014, "Site Selection and Workplan Report for the Geochemical Natural Analog Research Project." San Antonio, Texas: Center for Nuclear Waste Regulatory Analyses. 1992.

3 HYDROLOGIC CHARACTERIZATION

The Nopal I deposit is located in the oxidizing, hydrologic unsaturated zone 100 m [328 ft] or more above the water table (Pearcy, et al., 1994) (Figure 3-1). The deposit occurs in tuffaceous host rocks of the Nopal and Coloradas Formations, which are separated by a basal argillaceous zone, interpreted to be a vitrophyre. The Nopal Formation is a densely welded rhyolitic tuff deposited by pyroclastic air fall, and the Coloradas Formation is a densely welded rhyolite tuff of air flow origin (Pearcy, et al., 1991). The uranium deposit at Nopal I is interpreted to have formed by hydrothermal solutions that precipitated uraninite as they moved through a highly fractured zone within the welded tuffs (Pearcy, et al., 1994). All of the known uranium deposits in the Peña Blanca district are located above the water table in the unsaturated zone. At present, oxidizing meteoric groundwaters episodically penetrate the deposits through fractures in the unsaturated tuffs. The climate of the Peña Blanca area is arid, with annual precipitation of about 24 cm [9.45 in] (USDOC, 1965).

3.1 Groundwater Hydrology

The groundwater hydrological system in the Peña Blanca area has been interpreted from limited available data to be a two-aquifer system composed of an upper and a lower aquifer (Pearcy, et al., 1991). The upper aquifer, herein referred to as the “upper saturated unit,” is defined to be of limited extent and found only at higher elevations. The lower aquifer appears to be regional in extent and is interpreted to span several basins and ranges.

The upper saturated unit is interpreted to be a water-table unit of low permeability (Pearcy, et al., 1991). The extent of the upper saturated unit is controlled by the topography and the geologic structure of the region. In general, the upper saturated unit is only present at higher elevations. The base of the upper saturated unit has been tentatively interpreted to be limited, and it is possible that the upper saturated unit is perched if its base is situated on an impermeable horizon. The upper saturated unit is interpreted to be of low permeability with limited recharge because there are only isolated occurrences of groundwater discharge at the surface (e.g., springs, seeps) even though the potentiometric surface is inferred to be close to the ground surface at a multitude of locations including many dry streambeds. Water flow is interpreted to occur essentially in the fractures with negligible water flow through the rock matrix. The limited areal extent and recharge of the upper saturated unit, in conjunction with its low permeability, define this unit as an aquifer with limited capability of providing a significant quantity of water. The only use of the upper saturated unit has been the installation of catchments along streambeds for use as stock ponds. No operational wells set in the upper saturated unit have been identified, which supports the premise that the upper saturated unit is incapable of sustaining a well due to its low permeability and/or limited extent.

The mesa containing the Nopal I deposit does not exhibit perennial springs in surrounding streambeds at lower elevations. However, this mesa could potentially have a perched water unit in its highest elevations, at least episodically. Supporting the prospect of an upper saturated unit in the Nopal I mesa is the presence of water detected in several boreholes located on the +10-meter level of the Nopal I deposit (Pickett and Murphy, 1999).

During NRC-funded investigations there was limited information available on the lower aquifer. A total of four water wells located at three locations in the eastern portion of the Sierra Peña Blanca provided information on this water-bearing unit (Pearcy, et al., 1991). Three wells installed for mining-related purposes are not currently used, but are reported to have been capable of providing significant amounts of water.[1] Two of these wells are located at the Margaritas mining camp northwest of the Nopal I deposit, and the other well is located in a streambed southeast of the Nopal I deposit. The fourth well is a ranch well located east of the Sierra Peña Blanca in the Laguna el Cuervo basin. This well currently supplies water to a reservoir and associated stock ponds.

The depths to water in the wells at the Margaritas mining camp {with surface elevations of about 1,420 m [4,659 ft] above mean sea level (msl)} are reported to exceed 100 m [328 ft].[2] The depth to water at the mining well located along the streambed to the southeast of Nopal I {with a surface elevation of about 1,340 m [4,396 ft] msl} was measured to be 85 m [279 ft], indicating the groundwater elevation is about 1,255 m [4,118 ft] msl at this point. A ranch worker reported the depth to water in the ranch well {with a surface elevation of about 1,260 m [4,134 ft] msl} was about 60 to 70 m [197 to 230 ft], indicating a groundwater elevation of about 1,200 m [3,937 ft] msl.

The elevation of groundwater in these wells, therefore, appears to be approximately 1,200 to 1,300 m [3,937 to 4,265 ft] msl. The elevation of the lower aquifer would, therefore, be about 200 m [656 ft] below the ground surface at the Nopal I deposit. The elevation of the potentiometric surface of the upper aquifer in the area proximal to these wells has been estimated to be about 1,450 to 1,650 m [4,757 to 5,413 ft] msl or about 150 to 450 m [492 to 1,476 ft] above the elevation of the lower aquifer, thus supporting the hypothesis that there are two distinct hydrologic units. Subsequent drilling of the PB-1 well at the Nopal I site (Levy, et al., 2011) indicated that the water table is about 223 m [732 ft] below the +10 level of Nopal I, confirming our earlier estimates.

3.2 Hydraulic Characterization of Hydrothermally Altered Nopal Tuff

The low permeability of tuff rocks potentially hosting an upper saturated unit or perched zone at the Nopal I deposit has been confirmed by measurements of the matrix hydraulic properties of Nopal Formation tuff samples collected at the Nopal I site (Green, et al., 1995). Nopal Formation tuff samples were collected from the Nopal I site to evaluate the hydraulic properties of tuffs exhibiting varying degrees of hydrothermal alteration associated with formation of the uranium deposit. The degree of alteration ranges from highly altered rock located at the edge of the uranium deposit (sample NRG1) to unaltered rock located about 400 m [1,312 ft] from the deposit (sample NRG4) (Figure 3-2). The entire sample sequence from most altered to least altered is NRG1 (at edge of deposit), NRG2 {18 m [59 ft] from the deposit}, NRG5 {22 m [72 ft] from the deposit}, NRG3 {50 m [164 ft] from the deposit}, and NRG4 {400 m [1,312 ft] from the deposit}.

---

[1] J. Altamirano, personal communication.
[2] Ibid.

Effective porosity measurements of the five Nopal tuff samples as measured by gravimetric and gas pycnometer methods are summarized in Tables 3-1 and 3-2, respectively. Both measurement techniques indicate porosity increasing with increasing hydrothermal alteration toward the deposit. With the exception of NRG3, measured gas pycnometer values are greater than gravimetric values. Variation in measured porosity is high with a coefficient of variation ranging from 0.029 to 0.229 for the gravimetric method and 0.041 to 0.706 for the gas pycnometer method. The total range of porosity of the Nopal samples is large, from 0.036 to 0.270 percent by the gravimetric method and 0.02 to 0.34 percent for the gas pycnometer method.

Saturated hydraulic conductivity values determined for the five Nopal tuff samples using the constant head permeameter method are summarized in Table 3-3. The hydraulic conductivity values generally increase with increasing hydrothermal alteration toward the deposit. Hydraulic conductivity measurements varied by more than four orders of magnitude {i.e., 6.22×10^{-12} to 1.5×10^{-7} cm/s [2.43×10^{-12} to 5.85×10^{-8} in/s]}. Median saturated hydraulic conductivity varied from 1.06×10^{-7} cm/s [4.13×10^{-8} in/s] in NRG1 to 7.97×10^{-11} cm/s [3.11×10^{-11} in/s] in NRG3.

Bulk permeabilities of the five Nopal tuff samples were calculated based on measured matrix hydraulic properties of each tuff sample and assumed fracture properties. Fracture porosity values for the Nopal I site were determined by multiplying measured surface fracture density measurements with estimated average fracture apertures. Fracture porosities of 2×10^{-5}, 2×10^{-4}, and 2×10^{-3} were calculated using an average fracture density of 2 m/m^2 [0.61 ft/ft^2] measured at the Nopal I site (Pearcy, et al., 1994) and estimated average fracture apertures of 1, 10, 100, and 1,000 µm. Calculated bulk permeabilities for the tuff samples are summarized in Table 3-4 and range from 8.46×10^{-20} m^2 [9.11×10^{-19} ft^2] for a fracture aperture of 10 µm to 3.34×10^{-13} m^2 [3.59×10^{-12} ft^2] at a fracture aperture of 1,000 µm. As with effective porosity and hydraulic conductivity, calculated bulk permeabilities generally increase with increasing hydrothermal alteration toward the deposit.

3.3 Unsaturated Zone Water Chemistry

Past excavation associated with uranium mining at the Nopal I deposit has provided opportunities for sampling unsaturated zone waters. Perched and seep water samples collected at the deposit have yielded information on both radionuclide content and chemical characteristics of waters that have interacted with host rocks and ore minerals (Pickett and Murphy, 1999). This section presents chemical data on these waters. Uranium-series isotopic systematics on these waters are discussed in Chapter 6 of this report.

Perched water samples at the deposit were collected from a 10.7-m [35.1-ft]-deep uncased borehole on Level +10 of the deposit (BH-12 in Figure 3-2). The hole, which was drilled but not used for blast excavation, contained water for several years and was capped and sealed three months prior to sampling to ensure isolation from surface infiltration. Seepage water samples were collected in an adit on Level +00 of the deposit (ADIT95-6 and ADIT95-9 in Figure 3-2). Seepage water entering the adit traversed at least 8 m [26 ft] of rock before being collected. In addition, saturated zone aquifer samples were collected from the well in the regional carbonate aquifer located 1.3 km [0.8 mi] southeast of the Nopal I deposit {water depth 94 m [308 ft]}.

Results of chemical analyses on the seep, perched, and aquifer waters collected at the Nopal I site are displayed in Table 3-5. The perched and aquifer samples are calcium-bicarbonate dominated waters, with appreciable sodium and silica, and with chloride and sulfate as

subordinate anions. In contrast, the seep waters are more dilute and have relatively higher sulfate. Based on EQ3NR (speciation) thermodynamic calculations using the data0.com.R2 database (Wolery, 1992), the perched waters, like the aquifer waters, are near saturation with respect to calcite, which is consistent with the presence of caliche and vein calcite in fractured tuff at the deposit (see Chapters 5 and 6). The perched and aquifer waters are also supersaturated with respect to quartz, which is a common state among waters from the Yucca Mountain area (Yang, et al., 1996). One of the seep waters is undersaturated with quartz, and both are undersaturated with calcite, which is consistent with short water–rock contact time.

The Nopal I perched water is generally intermediate in composition between unsaturated zone perched and pore waters from the Yucca Mountain area (Yang, et al., 1996). Tuff-hosted Yucca Mountain perched waters tend to contain fewer dissolved solids, calcium, and bicarbonate—but more silicon, sodium, sulfate, and nitrate—than Nopal I perched water. This contrast is likely due to the near-surface location of the perched water, reflecting less interaction with tuffs and greater influence of quickly reacting carbonate solids. The higher carbonate in the perched water would tend to enhance uranium mobility (Clark, et al., 1995).

Uranium and thorium data reveal differences among the three Nopal water types. Both uranium and thorium are highest in the perched waters and lowest in the aquifer waters. Based on geochemical speciation modeling, the BH-12 perched waters are close to saturation with respect to the calcium uranyl silicate mineral haiweeite [$Ca(UO_2)_2(Si_2O_5)_3 \cdot 5H_2O$], suggesting solubility control by this mineral. Although host rocks in the vicinity of BH-12 are visibly devoid of uranium minerals, this result raises the possibility that haiweeite may occur outside the zone of visible uranium mineralization as a trace phase. Haiweeite has been detected by x-ray diffractometry (XRD) in fracture fill in vitrophyre a few meters outside the visible uranium deposit (see Chapter 5). The seep waters collected in the adit are mildly to strongly undersaturated with respect to uranium phases, with haiweeite and soddyite being the least undersaturated phases, depending on silicon content. This result is consistent with rapidly moving waters that are less likely to equilibrate with solid phases—despite the fact that the adit waters may have interacted with more uranium-rich rocks closer to the margin of the deposit (see Figure 3-2). The carbonate-rich aquifer water, sampled 1.3 km [0.8 mi] from the deposit, is strongly undersaturated in uranium phases.

Thorium concentrations are consistently well above thorianite solubility (10^{-14} to 10^{-13} molal) in all waters, suggestive of association with colloids less than 200 nm in size (based on filtration conditions). Therefore, colloid mobilization of sparingly soluble radionuclides may be an important process at Nopal I. The highest thorium concentrations are in perched waters, which have had relatively prolonged contact with the host tuffs and thus may have higher colloid contents.

3.4 References

Clark, D.L., D.E. Hobart, and M.P. Neu. “Actinide Carbonate Complexes and Their Importance in Actinide Environmental Chemistry.” *Chemical Reviews*. Vol. 95. p. 25. 1995.

Green, R.T., G. Rice, and K. Meyer-James. NUREG/CR–6356, CNWRA 94–027, “Hydraulic Characterization of Hydrothermally Altered Nopal Tuff.” San Antonio, Texas: Center for Nuclear Waste Regulatory Analyses. 1995.

Levy, S., S. Goldstein, P.F. Dobson, P. Goodell, T.-L. Ku, A. Abdel-Fattah, G. Saulnier, M. Fayek, and R. de la Garza. "Peña Blanca Natural Analogue Project: Summary of Activities." Proceedings of the 13th International High-Level Radioactive Waste Management Conference, Albuquerque, New Mexico, April 10–14, 2011. La Grange Park, Illinois: American Nuclear Society. pp. 330–341. 2011.

Pearcy, E.C., J.D. Prikryl, W.M. Murphy, and B.W. Leslie. "Alteration of Uraninite From the Nopal I Deposit, Peña Blanca District, Chihuahua, Mexico, Compared to Degradation of Spent Nuclear Fuel in the Proposed U.S. High-Level Nuclear Waste Repository at Yucca Mountain, Nevada." *Applied Geochemistry*. Vol. 9. pp. 713–732. 1994.

Pearcy, E.C., W.M. Murphy, R.T. Green, B.W. Leslie, and J.D. Prikryl. NUREG/CR–5817, CNWRA 91–01A, "Geochemical Natural Analogs, in NRC High-Level Radioactive Waste Research at CNWRA, Calendar Year 1991." Vol. 2. W. Patrick, ed. San Antonio, Texas: Center for Nuclear Waste Regulatory Analyses. 1991.

Pickett, D.A. and W.M. Murphy. "Unsaturated Zone Waters From the Nopal I Natural Analog Chihuahua, Mexico—Implications for Radionuclide Mobility at Yucca Mountain." Scientific Basis for Nuclear Waste Management XXII. D.J. Wronkiewicz and J. Lee, eds. Materials Research Society. Warrendale, Pennsylvania: Symposium Proceedings. Vol. 556. pp. 809–816. 1999.

U.S. Department of Commerce. "World Weather Records 1951–1960." Vol. 1 North America. Washington, DC: U.S. Department of Commerce. 1965.

Wolery, T.J. "EQ3NR, a Computer Program for Geochemical Aqueous Speciation–Solubility Calculations: Theoretical Manual, User's Guide, and Related Documentation (Version 7.0)." UCRL–MA–110662, Pt. 3. Livermore, California: Lawrence Livermore National Laboratory. 1992.

Yang, I.C., G.W. Rattray, and P. Yu. "Interpretation of Chemical and Isotopic Data From Boreholes in the Unsaturated Zone at Yucca Mountain, Nevada." U.S. Geological Survey Water-Resources Investigations Report 96–4058. 58 pp. 1996.

Table 3-1. Gravimetric Porosity of Nopal Tuff Samples*					
Porosity (Gravimetric)					
Sample	**NRG1**	**NRG2**	**NRG5**	**NRG3**	**NRG4**
Mean	0.255	0.210	0.183	0.083	0.078
Coefficient of Variation	0.029	0.061	0.060	0.229	0.149
Minimum	0.235	0.169	0.154	0.036	0.053
Median	0.256	0.213	0.188	0.089	0.074
Maximum	0.270	0.226	0.021	0.126	0.113

*Green, R.T., G. Rice, and K. Meyer-James. NUREG/CR–6356, CNWRA 94–027, "Hydraulic Characterization of Hydrothermally Altered Nopal Tuff." Washington, DC: NRC. 1995.

Table 3-2. Pycnometric Porosity of Nopal Tuff Samples*					
Porosity (Gas Pycnometric)					
Sample	**NRG1**	**NRG2**	**NRG5**	**NRG3**	**NRG4**
Mean	0.295	0.264	0.211	0.083	0.128
Coefficient of Variation	0.041	0.124	0.115	0.706	0.551
Minimum	0.28	0.23	0.18	0.02	0.04
Median	0.29	0.25	0.20	0.06	0.12
Maximum	0.32	0.34	0.26	0.18	0.31

*Green, R.T., G. Rice, and K. Meyer-James. NUREG/CR–6356, CNWRA 94–027, "Hydraulic Characterization of Hydrothermally Altered Nopal Tuff." Washington, DC: NRC.. 1995.

Table 3-3. Saturated Hydraulic Conductivity (cm/s)* of Nopal Tuff Samples†					
Sample	**NRG1**	**NRG2**	**NRG5**	**NRG3**	**NRG4**
Mean	9.49×10^{-8}	4.09×10^{-8}	1.95×10^{-8}	1.09×10^{-10}	2.17×10^{-10}
Coefficient of Variation	0.556	0.191	0.509	0.995	0.312
Minimum	1.15×10^{-8}	2.78×10^{-8}	9.67×10^{-9}	6.22×10^{-12}	1.17×10^{-10}
Median	1.06×10^{-7}	4.23×10^{-8}	1.91×10^{-8}	7.97×10^{-11}	2.42×10^{-10}
Maximum	1.5×10^{-7}	5.19×10^{-8}	3.67×10^{-8}	2.20×10^{-10}	2.65×10^{-8}

*1 cm/s = 0.394 in/s

†Green, R.T., G. Rice, and K. Meyer-James. NUREG/CR–6356, CNWRA 94–027, "Hydraulic Characterization of Hydrothermally Altered Nopal Tuff." Washington, DC: NRC. 1995.

Table 3-4. Bulk Permeability K_b (m^2)* for Nopal Tuff Samples†					
Fracture Aperture (µm)	**NRG1**	**NRG2**	**NRG5**	**NRG3**	**NRG4**
1	1.06×10^{-16}	4.31×10^{-17}	1.95×10^{-17}	8.13×10^{-20}	2.47×10^{-19}
10	1.06×10^{-16}	4.31×10^{-17}	1.95×10^{-17}	8.46×10^{-20}	2.50×10^{-19}
100	1.39×10^{-16}	7.65×10^{-17}	5.29×10^{-17}	3.35×10^{-17}	3.36×10^{-17}
1,000	3.34×10^{-13}	3.34×10^{-13}	3.34×10^{-13}	3.34×10^{-13}	3.34×10^{-13}

*1 m^2 = 10.8 ft^2

†Green, R.T., G. Rice, and K. Meyer-James. NUREG/CR–6356, CNWRA 94–027, "Hydraulic Characterization of Hydrothermally Altered Nopal Tuff." Washington, DC: NRC. 1995.

Table 3-5. Nopal I Water Chemistry Data*†

Component	ADIT95-6 Seep	ADIT95-9 Seep	BH12W95-04 Perched	BH12W95-05 Perched	BH12W95-11 Perched	WVW95-02 Aquifer	WVW95-03 Aquifer
pH	—	—	7.32	7.26	7.34	7.72	—
T (°C)	—	—	26.4	25.6	26.0	29.3	—
Diss. O_2	—	—	—	0.64 mg/l	—	—	1.03 mg/l
Conduct.‡	179	79	557	551	550	278	276
HCO_3^-§	8.0×10^{-04}	2.0×10^{-04}	—	5.7×10^{-03}	—	—	2.5×10^{-03}
Cl^-	2.7×10^{-05}	2.0×10^{-05}	1.9×10^{-04}	1.9×10^{-04}	1.9×10^{-04}	1.5×10^{-04}	1.7×10^{-04}
F^-	1.2×10^{-04}	1.3×10^{-05}	4.6×10^{-05}	4.7×10^{-05}	4.5×10^{-05}	4.9×10^{-05}	5.0×10^{-05}
NO_3^-	1.9×10^{-05}	6.7×10^{-06}	5.2×10^{-05}	5.3×10^{-05}	5.8×10^{-05}	2.1×10^{-05}	2.2×10^{-05}
PO_4^{3-}	$<1 \times 10^{-06}$	$<1 \times 10^{-06}$	6.6×10^{-06}	8.0×10^{-06}	7.9×10^{-06}	$<1 \times 10^{-06}$	$<1 \times 10^{-06}$
SO_4^{2-}	1.9×10^{-04}	1.3×10^{-04}	7.5×10^{-05}	7.4×10^{-05}	7.7×10^{-05}	1.2×10^{-04}	1.3×10^{-04}
Al	$<7 \times 10^{-07}$	7.8×10^{-07}	1.1×10^{-06}	1.2×10^{-06}	1.5×10^{-06}	1.0×10^{-06}	9.6×10^{-07}
B	$<2 \times 10^{-06}$	$<2 \times 10^{-06}$	3.3×10^{-06}	3.4×10^{-06}	3.2×10^{-06}	4.6×10^{-06}	4.5×10^{-06}
Ca	5.3×10^{-04}	2.1×10^{-04}	2.6×10^{-03}	2.6×10^{-03}	2.6×10^{-03}	8.0×10^{-04}	8.0×10^{-04}
Mg	3.3×10^{-06}	6.4×10^{-06}	2.3×10^{-04}	2.3×10^{-04}	2.3×10^{-04}	3.1×10^{-04}	3.1×10^{-04}
Mn	5.5×10^{-08}	3.7×10^{-05}	3.7×10^{-05}	3.4×10^{-05}	2.2×10^{-06}	2.1×10^{-06}	$<4 \times 10^{-08}$
K	3.7×10^{-05}	5.3×10^{-05}	1.6×10^{-04}	1.5×10^{-04}	1.5×10^{-04}	1.0×10^{-04}	1.1×10^{-04}
Si	5.2×10^{-04}	2.3×10^{-05}	6.7×10^{-04}	6.7×10^{-04}	$.6 \times 10^{-04}$	2.6×10^{-04}	2.6×10^{-04}
Na	3.0×10^{-04}	4.0×10^{-05}	8.5×10^{-04}	8.4×10^{-04}	8.3×10^{-04}	4.5×10^{-04}	4.7×10^{-04}
U	8.3×10^{-10}	3.72×10^{-09}	—	2.012×10^{-08}	2.426×10^{-08}	—	7.1×10^{-10}
Th	1.9×10^{-12}	5.31×10^{-12}	—	1.16×10^{-09}	6.74×10^{-10}	—	6.16×10^{-13}

*Cation and anion values are in molal

†Pickett, D.A. and W. M. Murphy. "Unsaturated Zone Waters From the Nopal I Natural Analog Chihuahua, Mexico—Implications for Radionuclide Mobility at Yucca Mountain." Scientific Basis for Nuclear Waste Management XXII. Symposium Proceedings. D.J. Wronkiewicz and J. Lee, eds. Warrendale, Pennsylvania: Materials Research Society. Vol. 556. pp. 809–816. 1999.

‡Conductivity is expressed in μS/cm

§HCO_3^- is calculated from measured alkalinity for seep samples and measured bicarbonate alkalinity in the field for others

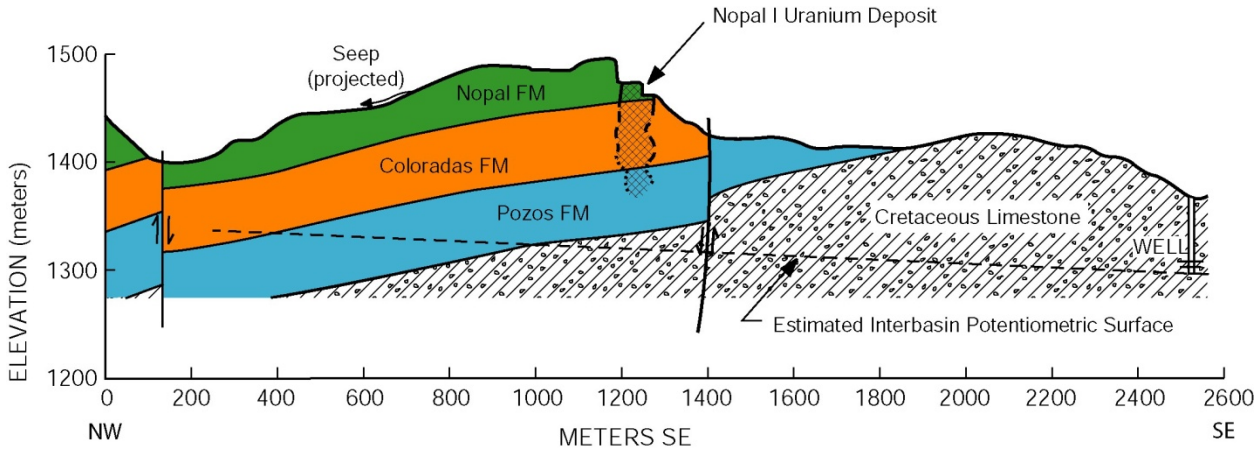

Figure 3-1. Vertical Cross Section of the Nopal I Uranium Deposit Illustrating Its Location Above the Water Table and Within Welded Silicic Tuffs of the Nopal and Coloradas Formations (Modified From Pearcy, et al., 1994)

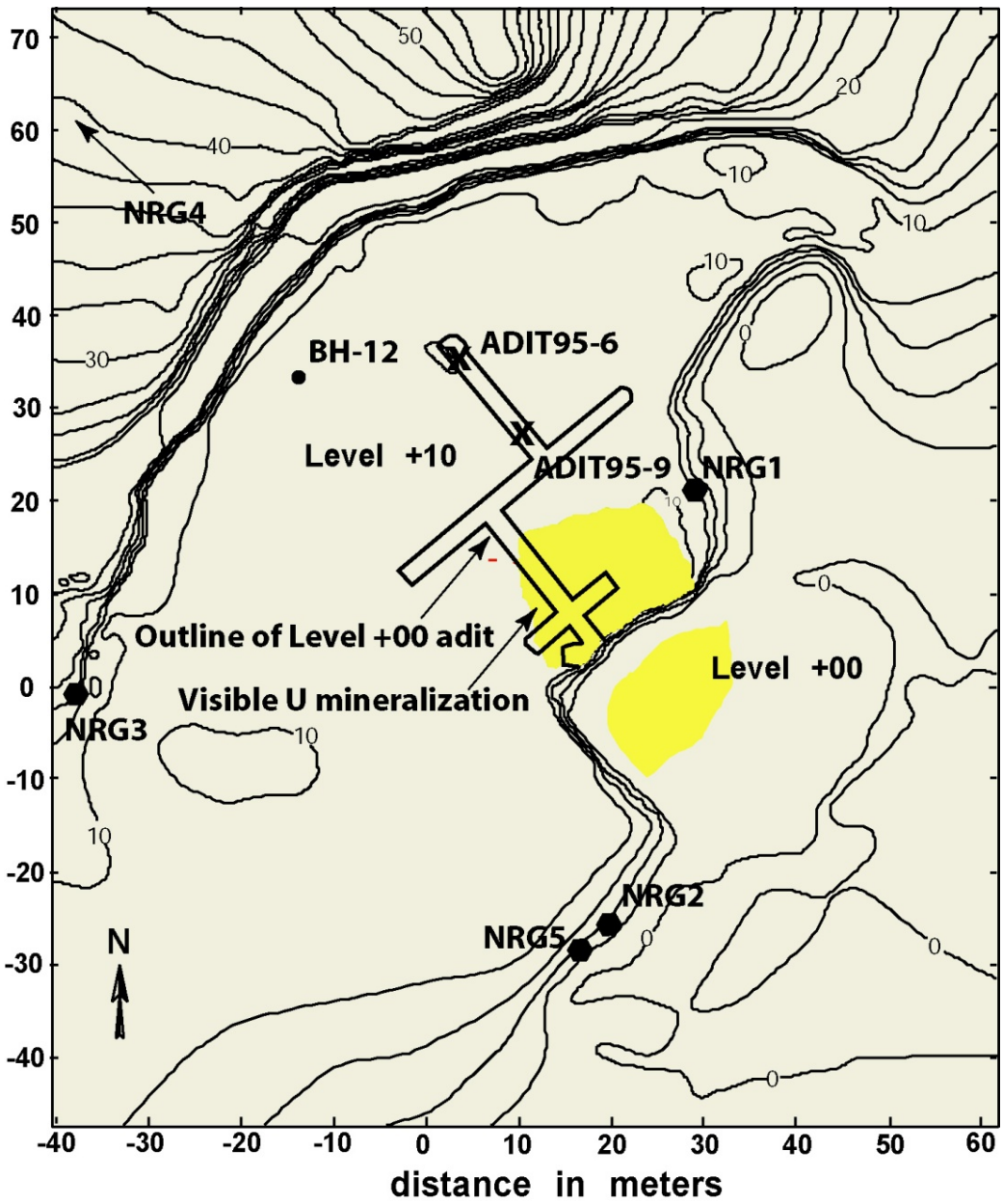

Figure 3-2. Map of the Level +00 and Level +10 Exposures at Nopal I Showing Nopal Formation Tuff and Water-Sampling Locations. Tuff Samples Were Collected at Locations NRG1, NRG2, NRG3, and NRG5. Tuff Sample NRG4 Was Collected About 400 m [1,312 ft] From the Zone of Visible U Mineralization. Water Was Collected at Borehole 12 (BH-12) and in the Level +00 Adit at Projected Locations Marked by Xs. Yellow Shading Indicates the Zone of Visible Uranium Mineralization, or Uranium Deposit. Contour Interval Is 2 m [6.6 ft], Referenced at Zero at Level +00.

4 FRACTURE CHARACTERIZATION

A major objective of Nopal I studies was to understand evidence of fracture transport of uranium away from the deposit. This chapter summarizes comprehensive fracture mapping efforts and provides some characteristics of the fractures from the mapped surfaces. Chapter 6 presents a summary of the timing, extent, and mechanisms of release of uranium and other radionuclides from the ore body, including transport in fractures.

4.1 Detailed Mapping

The Nopal I deposit consists of a series of mined horizontal benches. The benches are vertically separated by 10 m [33 ft]. Study participants cleared portions of Levels +10 and +00 benches and established a grid system to allow detailed mapping. The vertical walls between benches (Figure 4-1), and cleared benches (Figure 4-2) were mapped at a scale of 1:25, primarily by Ignacio Reyes-Cortés (Universidad Autonoma de Chihuahua). Pearcy (1994) described the clearing of the benches, the grid system, and the comprehensive fracture mapping of the cleared benches on Levels +00 and +10 (11,374 individual fractures). Reyes-Cortés (1997) provided stereograms of the strikes and dips of mapped structures, and Rose diagrams of strikes of the structures for the cleared benches and the walls. Center for Nuclear Waste Regulatory Analyses (CNWRA®) staff digitized the original field data for use in the ARC/INFO software.

4.2 Characteristics of Fractures

The digitized field data from the cleared benches were used to develop maps of the fractures in ARC/INFO, analyze fracture density patterns, and conduct fractal analysis computations (Pearcy, 1994). Pearcy (1994) characterized fracture density by length (sum of fracture lengths/m^2) and by frequency (number of fractures/m^2). He noted that fracture density by frequency shows a general increase close to the deposit. Pearcy (1994) determined, using a box-counting method, the fractal dimension of the fracture pattern on cleared benches was 1.8. At Nopal I the fracture frequency density has a fractal dimension of 2.4 and a fracture length density of 2.6 (Pearcy, 1994). Pearcy (1994) noted that interconnectedness (fracture intersections per unit area) of the fracture pattern also appeared to be fractal, though with a dimension of 1.5, it appeared to be less complex than the entire fracture network.

Later, Leslie, et al. (2005a,b) reassessed the available fracture characterization data and compared it to fracture characteristics of Yucca Mountain, Nevada. The fracture data from the cleared benches and the vertical walls at Nopal I were mapped and analyzed using ArcGIS. The orientation of the fractures from both cleared benches surfaces are provided in Figure 4-3 and are consistent with the six sets of fractures Pearcy (1994) identified. Both Pearcy (1994) and Leslie, et al. (1995b) noted that use of fracture information in subsequent analyses is critically dependent on correcting data for orientation bias. For instance, Pearcy (1994) noted that orientation of subhorizontal fracture sets was underrepresented on the nearly horizontal cleared benches. Mapped fractures and fracture density by length are presented for the walls separating Level +00 from Level +10 (Figure 4-4) and Level +10 from Level +20 (Figure 4-5). In general, fracture density by length on the vertical walls (Figures 4-4 and 4-5) appears to be lower {~0.4–~2.0 m/m^2 [~0.12–~0.61 ft/ft^2]} than on the cleared benches {Figure 4-6 ~0.4–~6.0 m/m^2 [~0.12–~1.83 ft/ft^2]. Fracture density by length can be greater than 6 m/m^2 [1.83 ft/ft^2] within the ore deposit, but is not significantly different than outside the ore deposit.

The intensive mapping at Nopal I allowed a better understanding of the transport processes for radionuclide migration at the site and provided the context for interpreting the mineralogical, geochemical, and radiological analyses of rock samples at the site.

4.3 References

Pearcy, E.C. "Fracture Transport of Uranium at the Nopal I Natural Analog Site." CNWRA 94–011. San Antonio, Texas: Center for Nuclear Waste Regulatory Analyses. 1994.

Leslie, B.W., K.J. Smart, and E.C. Pearcy. "Characterization of Fractures at the Nopal I Site and Comparison to Fracture Characteristics of Yucca Mountain, Nevada." *Geological Society of America Abstracts with Programs.* Vol. 37, No. 7. p. 196. 2005a.

_____. "Characterization of Fractures at the Nopal I Site and Comparison to Fracture Characteristics of Yucca Mountain, Nevada." Presentation Slides, ADAMS ML052800172. City, state: publisher. 2005b.

Reyes-Cortés, I.A. "Geologic Studies in the Sierra de Peña Blanca, Chihuahua, Mexico." Ph.D. dissertation. The University of Texas at El Paso. El Paso, Texas. 1997.

Figure 4-1. A Photo, Shot Looking to the Northeast, of the Vertical Walls Separating Benches of the Nopal I Uranium Deposit. These Walls as Well as the Wall Separating Levels +10 and +00 Benches Were Mapped at a Scale of 1:25.

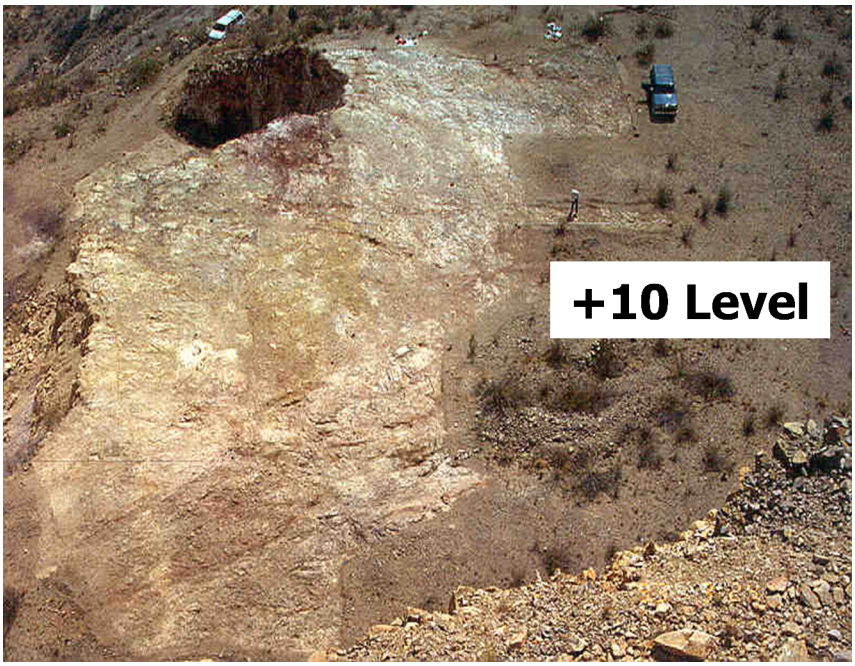

Figure 4-2. A Photo, Shot Looking to the South From the +40 Level Down to the Level +00, Shows the Cleared Area of the Level +10 Bench and a Portion of Level +00 Bench. The Cleared Areas of Levels +10 and +00 Were Mapped at a Scale of 1:25.

Summary of Fracture Orientations (Trend) for Nopal Pavements

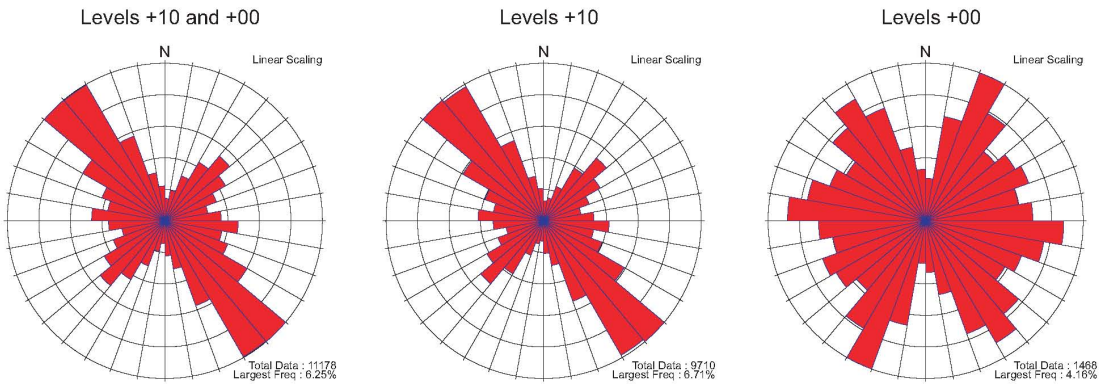

Figure 4-3. Summary of Fracture Trends for 11,178 Mapped Fractures on the Cleared Benches

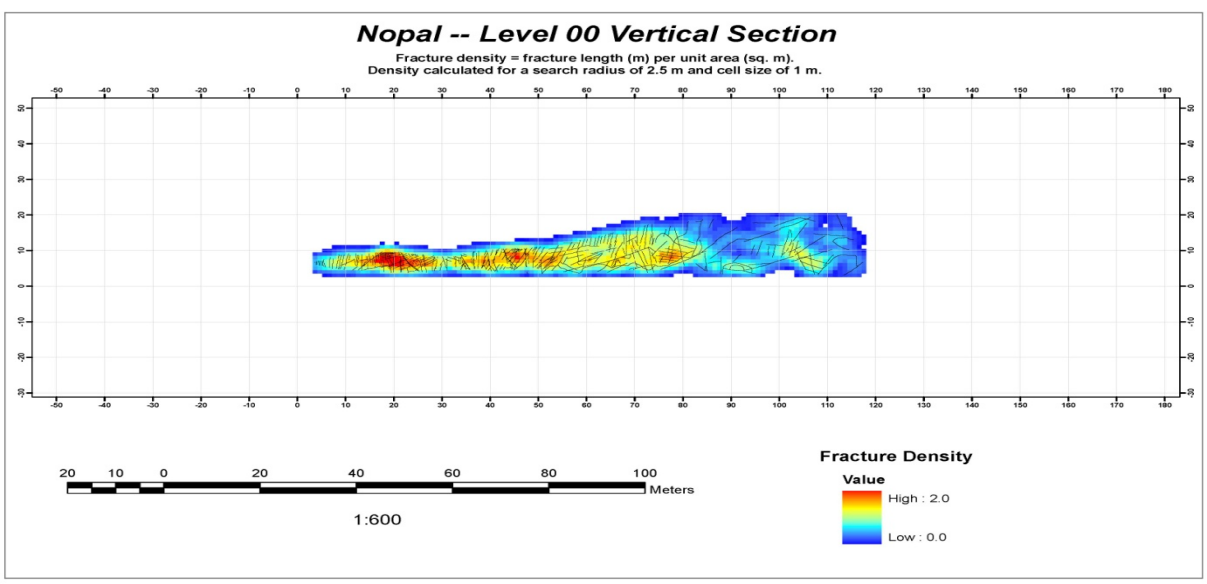

Figure 4-4. Mapped Fractures and Calculated Fracture Density on the Wall Between Level +00 and Level +10

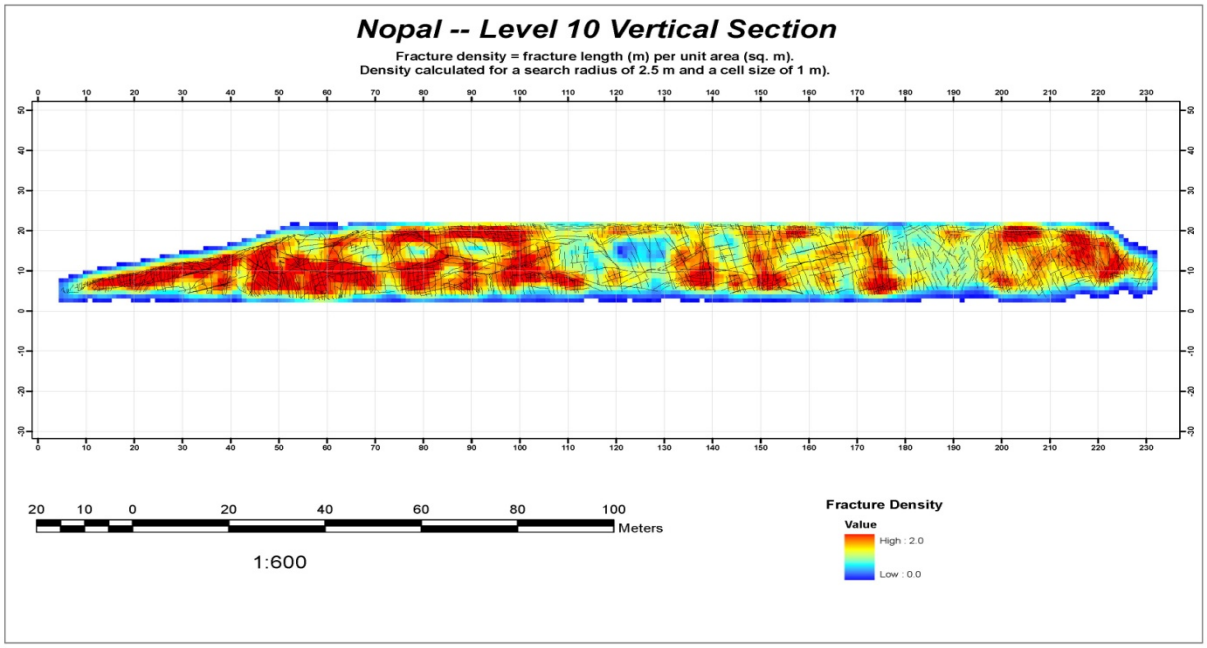

Figure 4-5. Mapped Fractures and Calculated Fracture Density on the Wall Between Level +10 and Level +20

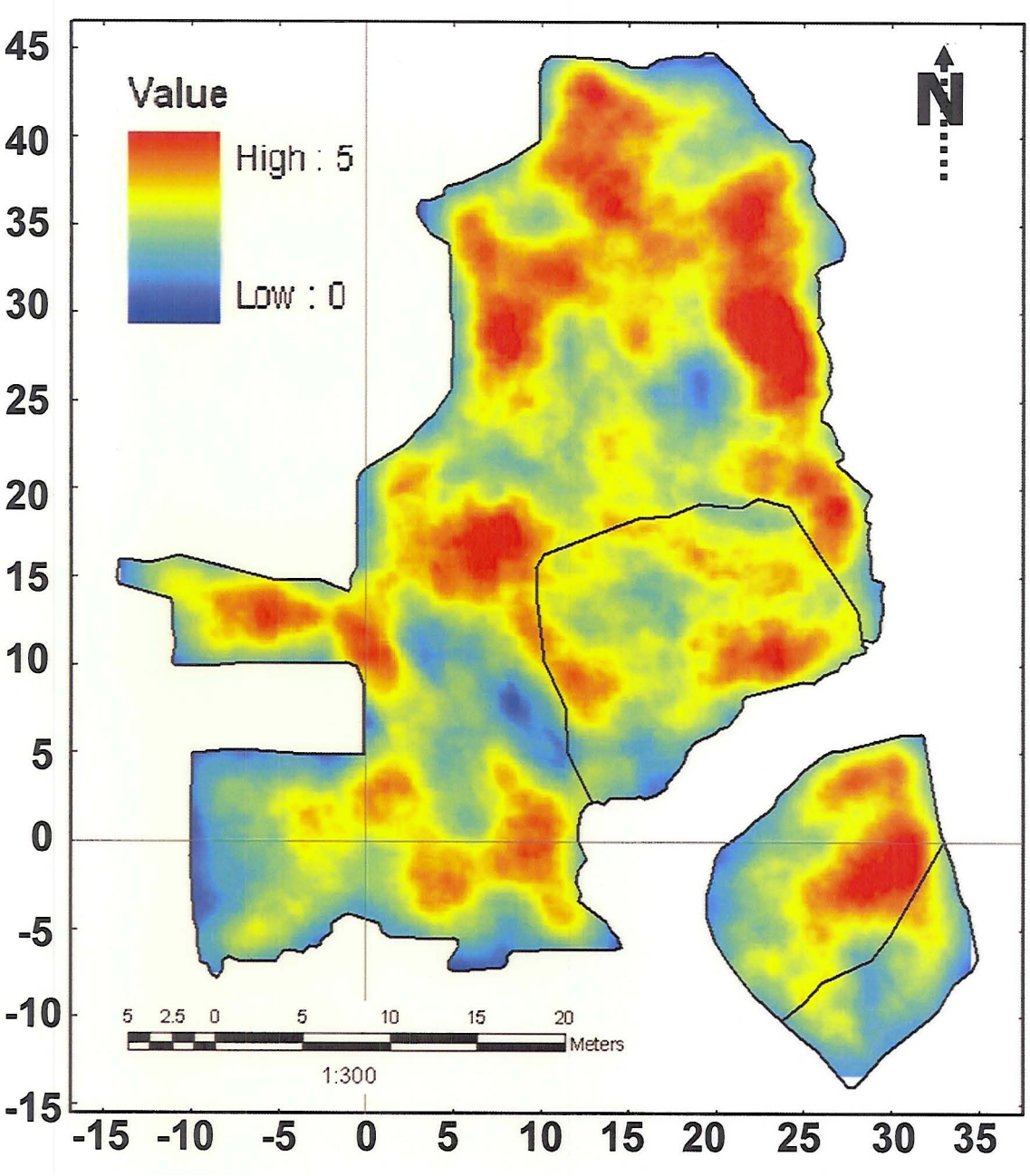

Figure 4-6. Calculated Fracture Density by Length on the Level +00 and Level +10 Benches. The Break Between the Upper Left and Lower Right Portions of the Mapped Area Reflects the Wall Area Between the Two Levels (Level +00 is in the Lower Right).

5 NOPAL I MINERALOGY

As described in Chapter 1, the Nopal I uranium deposit is a small, well-exposed, high-grade uranium deposit in the Peña Blanca district in the state of Chihuahua, Mexico (see Figure1-1). Along with the Nopal I deposit, the Peña Blanca district contains more than 100 occurrences of concentrated uranium hosted in Tertiary volcanic tuffs (Reyes-Cortés, 2002). Uranium deposits in the Peña Blanca district are associated with hydrothermal alteration at faults and fractures and within breccias (Calas, 1977; Goodell, 1981; Cardenas-Flores, 1985; George-Aniel, et al., 1985; Ildefonse, et al., 1990; Muller, et al., 1990; Murphy, et al., 1997). At present, most of the uranium mineralization in the district is oxidized; uranyl (UO_2^{2+}) minerals, predominantly uranyl silicates, are most common.

5.1 Geologic Setting of the Nopal I Deposit

Calas (1977), Goodell (1981), and Reyes-Cortés (2002) provide informative descriptions of the geologic setting of the Nopal I uranium deposit. The uranium deposit at Nopal I is part of a west-dipping horst block composed of siliceous Tertiary volcanic tuffs underlain by carbonate sedimentary rocks. The deposit consists of a near-vertical breccia pipe, which extends over a vertical interval of at least 100 m [328 ft] (Figure 5-1). The deposit is bounded by intersecting high angle faults (Goodell, 1981; Pearcy, et al., 1995; Fayek, et al., 2006). The deposit is located above the water table and is hosted by heavily fractured, rhyolitic tuffs of the Nopal and Coloradas Formations, which are separated by an argillaceous zone interpreted to be an altered vitrophyre. The tuffs contain background uranium concentrations of about 10 ppm (George-Aniel, et al., 1991). Fractures within the tuffs served as pathways for fluid flow, routes for uranium migration, and sites for uranium mineral precipitation (Pearcy, et al., 1995).

The Nopal Formation (the youngest of the host rocks for the Nopal I deposit) has been dated at 43.8 Ma (Alba and Chavez, 1974). Comparison of the chemical composition (major oxide abundance) between the Nopal and Coloradas Formations with that of the Topopah Spring Member of the Paintbrush Tuff Formation (the proposed repository horizon at Yucca Mountain) illustrates chemical similarities between the units (Table 5-1). At depth the Nopal I ore body extends into the Pozos Formation, which is largely a limestone conglomerate deposited on Cretaceous limestones.

The Nopal I deposit is estimated to have formed about 8 $\pm$ 5 Ma (Pearcy, et al., 1994). After formation and possible hydrothermal alteration, the deposit was lifted above the water table by Basin and Range deformation and exposed at the surface along the eastern face of a horst (Goodell, 1981). In its present position, the deposit has been subject to weathering processes common to the desert areas of northern Mexico {i.e., annual rainfall of about 25 cm [9.84 in] (U.S. Department of Commerce, 1965), occurring in episodic downpours}.

5.2 Mineralogic Mapping

Open pit mining during the late 1970s and early 1980s exposed the upper portion of the Nopal I deposit on two broad horizontal surfaces with about 10 m [33 ft] vertical separation (Levels +00 and +10; Figure 5-2). Clearing and geologic mapping of the Levels +00 and +10 surfaces show that the area of uranium mineralization is easily visible on the outcrop, is roughly elliptical in form, and has maximum horizontal dimensions of about 18 by 30 m [59 by 98 ft] (Figures 5-3 and 5-4). The limits of uranium mineralization on Levels +00 and +10 have been further defined by a field gamma survey (Figure 5-5). Gamma intensity measurements show a roughly annular

pattern corresponding to variations in uranium and nonuranium occurrence (Pearcy, et al., 1995). A contact gamma reading of 1.0 mR/hr [0.26 μC/kg/hr] is the apparent limiting value for the presence of visible uranium minerals on the deposit surface. The Level +10 exposure contains an interior zone with low gamma intensities {<1.0 mR/hr [0.26 μC/kg/hr]}, which corresponds to an area of strongly hematized tuff with no observable uranium minerals. An outer ring of relatively high gamma intensities {up to 28 mR/hr [7.2 μC/kg/hr]} containing abundant but irregularly distributed uranium minerals surrounds this interior zone. Uranium minerals visible on the outcrop generally occur in fractures and consist almost exclusively of uranyl silicates.

The host rock exposed in the cleared areas, Nopal Formation tuff, has been altered in the vicinity of the deposit. Secondary minerals observed in the host rock are clays {variably kaolinite [$Al_2Si_2O_5(OH)_4$] and smectite [$(Na, K, Mg, Ca)_{0.33}Al_2Si_4O_{10}(OH)_2 \cdot nH_2O$], calcite [$CaCO_3$], and iron oxides [variably hematite (Fe_2O_3) and goethite (α-FeO·OH)}. On the Level +10 surface, kaolinite is the predominant clay and tends to increase close to the deposit. On the Level +00 surface, Nopal tuff along the southeast boundary of the deposit, corresponding to the downslope direction of the premining surface, is heavily weathered to smectite. The vitrophyre separating the Nopal and Coloradas Formations has also been exposed on Level +00 and is similarly heavily weathered to smectite.

5.3 Mineralogic Studies

Petrography and scanning electron microscope analyses indicate formation of the Nopal I deposit by emplacement of uranium minerals in fractures, cavities, and intergranular spaces within a brecciated host tuff. The sequence of uranium mineral formation is relatively simple, consisting of primary uraninite, followed by uranyl oxide hydrates, followed by uranyl silicates. In addition to secondary uranium mineral formation, the Nopal I deposit has undergone substantial alteration associated with uranium movement within and around the deposit and formation of secondary nonuranium- and uranium-bearing minerals. Mineralogic aspects of the Nopal I deposit are described by Calas (1977), Goodell (1981), George-Aniel, et al. (1985), Ildefonse, et al. (1990), Pearcy, et al. (1994), Murphy, et al. (1997), Prikryl, et al. (1997), Fayek, et al. (2006), and Murphy (2007).

5.3.1 Primary Mineralization

Uraninite, with formulae between UO_2 and $UO_{2.33}$, was the first uranium mineral to be deposited at Nopal I (Pearcy, et al., 1994). Uraninite is preserved as micron- to millimeter-sized masses within small volumes of strongly silicifed, brecciated tuff. The breccia is composed of silicified, angular, tuff fragments cemented by a uraninite-bearing fine crystalline matrix (Figure 5-6). Minerals associated with primary uraninite in the fine matrix are pyrite, kaolinite, and quartz (Pearcy, et al., 1994) (Figure 5-7). The uranium deposit is interpreted to have formed from hydrothermal solutions, which leached uranium from volcanic glass in the surrounding tuffs and precipitated a uraninite-pyrite-kaolinite-quartz assemblage in voids and fractures as they moved through a subvertical, brecciated zone. The reduced permeability of the silicified breccia likely contributed to the preservation of uraninite at Nopal I by restricting access of altering fluids to preexisting mineralized zones (Pearcy, et al., 1994).

Calas (1977) concluded that uraninite deposition at Nopal I was coincident with hydrothermal alteration at low temperatures as evidenced by montmorillonite (smectite) occurrences. Silica released by hydrothermal alteration of glass and feldspars encased some uraninite and prevented its oxidation. Goodell (1981) proposed an epithermal origin for the uranium ore

deposit at Nopal I in which uranium was derived from the alteration and leaching of volcanic glass by geothermal convective groundwater systems. George-Aniel, et al. (1985) proposed that primary uranium mineralization at Nopal I occurred in stages. Initially, uraninite precipitated in microcracks inside volcanic ilmenites. A high temperature {400 °C [752 °F]} was determined from vapor phase fluid inclusions in quartz, which were related to the first stage of uranium mineralization. The ilmenite-uraninite association was subsequently replaced by a uraninite-pyrite-kaolinite association. George-Aniel, et al. (1985) concluded that uraninite and kaolinite formation occurred at temperatures of 150 to 250 °C [305 to 482 °F]. Hydrothermal formation of uraninite and pyrite, coincident hydrothermal deposition of kaolinite, and subsequent uranium mobilization by oxidizing solutions was also recognized by Ildefonse, et al. (1990).

Pearcy, et al. (1994) identified three texturally distinct forms of uraninite (referred to as "granular," "euhedral," and "colloform") at Nopal I. Relations between uraninite textures and chemistry suggest that granular and euhedral uraninite formed early and then were partially dissolved and reprecipitated as colloform uraninite. Texturally, granular and euhedral uraninite are typically intergrown with kaolinite and pyrite (Pearcy, et al., 1994) (Figures 5-7 and 5-8), whereas colloform uraninite is free of discernible primary mineral intergrowths and is generally observed growing from granular uraninite or quartz substrates (Figures 5-8 and 5-9). Chemically, colloform uraninite is enriched in sulfur and depleted in cations (e.g., calcium, sodium, and lead) when compared to granular and euhedral uraninite (Table 5-2).

The textural and chemical evidence Pearcy, et al. (1994) presented is consistent with an alteration scenario in which an acid sulfate solution generated by pyrite oxidation interacted with early-formed euhedral and granular uraninite. Portions of the euhedral and granular uraninite were dissolved, and uranium may have been transported a short distance (millimeters to centimeters) and reprecipitated as colloform uraninite. This process leached calcium, sodium, and lead and other cations from the early-formed uraninite, and precipitated colloform uraninite enriched in sulfur, depleted in cations, and free of kaolinite and pyrite.

Murphy, et al. (1997) proposed a geochemical model for primary uranium ore genesis at Nopal I based on fluid mixing in a fractured, high permeability breccia zone created by deformation and faulting in the existing tuffs. In this model, reducing water from underlying carbonates containing dissolved ferrous iron and sulfide mixed in the breccia zone at the intersection of faults with oxidizing water percolating through the tuffs and carrying aqueous uranyl. The primary mineral assemblage at the Nopal I deposit (i.e., uraninite, pyrite, kaolinite, and quartz) was produced by the reaction

$$UO_2^{2+} + Fe^{2+} + 2HS^- + H_2O + 2KAlSi_3O_8 \rightarrow UO_2 + FeS_2 + Al_2Si_2O_5(OH)_4 + 4SiO_2 + 2K^+$$

which couples sulfur oxidation, uranium reduction, and incongruent feldspar alteration.

Based on concentrations of uranium and lead in the late-forming, cation-poor, colloform uraninite specimens, Pearcy, et al. (1994) reported a chemical uranium-lead age of 8 ± 5 Ma for the primary mineralizing event at Nopal I. Fayek, et al. (2006) identified two stages of uraninite formation at Nopal I. Stage I uraninite was dated at 32 ± 8 Ma (by the uranium-lead method), and stage 2 uraninite, which corresponds to the colloform uraninite Pearcy, et al. (1994) described, was dated at 1.6 ± 0.5 Ma. Fayek, et al. (2006) also obtained an age of less than 1 Ma (based on uranium-lead data) for uraninite from the Pozos Formation, which was collected from a borehole core nearly 100 m [328 ft] below the surface exposure of the Nopal I deposit.

5.3.2 Secondary Mineralization

Where fluids and oxygen have penetrated the Nopal I deposit, the primary uraninite has been oxidized, remobilized, and reprecipitated as secondary uranyl minerals and as components of iron oxides, opal, and calcite (Pearcy, et al., 1994; Prikryl, et al., 1997). The ore deposit presently occurs in the unsaturated hydrologic zone above the groundwater table; however, some degree of oxidation and migration of uranium likely occurred earlier under groundwater-saturated and possibly hydrothermal conditions.

5.3.2.1 Uranyl Minerals

Secondary uranium minerals identified at the Nopal I deposit are listed in Table 5-3. The Nopal I deposit has fewer uranium minerals than most other uranium deposits that have undergone oxidative alteration of the primary mineral assemblage. The limited number of uranium phases at Nopal I is a result of the comparative youth of the deposit and the relatively simple chemistry of the system. Pearcy, et al. (1994) characterized the paragenetic sequence of secondary uranyl mineralization at Nopal I concluding that it progressed from uranyl oxide hydrates (notably varieties of schoepite) to uranyl silicates (notably soddyite, weeksite, boltwoodite, and especially uranophane) (Figure 5-10).

The initial products of uraninite oxidation at Nopal I are uranyl oxide hydrates that directly replace uraninite and fill voids lined by colloform uraninite (Figures 5-8 and 5-9). The most common uranyl oxide hydrates at Nopal I are the mixed-valence phase ianthinite, schoepite, and dehydrated schoepite. Ianthinite, a uranyl oxide hydrate containing both U^{+4} and U^{+6}, is rarely preserved in most uranium deposits but is relatively common in uraninite-bearing specimens from Nopal I (Figure 5-11). Ianthinite is unstable and converts to schoepite when exposed to air. The occurrence of ianthinite at Nopal I demonstrates effective isolation of minerals from oxidizing fluids over long periods of time in an environment perceived to be pervasively oxidizing. Schoepite and dehydrated schoepite are the most common uranyl oxide hydrates at Nopal I. Dehydration of schoepite proceeds directly to dehydrated schoepite. Becquerelite, a calcium-bearing uranyl oxide hydrate, has been identified by x-ray diffractometry (XRD) analysis but has not been observed optically in specimens from Nopal I. In samples containing multiple uranyl oxide phases, ianthinite is the earliest formed and is followed by schoepite and/or dehydrated schoepite (Figure 5-12).

Uranyl oxide hydrates are followed paragenetically by uranyl silicates, which are the dominant uranium mineral phases at Nopal I. Uranyl silicates occur as replacements of earlier formed uranium minerals and as euhedral crystals within voids and fractures. In voids lined by uraninite, a clear progression from uraninite to uranyl oxide hydrates to uranyl silicates is frequently preserved (Figures 5-13 and 5-14). Uranophane is the most abundant uranyl silicate at Nopal I and occurs throughout the deposit. Uranophane in voids and fractures generally forms clusters of yellow acicular crystals (Figure 5-15). Beta-uranophane, a polymorph of uranophane, is also observed at Nopal I where it occurs in the interior of the deposit (Figure 5-16). Soddyite, weeksite, and boltwoodite are also common at Nopal I but have much more limited occurrences than uranophane. Soddyite at Nopal I occurs in fractures close to uraninite-bearing zones, typically follows uranyl oxide hydrates, and is often intergrown with other uranyl silicates (Figure 5-17). Euhedral, rhombic-shaped soddyite crystals have been observed in fractures rich in iron oxides and clays (e.g., kaolinite and smectite) (Figure 5-18). Weeksite and boltwoodite have a much more limited occurrence at Nopal I than uranophane and soddyite and occur as either fine equigranular or coarser acicular crystals precipitated in

open space (Figure 5-19). XRD has detected haiweeite, a calcium-bearing uranyl silicate, in fracture fill in the altered vitrophyre a few meters outside the deposit.

Uranyl silicates are generally complexly intergrown in oxidized samples from Nopal I (Figure 5-20). Weeksite and boltwoodite tend to occur somewhat further from remnant uraninite than uranophane and soddyite, suggesting their formation later in the sequence. However, on a deposit-wide scale, a clear progression from one uranyl silicate to another is not observed. The evidence suggests that the specific uranyl silicate formed in a given area depended on local geochemical conditions (e.g., cation activity) rather than a broad evolution of the oxidizing system. Such local variability is characteristic of natural systems.

With respect to the timing of secondary uranium mineralization, Pickett and Murphy (1997) reported a uranium phase oxidation event at 3.2 to 3.4 Ma based on uranium-lead isotopic data from three samples of late-forming uranophane from Nopal I. Fayek, et al. (2006) also calculated ages of secondary uranyl minerals from the main Nopal I ore body using uranium decay series methods. Uranophane had an age of 3.1 $\pm$ 0.5 Ma, which is consistent with results from Pickett and Murphy (1997). In contrast, schoepite/dehydrated schoepite had an age of 85 $\pm$ 8 ka, and weeksite/boltwoodite from near the deposit margin yielded an age of 41 $\pm$ 5 ka.

The composition of the secondary uranium phases at Nopal I indicates that the fluids that altered the uraninite were oxidizing and contained substantial silicon, calcium, and potassium. This composition reflects interaction of the altering fluids with the host tuffs, which have abundant silica and significant amounts of CaO and K_2O (see Table 5-1). Calcium may also have been supplied by limestones, which underlie the volcanic sequence, or by interaction of meteoric fluids with caliche near the surface (Murphy, et al., 1991) and/or with abundant calcite veinlets in the deposit area.

5.3.2.2 Nonuranium- and Uranium-Bearing Minerals

As exposed on Level +10 of Nopal I, an interior portion of the deposit consists of strongly hematized tuff with no observable uranium minerals (see Figure 5-5). Petrography and XRD analyses of this interior zone indicate the occurrence of abundant alunite [$KAl_3(SO_4)_2(OH)_6$] and jarosite [$KFe_3(SO_4)_2(OH)_6$] (Leslie, et al., 1993). Alteration of pyrite associated with the primary ore assemblage by interaction with oxidizing fluids is a likely mechanism leading to formation of hematite, alunite, and jarosite (Bladh, 1982; Nordstrom, 1982). Conditions that favor iron-oxide and sulfate formation (oxidizing, low pH) are also conditions that tend to mobilize uranium. Thus, the absence of uranium minerals in the central part of the deposit likely resulted from mobilization of uranium associated with pyrite oxidation.

Jarosite has also been observed outside the deposit as a late-forming precipitate in a major fracture that crosscuts the deposit (Figure 5-21) (Pearcy, et al., 1995; Prikryl, et al., 1997). The fracture also contains hematite, goethite, and amorphous iron-oxides with anomalous uranium concentrations (up to thousands of ppm) but no observable uranium minerals. Petrographic observations indicate that the original assemblage in the fracture was a pyrite-kaolinite association (Figure 5-22). Like the strongly hematized interior zone on Level +10, the present mineral assemblage in the fracture is most likely the result of chemical weathering of pyrite. The high uranium contents of the iron-oxide phases and apparent absence of uranium minerals within the fracture indicate that uranium was sequestered during secondary mineral growth or sorbed on mineral surfaces. Uranium decay series data on three samples of iron oxide/oxyhydroxide fracture filling from Nopal I are consistent with an episode of uranium deposition around 400 ka (Murrell, et al., 2002).

Other uranium-bearing secondary materials found at Nopal I are caliche and opal. Uranium-rich caliche occurs within meters of the deposit in fractures and on surface exposures of tuff that were undisturbed by mining activities. In strongly oxidized fractures within the deposit, uranium-rich opal coats botryoidal hematite and uranophane (Leslie, et al., 1993). Uranium-series data from these materials provide information on the rates and the episodic nature of radionuclide migration (Pickett, et al., 2001). Opals have uranium as high as 10,000 ppm, while carbonate-rich caliches contain up to 350 ppm uranium. Most opals appear to be older than 600 ka. Caliches, however, have Th-230 ages ranging from 18 to 136 ka, clustering around 50 ka. In addition, one opal yielded a 54-ka age (Leslie and Pearcy, 1993), supporting episodic uranium deposition at this time. Uranium-series data on the iron-rich fracture fills, caliches, and opals are discussed further in Chapter 6.

5.3.3 Thermodynamic Properties of Uranyl Minerals at Nopal I

Murphy (2007) estimated thermodynamic properties and calculated relative stabilities of uranyl minerals under hydrothermal conditions relevant to Nopal I {e.g., at temperatures up to 200 °C [392 °F]}. The estimations focused on phase relations among metaschoepite, becquerelite, soddyite, and uranophane because they are the predominant minerals at Nopal I and represent primary variations in uranyl mineral chemistry at the site. Metaschoepite [nominally $UO_3 \cdot 2H_2O$] forms by partial dehydration of schoepite; however, schoepite and metaschoepite are optically and structurally similar and the terms “schoepite” and “metaschoepite” are often used interchangeably. Equilibrium phase relations among the uranyl minerals are illustrated as a function of temperature in Figure 5-23. With increasing temperature, the becquerelite stability field encroaches over the metaschoepite field and both the becquerelite and uranophane fields encroach on the soddyite field reflecting strong retrograde solubility of the Ca-bearing uranyl phases. Metaschoepite-soddyite equilibrium buffers aqueous silica activity and is a weak function of temperature. Uranophane-becquerelite equilibrium is essentially independent of temperature. The phase relations illustrated in
Figure 5-23 show that below 100 °C [212 °F] uranophane coexists with metaschoepite and above 100 °C [212°F] becquerelite coexists with soddyite.

Based on the calculated phase relations illustrated in Figure 5-23, Murphy (2007) reported that uranophane is the most stable uranyl phase over a broad range of moderate to elevated silica activities coupled with near-neutral to slightly alkaline pH and moderately low (and higher) Ca ion activity. Relative to other uranyl minerals, becquerelite stability is restricted to a narrow range of conditions at 25 °C [77 °F], and the stabilities of metaschoepite and soddyite are restricted to low Ca activities and/or acidic conditions at elevated temperatures.

Murphy (2007) concluded that uranophane stability relative to other uranyl minerals over the broad range of realistic geochemical conditions between 25 and 200 °C [77 and 392 °F] supports an interpretation that widely recognized assemblages of schoepite, soddyite, and uranophane are a consequence of persistent chemical potential heterogeneity. Preservation of uraninite in silicified tuff at Nopal I indicates the geologic stability of strong geochemical potential gradients in the mineralogical system. In addition, the occurrence of schoepite and soddyite at Nopal I in close proximity to uranophane (dated at more than 3 Ma) also attests to heterogeneity stability. The thermodynamic studies of Murphy (2007) in conjunction with petrographic evidence indicate that geochemical potential heterogeneity at Nopal I has been maintained on a geologic time scale.

5.4 References

Alba, L.A. and R. Chavez. "K-Ar Ages of Volcanic Rocks From the Central Sierra Peña Blanca, Chihuahua, Mexico." *Isochron West*. Vol. 10. pp. 21–23. 1974.

Bladh, K.W. "The Formation of Goethite, Jarosite, and Alunite During the Weathering of Sulfide-Bearing Felsic Rocks." *Economic Geology*. Vol. 77. pp. 176–184. 1982.

Calas, G. "Les Phénomènes D'Altération Hydrothermale et Leur Relation Avec les Minéralisations Uranifères en Milieu Volcanique: Le Cas des Ignimbrites Tertiaires de la Sierra de Peña Blanca, Chihuahua (Mexique)." *Sciences Géologique Bulletin.* Vol. 30. pp. 2–19. 1977.

Cárdenas-Flores, D. "Volcanic Stratigraphy and U-Mo Mineralizations of the Sierra Peña Blanca, Chihuahua, Mexico." *Uranium Deposits in Volcanic Rocks*. IAEA–TC–490/31. Vienna, Austria: International Atomic Energy Agency. pp. 125–136. 1985.

Fayek, M., M. Ren, P. Goodell, P. Dobson, A. Saucedo, A. Kelts, S. Utsunomiya, R.C. Ewing, L.R. Riciputi, and I. Reyes. "Paragenesis and Geochronology of the Nopal I Uranium Deposit, Mexico." International High-Level Radioactive Waste Management Proceedings, Las Vegas, Nevada. La Grange Park, Illinois: American Nuclear Society. pp. 55–62. 2006.

George-Aniel, B., J.L. Leroy, and B. Poty. "Volcanogenic Uranium Mineralizations in the Sierra Pena Blanca District, Chihuahua, Mexico: Three Genetic Models." *Economic Geology.* Vol. 86. pp. 233–248. 1991.

———. "Uranium Deposits of the Sierra Peña Blanca." *Uranium Deposits in Volcanic Rocks*. IAEA–TC–490/8. Vienna, Austria: International Atomic Energy Agency. pp. 175–186. 1985.

Goodell, P.C. "Geology of the Peña Blanca Uranium Deposits, Chihuahua, Mexico." Uranium in Volcanic and Volcanoclastic Rocks. P.C. Goodell, and A.C. Waters, eds. *AAPG Studies in Geology.* No. 13. pp. 275–291. 1981.

Ildefonse, P., J.P. Muller, B. Clozel, and G. Calas. "Study of Two Alteration Systems as Natural Analogues for Radionuclide Release and Migration." *Engineering Geology.* Vol. 29. pp. 413–439. 1990.

Leslie, B.W. and E.C. Pearcy. "Uranium Migration at the Pena Blanca Natural Analog Site." *Geological Society of America Abstracts With Programs*. Vol. 25. p. A–184. 1993.

Leslie, B.W., E.C. Pearcy, and J.D. Prikryl. "Oxidative Alteration of Uraninite Under Hydrologically Unsaturated Conditions at Pena Blanca, Chihuahua, Mexico: Contaminant Transport and Source-Term Constraints for the Proposed Repository at Yucca Mountain, Nevada." *Scientific Basis for Nuclear Waste Management XVI.* C.G. Interrante and R.T. Pabalan, eds. Symposium Proceedings 294. Pittsburgh, Pennsylvania: Materials Research Society. pp. 505–512. 1993.

Muller, J.P., P. Ildefonse, and G. Calas. "Para-Magnetic Defect Centers in Hydrothermal Kaolinite From an Altered Tuff in the Nopal Uranium Deposit, Chihuahua, Mexico." *Clays and Clay Minerals*. Vol. 38, No. 6. pp. 600–608. 1990.

Murphy, W.M. "Hydrothermal Phase Relations Among Uranyl Minerals at the Nopal I Analog Site." Materials Research Society Symposium Proceedings. Pittsburgh, Pennsylvania: Materials Research Society. Vol. 985. pp. 53–58. 2007.

Murphy, W.M., E.C. Pearcy, and D.A. Pickett. "Natural Analog Studies at Peña Blanca and Santorini." Seventh EC Natural Analogue Working Group Meeting. H. von Maravic and J. Smellie, eds. EUR 17851 EN. Brussels, Belgium: European Commission. pp. 105–112. 1997.

Murphy, W.M., E.C. Pearcy, and P.C. Goodell. "Possible Analog Research Sites for the Proposed High-Level Nuclear Waste Repository in Hydrologically Unsaturated Tuff at Yucca Mountain, Nevada." Fourth Natural Analogue Working Group Meeting and Pocos de Caldas Project Final Workshop, Pitlochry, Scotland, June 18–22, 1990. B. Come and N.A. Chapman, eds. Final Report EUR 13014 EN. Brussels, Belgium: Commission of the European Communities. pp. 267–276. 1991.

Murrell, M.T., S.J. Goldstein, and P.R. Dixon. "Uranium Decay Series Mobility at Peña Blanca, Mexico: Implications for Nuclear Repository Stability." Eighth EC Natural Analogue Working Group Meeting. H. von Maravic and W.R. Alexander, eds. EUR 19118 EN. Brussels, Belgium: European Commission. pp. 339–347. 2002.

Nordstrom, D.K. "Aqueous Pyrite Oxidation and the Consequent Formation of Secondary Iron Minerals." Acid Sulfate Weathering. *Soil Science Society of America, Special Publication No. 10.* pp. 37–56. Madison, Wisconsin: Soil Science Society of America. 1982.

Pearcy, E.C., J.D. Prikryl, and B.W. Leslie. "Uranium Transport Through Fractured Silicic Tuff and Relative Retention in Areas With Distinct Fracture Characteristics." *Applied Geochemistry.* Vol. 10. pp. 685–704. 1995.

Pearcy, E.C., J.D. Prikryl, W.M. Murphy, and B.W. Leslie. "Alteration of Uraninite From the Nopal I Deposit, Peña Blanca District, Chihuahua, Mexico, Compared to Degradation of Spent Nuclear Fuel in the Proposed U.S. High-Level Nuclear Waste Repository at Yucca Mountain, Nevada." *Applied Geochemistry.* Vol. 9. pp. 713–732. 1994.

Pickett, D.A. and W.M. Murphy. "Isotopic Constraints on Radionuclide Transport at Peña Blanca." Seventh European Commission Natural Analogue Working Group Meeting. H. von Maravic and J. Smellie, eds. EUR 17851 EN. Brussels, Belgium: European Commission. pp. 113–122. 1997.

Pickett, D.A., W.M. Murphy, and B.W. Leslie. "^{238}U-^{234}U-^{230}Th Ages of Secondary Deposits and Evidence on the Rate of Recent Radionuclide Migration at the Nopal I Natural Analog." Abstracts of the 8th International Conference on Chemistry and Migration Behaviour of Actinides and Fission Products in the Geosphere. *Migration '01.* p. 103. 2001.

Prikryl, J.D., D.A. Pickett, W.M. Murphy, and E.C. Pearcy. "Migration Behavior of Naturally Occurring Radionuclides at the Nopal I Uranium Deposit, Chihuahua, Mexico." *Journal of Contaminant Hydrology.* Vol. 26. pp. 61–69. 1997.

Reyes-Cortés, I.A. "Geologic Setting and Mineralization: Sierra Peña Blanca, Chihuahua, Mexico." Eighth European Commission Natural Analogue Working Group Meeting.

H. von Maravic and W.R. Alexander, eds. EUR 19118 EN. Brussels, Belgium: European Commission. pp. 321–331. 2002.

U.S. Department of Commerce. "World Weather Records 1951–1960, Vol. 1: North America." Washington, DC: U.S. Department of Commerce. 1965.

Table 5-1. Comparison of Chemical Compositions of the Nopal and Coloradas Formations and the Topopah Spring Member of the Paintbrush Tuff Formation (Values in Weight Percent)

Oxide	Nopal Formation*	Coloradas Formation*	Topopah Spring Member†
SiO_2	75.24	67.49	74.00
Al_2O_3	12.75	12.00	12.40
K_2O	6.48	4.13	4.00
Fe_2O_3	1.54	1.99	1.07
Na_2O	1.07	0.47	3.40
CaO	0.41	4.41	0.66
TiO_2	0.26	0.24	0.10
MgO	0.15	0.16	0.31
P_2O_3	0.07	0.04	1.01
MnO	0.06	0.11	0.08
LOI‡	2.60	8.17	3.79
Total	100.63	99.21	99.82

*Pearcy, E.C., W. M. Murhpy, and J. D. Prikryl. "Report on Research Activities for the Quarter April 1 Through June 30, 1991." CNWRA 91-02Q. San Antonio, Texas: Center for Nuclear Waste Regulatory Analyses. 1991. ML040360615.

†Broxton, D.E., R.G. Warren, R.C. Hagan, and G. Luedemann. "Chemistry of Diagenetically Altered Tuffs at a Potential Nuclear Waste Repository, Yucca Mountain, Nye County, Nevada." LA-10802-MS. Los Alamos, New Mexico. Los Alamos National Laboratory. 1986.

‡LOI = Loss on ignition

Table 5-2. Electron Microprobe Analyses of Nopal I Uraninite (Normalized to 100 Atom Percent)*															
Sample	**U**	**O**	**Na**	**Al**	**Si**	**P**	**As**	**Th**	**Pb**	**Ca**	**K**	**S**	**Fe**	**Mn**	**Ti**
Colloform Uraninite															
32-ts2-p1	32.34	66.42	0.11	0.01	0.33	0.00	0.03	0.01	0.05	0.00	0.24	0.20	0.00	0.01	0.06
32-ts2-p4	30.88	66.98	0.43	0.09	0.65	0.00	0.02	0.00	0.04	0.07	0.28	0.24	0.01	0.02	0.10
32-ts2-p5	33.78	64.65	0.16	0.31	0.34	0.03	0.01	0.00	0.02	0.04	0.26	0.16	0.02	0.00	0.03
32-ts2-p6	32.79	65.52	0.35	0.08	0.44	0.00	0.01	0.02	0.07	0.00	0.26	0.25	0.00	0.00	0.01
32-ts4-p2	29.75	66.86	0.85	0.16	0.32	0.02	0.15	0.01	0.58	0.65	0.26	0.16	0.04	0.00	0.00
32-ts4-p6	30.52	66.96	0.66	0.10	0.47	0.04	0.09	0.00	0.26	0.29	0.20	0.16	0.01	0.00	0.04
32-ts4-p19	29.61	68.38	0.32	0.07	0.46	0.00	0.06	0.02	0.28	0.04	0.28	0.21	0.00	0.03	0.00
32-ts4-p21	30.01	67.93	0.32	0.05	0.42	0.03	0.00	0.01	0.30	0.14	0.26	0.26	0.01	0.01	0.06
1-ts3-p1	30.28	68.09	0.17	0.12	0.45	0.00	0.04	0.01	0.05	0.00	0.26	0.27	0.01	0.02	0.03
1-ts3-p2	30.09	68.22	0.25	0.04	0.52	0.00	0.00	0.01	0.02	0.00	0.31	0.29	0.00	0.02	0.05
1-ts3-p6	30.76	67.44	0.20	0.17	0.58	0.00	0.00	0.00	0.03	0.01	0.32	0.21	0.02	0.00	0.07
30-ts2-p1	28.94	66.80	0.74	0.08	0.56	0.03	0.11	0.01	0.75	1.37	0.18	0.05	0.12	0.00	0.08
30-ts2-p2	29.05	67.46	0.60	0.00	0.50	0.04	0.13	0.01	0.61	10.3	0.22	0.04	0.09	0.00	0.03
30-ts2-p5	27.96	67.20	0.77	0.08	0.63	0.01	0.10	0.00	0.56	2.08	0.21	0.05	0.14	0.02	0.00
30-ts2-p6	27.65	69.22	0.58	0.06	0.42	0.00	0.07	0.00	0.57	0.82	0.29	0.09	0.08	0.03	0.02
30-ts2-p7	28.12	67.31	0.89	0.06	0.57	0.00	0.10	0.01	0.53	1.84	0.23	0.02	0.05	0.00	0.09
32-ts5-p5	27.65	68.69	0.91	0.22	0.31	0.06	0.10	0.01	0.51	0.85	0.27	0.07	0.06	0.00	0.08
32-ts5-p6	27.81	68.83	0.99	0.03	0.22	0.00	0.09	0.00	0.52	0.92	0.27	0.04	0.07	0.02	0.00
Average	29.89	67.39	0.52	0.09	0.46	0.01	0.06	0.01	0.32	0.56	0.26	0.15	0.04	0.01	0.04
Granular Uraninite															
32-ts4-p18	27.15	67.28	0.67	0.12	0.42	0.06	0.09	0.00	2.66	1.04	0.22	0.00	0.06	0.05	0.01
32-ts4-p20	27.10	68.09	0.68	0.18	0.47	0.00	0.07	0.01	1.38	1.50	0.25	0.00	0.03	0.01	0.03
32-ts4-p23	27.66	67.54	0.75	0.16	0.45	0.01	0.06	0.00	1.34	1.46	0.28	0.02	0.07	0.00	0.01
32-ts4-p24	28.48	67.68	0.78	0.22	0.44	0.00	0.17	0.00	0.31	1.36	0.28	0.01	0.00	0.07	0.00
32-ts4-p25	28.44	67.41	0.92	0.14	0.37	0.03	0.20	0.00	0.39	1.52	0.25	0.02	0.06	0.01	0.05
32-ts4-p27	28.19	67.78	0.77	0.15	0.40	0.01	0.16	0.00	0.42	1.62	0.23	0.02	0.03	0.00	0.03
1-ts3-p11	29.70	67.40	0.62	0.04	0.37	0.00	0.07	0.00	0.31	0.84	0.31	0.14	0.00	0.00	0.00

Table 5-2. Electron Microprobe Analyses of Nopal I Uraninite (Normalized to 100 Atom Percent)* (continued)															
Sample	**U**	**O**	**Na**	**Al**	**Si**	**P**	**As**	**Th**	**Pb**	**Ca**	**K**	**S**	**Fe**	**Mn**	**Ti**
Granular Uraninite															
1-ts3-p12	27.84	68.32	0.85	0.04	0.26	0.02	0.07	0.00	0.57	1.48	0.26	0.10	0.01	0.00	0.00
1-ts3-p14	27.49	67.94	0.90	0.34	0.48	0.00	0.05	0.00	0.80	1.43	0.28	0.02	0.00	0.01	0.06
1-ts3-p18	32.93	65.13	0.45	0.02	0.34	0.01	0.01	0.01	0.08	0.10	0.37	0.25	0.06	0.00	0.04
1-ts3-p19	31.82	66.70	0.29	0.02	0.32	0.01	0.00	0.00	0.05	0.02	0.30	0.11	0.08	0.00	0.08
Average	28.80	67.39	0.70	0.13	0.39	0.01	0.09	0.00	0.76	1.12	0.28	0.06	0.04	0.01	0.03
Euhedral Uraninite															
32-ts2-p9	29.34	66.27	0.84	0.08	0.71	0.02	0.04	0.00	0.07	2.00	0.26	0.11	0.01	0.00	0.05
32-ts4-p1	27.42	66.71	1.43	0.08	0.48	0.02	0.14	0.00	1.04	2.14	0.20	0.00	0.13	0.00	0.02
32-ts4-p4	27.43	67.02	1.34	0.04	0.40	0.01	0.13	0.01	0.90	2.14	0.20	0.02	0.12	0.00	0.03
32-ts4-p8	27.43	66.87	1.48	0.11	0.39	0.08	0.17	0.00	0.75	2.07	0.25	0.00	0.20	0.01	0.00
1-ts3-p10	27.06	66.91	10.6	0.20	0.42	0.06	0.00	0.01	2.05	1.65	0.27	0.00	0.00	0.07	0.04
1-ts3-p15	29.03	66.28	0.86	0.32	0.68	0.01	0.06	0.00	0.78	1.26	0.35	0.03	0.03	0.04	0.08
32-ts5-p1	27.43	66.56	1.13	0.10	0.24	0.09	0.11	0.00	0.58	3.16	0.23	0.03	0.14	0.02	0.00
32-ts5-p2	27.59	66.54	1.10	0.09	0.31	0.01	0.09	0.00	0.68	2.82	0.29	0.02	0.22	0.01	0.04
Average	27.84	66.65	1.15	0.13	0.45	0.04	0.09	0.00	0.86	2.15	0.25	0.03	0.11	0.02	0.03

*Pearcy, E.C., J.D. Prikryl, W.M. Murphy, and B.W. Leslie. "Alteration of Uraninite From the Nopal I Deposit, Peña Blanca District, Chihuahua, Mexico, Compared to Degradation of Spent Nuclear Fuel in the Proposed U.S. High-Level Nuclear Waste Repository at Yucca Mountain, Nevada." *Applied Geochemistry.* Vol. 9. pp. 713–732. 1994.

Table 5-3. Uranium Minerals Identified at the Nopal I Uranium Deposit	
Mineral	**Nominal Chemical Formula**
Uraninite	UO_{2+x}
Ianthinite	$U^{4+}(U^{6+}O_2)_5(OH)_{14} \cdot 3H_2O$
Schoepite	$UO_3 \cdot 2H_2O$
Dehydrated Schoepite	$UO_3 \cdot nH_2O$ (n<2)
Becquerelite	$Ca(UO_2)_6O_4(OH)_6 \cdot 8H_2O$
Soddyite	$(UO_2)_2SiO_4 \cdot 2H_2O$
Uranophane	$Ca(UO_2)_2Si_2O_7 \cdot 6H_2O$
Beta-uranophane	$Ca(UO_2)_2Si_2O_7 . 6H_2O$
Weeksite	$K_2(UO_2)_2Si_6O_{15} \cdot 4H_2O$
Boltwoodite	$KH(UO_2)SiO_4 \cdot 1.5H_2O$
Haiweeite	$Ca(UO_2)_2Si_6O_{15} \cdot 5H_2O$

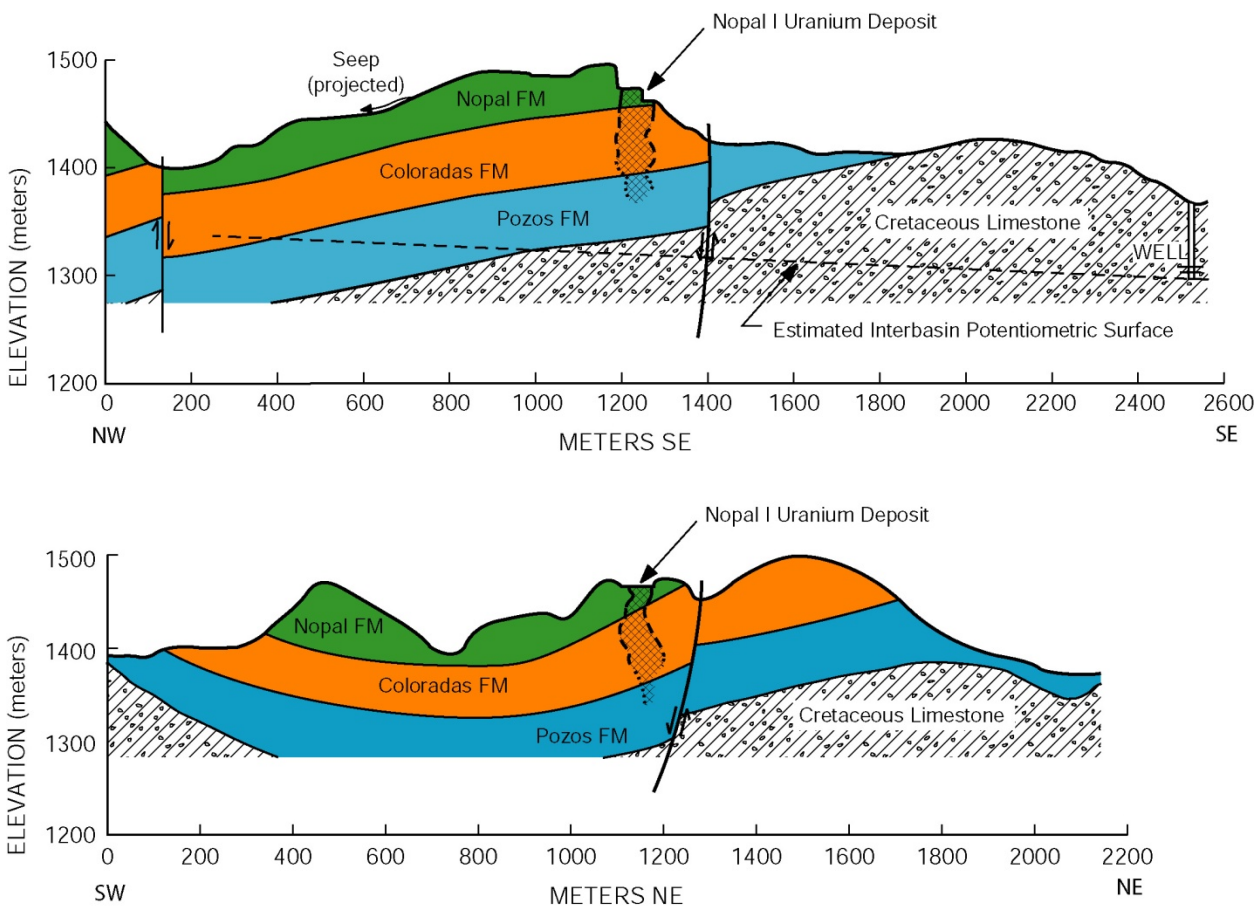

Figure 5-1. Schematic Cross-Section of the Nopal I Uranium Deposit. The Deposit Is Located Above the Water Table and Hosted in Silicic Tuffs of the Nopal and Coloradas Formations. The Deposit Extends Into the Pozos Formation, Which Is Largely a Limestone Conglomerate (Figure From Pearcy, et al., 1994).

Figure 5-2. Photograph of the Nopal I Uranium Deposit Looking to the Southwest; the Vertical Wall at the Left of the Photo Is About 10 m [33 ft] High and Separates the Level +00 and Level +10 Exposures

Figure 5-3. Photograph of the Nopal I Uranium Deposit Looking Toward the South and Showing the Level +10 Exposure After Clearing of Loose Rock and Soil

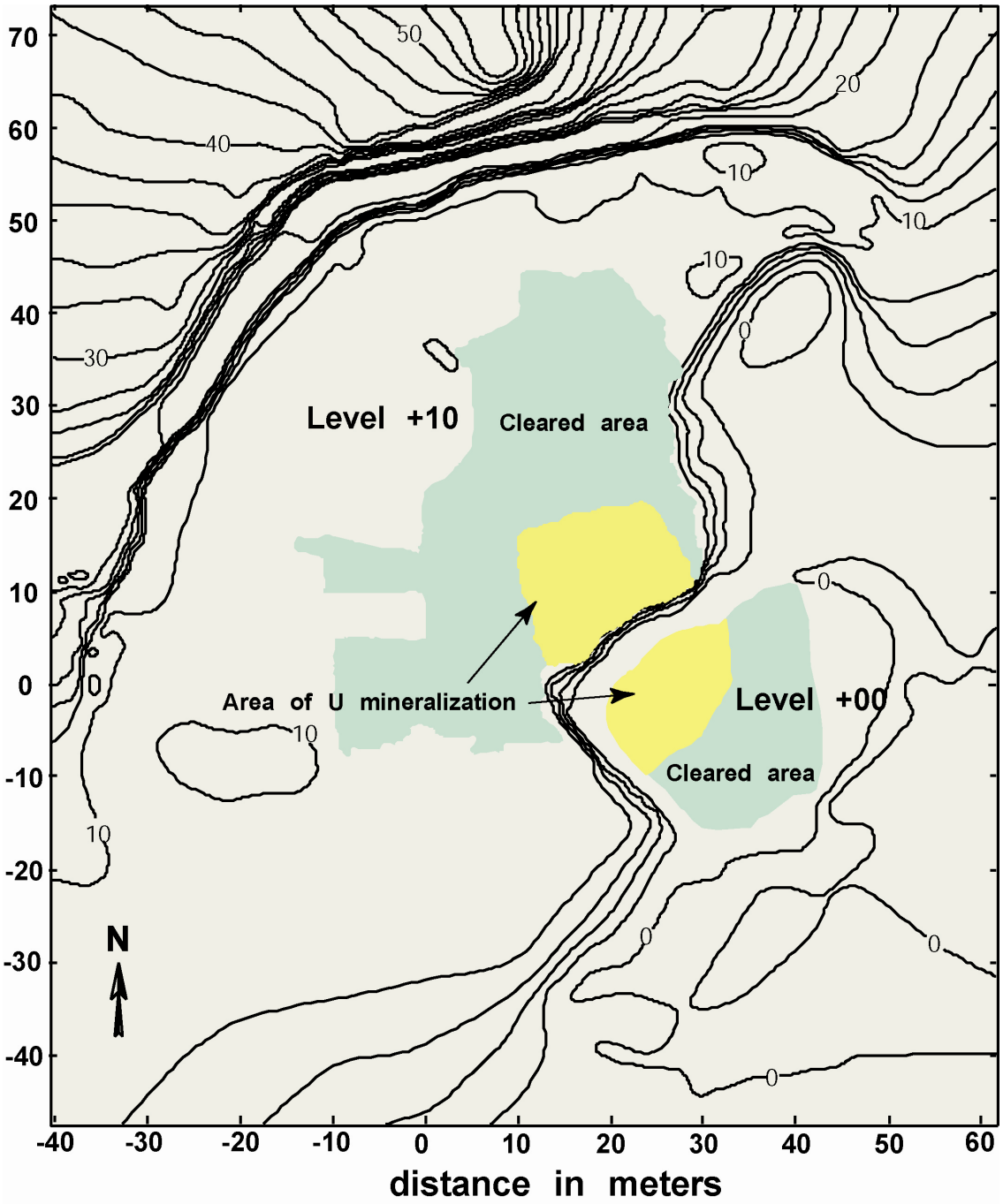

Figure 5-4. Plan View Map of the Nopal I Uranium Deposit Showing the Cleared Portions of Level +00 and Level +10 and the Area of Visible U Mineralization on the Cleared Outcrop. The Contour Interval on the Map Is 2 m [6.6 ft], Referenced at Zero on Level +00.

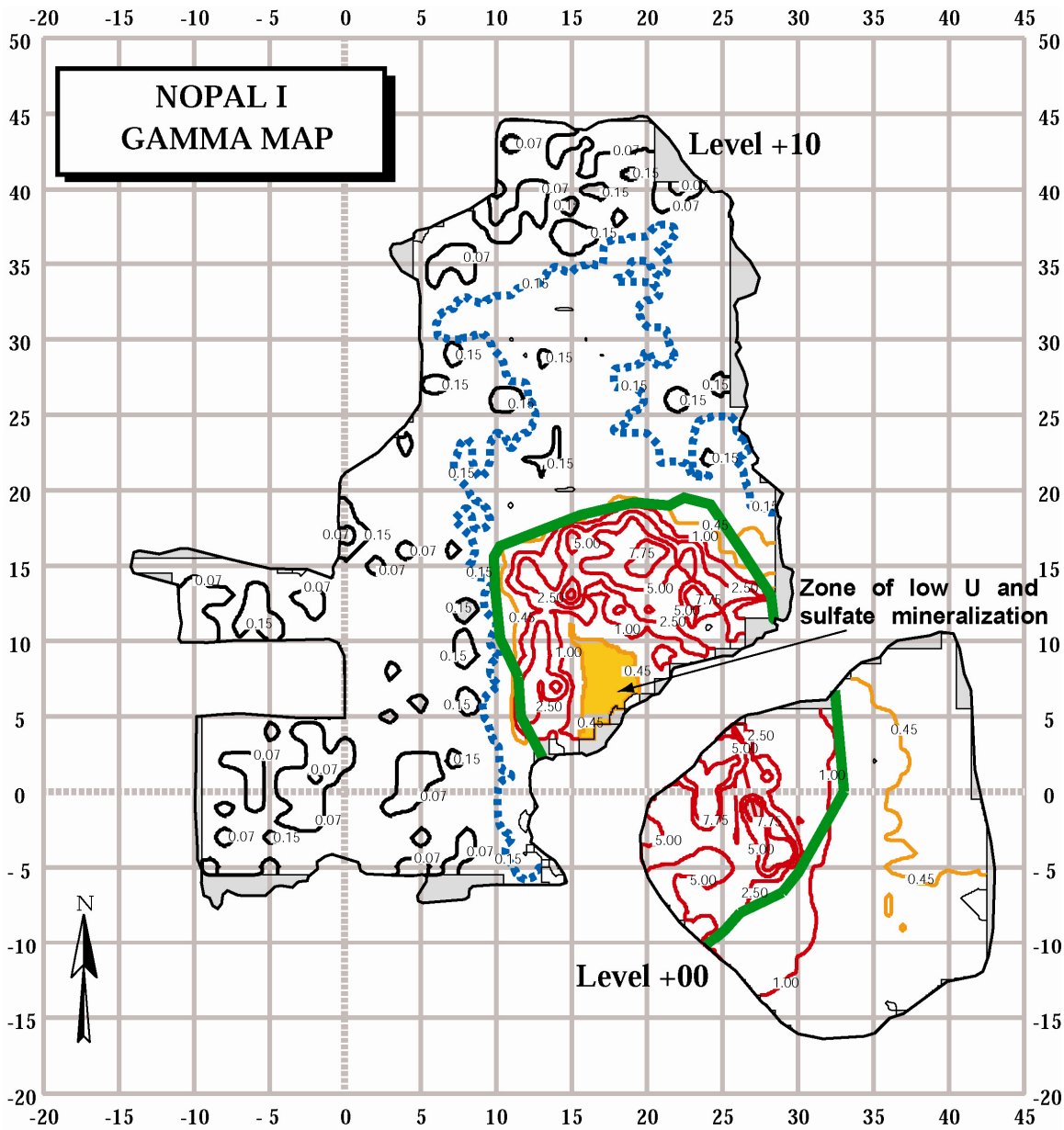

Figure 5-5. Plan View Map Showing Results of a Gamma Survey Conducted on the Cleared Areas of the Nopal I Deposit. The Heavy Green Line Indicates the Limit of Visible U Mineralization and Marks the Nominal Edge of the Deposit. The Orange Shaded Area in the Interior of the Ore Body on Level +10 Corresponds to a Zone of Low Gamma Intensities {<0.45 mR/hr [0.12 µC/kg/hr]}. This Zone Is Strongly Hematized, Contains Sulfate Minerals (Alunite and Jarosite), and Has No Observable U Minerals. The blue dashed line is the 0.15 mR/h boundary of the continuous area of anomalous U concentrations.
(Figure Modified From Pearcy, et al., 1995).

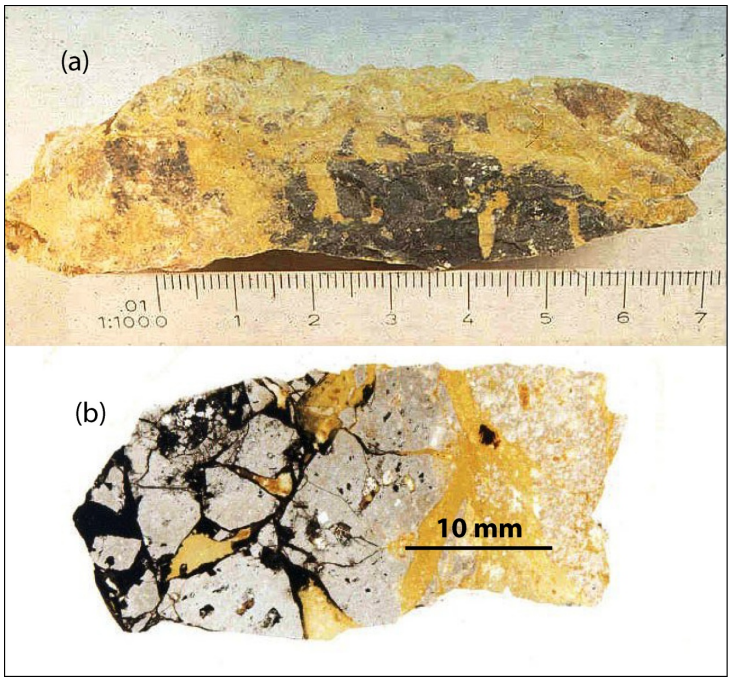

Figure 5-6. (a) Photograph of Rock Specimen of Uranium Ore From Nopal I Showing Brecciated Tuff Fragments Cemented by Uraninite-Bearing Fine Crystalline Matrix (Black Material). The Uraninite-Bearing Matrix Has Undergone Oxidative Alteration to Yellow-Colored Uranyl Minerals. (b) Photograph of a Rock Thin Section of Uranium Ore From Nopal Showing Silicified, Angular, Tuff Fragments Cemented by a Black-Colored, Uraninite-Bearing Fine Crystalline Matrix. In the Right Portion of the Section, Oxidation of the Uraninite Has Led to Formation of Yellow-Colored Uranyl Minerals.

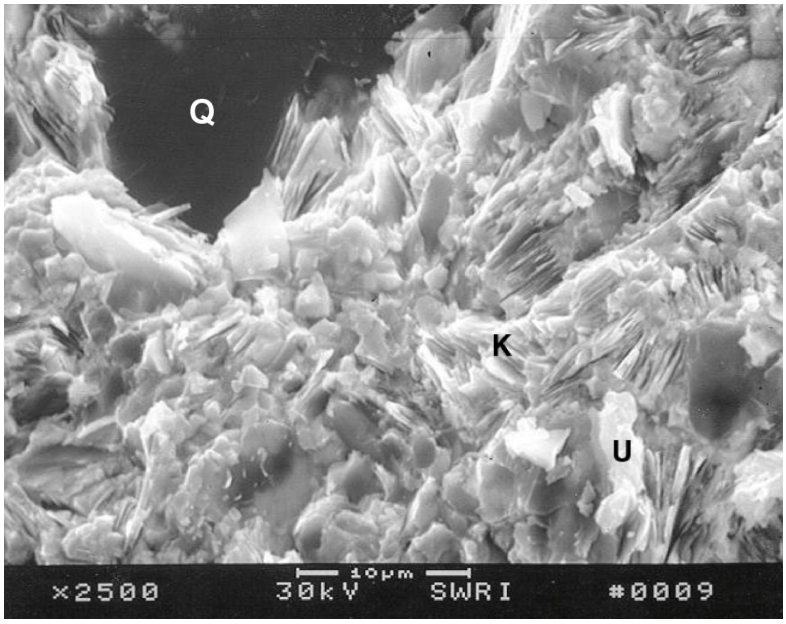

Figure 5-7. SEM Photograph of Fine Crystalline Uraninite-Bearing Matrix Cementing Tuff Fragments Composed of Quartz (Q). The Uraninite (U) Within the Matrix Is Intimately Intergrown With Kaolinite (K). This Texture Has Been Referred to as "Granular" Uraninite (Pearcy, et al., 1994).

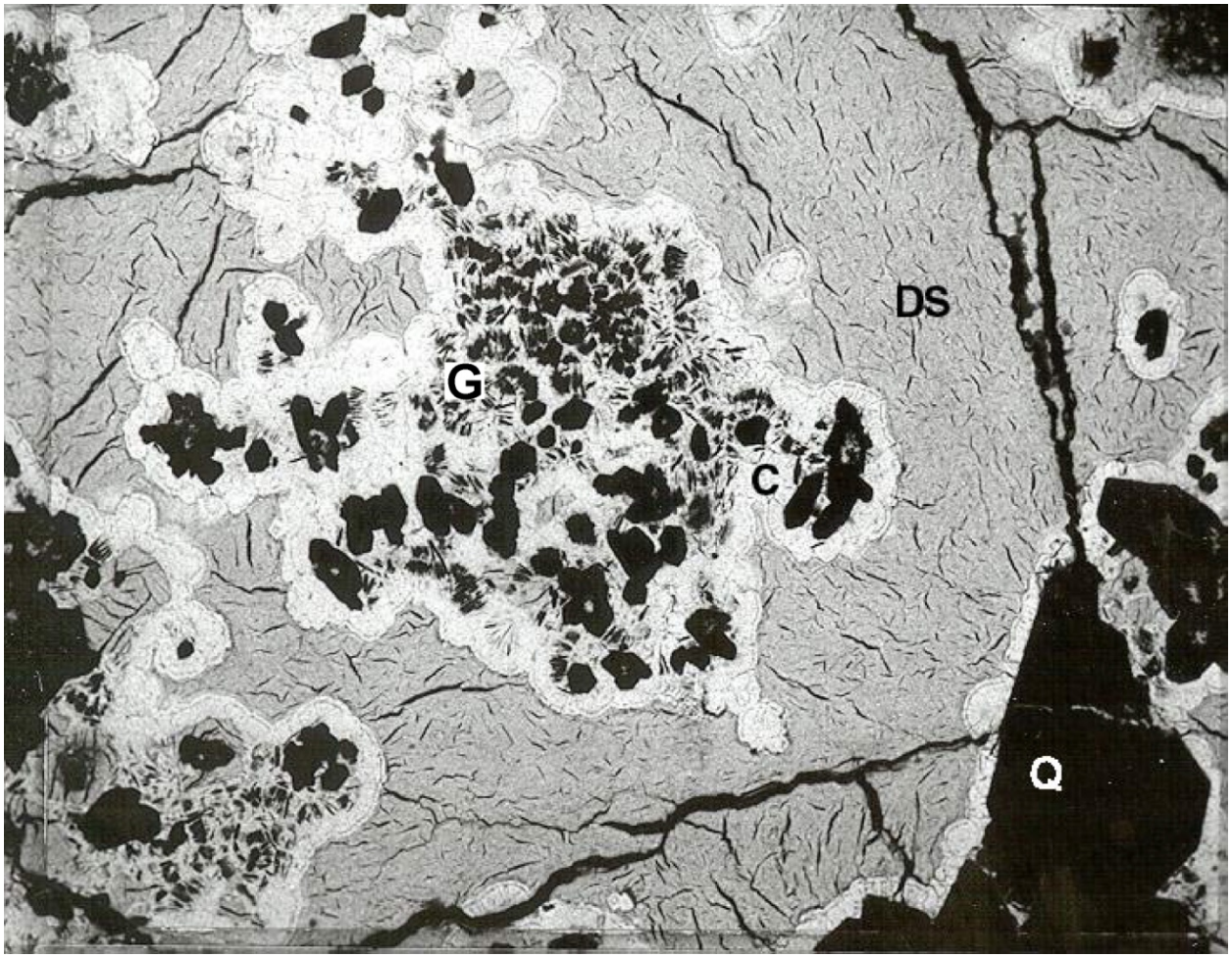

Figure 5-8. Backscattered Electron Photomicrograph of Uranium Phases Filling Open Space Within Brecciated Tuff. Granular Uraninite (G) Composed of Fine Crystalline Uraninite Intergrown With Kaolinite and Quartz Is Followed by Colloform Uraninite (C). The Colloform Uraninite Forms a Distinctive Rim, Which Signifies the End of the Primary Mineralizing Event. The Open Space Remaining After Uraninite Formation Is Filled By Dehydrated Schoepite (DS). Note the Euhedral Quartz Crystals (Q), Some With Double Terminations, Which Act as Substrates for Uraninite. Field of View is 0.4 mm [1.5×10^{-2} in] Across.

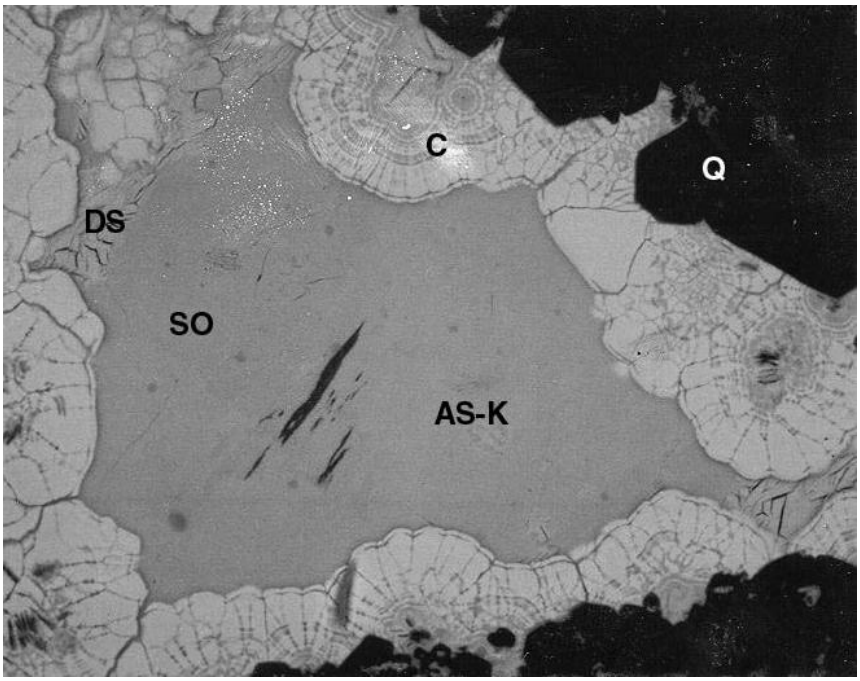

Figure 5-9. Backscattered Electron Photomicrograph of Colloform Uraninite (C) Lining a Fracture in Brecciated Tuff. Note the Radial and Concentric Microfractures Within the Colloform Uraninite Crystals. The Remaining Open Space Is Filled by Corroded, Dehydrated Schoepite (DS), Soddyite (SO), and an As- and K-Rich Uranyl Oxide Hydrate (AS-K). Field of View Is 0.1 mm [3.9 × 10^{-3} in] Across.

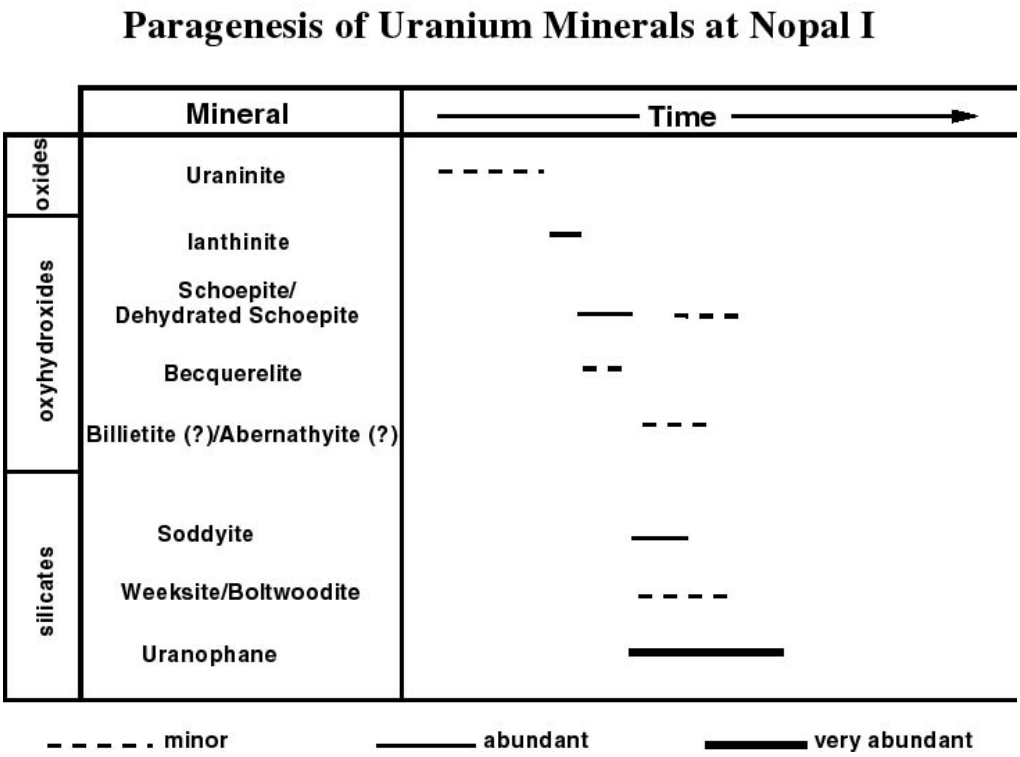

Figure 5-10. Relative Sequence of Formation and Abundance of Uranium Minerals at the Nopal I Deposit (From Pearcy, et al., 1994)

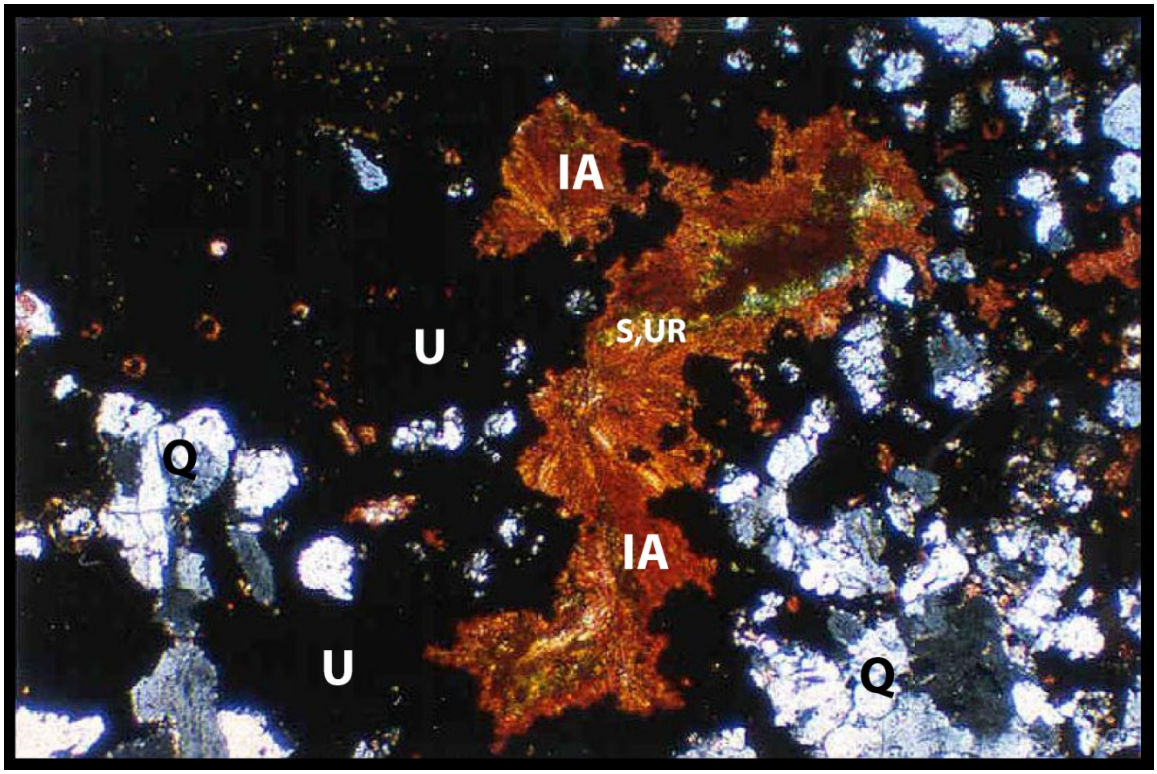

Figure 5-11. Transmitted Light Photomicrograph of Red-Colored Ianthinite (IA) Filling Open Space in Brecciated Tuff. The Ianthinite Is Being Replaced by Yellow-Colored Schoepite (S) and Uranophane (UR). The Black-Colored Material in the Photomicrograph Consists of Granular and Colloform Uraninite (U); the Brighter Colored White and Light Gray Material Is Quartz (Q). Field of View Is 0.8 mm [3.1 × 10^{-2} in] Across.

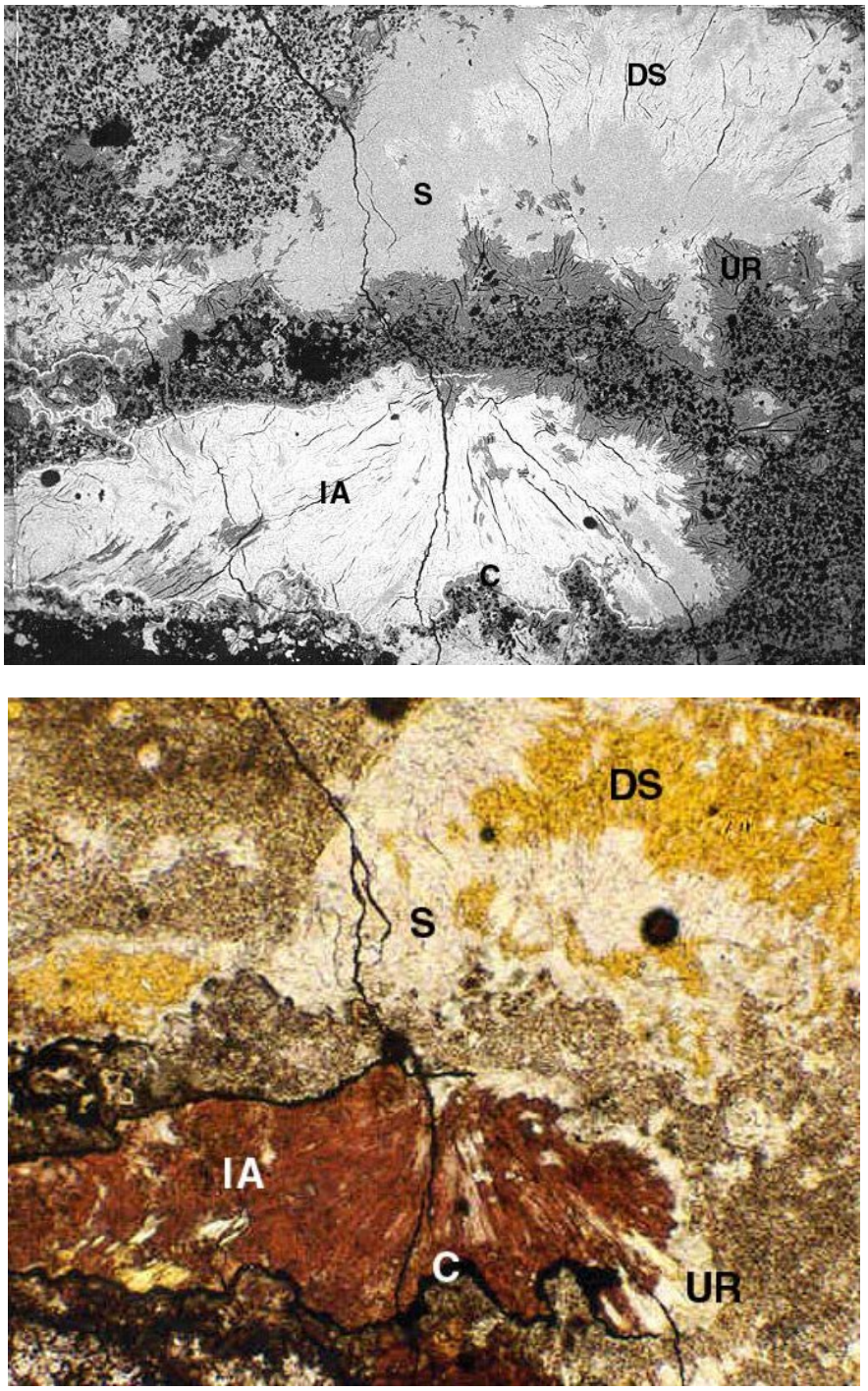

Figure 5-12. Backscattered Electron (Top Photo) and Corresponding Plane Light (Bottom Photo) Photomicrographs of Uranium Phases Filling Open Space in Brecciated Tuff. Open Space Is Filled by Ianthinite (IA) Followed by Schoepite (S) and Dehydrated Schoepite (DS). Uranophane (UR) Replaces the Uranyl Oxide Hydrates. Note the Thin Rim of Colloform Uraninite (C) Preserved Along the Margin of the Granular Material. Field of View Is 0.8 mm [3.1×10^{-2} in] Across.

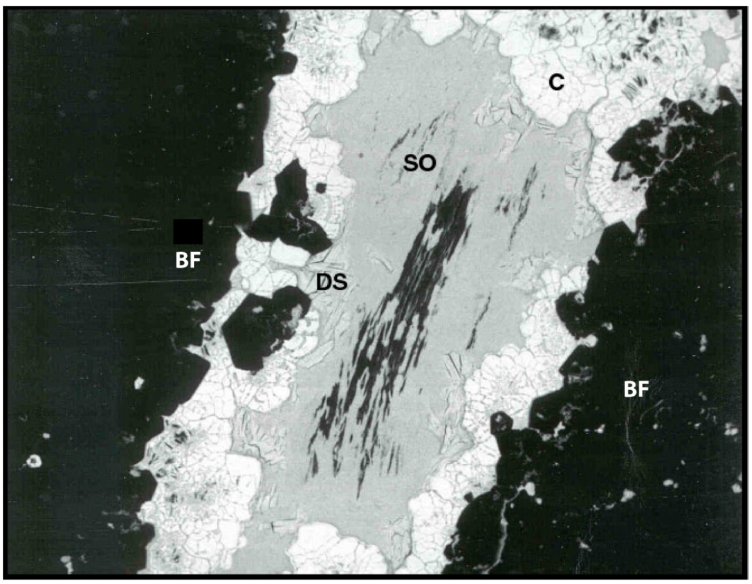

Figure 5-13. Backscattered Electron Photomicrograph of Colloform Uraninite (C) Lining Open Space Between Silicified Breccia Fragments (BF). The Remaining Open Space Is Filled by Dehydrated Schoepite (DS) Along the Margins, Which Has Been Replaced by Soddyite (SO). Field of View is 0.4 mm [1.5 × 10^{-2} in].

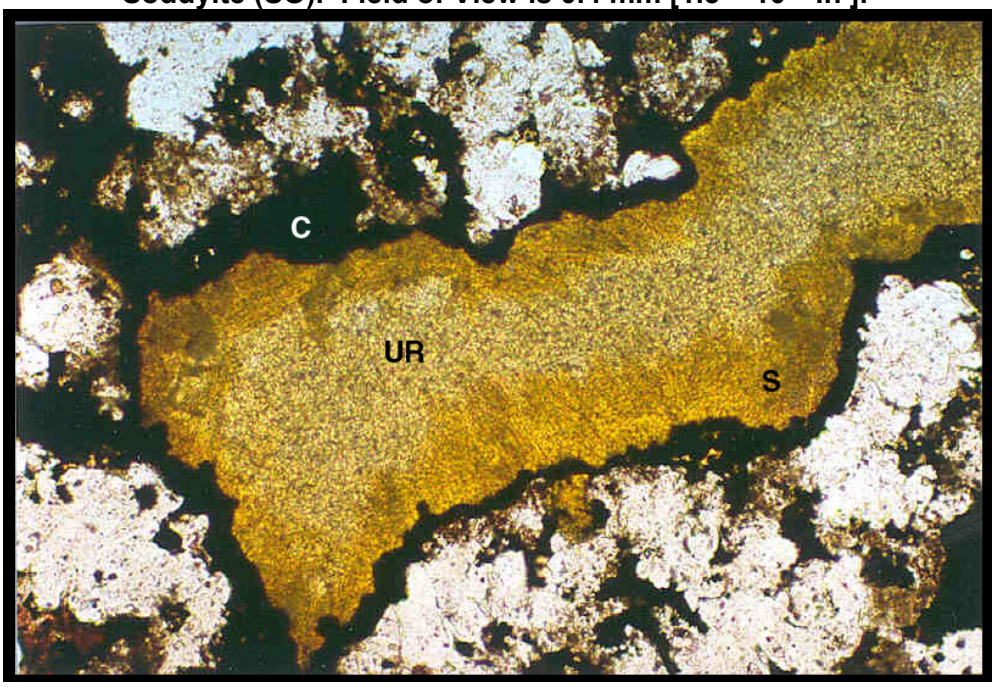

Figure 5-14. Transmitted Light Photomicrograph of Schoepite (S) and Uranophane (UR) Filling an Open Void. Schoepite Occurs at the Margin of the Void and Follows Colloform Uraninite (C), Which Lines the Void. Uranophane Occurs in the Middle of the Void and Replaces Schoepite. Field of View Is 0.8 mm [3.1 × 10^{-2} in] Across.

Figure 5-15. Scanning Electron Photomicrograph of Acicular Uranophane Crystals Within a Void at the Nopal I Deposit. Field of View Is 0.1 mm [3.9×10^{-3} in] Across.

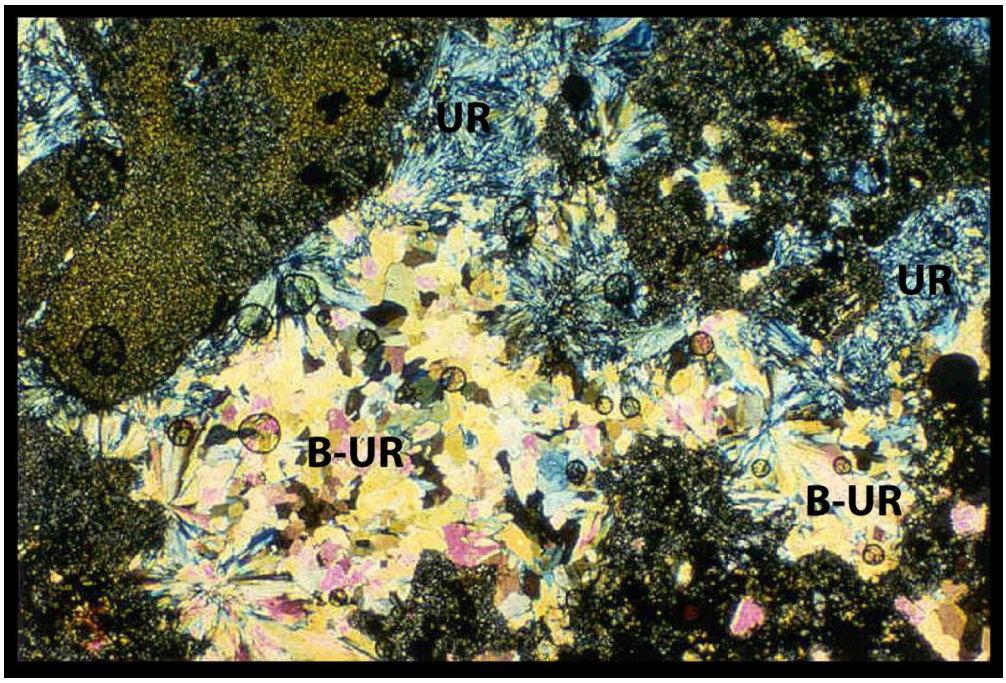

Figure 5-16. Transmitted Light Photomicrograph of Uranophane and Beta-Uranophane Filling Open Space in Brecciated Tuff. Beta-Uranophane (B-UR) Occurs as Equigranular, Yellow-Colored Crystals, Whereas Uranophane (UR) Is Composed of the Finer, Acicular, Blue-Green Crystals. Field of View Is 2.6 mm [0.1 in] Across.

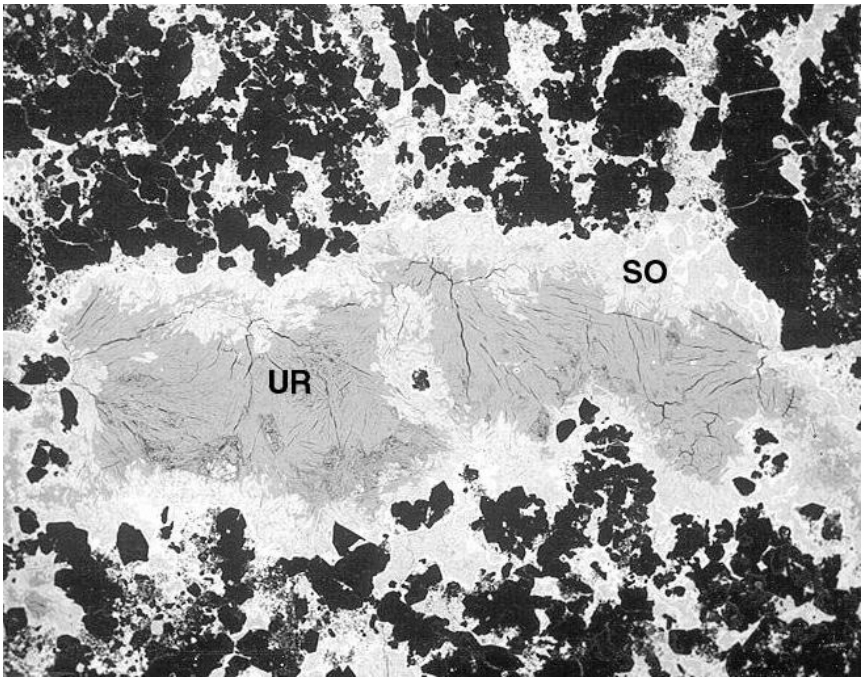

Figure 5-17. Backscattered Electron Photomicrograph of a Fracture Containing Predominantly Intergrown Soddyite (SO) and Uranophane (UR). Field of View Is 0.6 mm [2.3 × 10^{-2} in] Across.

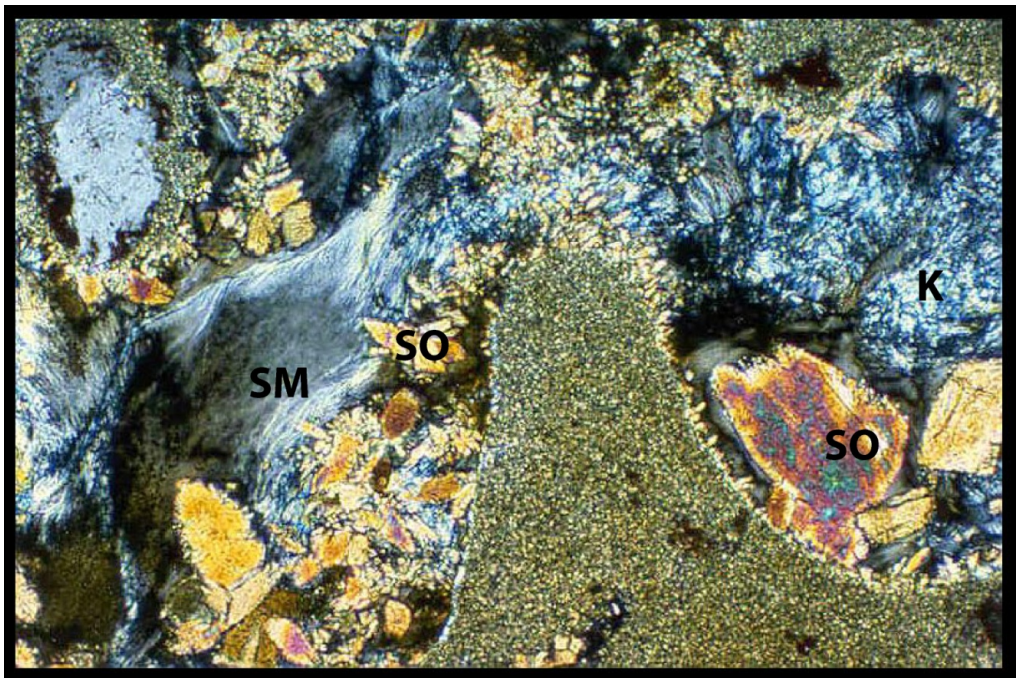

Figure 5-18. Transmitted Light Photomicrograph of Rhombic-Shaped Soddyite (SO) Crystals in a Fracture With Kaolinite (K) and Smectite (SM). Field of View Is

2.6 mm [0.1 in] Across.

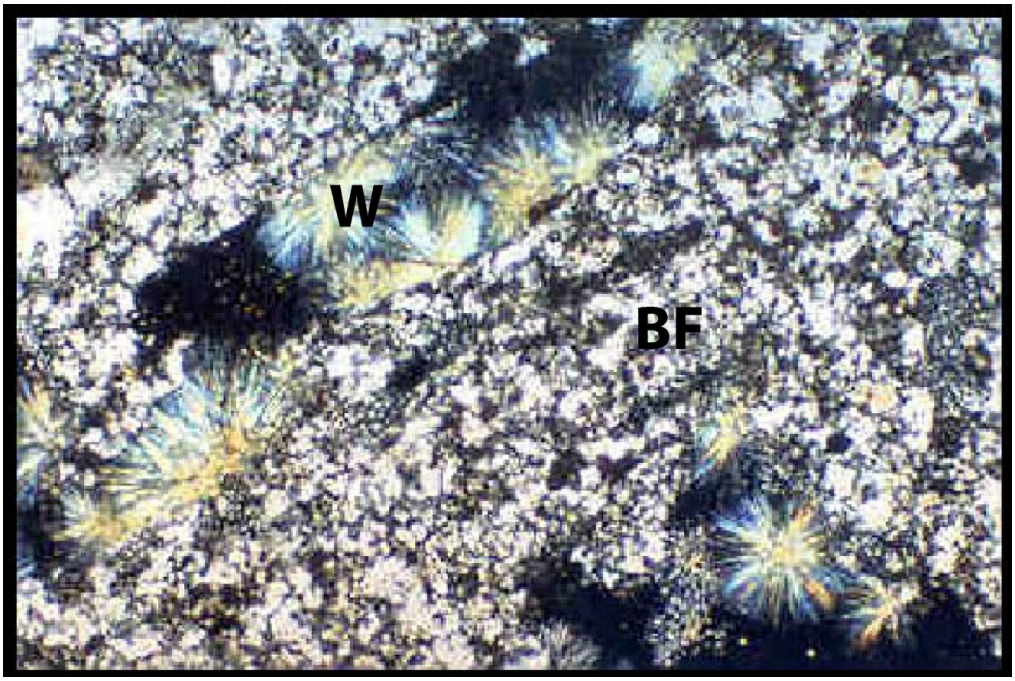

Figure 5-19. Transmitted Light Photomicrograph of Clusters of Acicular Weeksite (W) Crystals Within a Fracture in Brecciated Tuff (BF). Field of View Is 1.3 mm [5.1 × 10^{-2} in] Across.

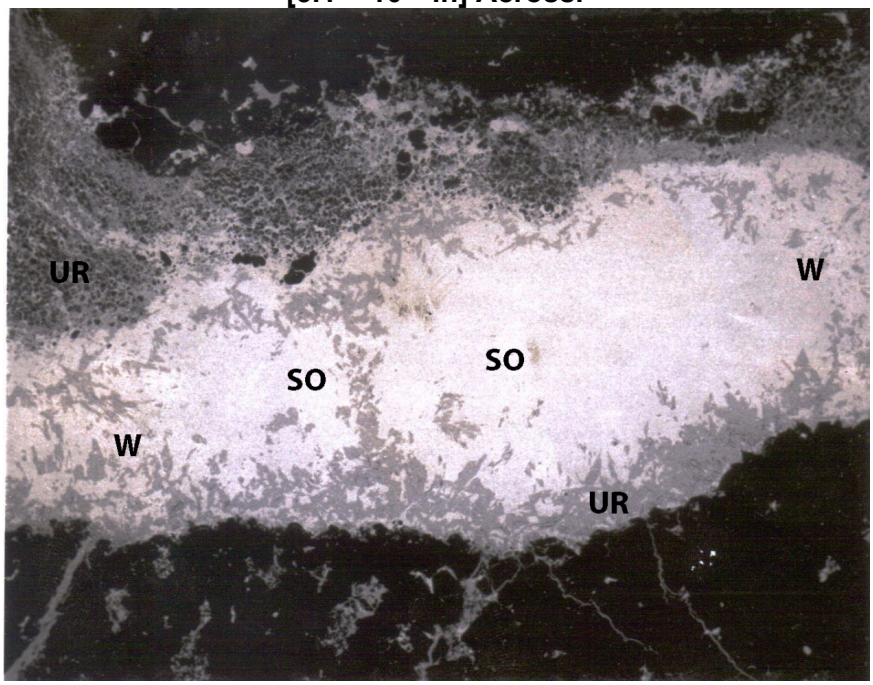

Figure 5-20. Backscattered Electron Photomicrograph of Intergrown Soddyite (SO), Uranophane (UR), and Weeksite (W) Filling a Fracture in Brecciated Tuff. At the Top Left, Original Granular Uraninite Has Been Replaced by Uranophane. Field of View Is 0.7 mm [2.7 × 10^{-2} in] Across.

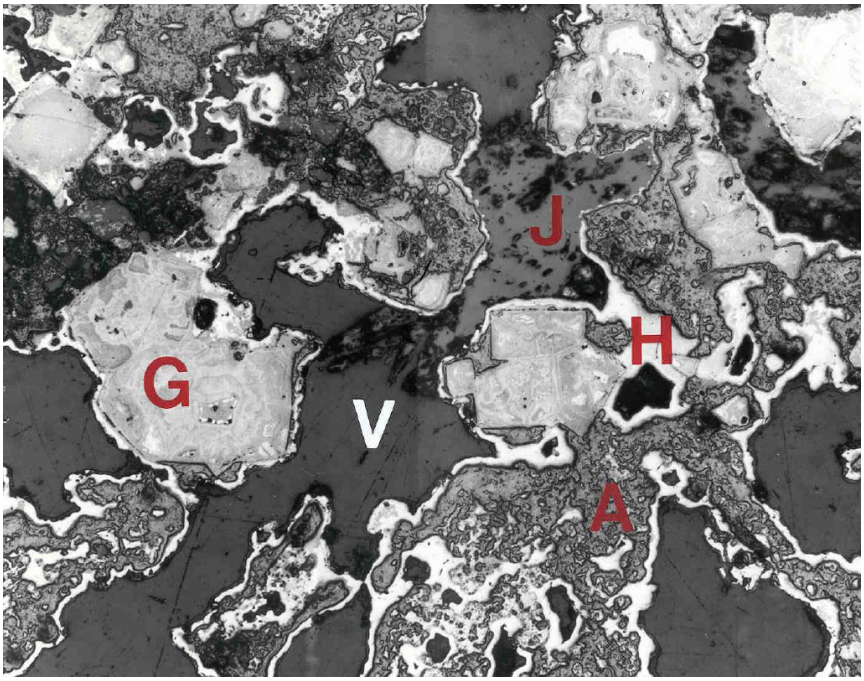

Figure 5-21. Reflected Light Photomicrograph of Iron Minerals Filling a Fracture at Nopal I. Hematite (H) Grows Into Open Space From Goethite (G) and Amorphous Iron-Oxyhydroxide (A) Substrates. Jarosite (J) Grows From Hematite Substrates Into Open Voids (V). Field of View Is 0.5 mm [1.9 × 10^{-2} in] Across.

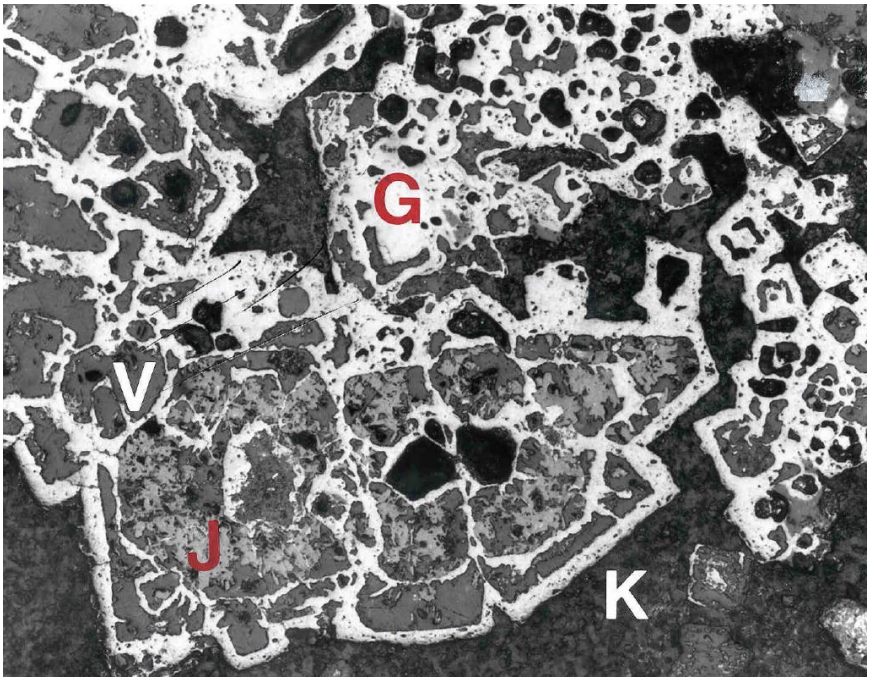

Figure 5-22. Reflected Light Photomicrograph of Iron Minerals Filling a Fracture at Nopal Showing Goethite (G) Partially Replacing Cubic Pyrite That Was Originally Intergrown With Kaolinite (K). Open Voids (V) Left by Pyrite Dissolution Are Partially Filled by

Jarosite (J). Field of View Is 0.5 mm [1.9 × 10^{-2} in] Across.

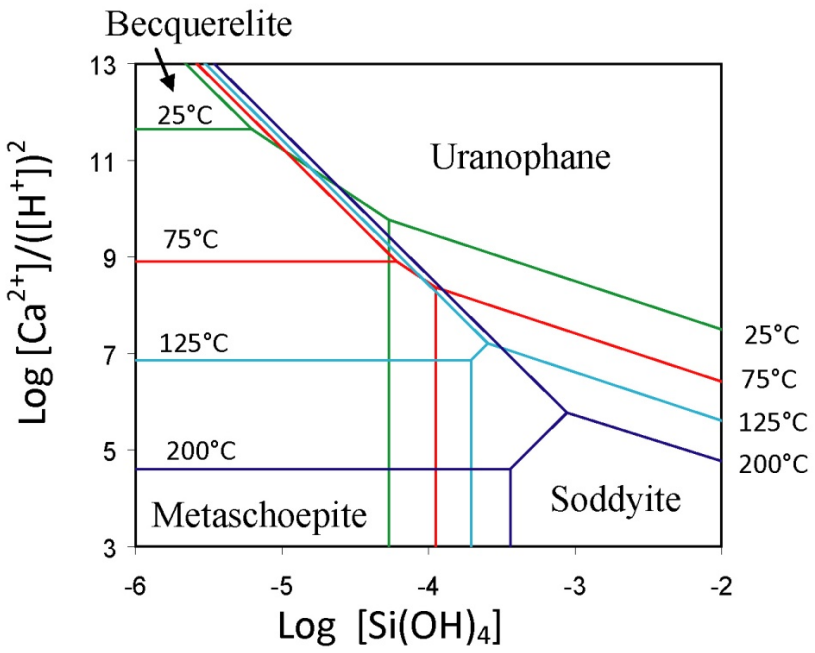

Figure 5-23. Fields of Uranyl Mineral Stability as a Function of Aqueous Solution Composition and Temperature (From Murphy, 2007)

6 RADIONUCLIDE MOBILITY

A major focus of Nopal I studies was to understand the timing, extent, and mechanisms of release of uranium and other radionuclides from the ore body and subsequent subsurface transport. The studies were conducted in the context of analogous transport conditions with respect to the proposed Yucca Mountain repository (unsaturated zone, arid climate, oxidizing geochemical setting, fractured tuff host rock, UO_2 source). Analyses included (i) *in-situ* gamma radiation mapping and alpha autoradiography measurements on hand samples; (ii) gamma spectrometry and alpha autoradiography on plant samples; (iii) bulk uranium analyses of ore, host tuff, and fracture-filling materials; (iv) bulk chemical analyses of ore, host tuff, and fracture-filling materials; (v) uranium-series data from unsaturated zone waters; (vi) uranium-series and uranium-lead isotopic measurements on ore, host tuff, and fracture-filling materials; and (vii) uranium-series and stable isotope measurements on fracture-filling carbonates and silicates.

6.1 Gamma and Alpha Radiation Measurements

At Nopal I, two types of radiation measurements have been used to map uranium transport at the field and micro scales. Contact gamma measurements—made *in situ* in the field on Nopal I Level +10—were used to map uranium concentrations and compare them with a detailed distribution of fractures (Leslie, et al., 1993; Pearcy, et al., 1995). These observations, combined with others, supported the conceptual model of fractures providing the most efficient pathways of uranium transport from the ore body.

Pearcy, et al. (1995) also reported alpha autoradiographic data on tuff matrix as a function of distance from uranium-enriched microfractures. The alpha intensity profiles were interpreted to represent diffusion of uranium through the tuff matrix. Transport through the matrix, however, was limited to distances less than 0.28 mm [0.011 in], even adjacent to uranium mineral-bearing fractures.

6.2 Vegetation Radiation

Plant specimens with high radiation levels, collected while growing on Nopal I ores that had been transported to a nearby site, were the subject of a study by Leslie, et al. (1999). The data indicated very high Ra-226 concentrations and suggested relatively high ore release rates for radium compared to uranium and thorium isotopes. Leslie, et al. (1999) reasoned that the data suggested that decay-series nuclides could be released at rates greater than would result simply from uranium mineral solubility and discussed implications for solubility-based waste form release models.

Leslie and Pickett (2000) further analyzed these concepts in a poster and concluded that apparent Ra-226 mobility and $^{226}Ra/^{230}Th$ disequilibrium in uranium ore at Nopal I points to the potential for preferential release of radionuclides from spent fuel relative to uranium. This notion is discussed more in Chapter 7 of this report.

6.3 Uranium Measurements in Tuff and Iron-Rich Fracture Filling

Leslie, et al. (1993), Pearcy, et al. (1995), and Prikryl, et al. (1997) published uranium measurements in rock samples from Nopal I (not including uranium minerals; see Chapter 5) . The uranium concentrations showed a well-defined boundary to the ore body, but also showed

elevated uranium outside the ore body in the tuff, consistent with transport facilitated by fractures and microfractures as revealed by the contact gamma data (Section 6.1). Data from a major fracture, characterized by iron oxyhydroxide fill and cross-cutting the ore body, shows uranium elevated relative to the adjacent tuff—consistent again with the importance of fractures in facilitating radionuclide transport. The data of Prikryl, et al. (1997) specifically showed uranium concentrations of several hundred to a few thousand parts per million (ppm) in the major fracture were associated with goethite, hematite, and amorphous iron oxyhydroxides in the fracture filling. In the fractures, goethite and hematite had uranium concentrations of 10^3 to 10^4 ppm. Although it was not clear whether the initial uranium deposition in the fracture was associated with the original pyrite-kaolinite hydrothermal assemblage, or whether uranium was deposited later when the present lower temperature minerals were formed, it is clear that the iron oxyhydroxide mineral species were effective at sequestering uranium.

6.4 Other Rock Chemistry Data Relevant to Ore Body Evolution and Radionuclide Mobility

Leslie and Pickett (2006) examined the implications of major and trace element chemical data on Nopal I rock samples for large-scale chemical alteration of and mobilization from the primary ore body. Of particular interest in the analog context are implications for uranium mineral evolution and radionuclide transport. The data and analyses supporting the meeting presentation slides are presented in more detail here.

6.4.1 Context of Analyses

The primary mineral assemblage of the uranium ore deposit consisted of uraninite, quartz, kaolinite, and pyrite, thought to have formed from hydrothermal reducing waters largely confined to a breccia pipe (Chapter 5). The ore body and adjacent tuff were subsequently altered to assemblages containing secondary uranium minerals, iron oxyhydroxides, iron oxides, alunite, and jarosite, with additional kaolinite generation. The combination of primary mineralization and subsequent element remobilization is evident in the uranium distribution pattern illustrated by the gamma intensity contours obtained on Level +10 of Nopal I (Figure 6-1). The objective of the Leslie and Pickett (2006) analysis was to gain further insights into these processes by applying other chemical and mineralogical data.

The gamma contours in Figure 6-1 (see also Section 6.1) illustrate not only the boundaries of the roughly cylindrical ore body, but also show a distinct low-uranium area in the center of the deposit where uranium minerals are also not visible (Leslie, et al., 1993; Pearcy, et al., 1995). Level +00, in contrast, is more homogeneous in uranium distribution. Also depicted in Figure 6-1 are the locations of three sampling traverses. Whole-rock tuff and ore samples were obtained from Traverses J and A, which are 20 and 2 m [66 and 6.6 ft] long, respectively. Sampling on the shorter Traverse A was on a finer scale—about every 20 cm [8 in]. Feature B is a major cross-cutting fracture, rich in iron oxyhydroxides, also discussed in Section 6.3. Fracture filling materials, rather than tuff, were sampled from B. The different sampling traverses provided contrasting information on fracture versus matrix behavior with respect to element mobility.

This study combined the contact gamma measurements with rock chemistry data and x-ray diffractometry (XRD) mineralogical analyses. Texas Tech University conducted whole rock chemical analyses, and all major and trace elements were determined by inductively coupled plasma mass spectrometry (ICP-MS), except (i) rubidium by flame atomic emission spectroscopy at Texas Tech, (ii) iron-oxide by titration at Texas Tech, and (iii) sulfur by x-ray

fluorescence at Southwest Research Institute® (Scientific Notebook 024; ML040490656). Uranium concentrations were measured by gamma spectrometry and have been reported in Leslie, et al. (1993) for Traverse J and Pearcy, et al. (1995) for Traverse A. Rare-earth elements (REE) were determined at the University of Texas at El Paso using the instrumental neutron activation analysis method (Scientific Notebook 084; ML040650390 and ML093270193). The XRD methods were described in Pearcy, et al. (1995).

6.4.2 Mineralogical Data

The XRD results reported here supplement and are consistent with those Pearcy, et al. (1995) reported. Figure 6-2 shows the two-theta angle distributions for five samples of fracture fill material at progressively greater distances from the edge of the uranium ore body. Prikryl, et al. (1997) reported that the primary fracture assemblage was pyrite and kaolinite, and that goethite, hematite, and jarosite resulted from pyrite oxidation. The relative proportions of the ferric minerals jarosite and goethite in the fracture change with increasing distance from the ore body. Jarosite decreases relative to goethite with distance, reflecting the decreasing influence of acidic fluids away from the ore body. Jarosite is a hydrous ferric sulfate indicative of acidic conditions on oxidation of primary pyrite during weathering (Pearcy, et al., 1995). Recall that the fracture fill is also uranium enriched (Section 6.3).

Figure 6-3 shows variation in the ratio of kaolinite to alkali feldspar in bulk tuff samples on Traverse J (i.e., not fracture fillings). The ore body is located at positions on the X axis of 12 m [39 ft] and greater. Kaolinite is highly, but variably, enriched relative to feldspar in the ore body. The kaolinite/feldspar ratio rapidly decreases as the edge of the ore body (denoted as the most westward occurrence of uranophane) is approached from the east and a relatively constant ratio of 0.5 is achieved within 2 m [6.6 ft]. Because kaolinite is a secondary clay mineral, the kaolinite/feldspar ratio is good indicator of bulk tuff alteration, though the variation within the ore body probably reflects overprinting by the secondary acid alteration.

The occurrences of uranophane, hematite, and alunite in the ore body show the results of bulk alteration, as opposed to that confined to the fracture. The primary iron mineral pyrite is no longer present. Hematite is the dominant iron phase, reflecting mobilization of iron out of the ore body interior during the secondary, acidic, oxidizing event. Likewise, no uranium minerals survive in the interior. Alunite—a hydrous potassium aluminum sulfate—reflects the extensive acid alteration of the interior. The influence of the secondary acidic event drops off rapidly in the bulk samples. It is seen outside of the ore body only along the confined fracture pathway, as illustrated by the jarosite occurrences in Figure 6-2.

Therefore, the evidence for precipitation of the reduced uraninite and pyrite assemblage and its subsequent oxidation is spatially limited.

6.4.3 Chemical Data

Major and trace element data from matrix tuff Traverses A and J are reported in Tables 6-1 through 6-4, and REE concentrations for selected Level +10 samples are in Table 6-5.

The Traverse A plot of Figure 6-4 shows that uranium decreases sharply over this 2-m [6.6-ft] distance. Zinc and iron both show concentration peaks outside the area of strong uranium enrichment. The two highest iron samples were those that had observed hematite from XRD analyses. It is likely that the elevated iron results point to the presence of small fractures, because iron is much better expressed in fractures than is uranium.

Larger scale elemental patterns can be seen in Traverse J (Figure 6-5). Uranium is enriched relative to tuff throughout the ore body {which is to the east of approximately the 12-m [39-ft] mark on the X axis}, but is strongly enriched in the outer “ring” of the ore body first identified on the basis of gamma contact data (Leslie, et al., 1993; Pearcy, et al., 1995). The remobilization of uranium to the “ring” is best explained as resulting from the acid oxidizing event suggested by the mineralogical data (Section 6.4.2), likely coinciding with the earliest formation of uranyl minerals (Pearcy, et al., 1994). Iron and zinc show similar behavior. The iron-enriched zone coincides with hematite occurrence (Figure 6-3), which has replaced primary pyrite. Though data are sparse, sulfur may be highest in the center of the ore body, where alunite was deposited by acid fluids resulting from pyrite oxidation (Figure 6-3).

Traverse J tuff trace elements (Figure 6-6) show a great deal of variability of nearly all the elements within the ore body, perhaps owing to its complex geochemical history. Those elements clearly enriched in the ore body relative to the host tuff include barium, strontium, vanadium, copper, and nickel. Rubidium is depleted throughout the deposit. Those, like uranium, showing depletion in the center of the ore body versus the margin include yttrium and copper.

Traverse J major elements (Figure 6-7) show that, consistent with rubidium (Figure 6-6), the alkali elements sodium and potassium are depleted throughout the ore body relative to the host tuff, suggesting this may be a feature of the primary hydrothermal mineralization event. There is a suggestion of calcium depletion from the center of the ore body. The highest calcium peak is in the region of abundant uranophane, which contains calcium. The high volatile content (loss on ignition, or LOI) in the center of the ore body is consistent with the abundance of the hydrous sulfate alunite, but may also partly reflect the abundant kaolinite that accompanied primary uranium mineralization.

REE are of interest because of their well-known systematic behavior, but also because they may serve as analogs of the actinides present in spent nuclear fuel. Five samples from within and near the ore body were selected for REE analyses (Table 6-5). The concentrations were chondrite-normalized using the scheme of Nakamura (1974), with the resulting patterns shown in Figure 6-8. The relatively unaltered Nopal tuff concentrations are consistent with published data by George-Aniel, et al. (1991). The sample from 2 m [6.6 ft] from the ore body is nearly identical to the unaltered tuff, reflecting the general immobility of REE in the matrix rock. There is no evidence of REE enrichment associated with original mineralization, except perhaps in the heavy REE in the uranium-rich sample. The acid-altered sample from the ore body interior has the most distinctive pattern, with the highest degree of depletion in the middle REE. This is consistent with the model of dissolution and mobilization out of the center of the ore body by acid sulfate waters. Depletion of REE is seen for altered silicic rocks that were subject to acidic-sulfate conditions (Fulginati, et al., 1999). The REE depletion in the “acid-altered” sample, then, reflects the complementary residue after partial depletion of REE, with the middle REE preferentially removed. It is possible that the light REE-depleted fracture filling could reflect the influence of the mobilized, middle REE-enriched water on initially REE-poor material.

6.4.4 Summary

While the interpretations of the combined mineralogical, major element, and trace element data are nonunique, they are consistent with published uranium mineralogical and uranium distribution observations from Nopal I. As a result of acid alteration of the uranium ore deposit, which originally contained the reduced mineral assemblage UO_2+pyrite+quartz+kaolinite, differential elemental mobility and enrichment patterns are recorded in tuff matrix and fracture

minerals. For instance, the distance traveled by mineralizing fluids was limited in the tuff matrix and was much greater in discrete mesofractures. Alkali metals were depleted throughout the ore body. Transition metals, uranium, and sulfur tended to be enriched throughout the deposit. There is limited evidence for coprecipitation of the actinide-analog REE in U(VI) minerals (i.e., uranium-rich samples are not particularly REE-rich), but the REE do show depletion (like uranium) in the acid-altered ore body interior.

6.5 Groundwater Radionuclide Data

Pickett and Murphy (1999) reported chemical and uranium-series data on three types of waters collected at and near Nopal I: seepage water in the Level +00 adit, perched water collected from a borehole in Level +10, and groundwater from a well 1.3 km [0.8 mi] southeast of the ore body. Geochemical modeling, also described in Chapter 3, suggested that the unsaturated zone waters (adit and perched) have chemical characteristics consistent with oxidizing waters that could have reacted with uraninite to form early schoepite (although the current uranium contents are not consistent with schoepite solubility control). Uranium-series isotopic systematics implied a greater degree of reaction with uranium-rich materials in the perched waters than in the seepage waters, consistent with the shorter duration of water–rock interaction in the seepage waters. The carbonate aquifer groundwater had no apparent connection to the Nopal I unsaturated zone waters.

6.6 Uranium-Series Systematics in Ore Body, Host Tuff, and Fracture-Filling Minerals

We detail here the results of an unpublished, NRC-approved report.[3] Uranium-series disequilibrium systematics have the potential to reveal much about radionuclide transport processes in natural systems. Presented here are data on uranium-series radionuclides in tuff and fracture infilling minerals within and surrounding the Nopal I deposit, with interpretations pertinent to the timing and nature of actinide transport. Included are analyses of bulk rocks and of products of sequential extraction of fracture infilling materials. The data reveal a complex, episodic, multistage history of uranium mobility.

The first published uranium-series isotopic data from Nopal I (Pearcy, et al., 1995) were $^{234}U/^{238}U$ activity ratios on bulk tuff samples on the 2-m [6.6-ft]-long Traverse A across the edge of the ore body (Figure 6-1). (Unless otherwise noted, uranium-series radionuclide ratios in this report are presented as activity ratios.) The ratios were interpreted to indicate open-system uranium behavior outside the ore body within the past 1 million years (Ma), with limited depletion of the uranium-rich ore body. Prikryl, et al. (1997) then reported a more extensive set of $^{234}U/^{238}U$ and $^{230}Th/^{234}U$ ratios from samples of iron-rich fracture filling materials from Traverse B (Figure 6-1), which includes rocks from inside and outside the area of visible uranium mineralization. Both activity ratios exceeded 1 in the fractures, which requires recent (<1 Ma), multistage history of aqueous uranium deposition and remobilization. A pattern of decreasing

---

[3]Pickett, D., J. Prikryl, W. Murphy, and E. Pearcy. "Uranium-Series Disequilibrium Investigation of Radionuclide Mobility at the Nopal I Uranium Deposit." Prepared for and approved by the U.S. Nuclear Regulatory Commission. Unpublished report (1996).

$^{234}U/^{238}U$ with distance from the ore body was observed, but a definitive explanation for the pattern was not possible.

Pickett and Murphy (1997) summarized uranium-series data from a larger number of tuff sample traverses on Level +10. The uranium-series data plotted in Pickett and Murphy (1997) are the same as those presented here in detail. However, this report includes a new evaluation of the $^{230}Th/^{234}U$ ratios previously reported.

6.6.1 Setting and Samples

The map of the site (Figure 6-9) shows two horizontal levels, separated vertically by 10 m [33 ft], exposed during exploratory mining at Nopal I. Samples were collected from Levels +00 and +10 along the eight horizontal traverses shown on the map. The uranium ore body is defined as the zone where uranium minerals are visible in the field. The uranium mineral suite is dominated by secondary uranyl [U(VI)] phases, such as uranophane, soddyite, and schoepite, with minor amounts of primary uraninite (Pearcy, et al., 1994). A chemical uranium-lead age of 8 ± 5 Ma was determined for uraninite (Pearcy, et al., 1994) and U/Pb isotopic data suggest an age of around 3 Ma for uranophane, which is the dominant uranium mineral in the ore body (Pickett and Murphy, 1997). The deposit is hosted by heavily fractured, silicic tuffs of the Tertiary Nopal and Coloradas Formations. Mineralogic descriptions and uranium-series data from fracture traverse B are detailed by Prikryl, et al. (1995) and summarized in Prikryl, et al. (1997).

Traverses B and E sampled infilling materials along major fracture sets (termed mesofractures to distinguish them from microfractures distributed throughout the tuff); the other traverses sampled bulk rocks, which may have included uranium minerals in samples from inside the ore boundary. Fracture samples are dominated by goethite, amorphous iron-oxyhydroxides, hematite, jarosite, kaolinite, and quartz (Prikryl, et al., 1995, 1997). Petrographic evidence suggests that goethite generally predates the other observed iron minerals and formed from oxidation of pyrite, which is now absent. Next in the iron mineral paragenetic sequence was amorphous iron-oxyhydroxides, followed by hematite and, finally, jarosite (Prikryl, et al., 1997). Kaolinite was an early-formed alteration mineral, generally predating the iron minerals, and quartz represents fragments of the host tuff. The fractures both inside and outside the ore body contain no detectable uranium minerals, observed down to the nanometer scale by transmission electron microscopy (TEM). Bulk rock samples from traverses other than B and E consist of generally fractured, extensively to mildly altered silicic tuff with an alteration assemblage dominated by kaolinite and iron oxides.

6.6.2 Methods

Samples were analyzed for decay-series radionuclides by either alpha or gamma spectrometry. Bulk rocks and fracture-infilling minerals were powdered in a SPEX 8000 Mixer/Mill using a tungsten carbide vial. For samples from traverses A through E, U-238, U-234, Th-232, and Th-230 were measured by isotope dilution/alpha spectrometry using the following procedure: (i) spiking with a U-232 + Th-228 solution, (ii) acid digestion (CEM MDS-2000 microwave system with Teflon PFA vessels), (iii) iron hydroxide coprecipitation, (iv) ion-exchange column separation and purification (BIORAD AG 1-x8 anion exchange resin), (v) deposition on membrane filters, (vi) alpha counting, and (vii) data reduction and analysis. Alpha spectra were measured on an EG&G ORTEC system that included model 676A and 576A spectrometers with ion-implanted silicon charged particle detectors, model 920-16 and 920-8 multichannel buffers,

ALPHAMAT (Version 1.00) analysis software for acquisition control, and MAESTRO II (Version 1.40) multichannel analyzer emulation software for analysis of spectral data.

Uranium-series activity ratios for a group of pitchblende (UO_2) and monazite [(Ce, La, Nd, Th)PO_4] ore standards are shown in Table 6-6. All of these standards are known to be in secular equilibrium and, therefore, should yield a value of 1 for all the tabulated ratios. For all measurements except DP2DM1, the $^{234}U/^{238}U$ ratio is within 5 percent of 1. The counting statistics error for DP2DM1 is 9 percent. We therefore consider 5 percent to be a reasonable value for the uncertainty in the $^{234}U/^{238}U$ measurement, unless the counting error is larger. For $^{230}Th/^{234}U$ and $^{230}Th/^{238}U$, the measurements are always within 10 percent of 1; we therefore consider 10 percent to be a reasonable value for the uncertainty in these ratios. Note that these standards measurements were made after the bulk of the isotopic measurements were made on the unknown samples.

In traverses F through H, uranium was determined by gamma spectrometry with a germanium detector system (Pearcy, et al., 1995) utilizing gamma emission lines for (i) Th-234 for samples with >1,000 ppm uranium or (ii) Bi-214 and Pb-214 in lower uranium samples. Due to the likelihood that uranium-series disequilibrium in most samples could introduce large errors when using daughter nuclides for U-238 determination, the uranium concentration data from traverses F, G, and H must be considered semiquantitative and interpretable only in terms of patterns and differences at the order-of-magnitude scale.

Because bulk rock samples reveal little about the relative mobility and physical siting of elements in the rock, a sequential, selective extraction procedure was applied to ~ 2.5 g [0.088 oz] aliquots of six samples of infilling material from the B fracture traverse. The reagents used in each extraction step and the phases separated are listed in Table 6-7. This procedure was based on work by Yanase, et al. (1991), Ivanovich, et al. (1994), and Suksi, et al. (1994) in other analog studies and with reference to more general studies (Martin, et al., 1987; Tessier, et al., 1979). After each extraction step, the remaining residue was separated from the leachate by centrifugation, washed with 0.05 M ammonia, dried, and weighed. The final resistate (RES) was analyzed for uranium and thorium using the alpha spectrometry procedure described in this section. The leachates were spiked with a U-232 + Th-228 solution. An aliquot of the ion exchangeable (IE) fraction was analyzed for uranium and thorium using steps (iii) through (vii) of the previous procedure. Aliquots of the adsorbed (AD), amorphous iron-oxyhydroxide (AM), and crystalline iron-oxide (CR) fractions were evaporated to dryness, refluxed in 50:50 (volume ratio) HNO_3 + $HClO_4$, again evaporated to dryness, dissolved in 4 M HCl, and analyzed using steps (iii) through (vii) of the previous procedure. Because the behavior of thorium during these extraction steps can be difficult to control (e.g., Martin, et al., 1987), the thorium data should be interpreted with caution.

6.6.3 Results

6.6.3.1 Bulk Rocks

Bulk rock alpha spectrometry results are shown in Table 6-8. Uranium concentrations from rock samples along the seven traverses that trend radially from, and in most cases cross, the ore body boundary are depicted in Figure 6-10, with alpha and gamma spectrometry data presented in separate plots. The most striking feature of the traverses is the typically dramatic, but smoothly varying, decrease in uranium away from the ore body. This is suggestive of transport of uranium up to tens of meters away from the ore body, though at varying rates and/or magnitudes. For most traverses, uranium contents do not reach background levels appropriate

for the host tuff (generally 8–23 ppm; Leslie, et al., 1993) at distances less than about 20 m [66 ft] from the ore body; traverse H is the exception. Thorium contents do not generally show a pattern with distance. Some elevated values from near the ore body (traverses C, B, and E; Table 6-8) suggest limited local mobility of thorium, though on a much smaller scale than uranium. Otherwise, thorium is limited to the range 15–47 ppm, which is similar to the previously reported range for Nopal I host tuff (Leslie, et al., 1993).

Variations in uranium-series nuclide activity ratios along the traverses are shown in Figure 6-11. The two bulk rock traverses (A and C) show near-equilibrium (i.e., ±10 percent) $^{234}U/^{238}U$ within the deposit and up to 50 percent disequilibrium outside with no spatial pattern. (Note that the limited lengths of A and C preclude full evaluation of possible spatial trends in activity ratios.) The two fracture-related traverses (B and E) show a systematic decrease away from the ore body, with a large digression to high $^{234}U/^{238}U$ at 9 to 11 m [30 to 36 ft] distance in traverse E. In traverse D, which is located 10 m [33 ft] from the ore body boundary and aligned roughly parallel to it (Figure 6-9), $^{234}U/^{238}U$ varies from 1.0 to 1.5. This shows that wide variation is possible for a given distance from the deposit and suggests that spatial trends are by no means monotonic or tightly constrained. For $^{230}Th/^{234}U$, both types of traverses (bulk rock and fracture) generally show ratios of about 1 to 1.5 near the boundary, with all but one traverse showing no spatial pattern. Fault-related traverse E does show a distinct trend toward higher $^{230}Th/^{234}U$ with distance from the ore body. Observation of uranium-series disequilibrium in these rocks implies open-system mobility of uranium within the past approximately 1 Ma.

Powder splits on 10 samples that were measured by alpha spectrometry at the Center for Nuclear Waste Regulatory Analyses (CNWRA®) were also measured by the more precise thermal ionization mass spectrometric method at Los Alamos National Laboratory (CRWMS M&O, 2000). Within uncertainty, all but one of the samples measured at Los Alamos plotted outside the “forbidden zone” (Section 6.6.4.2), and the one exception was not far inside the zone. The Los Alamos investigators concluded that, with few exceptions, the data could be explained by single-stage uranium-thorium processes that have been dormant for around 300,000 years. The differences from CNWRA results were largely due to the CNWRA $^{230}Th/^{234}U$ ratios being significantly higher. For example, for sample NOPI-404, we measured $^{230}Th/^{234}U$ of 1.44 (Table 6-8), while the Los Alamos group reported 1.06. If our $^{230}Th/^{234}U$ ratios were too high, the multistage interpretation may not be supported by the data. The biggest discrepancies were seen in lower-uranium samples. The alpha spectrometric and mass spectrometric $^{230}Th/^{234}U$ values for NOPI-410, for example, were 2.13 (Table 6-8) and 1.03, respectively, in a fracture fill sample with only 11 ppm uranium. We were otherwise unable to find any potential systematic errors to explain why we might have measured erroneously high Th-230. As noted in Section 6.6.2, our standards measurements of $^{230}Th/^{234}U$ were within 10 percent of equilibrium, but those measurements were conducted later than the data in Table 6-8.

Because (i) we cannot explain the differences in the two sets of measurements, (ii) we cannot unequivocally rely on our standards measurements, and (iii) there is no reason to question the Los Alamos data, this report will deemphasize the previous interpretations based on CNWRA Th-230 measurements. We consider our $^{234}U/^{238}U$ ratios to be reliable within 5 percent, unless the counting error is larger.

6.6.3.2 Sequential Extraction of Fracture Infilling

Uranium contents in the sequential extraction fractions from traverse B (Table 6-9) are represented in Figure 6-12 according to the amount of uranium per gram of sample. The

crystalline oxides (CR; i.e., goethite and hematite) are the dominant uranium-bearing fracture phases, accounting for 60–74 percent of sample uranium. This is consistent with high concentrations in goethite and hematite observed by electron microprobe (Prikryl, et al., 1997). The AD (adsorbed) and AM (amorphous iron-oxyhydroxide) fractions each contain 10–20 percent of the uranium; RES (resistate) has 1–10 percent and IE (ion exchangeable) has very small proportions (one at 1.9 percent, others <0.3 percent). Uranium concentrations calculated using mass changes between extraction steps are very high in AM (3,000 to 30,000 ppm) and CR (600 to 9,000 ppm). RES shows a broad range of 26 to 1,600 ppm, demonstrating that host tuff fragments along the fracture are also enriched in uranium; in RES, uranium is likely concentrated in secondary phases such as kaolinite. While uranium contents tend to decrease with distance from the ore body (Figure 6-12), the proportions of uranium among the fractions change little; that is, all fractions mimic the observed bulk rock uranium trend [traverse B in Figure 6-10(a)].

Spatial trends of $^{234}U/^{238}U$ (Figure 6-13) reveal the contrasting, highly variable activity ratios observed in the fractions. $^{234}U/^{238}U$ is less than unity in AD, AM, and IE proximal to the ore body, but U-234 is enriched (as in most bulk rocks) in CR, RES, and distal IE. These observations suggest that all fracture-infilling phases and sites have been involved in recent open-system uranium mobility and imply distinct differences in histories. Because CR dominates the uranium budget, its activity ratios are reflected most in bulk rock analyses, masking the true complexity of the history of uranium transport behavior. For most fractions, trends with distance from the ore body are subtle or absent. A strong trend is seen in IE (increasing $^{234}U/^{238}U$), while weak trends are observed in AD (increasing $^{234}U/^{238}U$) and CR (decreasing $^{234}U/^{238}U$).

6.6.4 Discussion

6.6.4.1 Bulk Rock Uranium Contents

The differences in uranium gradients among different traverses (Figure 6-10) have implications for the nature of radionuclide mobility in fractured tuffaceous rock. Mesofracture-related traverses B and E, for example, have higher uranium concentrations for a given distance outside the ore body than all other traverses. This is consistent with previous conclusions (Pearcy, et al., 1995) that mesofractures provided the dominant advective pathways for uranium transport at Nopal I.

Among the traverses located in generally fractured tuff, a correlation is suggested between the intensity of uranium transport and the relative fracture density. In Figure 6-10(b), uranium concentrations are progressively higher from H to G to F; inspection of the fracture density contour map of Nopal I (Pearcy, 1994, Figure 4-4 based on Pearcy, et al., 1995, Figure 3) reveals that traverse F is located in the most fractured portion of Level +00 {~20 fractures per m^2 [~2 per ft^2]}, while H is in the least fractured portion {~10 fractures per m^2 [~1 per ft^2]}. Contours of apparent uranium concentration in the contact gamma intensity map (Pearcy, et al., 1995) are consistent with this trend on Level +00. Alternatively, the H to F progression could be related to the more downslope position of F in the premining topography (see elevation contours in Figure 6-9); that is, transport of uranium from the deposit by infiltrating groundwater could have been more effective in the downslope direction (Pearcy, et al., 1995). A rough correspondence among uranium contents, contact gamma intensity, and fracture density is suggested by comparing traverses A and C (east and north, respectively, of the deposit) on Level +10, but quantitative correlations on both levels have proven elusive. If a correspondence among fracturing and uranium transport is present, it confirms the intuitive expectation that,

while uranium transport was more limited in generally fractured tuff than in mesofractures, more intensely fractured tuff provided more pathways for uranium transport than less fractured tuff.

Previous microprobe data (Prikryl, et al., 1997) and the sequential extraction data reported here from the traverse B mesofracture imply that uranium transport was retarded by sorption and/or coprecipitation of aqueous uranium during mineral growth within fractures, particularly of iron-oxides and iron-oxyhydroxides. No such direct data exist from the bulk rock traverses, but the interpreted association of uranium content with fracture density suggests a similar mechanism.

The uranium transport at Nopal I, while evidently limited to only a few tens of meters in horizontal extent, nevertheless is consistent with the high uranium mobility expected in an oxidizing environment such as Nopal I relative to a reducing environment (Osmond and Cowart, 1992). Evidence for long-term dominance of oxidizing conditions at Nopal I includes the presence of uranyl minerals (for perhaps as long as 3 Ma), near-surface deposits (caliche and opal) dating back at least 54 ka, and present-day hydrochemical conditions (Pearcy, et al., 1994; Pickett, et al., 1996). It is likely that the horizontal component of transport vastly underrepresents the true extent of transport, considering that the major vector of hydrochemical transport in the unsaturated zone is vertical due to downward percolation and fracture flow of meteoric waters. The empirical relationship between transport and fracturing at Nopal I shows that hydraulic conductivity was the overriding factor in determining extent of radionuclide migration. A major portion of uranium migration occurred during growth (or at the least, concomitant dissolution-reprecipitation) of ferric mineral phases in fractures. The lack of significant thorium mobility over this period is consistent with its low solubility in groundwaters. The suggestion of finite, though limited, thorium mobility in fracture traverses B and E may be related to earlier stages of mineralogic development when more acidic conditions may have prevailed (Prikryl, et al., 1997).

6.6.4.2 Bulk Rock Uranium-Series Activities

The uranium-series activity data demonstrate that geochemical processes affecting uranium mobility at Nopal I were active at least as recently as the last few hundred thousand years. $^{234}U/^{238}U$ ratios in the traverses are generally ≥1 outside of the ore body, consistent with recent uptake of uranium from U-234 enriched groundwater (Figure 6-11a). In the bulk rock traverses (A and C), samples from inside the ore deposit are near $^{234}U/^{238}U$ equilibrium because their uranium budget is likely dominated by older uranium minerals. The combined ^{230}Th-^{234}U-^{238}U systematics measured by mass spectrometry (CRWMS M&O, 2000) suggest that uranium and thorium have, in most cases, behaved as a closed system for the past 300,000 years. CRWMS M&O (2000) does report an age of 88,000 years on a sample from Transect F; our alpha spectrometric ratios on the same sample (not reported here) were the same within uncertainty.

A uranium-series evolution model based on CNWRA alpha spectrometry measurements of bulk rocks was originally published by Pickett and Murphy (1997) and is illustrated in Figure 6-14, which includes data from traverse D. The $^{234}U/^{238}U$ versus $^{230}Th/^{238}U$ plot (Osmond, et al., 1983; Thiel, et al., 1983) is useful for interpreting uranium-series activity data from rocks affected by aqueous uranium mobilization. Trajectories of uranium addition are to the left, with a possible upward component if U-234 is relatively enriched, while uranium removal moves a rock to the right, with a possible downward component if U-234 is preferentially leached. The “forbidden” or “multiple event” zone refers to areas of the plot inaccessible by single events, whether sudden, continuous, or steady state (Ivanovich, et al., 1992; Osmond and Ivanovich, 1992; Scott, et al.,

1992). Most of the studied bulk rocks plot in this zone, apparently requiring a multistage history. In the model, a host rock begins at or near secular equilibrium and aqueous uranium, which is enriched in U-234 due to recoil processes, is added. (As a result of alpha recoil, a decaying U-238 atom in a rock may be displaced when an alpha particle is emitted, causing either direct ejection of the daughter Th-234 into water or lattice damage that makes the Th-234 and its daughters, such as U-234, more susceptible to mobilization in water. Both processes lead to enrichment of U-234 relative to U-238 in water.) An aqueous $^{234}U/^{238}U$ ratio of 2 is used for illustrative purposes (Figure 6-14), but any value that is at least twice as enriched in U-234 as the present rock would be appropriate (this factor accounts for subsequent decay of around half of the excess U-234 during Th-230 ingrowth). This ten- to one thousandfold uranium enrichment drives $^{230}Th/^{238}U$ toward near-zero values. The observation that only a few rocks still have $^{230}Th/^{238}U$ <1 implies that a subsequent period of hundreds of thousands of years is required for Th-230 ingrowth toward secular equilibrium with U-234 (samples with $^{234}U/^{238}U = 1$ may have evolved long enough to have reached equilibrium). If uranium addition is a more continuous process, the times required may exceed those depicted on the time curve (Figure 6-14). Reaching the "forbidden" zone in this model requires a third stage—uranium removal. As discussed in Section 6.6.3.1, however, we are no longer confident in our interpretations based on the apparent presence of samples in the "forbidden zone" because the $^{230}Th/^{238}U$ ratios are questionable.

Three samples from traverse E have markedly higher $^{234}U/^{238}U$ than the rest of the samples [Figure 6-11(a)]. These three (NOPI-399, NOPI-400, and NOPI-401 in Table 6-8) are all from one short segment of the traverse E fault at 9 to 11 m [30 to 36 ft] from the ore body, where uranium concentrations decrease significantly [Figure 6-10(a)]. The most plausible explanation for these anomalous samples is that the groundwater that was the original source of transported uranium in this portion of the fault may have had unusually high $^{234}U/^{238}U$ (significantly >2.5). A correspondence between low uranium and high $^{234}U/^{238}U$ in transported uranium is common (Osmond and Cowart, 1992; Osmond and Ivanovich, 1992) and reflects the tendency for the alpha recoil uranium component to be relatively emphasized when bulk uranium is less mobile.

The few samples with $^{234}U/^{238}U$ clearly below 1 (NOPI-374, -380, -382, and -407 in Table 6-8) must have been subject to some degree of uranium removal. The fact that they are also still uranium-rich suggests that these rocks have indeed seen a multistage history.

The spatial trends in $^{234}U/^{238}U$ [Figure 6-11(a)] shed further light on the apparent complexity of uranium mobilization processes at Nopal I. The decrease in $^{234}U/^{238}U$ away from the ore body in traverse B can be attributed to multistage uranium deposition along the fracture or to a higher frequency of depositional episodes in the portions of the fracture closest to the ore deposit (Prikryl, et al., 1997). That is, more frequent uranium enrichment closer to the ore body would yield a lower average age for the uranium, consistent with $^{234}U/^{238}U$ closer to 1. A similar trend in $^{234}U/^{238}U$ is observed in traverse E, except for the aforementioned anomaly at 9 to 11 m [30 to 36 ft] from the ore body; this trend may more accurately be characterized as a restriction to near-equilibrium values beyond 14 m [46 ft] from the ore body. The near-equilibrium $^{234}U/^{238}U$ in the distal samples is clearly a result of long time duration since initial enrichment.

An event of possible significance in the late-stage history occurred at 54 ka; that age has been determined from ^{230}Th-^{234}U-^{238}U analyses of uranium-rich opal (Section 6.7.4.3) and caliche (Pearcy, et al., 1994) from on and adjacent to the ore deposit. While the nature of the event is unknown, it was clearly marked by significant water movement and uranium mobilization in a weathering environment. Because the initial uranium enrichment in the studied rocks from outside the ore deposit is constrained by uranium-series activity ratios to have occurred at least

a few hundred thousand years ago, the 54-ka event may represent uranium removal from the altered tuffs and fracture assemblages.

6.6.4.3 Sequential Extraction Uranium-Series Activities

Each of the sequential extraction fractions has rather distinctive uranium and $^{234}U/^{238}U$ characteristics (Table 6-9; Figures 6-12 and 6-13), demonstrating that they have had distinct uranium mobilization histories. Th-230 behavior is not addressed in this section, due to uncertainties in the measurement of this nuclide and its behavior during the leaching process (Sections 6.6.2 and 6.6.3.1).

IE. This represents a very low proportion of the rock uranium budget (Figure 6-12). There does appear to be a real pattern of increasing $^{234}U/^{238}U$ with distance from the ore deposit (Figure 6-13). This trend may reflect the changing influence along the fracture of two sources of exchangeable uranium: U-234 depleted from AD and AM (see next) and U-234 enriched from present groundwater. Lower uranium contents in AD and AM further from the deposit are consistent with a decreasing contribution to IE from the low-U-234 component.

AD. The less-than-unity $^{234}U/^{238}U$ ratios in the adsorbed uranium preclude groundwater as the dominant uranium source. Note the similar $^{234}U/^{238}U$ ratios in AD and AM in Figure 6-13. These similarities and the lack of another potential uranium source with $^{234}U/^{238}U$ <1 suggest that AM was the source of adsorbed uranium in the fracture rocks; note that this is the uranium as now present in AM, not that which was removed earlier to yield $^{234}U/^{238}U$ <1 (see next). Figure 6-13 suggests a trend to higher $^{234}U/^{238}U$ in AD away from the deposit; as in the case of IE, this may reflect the increasing influence of groundwater uranium with $^{234}U/^{238}U$ >1. One feature unexplained by this model is the lower $^{234}U/^{238}U$ in AD compared to AM in four of the six samples. Preferential desorption of U-234 from AD sorption sites seems an unlikely explanation because the AD fraction is unlikely to have remained a closed system long enough for alpha recoil to effect uranium isotopic fractionation.

AM. This fraction, which contains an appreciable proportion (10–18 percent) of the uranium budgets of samples, is also marked by $^{234}U/^{238}U$ <1, in contrast to bulk rock ratios (Figure 6-13). These ratios most likely reflect partial loss of uranium from previously uranium-enriched AM. The lower $^{234}U/^{238}U$ in AM compared to crystalline iron oxides (Figures 6-13) may also be related to higher leachability of noncrystalline compared to crystalline iron minerals. The amorphous iron phases, therefore, appear to have acted most recently as sources of mobile uranium.

CR. Because CR accounts for 59 to 74 percent of the traverse B mesofracture rock uranium budgets (Figure 6-12), CR activity ratios are similar to bulk rock values discussed previously. The bulk rock uranium mobility history discussed previously, then, is appropriate for fracture-filling goethite and hematite. The weak trend in CR of decreasing $^{234}U/^{238}U$ with distance (Figure 6-13) may, like the bulk rock trend in traverse B, be related to the episodic nature of uranium enrichment along the fracture.

RES. RES $^{234}U/^{238}U$ ratios are mostly lower than those in CR, but still greater than 1 (Figure 6-13), suggesting a similar but—on average—older uranium mobilization history for clays and/or other minerals associated with the host tuff. One anomalous RES sample that defies simple explanation is noted, with higher $^{234}U/^{238}U$ than all other fractions (Figure 6-13) and all measured traverse B bulk rocks (Figure 6-11a).

In summary, the CR and RES $^{234}U/^{238}U$ ratios are interpreted to have evolved from the history for bulk rocks discussed previously. Uranium enrichment in these phases is interpreted to have occurred within the last few hundred thousand years, followed—possibly, but not necessarily—by a more recent uranium removal.

The AM have also clearly seen a uranium enrichment event, given their high uranium contents (Table 6-9), but their consistently less-than-one $^{234}U/^{238}U$ ratios indicate that they have most recently been subjected to uranium removal. It is not surprising that an amorphous phase with high surface area would be more leachable than crystalline iron phases. Recent uranium loss from AM is consistent with the uranium mobility apparent in the 54-ka uranium-rich opal and caliche. If uranium loss is not actually linked to a single such event, at the least the 54-ka event may be representative of the uranium-removal environment.

6.6.5 Summary

The uncertainty in the reliability of the alpha spectrometric $^{230}Th/^{234}U$ data decreases our confidence in the pervasiveness of multistage uranium mobilization behavior at Nopal I as depicted in Figure 6-14. The mass spectrometric data (CRWMS M&O, 2000) allow for a history characterized more by relatively closed uranium-thorium behavior for about 300,000 years subsequent to major uranium enrichment. Nevertheless, enough evidence exists (e.g., some much younger uranium-rich fracture fillings and $^{234}U/^{238}U < 1$ in amorphous iron phases) that more recent behavior has been characterized by uranium mobility.

If more recent behavior in the iron-rich fractures around the ore body is indeed characterized by uranium removal, the shift from uranium accumulation may be related to the cessation of growth of the secondary fracture assemblage, which had provided for uranium accumulation by coprecipitation. Alternatively, this shift could be related to changes in the flow regime, which effectively diminished the role of the ore deposit as a source of transported uranium.

U/Pb data suggest an age of about 3 Ma for uranophane, which is a product of oxidation of primary, reduced uraninite at Nopal I (Pickett and Murphy, 1997). Earlier work (Prikryl, et al., 1997) suggests that this oxidation event may coincide with the initial growth of iron-oxides and iron-oxyhydroxides in fractures, which formed as a consequence of pyrite oxidation (see also Section 6.4). This seemingly conflicts with the conclusion of this section that uranium-rich crystalline iron-oxides are no more than a few hundred thousand years old. However, simulations of uranium-series evolution in water–rock systems (Scott, et al., 1992) show that time scales may be considerably longer if decay toward secular equilibrium is accompanied by continued uranium enrichment. Therefore, initial growth of the fracture assemblages could have been as old as 3 Ma, but subsequent open-system behavior during continuing uranium enrichment (perhaps including dissolution-recrystallization, reaction of amorphous phases to crystalline oxides, and episodic uranium removal) helped preserve the disequilibrium reflected in $^{234}U/^{238}U$ ratios greater than one in CR+RES. These views on the history of uranium mobilization at Nopal I informed a summary conference paper by Pickett and Murphy (2001).

6.7 Uranium-Series and Stable Isotope Data for Carbonate and Silicate Fracture Deposits at Nopal I

Some fractures in and around the Nopal I ore body contain uranium-rich calcite, caliche, and opal. CNWRA studied these materials as tracers of radionuclide mobility. Analyses included uranium-series radionuclide isotopes for age information and stable oxygen and carbon isotopes for implications for conditions of deposition. The results of this study were presented at

conferences (Pickett, et al., 2000, 2001; Pickett and Leslie, 2005) but were not published as a report or paper.

6.7.1 Introduction

Previous studies of tuffs and iron-oxyhydroxide-rich fracture fills from the vicinity of the Nopal I ore body (Sections 6.1, 6.3, and 6.6) show that uranium has been mobilized out of the ore body, preferentially along fractures in the tuff, and partially redeposited with the iron-oxyhydroxide fracture fills. Evidence on remobilization of uranium from the fracture fills in the last few hundred thousand years has been ambiguous because of differing analytical results (Section 6.6.3.1).

Episodes of significant uranium mobility in the recent past are strongly indicated by uranium-rich fracture-filling caliches and opals with a previously reported age of 54 ka (Pearcy, et al., 1994). The purpose of the study presented in this section is to review uranium concentrations, uranium-series disequilibrium ages, and stable isotope data in such materials from within a few tens of meters [about 100 ft] of the Nopal I ore body that will shed light on the timing and conditions of uranium mobilization. Any clustering of ages could provide evidence of episodes of release rates more rapid than indicated by long-term averages.

6.7.2 Setting and Samples

The primary ore mineral at Nopal I was uraninite, only a few remnants of which remain (Pearcy, et al., 1994). The primary mineralization age is constrained by a chemical U/Pb age of 8±5 Ma (Pearcy, et al., 1994). (While subsequent uranium mineral ages have been reported in DOE-sponsored studies, discussion of these results is beyond the scope of the present report, and they do not affect the interpretations.) The uraninite was subsequently oxidatively altered to a series of uranyl phases; previous U/Pb dates on late-stage uranophane, the most abundant uranyl mineral, suggest a minimum oxidation age of around 3 Ma (Pickett and Murphy, 1997).

Uranium-series analyses of host tuff and fracture filling materials indicate that uranium has been mobile within the past few hundred thousand years (Section 6.6). CNWRA analyses suggested that uranium had subsequently been partially remobilized from these secondary deposits in more recent times. However, analyses at Los Alamos National Laboratory indicate that, for the most part, uranium has been immobile at the site for the last 300,000 years. A counter-argument to this conclusion lies in the previously reported ages on uranium-rich caliches and opals of 54 ka. These secondary carbonate and silicate fracture-filling deposits are remnants of episodes of significant deposition of uranium outside the ore body. The purpose of the work reported here is to (i) document the extent to which uranium has been mobilized during deposition of these materials, (ii) describe ^{230}Th-^{234}U-^{238}U dates on these materials, and (iii) use stable isotope data to constrain the conditions of deposition.

Three types of samples were studied: crystalline calcite, fracture-filling caliche, and opal coatings. Sample locations are shown in Figure 6-15. The calcites, which both fill tuff fractures and coat free surfaces with euhedral crystal forms, up to more than 1 cm [0.4 in] across, range from clear and colorless to opaque and dark reddish brown (Figure 6-16). Some calcite masses grade from clear to gray within the same crystalline structure. Caliches (Figure 6-17) were sampled from tuff fracture faces from outcrops exposed by mine and road excavations, occurring from just below to 2 m [6.6 ft] below the preexcavation surface (Figure 6-18). The caliches occur in layers typically ranging from 1 to 10 mm [0.04 to 0.4 in] thick occurring in masses that may be as much as 15 cm [6 in] thick. The caliche layers range in color from

nearly pure white to grayish beige, and in fine-grained texture from friable to hard. X-ray diffraction analyses of the caliches reveal them to consist of calcite, with (typically) lesser amounts of quartz and sanidine. Opal occurs as a coating on tuff or tuff breccia in limited portions of the Nopal I exposure (Figure 6-19). In some occurrences, the opal occurs with uranophane. The opal is found in different textural relationships, both coating earlier uranophane and being overlain by uranophane needles (Figure 6-20). The outer surface of the opal typically has a botryoidal character (Figure 6-19). In the absence of uranophane, the opal ranges in color from nearly transparent with a faint greenish tint to milky white. When associated with uranophane, the color may also grade to deep yellow, suggestive of incorporation of microcrystals of a uranyl phase.

6.7.3 Methods

Samples of calcite and caliche were crushed in an agate or stainless steel mortar and pestle and sieved to produce grain-size fractions of >250 µm, 125–250 µm, 63–125 µm, and <63 µm [>0.0098 in, 0.0049–0.0098 in, 0.0025–0.0049 in, and <0.0025 in]. The two largest size fractions were subsequently further crushed in the agate mortar and pestle to reduce grain size for ease of further preparation. Aliquots of selected subsamples were dried overnight in glass beakers at 100 °C [212 °F]. The dried aliquots were then placed in porcelain crucibles and fired in a muffle furnace at 900 °C [1,652 °F] for 4 hours. The mass change from firing was assumed to result from CO_2 release and was used to estimate the carbonate content of the rock. Samples of opals and, in one case, uranophane were obtained from sample surfaces and cleaned in deionized water; they were not subjected to further sample preparation.

Uranium and thorium isotopic data were measured by Larry Mack at the Department of Geological Sciences, University of Texas at Austin, using thermal ionization mass spectrometric procedures, with concentrations obtained by isotope dilution. Initially, total rock dissolutions were performed on calcites and caliches (using typical procedures that include hydrofluoric acid to afford complete dissolution of any silicates) and uranium and thorium concentrations were measured as a scoping test. Uranium and thorium concentrations and U/Th ratios were reproducible on blind replicates to within 6 percent.

Later, uranium and thorium isotopic data were obtained on some of these total-rock dissolutions and on leachates of the same selected samples. The leachates were prepared from selected fired caliche and calcite samples using 0.1 M HNO_3. Bischoff and Fitzpatrick (1991) suggested using this approach if a significant spread in U/Th ratios is not obtained from total-dissolution subsamples prepared (e.g., by grain-size discrimination as was used in this study). All opal and uranophane uranium-thorium analyses were performed on total dissolutions. Uranium-series evolution plots used in this section were prepared using K. Ludwig's Isoplot add-in for Microsoft® Excel®.

For calcites and caliches, oxygen and carbon isotope ratios were measured on (i) orthophosphoric acid leachates and (ii) residues at the Department of Geological Sciences, Southern Methodist University.

6.7.4 Results

6.7.4.1 Uranium and Thorium Concentration Data for Calcites and Caliches

Table 6-10 shows uranium and thorium concentrations of calcite and caliche samples. Table 6-10 also provides an estimate of the percentage of noncarbonate in each sample (determined

from the difference between total sample mass and the estimated mass of carbonate determined from the CO_2 release). Most clear calcite samples have a low noncarbonate component, as expected. Gray calcites can have appreciable noncarbonate. Most caliches have more than 10 percent noncarbonate. The x-ray diffraction data suggest that this is mostly quartz and sandine, though amorphous silica cannot be ruled out. (We will use the general term "silicate" for this noncarbonate component.) One rock (NOPI-458) that had a field appearance consistent with caliche in fact is nearly entirely quartz; we will discuss it in the context of the caliches because of its similar field appearance.

Two features of the uranium-thorium concentration data are notable. First, although the calcites have lower uranium than the caliches, most of the samples have relatively high uranium for authigenic carbonate-rich rocks (which typically have less than 10 ppm uranium; Reeder, et al., 2001). This is perhaps not surprising in this environment, but it does provide more evidence for significant uranium transport along fractures around Nopal I. Distribution of uranium concentrations around the Nopal I ore body is shown in Figure 6-15. In addition, the authigenic nature of these rocks is reflected in the typically low Th/U ratios.

Second, pairs of powders representing different grain-size fractions from the same hand sample showed little variation in uranium and thorium concentrations and Th/U ratios. The grain-size fractions were prepared to attempt to obtain splits with different amounts of carbonate and silicate components. In most cases of "dirty calcites," the carbonate component is authigenic with a low Th/U, while the silicate component is an old detrital contaminant with higher Th/U that needs to be corrected to obtain meaningful uranium-series ages. In the samples in Table 6-10, this objective was not met. This is illustrated in Figure 6-21, in which these grain-size pairs are connected by lines; if the line is not visible, the points are very close together. The similarities in uranium-thorium characteristics mean that these grain-size fraction pairs are unsuitable for total-dissolution isochron uranium-series dating (e.g., Bischoff and Fitzpatrick, 1991).

These results raised questions about the disposition of uranium in these carbonate-rich rocks. A series of leaching tests were conducted on nonfired splits of some of the samples; results are not detailed here because they merely served to guide subsequent analyses. Sample powders were reacted with 1 M HNO_3 until they no longer effervesced, and uranium and thorium were measured in the leachates by ICP-MS at Southwest Research Institute. The leached masses of the two elements were compared to what should be in the sample based on previous concentration analyses. The tests showed that uranium and thorium were present in both soluble (carbonate) and insoluble (silicate) components in substantial amounts. The leachates contained 12 to 100 percent of the uranium and 4 to 67 percent of the thorium. These results suggest that both the carbonate and silicate components of the calcites and caliches are authigenic.

The leach test also provided a second estimate of the mass fraction of noncarbonate component (calculated from the mass remaining after leaching) to compare with the previous estimates based on mass loss on firing. Among the 19 samples analyzed this way, the two estimates were within 8 percent—typically better than 4 percent. This result lends confidence to the use of fired samples in analyses involving leaching. The percentage of noncarbonates based on leaching was typically a few percent higher than that based on firing. This is not surprising, because firing would lead to H_2O loss in addition to CO_2 loss, whereas leaching would not affect hydrous components.

6.7.4.2 Uranium-Series Isotopic Results for Calcites and Caliches

Uranium-series isotopic data for total dissolutions and leachates on selected calcite and caliche samples are presented in Table 6-11. Note that NOPI-305-L1 and NOPI-305-L2 are adjacent caliche layers from the same hand sample; two grain-size fractions were measured from the latter. Because the concentration data showed that the calcite and caliche grain-size fractions were not suitable for total-dissolution ^{230}Th-^{234}U-^{238}U isochron dating (Section 6.7.4.3), uranium and thorium isotopes were measured on leachates from selected samples, prepared by reacting with 0.1 M HNO_3.

Table 6-12 shows the estimated weight percent carbonate in these selected samples based on the mass change during 0.1 M HNO_3 leaching, corrected for the loss of mass during firing of the original samples. The leachate uranium "concentrations" in Table 6-11 (which were based on total sample mass) were corrected to estimated carbonate concentrations (Table 6-12) using the weight percent carbonate. Using this value and the corresponding total rock uranium concentration, the uranium concentration in the silicate fraction may be estimated. These calculations are inexact, involving assumptions about sample behavior during firing. Nevertheless, based on reasonable comparisons between firing and leaching estimates of carbonate content (Section 6.7.4.1), the estimates are not likely to be grossly in error. What the results of Table 6-12 show is that both carbonate and silicate fractions of these rocks can contain comparable concentrations of uranium. The insoluble silicate-rich fractions in the calcites and caliches do not appear to consist of host tuff, which is not particularly rich in uranium. This result is consistent with the earlier leaching tests summarized in Section 6.7.4.1. The one exception—N99-11 with much lower carbonate uranium—is also the only calcite sample in the table. Uranium contents tend to be low in measured calcites (Table 6-10 and Figure 6-21).

All total-dissolution Th-230 dates are shown in Table 6-11 and on a map of Nopal I in Figure 6-22. We first discuss Th-230 dates on the five samples for which leachates were not obtained (N99-1, -4, -5, -16, and -35). These rocks either give dates of 370 ka or greater (N99-4 and N99-16) or have activity ratios near secular equilibrium that cannot yield a single-stage age. The former two do not provide age information different from that obtained from iron-rich fracture fills (Section 6.6), and the latter three will be discussed again along with opal and uranophane data. (One of these, N99–35 is the "caliche" that, in fact, consists almost entirely of quartz.) All measured calcites but one fall in these categories, indicating that calcites are in general older than caliches.

The remaining samples—1 calcite and 7 caliches—give total-dissolution and leachate ages ranging from 17 to 213 ka (Table 6-11). An attempt was made to calculate total dissolution–leachate isochron dates using the pair of data points from each sample, in the absence (Section 6.7.4.1) of good spreads in Th/U in total dissolution splits (Bischoff and Fitzpatrick, 1991; Luo and Ku, 1991; Kaufman, 1993). Examples of such plots are shown in Figure 6-23. The N99-28 total dissolution–leachate pair in the figure yields an apparently reasonable age, but the N99-32 pair does not. Another sample not shown—N99-11—yields a negative isochron age, and it must be concluded that we have little information about its age. There is only one pair of coexisting total dissolution powders for which isotopic data were obtained: N99–29 and N99–30, which are two grain-size fractions from the same sample powder. Although the isochron age (Figure 6-23 bottom) is apparently reasonable, it includes only two points.

The variable behavior of the isochrons probably reflects the breakdown of the inherent assumptions in this type of analysis in an environment that may contain more than one uranium-rich authigenic component. For example, initial uranium and thorium isotopic characteristics may not have been uniform within a sample. There may also have been some redistribution of uranium and thorium between leachate and solid, which is a typical problem in this type of analysis. The isochrons do not, therefore, provide reliable age information.

The total dissolution–leachate pairs are plotted in the uranium-series evolution plot of Figure 6-24. With one exception (the one calcite), the leachate date is within 11 percent of the total dissolution date (see also Table 6-11). The calcite N99-11, which plots on the right side of Figure 6-24a, does not provide any reliable age information. For all samples, the leachate activity ratios are not consistently higher or lower than total dissolution ratios, consistent with the observations of variable isochron behavior in the previous paragraphs. We believe this reflects the fact that both carbonate and silicate fractions are authigenic and uranium-rich. The relatively small difference between total rock and leachate dates most likely results from a continuum of ages within the sampled caliche layers and between the carbonate and silicate authigenic fractions. It does not appear, however, that the dates reflect an average age over very long time scales of deposition. If that were the case, it would be surprising that the leachate-total dissolution pairs would yield dates within 11 percent. It is notable that, for the two size fractions from the same sample (N99–29 and N99–30), all total dissolution and leachate dates lie within the range 40 to 47 ka. The two dates from a sample of an adjacent caliche layer in the same hand sample (N99–28) were 44 and 48 ka. Such systematic behavior would not be expected if these materials were recording long-term average ages.

These observations suggest that, for the caliches, the total dissolution dates are good approximations of deposition ages within 10 or 15 percent. The lack of age information on some calcites, and the recognition of ages greater than 370 ka on others, does not detract much from the objectives of this study, because the calcites are generally lower in uranium and therefore are not as relevant to uranium mobilization as are the caliches.

6.7.4.3 Uranium-Series Isotopic Results for Opals and Uranophane

Fracture-coating opal was collected from the samples shown in Figures 6-19 and 6-20, and latest stage uranophane needles were collected from the outer surface of opal in Figure 6-20. As seen in the uranium-series activity ratios of Table 6-13, the two opal layers in Figure 6-20 are, within uncertainty, at secular equilibrium, while the uranophane that overgrew them has an age of 343 ka. (Note that the four samples in Table 6-13 with the prefix IR-99 were measured by thermal ionization mass spectrometry as described in Section 6.7.3.) These ages are consistent with textural relationships between the opals and uranophane. Before later isotopic data from DOE-sponsored studies indicated even younger ages (Levy, et al., 2011), this was the youngest measured uranium mineral age from Nopal I. The other opal yields an age of about 600 ka. Table 6-13 also shows alpha spectrometric data from the CNWRA laboratory that yielded an age of 54 ka.

These relationships are illustrated in Figure 6-25. The younger ages for the uranophane and one opal are evident, whereas the error ellipses for the IR-99-1 opals overlap with the secular equilibrium point. Also shown on this plot are the previously mentioned (Section 6.7.4.2) data for the calcites and quartz-rich “caliche” that did not yield Th-230 ages (Table 6-11). The displacement of these data points to the right and lower right from secular equilibrium is evidence for a degree of recent uranium removal from the rocks.

Note that the reported uranium concentration of the uranophane of 10.7 weight percent (Table 6-13) is lower than that of the yellow opal and lower than the expected stoichiometric uranium concentration—55 percent based on the formula $Ca(UO_2)_2Si_2O_7 \bullet 6H_2O$. While great care was taken during sampling of the uranophane needles from the surface of the opal, contaminants were noted in the material, which may have included yellow opal that was not identified. (The yellow opal, if present, would not have been responsible for the young opal age, because that opal was found to be in secular equilibrium.) The mass of uranophane sample material weighed for transport to the analysts was only 1.7 mg, so it is possible that some mass was lost during sample processing and subsequent aliquoting. Another possible source of mass error could have been incomplete dissolution of the uranophane, which was delivered to the analysts as small chips rather than fine powder. These possible explanations are speculative, and it cannot be stated with certainty that contamination of the uranophane was insignificant or that another uranium phase was involved. Based on observations during sampling, the sample is predominantly a uranyl mineral.

6.7.4.4 Oxygen and Carbon Isotopic Analyses of Calcites and Caliches

Stable isotopes of oxygen and carbon in authigenic materials can be used as tracers of geochemical processes because they provide information on the source of aqueous components and the temperature of deposition. The $\delta^{18}O$ and $\delta^{13}C$ values for materials precipitated from water reflect not only the aqueous $^{18}O/^{16}O$ and $^{13}C/^{12}C$ ratios, which can provide information on the source and history of the water; the values also indicate thermal conditions because of the temperature dependence of mass-based isotopic fractionation. Oxygen and carbon isotope ratios measured on orthophosphoric acid leachates reflect the carbonate component, and the ratios on the residue reflect the silicate component (Table 6-14).

The oxygen isotope ratios in the two components reveal genetic differences between the calcites and caliches (Figure 6-26). For both rock types, $\delta^{18}O$ is much more heterogeneous among the residues than the carbonate fractions, likely due to the influence on the residue values of nonauthigenic silicates and oxides. The caliche residues have higher $\delta^{18}O$ than most of the calcite residues, suggesting that caliche residues contain a higher proportion of authigenic silica in the residues than for calcites. This is because low-temperature oxygen isotope fractionation between silica and carbonate leads to higher $\delta^{18}O$ in silica by about 7 to 8 permil relative to carbonate, consistent with the approximate difference between the values in most of the caliche carbonates (22 to 24 permil) and the cluster of caliche residue $\delta^{18}O$ values at around 30 permil. Because there is no analogous relationship between the residues and carbonates in the calcites in Figure 6-26—in fact, most calcite residues have lower $\delta^{18}O$ than the carbonate fractions—there is no evidence for a genetic relationship between the two fractions in the calcites.

Caliche carbonate $\delta^{18}O$ values of 22 to 24 permil are consistent with low-temperature {15 to 20 °C [60 to 70 °F]} fractionation relative to water with the characteristics of regional meteoric water ($\delta^{18}O$ of about −7 permil). $\delta^{18}O$ values in the calcite carbonate fractions are consistently lower than in the caliches. If the calcites had higher formation temperatures {by 10 or more °C [20 or more °F]}, the difference could result in lesser fractionation relative to meteoric water. This interpretation is limited, however, by our lack of knowledge of the isotopic nature of the water that formed the calcites.

The oxygen isotope data are combined with uranium-series age information in Figure 6-27. In both fractions, younger caliches tend toward higher $\delta^{18}O$ than do calcites and old caliches. (The youngest caliche, which counters this trend with its low residue $\delta^{18}O$, contained large

amounts of visible tuff detritus, which would tend to lower the residue $\delta^{18}O$.) This observation is consistent with lower temperatures during more recent caliche formation, but source variation and water–rock interaction effects are also possible. To illustrate oxygen isotope differences between two materials, the $\Delta^{18}O$ value is used; this is calculated as the difference between $\delta^{18}O$ values in permil in the two materials. In general, a small $\Delta^{18}O$ for two materials that formed at the same time reflects high temperatures, because mass-dependent oxygen isotope fractionation is less pronounced at elevated temperatures. Young, high-uranium caliches (Figure 6-28) have high $\Delta^{18}O$ (residue-carbonate), consistent with low-temperature formation of coexisting authigenic silica and carbonate.

Overall, $\delta^{13}C$ is lower in caliches than in calcites (Figure 6-29). The only exceptions to this relationship on the figure are the very oldest and very carbonate-poor quartz "caliche" and the very youngest caliche. If the aqueous carbon source $\delta^{13}C$ was similar for all deposits, the lower caliche values compared to calcites could reflect lower temperatures, because they would result from a lower degree of carbon isotope fractionation between calcium carbonate and aqueous bicarbonate. (The relationship between temperature and degree of isotope fractionation in this case is the opposite of the case for oxygen isotopes.) However, carbon isotope fractionation is not as sensitive to temperature as oxygen, so variation in the aqueous carbon source is also a likely effect. There may have been more influence on the carbon source by vegetation, which tends to lower $\delta^{13}C$, for the more recent caliches. It is also possible that the carbon source for the calcites was influenced by the underlying, higher $\delta^{13}C$ marine limestone. The carbon isotope data, while distinctive, are less constraining than the oxygen data.

6.7.5 Discussion

Uranium-series data on the opals and uranophane are consistent with the picture of high uranium mobility up to about 300,000 years ago that is evident in the data on tuffs and iron-rich fracture fills discussed in Section 6.6. The 343-ka age on uranophane shows that precipitation of oxidized uranyl phases persisted well past the previously determined period of 3 million years ago. The calcites also date from that period; while they have rather high uranium contents for coarsely crystalline calcites, the calcites do not reflect the degree of mobilization and deposition of uranium seen in the opals and uranophane. There is some evidence in calcites and the silica "caliche" for more recent partial removal of uranium.

Leaching tests suggest that total dissolution Th-230 dates provide a reasonable estimate of the deposition ages of the Nopal I caliches, which typically contain authigenic carbonate and silicate components. These ages are plotted with uranium concentrations in Figure 6-30. The data suggest a period of enhanced mobility around 40 to 60 ka, as demonstrated by high uranium in that period. The samples showing this apparent episode are from same area just south of the Nopal I ore body, but they are from distinct layers and fractures. Enhanced uranium mobility in this period is supported by an existing 54-ka age for an opal with 6,900 ppm uranium. The causes of this apparent episode, and of other events of uranium mobility evident in the uranium-series data, have not yet been explored in detail, but environmental variations due to climate change (affecting infiltration) or uplift/denudation may be important. However, the entire uranium mobilization history recorded in the uranium-series systematics probably occurred in a generally oxidizing regime.

The stable isotope data are consistent with the youngest uranium-rich aqueous deposits having formed in a lower temperature {15 to 20 ºC [60 to 70 ºF]}, near-surface environment. This is not surprising for a material recently deposited within 2 m [6.6 ft] of the current ground surface. The data also suggest, however, that the environment of deposition has changed steadily to lower

temperatures since the calcites formed more than 300,000 years ago. The stable isotope data are also consistent with the observations based on uranium-series data that the caliches contain both authigenic carbonate and authigenic silicates.

6.7.6 Summary

Recent uranium migration from and around the Nopal I ore body is reflected in the uranium contents of deposits of caliche, opal, and—to a lesser extent—calcite. Caliche deposits record the most recent mobilization, within the past 100 ka. The uranium-thorium isotopic systematics in the caliches do not simply reflect carbonate–detritus mixing, as is often the case for calcites that have insoluble silicate residues. Rather, uranium has been deposited in both carbonate and silicate authigenic phases, which appear to be similar in age. Leaching tests suggest that total dissolution ^{230}Th-^{234}U-^{238}U ages are reasonable estimates for the ages of the caliches, within perhaps 10 to 15 percent.

Deposition of high-uranium caliches and opal at around 40 to 60 ka suggests an episode of elevated uranium migration at rates greater than long-term estimates. Nopal I has not acted as a closed system with respect to uranium in recent millennia. High-uranium opals and uranophane record older episodes of uranium mobilization of earlier than 300 ka, consistent with data on iron-rich fracture fills (Section 6.6). A uranophane age of 340 ka was the youngest reported Nopal I uranium mineral age at the time it was measured.

Oxygen and carbon isotope data are consistent with aqueous deposition of the younger uranium-rich caliches in a lower temperature {15 to 20 ºC [60 to 70 ºF]}, near-surface environment. The data are consistent with the uranium-series evidence for roughly coeval deposition of carbonate and silicate caliche components. Older calcite and quartz appear to have formed at higher temperatures.

The uranium-series data show that, in the silicic tuff around Nopal I, fractures are efficient transport pathways for uranium. There is evidence that this transport may have a degree of episodicity, likely related to varying water infiltration rates.

6.8 References

Bischoff, J.L. and J.A. Fitzpatrick. “U-Series Dating of Impure Carbonates: An Isochron Technique Using Total-Sample Dissolution.” *Geochimica et Cosmochimica Acta*. Vol. 55. pp. 543–554. 1991.

CRWMS M&O. “Natural Analogs for the Unsaturated Zone.” ANL–NBS–HS–000007. Rev. 00. Las Vegas, Nevada: Civilian Radioactive Waste Management System Management and Operations Contractor. 2000.

Fulignati, P., A. Gioncada, and A. Sbrana. “Rare-Earth Element (REE) Behaviour in the Alteration Facies of the Active Magmatic-Hydrothermal System of Vulcano (Aeolian Islands, Italy).” *Journal of Volcanology and Geothermal Research*. Vol. 88. pp. 325–342. 1999.

George-Aniel, B., J.L. Leroy, and B. Poty. “Volcanogenic Uranium Mineralization in the Sierra Peña Blanca District, Chihuahua, Mexico—Three Genetic Models.” *Economic Geology*. Vol. 86. pp. 233–248. 1991.

Ivanovich, M., A.G. Latham, G. Longworth, and M. Gascoyne. "Chapter 17: Applications to Radioactive Waste Disposal Studies." *Uranium-Series Disequilibrium: Applications to Earth, Marine, and Environmental Sciences*. M. Ivanovich and R.S. Harmon, eds. Oxford, England: Clarendon Press. pp. 583–630. 1992.

Ivanovich, M., A. Hernandez Benitez, A.V. Chambers, and S.E. Hasler. "Uranium Series Isotopic Study of Fracture Infill Materials From El Berrocal Site, Spain." *Radiochimica Acta*. Vol. 66/67. pp. 485–494. 1994.

Kaufman, A. "An Evaluation of Several Methods for Determining ^{230}Th U Ages in Impure Carbonates." *Geochimica et Cosmochimica Acta*. Vol. 57. pp. 2,303–2,317. 1993.

Leslie, B.W. and D. Pickett. "What Can U-series Measurements Tell Us About Radionuclide Mobilization and Migration in a Low-Water Flux, High-Uranium Concentration Setting?" *EOS Transactions of American Geophysical Union*. Vol. 81, Supplement 19. pp. S442–S443. 2000.

Leslie, B.W. and D. Pickett. "Chemical Alteration and Elemental Mobility at the Nopal I Mine, Peña Blanca District, Mexico." *Geological Society of America Abstracts with Programs*. Vol. 38, No. 7. p. 14. 2006.

Leslie, B.W., E.C. Pearcy, and J.D. Prikryl. "Oxidative Alteration of Uraninite Under Hydrologically Unsaturated Conditions at Peña Blanca, Chihuahua, Mexico: Contaminant Transport and Source Term Constraints for the Proposed Repository at Yucca Mountain, Nevada." *Scientific Basis for Nuclear Waste Management XVI.* C.G. Interrante and R.T. Pabalan, eds. Symposium Proceedings 294. Pittsburgh, Pennsylvania: Materials Research Society. pp. 505–512. 1993.

Leslie, B.W., D.A. Pickett, and E.C. Pearcy. "Vegetation-Derived Insights on the Mobilization and Potential Transport of Radionuclides From the Nopal I Natural Analog Site, Mexico." *Scientific Basis for Nuclear Waste Management XXII*. D.J. Wronkiewicz and J.H. Lee, eds. Symposium Proceedings 556. Warrendale, Pennsylvania: Materials Research Society. pp. 833–842. 1999.

Levy, S., S. Goldstein, P.F. Dobson, P. Goodell, T.-L. Ku, A. Abdel-Fattah, G. Saulnier, M. Fayek, and R. de la Garza. "Peña Blanca Natural Analogue Project: Summary of Activities." Proceedings of the 13th International High-Level Radioactive Waste Management Conference, Albuquerque, New Mexico, April 10–14, 2011. La Grange Park, Illinois: American Nuclear Society. pp. 330–341. 2011.

Luo, S. and T.-L. Ku. "U-series Isochron Dating: A Generalized Method Employing Total-sample Dissolution." *Geochimica et Cosmochimica Acta*. Vol. 55. pp. 555–564. 1991.

Martin, J.M., P. Nirel, and A.J. Thomas. "Sequential Extraction Techniques: Promises and Problems." *Marine Chemistry*. Vol. 22. pp. 313–341. 1987.

Nakamura, N. "Determination of REE, Ba, Fe, Mg, Na, and K in Carbonaceous and Ordinary Chondrites." *Geochimica et Cosmochimica Acta*. Vol. 38. pp. 757–775. 1974.

Osmond, J.K. and J.B. Cowart. "Chapter 9: Ground Water." *Uranium-Series Disequilibrium: Applications to Earth, Marine, and Environmental Sciences*. M. Ivanovich and R.S. Harmon, eds. Oxford, England: Clarendon Press. pp. 290–333. 1992.

Osmond, J.K. and M. Ivanovich. "Chapter 8: Uranium-Series Mobilization and Surface Hydrology." *Uranium-Series Disequilibrium: Applications to Earth, Marine, and Environmental Sciences*. M. Ivanovich and R.S. Harmon, eds. Oxford, England: Clarendon Press. pp. 259–289. 1992.

Osmond, J.K., J.B Cowart, and M. Ivanovich. "Uranium Isotopic Disequilibrium in Ground Water as an Indicator of Anomalies." *International Journal of Applied Radiation and Isotopes*. Vol. 34. pp. 283–308. 1983.

Pearcy, E.C. "Geochemical Natural Analog Research." *NRC High-Level Radioactive Waste Research at CNWRA January–June 1994*. CNWRA 94–01S. B. Sagar, ed. San Antonio, Texas: Center for Nuclear Waste Regulatory Analyses. 1994.

Pearcy, E.C., J.D. Prikryl, and B.W. Leslie. "Uranium Transport Through Fractured Silicic Tuff and Relative Retention in Areas With Distinct Fracture Characteristics." *Journal of Applied Geochemistry.* Vol. 10. pp. 685–704. 1995.

Pearcy, E.C., J.D. Prikryl, W.M. Murphy, and B.W. Leslie. "Alteration of Uraninite from the Nopal I Deposit, Peña Blanca, District, Chihuahua, Mexico, Compared to Degradation of Spent Nuclear Fuel in the Proposed US High-Level Nuclear Waste Repository at Yucca Mountain, Nevada." *Journal of Applied Geochemistry*. Vol. 9. pp. 713–732. 1994.

Pickett, D.A. and B.W. Leslie. "Mobilization of Uranium from the Nopal I Analog and Implications for Nuclear Waste Repository Performance." *Geological Society of America Abstracts with Programs*. Vol. 37, No. 7. pp. 268. 2005.

Pickett, D.A. and W.M. Murphy. "Uranium Chemistry and Isotropy in Waters and Rocks at Peña Blanca, Mexico." The 8th European Commission Natural Analogue Working Group Meeting—Proceedings. H. von Maravic and W.R. Alexander, eds. EUR 19118. Luxembourg, Germany: European Commission. pp. 333–337. 2001.

Pickett, D.A. and W.M. Murphy. "Unsaturated Zone Waters From the Nopal I Natural Analog, Chihuahua, Mexico—Implications for Radionuclide Mobility at Yucca Mountain." *Scientific Basis for Nuclear Waste Management XXII*. D.J. Wronkiewicz and J. Lee, eds. Symposium Proceedings 556. Warrendale, Pennsylvania: Materials Research Society. pp. 809–816. 1999.

Pickett, D.A. and W.M. Murphy. "Isotopic Constraints on Radionuclide Transport at Peña Blanca." The 7th European Commission Natural Analogue Working Group Meeting. H. von Maravic and J. Smellie, eds. EUR 17851 EN. Luxembourg, Germany: European Commission. pp. 113–122. 1997.

Pickett, D.A., W.M. Murphy, and B.W. Leslie. "^{238}U-^{234}U-^{230}Th Ages of Secondary Deposits and Evidence on the Rate of Recent Radionuclide Migration at the Nopal I Natural Analog." The 8th International Conference on the Behaviour of Actinides and Fission Products in the Geosphere, Bregenz, Austria. *Migration '01, Abstracts.* p. 103. 2001.

Pickett, D.A., B.W. Leslie, W.M. Murphy, and M. Nugent. "Estimating Radionuclide Release From a Uranium Deposit Through Uranium-Series Systematics in Carbonates and Opal. Goldschmidt 2000 Conference Abstracts. *Journal of Conference Abstracts*. Vol. 5. p. 797. 2000.

Pickett, D.A., J.D. Prikryl, and E.C. Pearcy. "Geochemical Natural Analog Research." *NRC High-Level Radioactive Waste Research at CNWRA, July Through December 1995*. B. Sagar, ed. CNWRA 95–02S. San Antonio, Texas: Center for Nuclear Waste Regulatory Analyses. 1996.

Prikryl, J.D., D.A. Pickett, and E.C. Pearcy. "Geochemical Natural Analog Research." *NRC High-Level Radioactive Waste Research at CNWRA, January Through June 1995*. CNWRA 95–01S. B. Sagar, ed. San Antonio, Texas: Center for Nuclear Waste Regulatory Analyses. 1995.

Prikryl, J.D., D.A. Pickett, W.M. Murphy, and E.C. Pearcy. "Migration Behavior of Naturally-Occurring Radionuclides at the Nopal I Uranium Deposit, Chihuahua, Mexico." *Journal of Contaminant Hydrology*. Vol. 26. pp. 61–69. 1997.

Reeder, R.J., M. Nugent, C.D. Tait, D.E. Morris, S.M. Heald, K.M. Beck, W.P. Hess, and A. Lanzirotti. "Coprecipitation of Uranium(VI) with Calcite: XAFS, Micro-XAS, and Luminescence Characterization." Geochimica et Cosmochimica Acta. Vol. 65. pp. 3491-3503. 2001.

Scott, R.D., A.B. MacKenzie, and W.R. Alexander. "The Interpretation of ^{238}U-^{234}U-^{230}Th-^{226}Ra Disequilibria Produced by Rock-Water Interactions." *Journal of Geochemical Exploration*. Vol. 45. pp. 323–343. 1992.

Suksi, J., T. Ruskeeniemi, and L. Saarinen. "Selective Extractions in Uranium Migration Studies—Findings From a Natural Analogue Study at Palmottu." Fourth International Conference on the Chemistry and Migration Behaviour of Actinides and Fission Products in the Geosphere. J.P. Adloff, G.R. Choppin, and J.I. Kim, eds. Munich, Germany: R. Oldenbourg Verlag. pp. 589–594. 1994.

Tessier, A., P.G.C. Campbell, and M. Bisson. "Sequential Extraction Procedure for the Speciation of Particulate Trace Metals." *Analytical Chemistry*. Vol. 51. pp. 844–851. 1979.

Thiel, K., R. Vorwerk, R. Saager, and H.D. Stupp. "^{235}U Fission Tracks and ^{238}U-Series Disequilibria as a Means To Study Recent Mobilization of Uranium in Archaean Pyritic Conglomerates." *Earth and Planetary Science Letters*. Vol. 65. pp. 249–262. 1983.

Yanase, N., T. Nightingale, T. Payne, and P. Duerden. "Uranium Distribution in Mineral Phases of Rock by Sequential Extraction Procedure. *Radiochimica Acta.* Vol. 52/53. pp. 387–393. 1991.

Table 6-1. Major Element Analyses of Rocks Collected From Transect J on Nopal I Level +10*

Distance West (m)	SiO_2	TiO_2	Al_2O_3	Total Fe as Fe_2O_3	FeO	Fe_2O_3†	MnO	MgO	CaO	Na_2O	K_2O	P_2O_5	LOI‡	Total
2.55	76.38	0.24	12.79	0.72	0.16	0.53	0.01	0.12	0.13	0.53	6.36	0.02	2.49	99.78
4	76.57	0.23	12.32	0.93	0.27	0.62	0.01	0.07	0.19	0.59	6.43	0.03	2.25	99.62
5.2	77.98	0.25	11.93	0.60	1.19	-0.68	0.01	0.06	0.17	0.57	5.88	0.02	2.38	99.84
6.2	77.28	0.24	12.37	0.48	0.24	0.21	0.01	0.06	0.16	0.53	6.05	0.04	2.48	99.69
7.45	76.33	0.25	13.03	0.54	0.08	0.44	0.00	0.06	0.17	0.54	6.38	0.03	2.51	99.84
8.15	76.27	0.25	13.21	0.61	0.06	0.53	0.01	0.06	0.15	0.60	6.61	0.04	2.40	100.21
9	77.01	0.25	13.28	0.57	0.18	0.36	0.00	0.01	0.11	0.43	5.77	0.02	2.83	100.28
9.7	76.42	0.25	12.87	0.59	0.10	0.47	0.00	0.03	0.10	0.54	6.06	0.01	2.41	99.28
10.3	78.25	0.23	12.65	0.57	0.08	0.47	0.00	0.02	0.07	0.31	4.77	0.02	3.12	100.02
10.8	77.02	0.26	13.73	0.44	0.10	0.32	0.00	0.03	0.10	0.31	4.63	0.01	3.26	99.80
11.55	77.33	0.24	12.87	0.61	0.09	0.50	0.01	0.03	0.10	0.31	4.92	0.03	2.94	99.36
11.9	75.29	0.21	9.27	4.42	0.51	3.75	0.01	0.01	0.44	0.09	1.98	0.03	4.29	96.02
12.5	77.46	0.22	12.37	0.71	0.01	0.68	0.00	0.02	0.13	0.31	4.25	0.01	3.22	98.72
12.95	73.11	0.19	9.19	10.52	0.06	10.15	0.01	0.01	0.14	0.18	2.83	0.01	3.42	99.60
13.5	76.55	0.22	11.09	4.11	0.11	3.88	0.01	0.03	0.11	0.24	3.65	0.01	3.42	99.41
13.95	60.09	0.15	8.52	25.37	0.27	24.34	0.01	0.02	0.15	0.07	0.98	0.02	4.72	100.07
14.45	79.17	0.25	10.71	2.39	0.16	2.15	0.01	0.05	0.11	0.24	3.22	0.04	3.48	99.64
15	74.66	0.22	10.97	6.56	0.09	6.27	0.01	0.05	0.19	0.26	3.38	0.03	3.71	100.05
15.6	66.17	0.29	16.09	8.25	0.16	7.84	0.01	0.05	0.19	0.14	1.55	0.07	7.08	99.88
16.4	74.95	0.21	11.24	6.90	0.13	6.56	0.00	0.03	0.10	0.14	2.13	0.02	4.22	99.93
17	73.00	0.23	15.37	3.33	0.12	3.11	0.00	0.01	0.09	0.11	1.67	0.02	6.56	100.38
17.4	71.77	0.20	15.45	3.25	0.13	3.02	0.00	0.04	0.06	0.06	0.55	0.01	8.21	99.60
18.05	71.85	0.20	13.07	6.34	0.19	5.95	0.00	0.02	0.05	0.05	0.65	0.01	7.46	99.67
18.35	72.72	0.21	14.11	0.77	0.17	0.57	0.00	0.02	0.05	0.06	1.58	0.01	10.74	100.28
18.6	74.47	0.22	14.61	0.64	0.15	0.46	0.00	0.02	0.07	0.07	0.89	0.02	8.33	99.33
19	78.20	0.22	10.83	0.94	0.23	0.67	0.01	0.07	0.06	0.11	1.07	0.02	8.16	99.67
19.65	74.18	0.21	12.45	1.37	0.23	1.09	0.00	0.08	0.07	0.06	1.32	0.01	9.31	99.08
20.1	74.32	0.23	14.13	1.54	0.16	1.33	0.00	0.04	0.06	0.08	1.48	0.03	8.22	100.13
20.65	77.38	0.25	12.27	0.56	0.14	0.40	0.00	0.04	0.06	0.20	2.77	0.04	6.10	99.66

*Concentrations as oxide in weight percent

†Ferric iron concentrations calculated by difference between total iron (ICP-MS) and FeO (titration)

‡Loss on ignition in weight percent

Table 6-2. Trace Element Analyses of Rocks Collected From Transect J on Nopal I Level +10*

Distance West (m)	S	Sc	V	Cr	Ni	Cu	Zn	Nb	Y	Zr	Ba	Sr	Rb	U
2.55	232	3.3	20	8	23	2	113	36	38.9	241	72	31	341	29
4	—	3.8	24	—	—	3	130	35	35.3	—	74	22	360	28
5.2	—	3.6	18	—	—	2	117	32	33.9	—	68	33	324	24
6.2	—	4	25	—	—	2	101	35	34.3	—	70	41	318	26
7.45	—	4.8	31	—	—	1	105	35	40.4	—	75	32	357	31
8.15	—	3.05	26.5	—	—	2.5	113	41	35.1	—	67	64	357.5	22
9	50	4.4	56	5	9	5	88	36	77.4	305	85	33	300	60
9.7	50	3.1	19	4	7	4	87	30	36.9	256	69	38	338	22
10.3	50	2.6	64	7	18	5	140	35	33.3	243	128	52	245	67
10.8	197	3.5	44	8	14	4	132	36	37.6	258	82	51	245	50
11.55	270	1.6	170	6.5	9.5	18.5	213	34	41.5	240	117	42	243.5	91
11.9	891	4.4	184	40	13	45	870	50	77.4	291	397	100	81	23,300
12.5	122	1.7	29	12	16	7	182	27	25.4	215	85	57	228	2,910
12.95	198	2.5	87	10	3	12	206	19	31.4	257	492	49	137	3,910
13.5	435	2.4	92.5	3	2.5	10.5	222	35	16.5	219	126	61.5	169	309
13.95	422	7.75	324.5	10	28	29.5	1,000	24	55.45	523.5	246	54.5	41.5	1,230
14.45	—	2.7	75.5	—	—	6	189.5	47	17.15	—	127	64	140	256
15	—	2.6	127	—	—	9	285	41	16.3	—	105	57	156	426
15.6	—	13.2	332	—	—	22	374	37	43	—	294	231	67	546
16.4	—	3.6	75	—	—	6	64	30	12.4	—	130	62	96	204
17	4,351	9.4	60	36	69	9	30	32	11.9	213	144	118	59	115
17.4	—	12.2	138	—	—	8	98	31	11.9	—	227	158	10	148
18.05	—	15.7	115	—	—	6	32	30.5	10.95	—	524.5	294.5	9.5	328
18.35	—	36.8	124	—	—	4	37	38	12.1	—	451	362	12	222
18.6	—	28.7	133	—	—	4	36	35	10.9	—	233	190	12	187
19	—	26.7	112	—	—	6	42	36	11.9	—	409	177	14	334
19.65	—	24.9	142	—	—	11	57	34	12.4	—	345	287	16	288
20.1	—	18.6	191	—	—	8	56	35	11	—	292	194	39	526
20.65	—	15.5	104.5	—	—	5	25.5	39	13.75	—	164.5	147	104	356

*Concentrations in parts per million (ppm). A blank entry indicates that the element was not analyzed for that sample.
S = Sulfur, Sc = Scandium, V = Vanadium, Cr = Chromium, Ni = Nickel, Cu = Copper, Zn = Zinc, Nb = Niobium, Y = Yttrium, Zr = Zirconium, Ba = Barium, Sr = Strontium, Rb = Rubidium, U = Uranium

Table 6-3. Major Element Analyses of Rocks Collected From Transect A on Nopal I Level +10*

Distance West (m)	SiO_2	TiO_2	Al_2O_3	Total Fe as Fe_2O_3	FeO	Fe_2O_3†	MnO	MgO	CaO	Na_2O	K_2O	P_2O_5	LOI‡	Total
11	76.59	0.24	12.02	1.34	0.16	1.13	0.01	0.04	0.09	0.28	4.50	0.06	3.50	98.66
11.22	76.31	0.27	13.04	2.45	0.15	2.22	0.01	0.06	0.09	0.16	3.19	0.04	4.53	100.14
11.4	73.99	0.26	14.10	1.14	0.11	0.99	0.01	0.04	0.08	0.30	5.18	0.05	4.03	99.17
11.6	77.97	0.20	8.97	5.66	0.15	5.34	0.01	0.01	0.11	0.13	2.27	0.06	4.00	99.38
11.78	77.17	0.21	10.07	4.65	0.26	4.24	0.01	0.02	0.11	0.15	2.94	0.06	3.81	99.19
12	71.94	0.18	12.78	6.19	0.21	5.79	0.01	0.05	0.17	0.11	1.98	0.04	5.84	99.29
12.18	77.27	0.22	10.07	3.95	0.30	3.52	0.01	0.02	0.12	0.15	2.83	0.11	4.64	99.39
12.42	77.46	0.24	11.17	2.53	0.15	2.30	0.01	0.02	0.12	0.21	3.47	0.03	4.02	99.27
12.65	78.83	0.24	11.06	1.67	0.12	1.49	0.01	0.03	0.14	0.24	4.09	0.04	3.49	99.80
12.87	76.92	0.22	11.72	1.63	0.12	1.46	0.01	0.02	0.09	0.30	4.59	0.01	3.27	98.78
13	74.93	0.22	11.45	3.91	0.08	3.71	0.01	0.02	0.10	0.32	4.84	0.04	3.29	99.12

*Concentrations as oxide in weight percent
†Ferric iron concentrations calculated by difference between total iron (ICP-MS) and FeO (titration)
‡Loss on ignition in weight percent

Table 6-4. Trace Element Analyses of Rocks Collected From Transect A on Nopal I Level +10*

Distance West (m)	S	Sc	V	Cr	Ni	Cu	Zn	Nb	Y	Zr	Ba	Sr	Rb	U
11	169	3	73	5	1	11	355	35	33.5	257	188	71	217	222
11.22	223	3.4	114	12	24	19	435	41	45.4	293	208	94	137	127
11.4	187	2.3	46	5	6	10	239	39	37.4	258	75	66	253	61.6
11.6	50	12.3	171	4	4	43	1900	32	275.1	554	310	82	96	640
11.78	500	9.25	162	4.5	4.5	38.5	1253	33	119.15	474.5	315.5	88.5	132.5	742
12	1031	12.9	173	4	3	38	2335	30	100.6	515	265	69	87	803
12.18	4200	10	128	7	5	16	807	35	81.4	511	410	219	123	1260
12.42	105	3	79	42	70	9	645	30	22	275	137	62	161	2250
12.65	237	2.5	51.5	11	14.5	3.5	369.5	31	15.75	248	149	65.5	184.5	3000
12.87	50	2	28	10	6	0	162	24	18.9	213	586	52	247	4580
13	55	1.4	36	8	1	0	196	20	21.2	222	616	42	243	5280

*Concentrations in parts per million (ppm)
S = Sulfur, Sc = Scandium, V = Vanadium, Cr = Chromium, Ni = Nickel, Cu = Copper, Zn = Zinc, Nb = Niobium, Y= Yttrium, Zr = Zirconium, Ba = Barium, Sr = Strontium, Rb = Rubidium, U = Uranium

Table 6-5. Rare-Earth Element Concentrations (ppm) in Selected Samples From Nopal I Level +10									
Sample	**Description**	**La**	**Ce**	**Nd**	**Sm**	**Eu**	**Tb**	**Yb**	**Lu**
NOPI-ECP-1	Nopal Tuff	48.3	96.2	37.8	6.97	0.66	0.93	3.20	0.49
9.7/7.35	2 m outside ore body	57.5	107	49.0	8.67	0.67	1.01	3.38	0.53
11.9/7.9	Uranium-rich ore	30.4	96.8	29.7	8.41	0.76	1.53	6.26	0.86
17.0/7.5	Acid-altered ore body	34.1	54.2	14.4	2.33	0.115	1.10	1.79	0.28
8.45/13.82	Fracture filling	15.4	30.3	13.0	4.95	0.57	1.96	2.24	0.29

La = Lanthanum, Ce = Cerium, Nd = Neodymium, Sm = Samarium, Eu = Europium, Tb = Terbium, Yb = Ytterbium, Lu = Lutetium

Table 6-6. Uranium-Series Activity Ratios on Ore Standards						
	$^{234}U/^{238}U$	Counting Error	$^{230}Th/^{234}U$	Counting Error	$^{230}Th/^{238}U$	Counting Error
BL-5*	0.973	0.031	1.069	0.026	1.040	0.025
BL-5	1.026	0.041	0.972	0.028	0.998	0.029
DP2†[b]	0.965	0.044	—	—	—	—
DP2	0.979	0.070	1.078	0.063	1.056	0.062
DP2	0.958	0.055	0.979	0.052	0.939	0.049
SP1‡	0.984	0.039	0.999	0.030	0.983	0.030
DP2DM1§	1.068	0.094	1.012	0.074	1.081	0.081

*Uranium ore standard from Canada Centre for Minerals and Energy Technology (CANMET), Ottawa, Ontario, Canada
†Diluted pitchblende ore from U.S. Environmental Protection Agency (EPA), Environmental Monitoring System Laboratory, Las Vegas, Nevada
‡Standard pitchblende ore from EPA, Environmental Monitoring System Laboratory, Las Vegas, Nevada
§Mixture of diluted pitchblende and diluted monazite ores from EPA, Environmental Monitoring System Laboratory, Las Vegas, Nevada

Table 6-7. Nopal I Traverse B Sequential Extraction Scheme		
Target Phase	**Reagent**	**Effects**
Ion-exchangeable (IE)	1 M $MgCl_2$ (magnesium chloride) at pH 7 shaken for 1 hour.	Displaces exchangeable nuclides.
Adsorbed (AD)	Morgan's reagent with 2×10^{-5} M EDTA shaken for 6 hours.	Releases nuclides held on surfaces.
Amorphous iron-oxyhydroxides (AM)	Tamm's acid oxalate shaken in dark for 4 hours. Repeated with fresh reagent for 1 hour.	Dissolves hydrous iron-oxyhydroxides.
Crystalline iron-oxides (CR)	Coffin's reagent with sodium dithionite shaken for 1 hour. Repeated with fresh reagents until residues are free of iron.	Dissolves crystalline iron-oxides and iron-hydroxides.
Resistates (RES)	HF/HNO_3 (hydrofluoric acid and nitric acid) digestion.	Dissolves remaining minerals.

Table 6-8. Bulk Rock Alpha Spectrometry Results*						
Traverse	NOPI-XXX Sample Number	Distance (m)†	U (ppm)	Th (ppm)	$^{234}U/^{238}U$	$^{230}Th/^{234}U$§
A	113	−0.80	7,230	44.1	1.00(2)	0.93(1)
	114	−0.67	6,060	36.3	0.99(2)	1.02(2)
	115	−0.45	4,080	33.6	0.97(2)	1.11(2)
	116	−0.22	3,630	35.1	1.06(2)	1.00(1)
	117	0.02	1,400	31.5	1.01(2)	1.21(2)
	118	0.20	994	33.2	1.08(2)	1.15(2)
	119	0.42	1,080	36.3	1.04(2)	0.99(2)
	120	0.60	1,020	40.3	1.01(3)	1.10(2)
	121	0.80	54.0	39.7	1.46(5)	1.03(3)
	122	0.98	123	38.6	1.28(3)	1.07(2)
	123	1.20	99.6	35.9	1.12(3)	1.17(3)
B‡	417	−5.6	3,640	16.9	1.29(3)	1.27(2)
	144	−2.0	5,370	18.7	1.15(2)	1.03(1)
	418	−1.5	3,530	19.5	1.28(3)	1.25(2)
	142	0.1	1,720	139	1.40(2)	1.19(1)
	419	1.2	787	73.4	1.63(4)	1.39(2)
	302	1.8	1,480	111	1.34(3)	1.10(2)
	420	4.0	1,620	35.9	1.29(3)	1.31(2)
	139	4.0	1,410	25.1	1.14(2)	1.24(1)
	301	4.1	1,570	38.2	1.16(3)	1.18(2)
	137	6.4	1,160	39.2	1.16(2)	1.06(1)
	421	7.0	2,510	50.8	1.18(2)	1.24(2)
	422	9.1	1,720	39.9	1.08(3)	1.21(2)
	423	12.3	472	27.9	1.12(3)	1.31(3)
	205	13.2	818	108	1.11(2)	1.14(2)
	424	16.3	768	32.2	1.05(4)	1.23(5)
	209	17.5	1,090	40.0	1.30(8)	1.16(5)
	425	20.0	455	27.3	1.11(3)	1.33(3)
	294	20.3	375	15.3	1.12(3)	1.23(3)
	298	22.4	484	55.7	1.10(2)	1.15(2)
C	372	−0.61	204	40.7	1.11(2)	1.28(2)
	373	−0.41	343	55.0	1.08(2)	1.16(2)
	374	−0.16	179	30.2	0.94(2)	1.26(3)
	375	0.09	787	41.6	1.09(2)	1.12(2)
	376	0.39	256	32.7	1.07(4)	1.47(4)
	377	0.59	218	44.2	1.26(3)	1.31(2)
	378	0.89	298	34.6	1.04(2)	1.03(2)
	379	1.09	214	31.5	1.18(3)	1.09(2)
	380	1.34	168	36.5	0.95(2)	1.20(2)
	381	1.64	1,000	35.0	1.16(2)	1.06(1)
	382	1.94	1,530	35.3	0.84(1)	1.09(1)
	383	2.09	316	17.8	1.06(2)	0.61(1)
	384	2.29	239	39.0	1.06(2)	1.01(2)
	385	2.44	216	39.8	1.03(2)	1.16(2)
	386	2.64	185	46.4	0.99(2)	1.14(2)

Table 6-8. Bulk Rock Alpha Spectrometry Results (continued)*						
Traverse	NOPI-XXX Sample Number	Distance (m)†	U (ppm)	Th (ppm)	$^{234}U/^{238}U$	$^{230}Th/^{234}U$§
	387	2.89	179	40.6	1.00(2)	1.19(2)
	388	3.19	97.0	46.6	1.15(3)	1.13(3)
	389	3.39	649	43.1	0.97(1)	1.18(1)
	390	3.69	422	38.7	1.09(2)	1.08(1)
	391	4.04	90.1	46.6	1.13(3)	1.21(3)
D	212	10.7	184	44.7	1.27(6)	1.01(5)
	214	12.0	63.9	40.2	1.54(4)	1.26(3)
	215	13.4	145	29.0	1.02(2)	1.12(3)
	216r	14.5	600	31.8	1.00(2)	1.00(2)
	217	15.4	175	20.8	1.01(2)	1.15(2)
	218	16.5	68.9	25.2	1.14(3)	1.15(4)
	219	17.6	47.5	40.9	1.24(4)	1.23(4)
	221	19.2	118	33.3	0.97(2)	1.17(3)
E	307	4.7	486	41.6	1.33(2)	1.11(2)
	397	6.6	976	58.3	1.32(2)	1.09(1)
	398	7.7	1,200	59.0	1.17(2)	1.05(1)
	399	9.5	117	46.4	1.84(5)	1.20(2)
	400	10.4	134	47.7	2.43(6)	1.15(2)
	401	12.2	165	32.6	1.94(5)	1.32(3)
	402	13.6	314	47.6	1.25(2)	1.14(2)
	403	14.8	298	30.7	0.99(2)	1.30(2)
	404	16.3	138	39.6	1.01(3)	1.44(4)
	405	17.3	474	41.2	0.96(2)	1.14(2)
	406	19.3	44.4	42.0	1.01(4)	1.56(6)
	407	22.0	448	42.7	0.91(2)	1.23(2)
	408	24.4	16.1	40.2	1.00(7)	1.32(8)
	409	29.2	9.77	15.8	1.02(9)	1.69(15)
	410	34.9	10.8	39.1	1.04(8)	2.13(17)
	411	35.9	16.0	33.4	1.02(7)	1.68(11)

*Uncertainties in parentheses on activity ratios are 1 sigma due to counting statistics

†Distances are measured outward from the margin of the zone of visible U mineralization; distances for traverse D are referenced to the east-west axis in Figure 6-9, rather than to the ore deposit

‡Traverse B data originally tabulated in Prikryl, J.D., D.A. Pickett, and E.C. Pearcy. "Geochemical Natural Analog Research." *NRC High-Level Radioactive Waste Research at CNWRA, January Through June 1995.* CNWRA 95–01S. B. Sagar, ed. San Antonio, Texas: Center for Nuclear Waste Regulatory Analyses. 1995.

§As discussed in Section 6.6.3.1, these ratios are not considered reliable

Table 6-9. Sequential Extraction Data From Traverse B

Distance* (m)	Fraction	wt. (g)	wt. %	µg U	U, ppm†	U, µg/g‡	µg Th	Th, ppm†	Th, µg/g‡	$^{234}U/^{238}U$§	$^{230}Th/^{234}U$§
-5.6 NOPI-417	IE	0.037	1.4	1.98×10^{2}	—	7.39×10^{1}	7.33×10^{-1}	—	2.74×10^{-1}	0.72(2)	0.060(3)
	AD	0.015	0.6	1.18×10^{3}	—	4.41×10^{2}	4.82×10^{-1}	—	1.80×10^{-1}	0.69(1)	0.040(1)
	AM	0.105	3.9	1.14×10^{3}	1.09×10^{4}	4.28×10^{2}	5.45×10^{0}	5.20×10^{1}	2.04×10^{0}	0.78(2)	1.28(2)
	CR	1.762	65.8	6.43×10^{3}	3.65×10^{3}	2.41×10^{3}	2.29×10^{0}	1.30×10^{0}	8.56×10^{-1}	1.37(2)	1.12(1)
	RES	0.757	28.3	1.22×10^{3}	1.61×10^{3}	4.55×10^{2}	6.35×10^{0}	8.40×10^{0}	2.38×10^{0}	1.13(2)	1.30(1)
	bulk‖	2.675		1.02×10^{4}	3.80×10^{3}	—	1.53×10^{1}	5.72×10^{0}	—	1.18	1.07
-1.5 NOPI-418	IE	0.046	1.8	2.23×10^{1}	—	8.86×10^{0}	4.09×10^{-1}	—	1.62×10^{-1}	0.89(3)	0.55(2)
	AD	0.024	0.9	4.51×10^{3}	—	1.79×10^{3}	1.44×10^{0}	—	5.74×10^{-1}	0.77(2)	0.020(1)
	AM	0.141	5.6	4.16×10^{3}	2.95×10^{4}	1.65×10^{3}	8.80×10^{0}	6.24×10^{1}	3.50×10^{0}	0.89(2)	1.25(2)
	CR	1.500	59.6	1.38×10^{4}	9.19×10^{3}	5.48×10^{3}	3.93×10^{1}	2.62×10^{1}	1.56×10^{1}	1.50(3)	1.05(1)
	RES	0.806	32.0	7.26×10^{2}	9.01×10^{2}	2.89×10^{2}	4.03×10^{0}	5.00×10^{0}	1.60×10^{0}	1.18(1)	4.56(3)
	bulk‖	2.518		2.32×10^{4}	9.22×10^{3}	—	5.40×10^{1}	2.14×10^{1}	—	1.24	1.06
4.0 NOPI-420	IE	0.012	0.5	3.09×10^{0}	—	1.22×10^{0}	6.57×10^{-1}	—	2.60×10^{-1}	0.74(8)	0.97(11)
	AD	0.030	1.2	2.99×10^{2}	—	1.18×10^{2}	9.57×10^{-2}	—	3.78×10^{-2}	0.87(1)	0.040(1)
	AM	0.048	1.9	3.13×10^{2}	6.48×10^{3}	1.24×10^{2}	3.40×10^{0}	7.03×10^{1}	1.34×10^{0}	0.97(1)	1.48(2)
	CR	1.205	47.6	2.25×10^{3}	1.87×10^{3}	8.91×10^{2}	2.56×10^{1}	2.13×10^{1}	1.01×10^{1}	1.27(2)	1.14(1)
	RES	1.234	48.8	1.77×10^{2}	1.44×10^{2}	7.00×10^{1}	9.45×10^{0}	7.66×10^{0}	3.74×10^{0}	1.13(2)	1.19(2)
	bulk‖	2.529		3.05×10^{3}	1.20×10^{3}	—	3.92×10^{1}	1.55×10^{1}	—	1.19	1.09
7.0 NOPI-421	IE	0.029	1.2	6.51×10^{0}	—	2.68×10^{0}	9.62×10^{-1}	—	3.96×10^{-1}	0.98(9)	1.26(10)
	AD	0.011	0.4	5.25×10^{2}	—	2.16×10^{2}	1.33×10^{0}	—	5.48×10^{-1}	0.79(1)	0.030(1)
	AM	0.096	3.9	7.43×10^{2}	7.75×10^{3}	3.06×10^{2}	1.11×10^{1}	1.15×10^{2}	4.55×10^{0}	0.86(2)	1.59(2)
	CR	1.288	53.0	3.79×10^{3}	2.94×10^{3}	1.56×10^{3}	3.48×10^{1}	2.70×10^{1}	$1.43E \times 10^{1}$	1.27(2)	1.10(1)
	RES	1.008	41.5	3.95×10^{1}	3.92×10^{1}	1.63×10^{1}	1.99×10^{1}	1.97×10^{1}	8.17×10^{0}	1.75(5)	1.77(4)
	bulk‖	2.431		5.10×10^{3}	2.10×10^{3}	—	6.80×10^{1}	2.80×10^{1}	—	1.16	1.09
12.3 NOPI-423	IE	0.010	0.4	3.01×10^{0}	—	1.19×10^{0}	8.64×10^{-1}	—	3.41×10^{-1}	1.13(11)	1.16(11)
	AD	0.024	0.9	2.16×10^{2}	—	8.50×10^{1}	1.26×10^{0}	—	4.98×10^{-1}	0.84(1)	0.080(2)
	AM	0.073	2.9	2.15×10^{2}	2.92×10^{3}	8.46×10^{1}	2.08×10^{1}	2.84×10^{2}	8.22×10^{0}	0.85(1)	1.63(2)
	CR	0.409	16.1	9.33×10^{2}	2.28×10^{3}	3.68×10^{2}	7.10×10^{1}	1.74×10^{2}	2.80×10^{1}	1.35(2)	1.31(1)
	RES	2.021	79.7	9.00×10^{1}	4.45×10^{1}	3.55×10^{1}	2.26×10^{1}	1.12×10^{1}	8.89×10^{0}	1.15(2)	1.43(3)
	bulk‖	2.537		1.46×10^{3}	5.74×10^{2}	—	1.17×10^{2}	4.59×10^{1}	—	1.19	1.22
20.0 NOPI-425	IE	0.021	0.8	3.54×10^{0}	—	1.40×10^{0}	2.26×10^{-1}	—	8.93×10^{-2}	1.21(15)	0.67(8)
	AD	0.028	1.1	2.49×10^{2}	—	9.85×10^{1}	1.96×10^{-1}	—	7.75×10^{-2}	0.92(1)	0.080(3)
	AM	0.043	1.7	1.72×10^{2}	3.98×10^{3}	6.79×10^{1}	1.62×10^{1}	3.75×10^{2}	6.40×10^{0}	0.88(2)	2.02(3)
	CR	1.215	48.1	7.52×10^{2}	6.18×10^{2}	2.97×10^{2}	1.28×10^{1}	1.05×10^{1}	5.05E+00	1.25(2)	1.24(1)
	RES	1.222	48.3	3.15×10^{1}	2.58×10^{1}	1.25×10^{1}	1.71×10^{1}	1.40×10^{1}	6.74E+00	1.00(4)	1.49(5)
	bulk‖	2.529		1.21×10^{3}	4.77×10^{2}	—	4.64×10^{1}	1.84×10^{1}	—	1.12	1.13

* Distances are measured outward from the margin of the zone of visible U mineralization.
†Based on mass change during extraction step; values are not shown for IE and AD, because these are essentially massless.
‡Micrograms in the fraction per gram of bulk rock.
§Uncertainties in parentheses on activity ratios are 1 sigma due to counting statistics. As discussed in Section 6.6.3.1, the $^{230}Th/^{234}U$ ratios are not considered reliable.
‖Bulk values are calculated by combining the extraction data.
IE = Ion Exchangeable, AD = Adsorbed, AM = Amorphous Iron-Oxyhydroxide, CR = Crystalline Oxides, RES = Resistates

Table 6-10. Uranium and Thorium Concentration of Total-Rock Calcite and Caliche							
Sample	NOPI Number	Rock Type*	Grain Size (µm)	Percent Noncarbonate†	U (ppm)	Th (ppm)	Th/U
N99-1	12-SEP1	cc	>250	4.8	29.8	1.06	0.0355
N99-2	501-W	cc	—	4.0	0.146	0.511	3.51
N99-3	19-SEP1-P	cc, gray	>250	6.4	11.1	0.195	0.0175
N99-4	19-SEP2	cc, gray	63–125	7.5	10.7	0.116	0.0108
N99-5	24-SEP1	cc	>250	3.6	17.7	0.534	0.0301
N99-6	24-SEP2	cc	63–125	5.6	14.4	0.586	0.0407
N99-7	29-SEP1	cc	>250	4.3	4.59	0.466	0.102
N99-8	29-SEP2	cc	63–125	6.4	4.11	0.603	0.147
N99-9	164-SEP1	cc, gray	>250	56.8	28.0	16.8	0.598
N99-10	164-SEP4	cc, gray	<63	31.2	33.8	17.3	0.512
N99-11	166-SEP1-P	cc, gray	>250	7.0	16.3	0.680	0.0417
N99-12	166-SEP2	cc, gray	63–125	8.1	13.4	0.721	0.0538
N99-13	179-SEP1-P	cc, gray	>250	15.0	9.20	4.57	0.497
N99-14	179-SEP2	cc, gray	63–125	13.2	8.53	3.88	0.455
N99-15	501-G-SEP1	cc, gray	>250	8.4	14.0	0.345	0.0247
N99-16	501-G-SEP3	cc, gray	63–125	6.0	13.3	0 .340	0.0256
N99-17	436-L1-SEP1	cal	>250	16.1	31.7	2.27	0.0717
N99-18	436-L1-SEP4	cal	<63	9.6	27.5	2.15	0.0781
N99-19	436-L2-SEP2	cal	125–250	17.8	24.2	6.45	0.266
N99-20	436-L2-SEP4	cal	<63	14.6	38.5	11.9	0.308
N99-23	499-L2-SEP1	cal	>250	27.8	38.1	8.26	0.217
N99-24	499-L2-SEP3	cal	63–125	24.4	27.1	8.14	0.300
N99-25	499-L3-SEP1	cal, sil	>250	32.7	51.5	0.280	0.00544
N99-26	499-L3-SEP4	cal, sil	<63	30.8	63.8	0.255	0.00400
N99-27	305-L1-SEP2	cal	125-250	24.5	174	0.457	0.00262
N99-28	305-L1-SEP4	cal	<63	22.2	143	0.214	0.00150
N99-29	305-L2-SEP1	cal	>250	26.4	192	0.184	0.000958
N99-30	305-L2-SEP4	cal	<63	18.7	157	0.257	0.00164
N99-31	306-SEP1	cal, sil	>250	38.3	336	0.469	0.00139
N99-32	306-SEP4	cal, sil	<63	35.9	322	0.389	0.00121
N99-33	434-SEP2	cal, sil	125–250	4.2	83.9	2.44	0.0290
N99-34	434-SEP4	cal, sil	<63	7.8	83.2	3.20	0.0384
N99-35	458-SEP1	cal, sil	>250	92.6	112	7.28	0.0648
N99-36	458-SEP4	cal, sil	<63	91.4	86.8	9.48	0.109

*cc = calcite (clear or gray); cal = caliche; cal, sil = caliche appearing rich in silica

†Calculated percentage of rock that is not $CaCO_3$, assuming all mass loss during firing is from CO_2 loss. Because the rocks may contain H_2O, these estimates are likely low.

Table 6-11. Uranium and Thorium Concentrations and Activity Ratios in Calcites and Caliches*

Sample	NOPI Number	Type	U (ppm)†	Th (ppm)†	$^{232}Th/^{238}U$	$^{230}Th/^{238}U$	$^{234}U/^{238}U$	^{230}Th date (ka)‡
N99-1	12-SEP1	cc	28.0	1.082	0.01260(9)	1.016(4)	1.004(3)	—
N99-4	19-SEP2	cc, gray	10.2	0.114	0.00369(2)	1.263(6)	1.227(4)	370
N99-5	24-SEP1	cc	17.4	0.555	0.01040(6)	1.021(7)	0.999(3)	—
N99-11	166-SEP1-P	cc, gray	15.2	0.693	0.01490(8)	1.449(8)	1.551(5)	213
N99-11 leach			8.0	0.420	0.01718(9)	1.526(6)	1.892(6)	148
N99-16	501-G-SEP3	cc, gray	11.4	0.292	0.00839(4)	1.273(6)	1.222(4)	406
N99-18	436-L1-SEP4	cal	28.6	2.067	0.0237(2)	0.813(6)	1.670(5)	69.2
N99-18 leach			18.3	0.874	0.01564(9)	0.749(3)	1.671(5)	62.0
N99-26	499-L3-SEP4	cal, sil	59.9	0.232	0.001270(6)	0.571(2)	2.066(6)	34.3
N99-26 leach			39.3	0.106	0.000884(4)	0.544(3)	1.953(6)	34.6
N99-26 leach§			36.7	0.086	0.000764(3)	0.504(3)	1.996(6)	31.1
N99-28	305-L1-SEP4	cal	122.3	0.190	0.000509(2)	0.446(2)	1.233(4)	48.3
N99-28 leach			98.7	0.090	0.000300(1)	0.414(2)	1.229(4)	44.3
N99-29	305-L2-SEP1	cal	188.1	0.173	0.000302(2)	0.412(2)	1.207(4)	45.0
N99-29 leach			109.7	0.083	0.0002470(9)	0.375(1)	1.213(4)	39.9
N99-30	305-L2-SEP4	cal	170.2	0.294	0.000566(3)	0.423(3)	1.209(4)	46.4
N99-30 leach			95.0	0.132	0.000456(2)	0.429(1)	1.210(4)	47.2
N99-32	306-SEP4	cal, sil	313.0	0.378	0.000396(3)	0.910(6)	1.237(4)	136
N99-32 leach			153.6	0.162	0.000344(1)	0.965(3)	1.242(4)	151
N99-33	434-SEP2	cal, sil	83.3	2.489	0.00973(8)	0.179(1)	1.109(3)	19.2
N99-33 leach			76.3	1.540	0.00660(5)	0.163(1)	1.114(3)	17.2
N99-35	458-SEP1	cal, sil	105.5	7.610	0.0236(2)	1.037(6)	0.992(3)	—

*Numbers in parentheses are estimated 2σ uncertainties on last digit
†For leachates, concentrations are based on the preleach sample mass; does not consider leachable mass of sample
‡Due to uncertainties in initial conditions (e.g., initial $^{230}Th/^{232}Th$ cannot be assumed), dates do not include initial ^{230}Th corrections; if applied, these change the dates by less than 1 ka. A blank means that a single-stage date could not be calculated.
§The U-Th spike was added after leaching for this replicate; in all other cases, the spike was added before leaching. The differences in the results are within about 10 percent.
cc = calcite (clear or gray); cal = caliche; cal, sil = caliche appearing rich in silica.

Table 6-12. Estimated Uranium Concentrations in Carbonate and Silicate Fractions in Nopal I Calcite (N99-11) and Caliches (Others)				
Sample	**Estimated Weight Percent Carbonate***	**Total Rock U (ppm)**	**Estimated Carbonate U (ppm)**	**Estimated Silicate U (ppm)**
N99-11	89.4	15.2	9	68
N99-18	84.9	28.6	22	68
N99-26	56.9	59.9	69	48
N99-26	57.3	59.9	64	55
N99-28	73.6	122.3	134	90
N99-29	61.7	188.1	178	205
N99-30	72.4	170.2	131	273
N99-32	61.5	313.0	250	414
N99-33	84.9	83.3	90	47

*Calculated from mass loss during leaching; corrected for the mass lost during firing of original powder

Table 6-13. Uranium and Thorium Concentrations and Activity Ratios in Opals and Uranophane*						
Sample	**Description**	**U (ppm)**	**Th (ppb)**	**^{230}Th/^{238}U**	**^{234}U/^{238}U**	**^{230}Th date (ka)**
IR-99-1 OPAL 1	Clear glassy opal, with faint greenish tint, forming the base in Figure 6-20	8,830	7.0	0.999(3)	1.003(3)	Secular equilibrium†
IR-99-1 OPAL 2	Translucent yellow opal with no visible uranium minerals, contiguous with lighter opal layer in Figure 6-20	122,800	280	1.000(3)	1.002(3)	Secular equilibrium†
IR-99-10 OPAL SEP 1	Clear glassy opal, with greenish tint, from sample depicted in Figure 6-19	7,970	60	1.020(3)	1.017(3)	600 +300/-100
IR-99-1 Uph 4	Bright yellow uranophane needles growing on opal surface shown in Figure 6-20	107,200	97	0.968(3)	1.009(3)	343 +18/-15
NOPI-ECP-19.0/5.0-1‡	Clear, glassy, colorless opal	6,923	3,297	0.396(4)	1.01(1)	54 ±2

*Numbers in parentheses are estimated 2σ uncertainties on last digit of the activity ratios. Estimated uncertainties on dates are shown directly.

†^{230}Th/^{238}U and ^{234}U/^{238}U are indistinguishable from 1

‡Measured by alpha spectrometry at CNWRA, 1993.

Table 6-14. Stable Isotope Data for Calcites and Caliches From Nopal I						
Sample	NOPI Number*	Type	Weight % Carbonate†	$\delta^{18}O$ Silicate‡	$\delta^{18}O$ Carbonate‡	$\delta^{13}C$ Carbonate§
N05-01	12-SEP1	cc	78.2	20.1	17.3	−0.8
N05-02	19-SEP1-P	cc	69.0	5.6	20.9	0.0
N05-03	19-SEP2	cc	80.7	5.7	20.9	−0.1
N05-04	24-SEP1	cc	76.6	21.6	18.8	−1.3
N05-05	24-SEP2	cc	78.3	n.d.	18.8	−1.3
N05-06	29-SEP1	cc	91.5	n.d.	19.8	−1.6
N05-07	29-SEP2	cc	78.8	n.d.	20.0	−1.6
N05-08	164-SEP1	cc	36.4	14.1	22.1	−3.1
N05-09	164-SEP2	cc	49.8	14.0	21.7	−3.4
N05-10	164-SEP3	cc	51.1	12.5	21.7	−3.6
N05-11	164-SEP4	cc	60.3	14.1	21.7	−3.6
N05-65	166-SEP1	cc	84.0	13.0	21.3	−0.6
N05-14	166-SEP2	cc	88.9	n.d.	21.4	−0.6
N05-15	179-SEP1-PB	cc	63.6	16.2	21.7	−4.9
N05-16	179-SEP2	cc	76.6	n.d.	21.7	−5.0
N05-17	436-L1-SEP1	cal	76.3	28.4	23.3	−5.7
N05-18	436-L1-SEP2	cal	79.8	29.3	23.7	−5.7
N05-19	436-L1-SEP3	cal	33.7	28.2	24.1	−5.5
N05-20	436-L1-SEP4	cal	81.7	25.4	23.6	−5.6
N05-21	436-L2-SEP1	cal	66.1	22.6	23.2	−6.4
N05-22	436-L2-SEP2	cal	80.0	22.2	23.0	−6.3
N05-23	436-L2-SEP3	cal	71.0	24.1	23.1	−6.5
N05-24	436-L2-SEP4	cal	75.8	n.d.	23.3	−6.5
N05-25	499-L2-SEP1	cal	59.9	21.9	23.3	−7.7
N05-26	499-L2-SEP2	cal	61.8	22.2	23.5	−7.6
N05-27	499-L2-SEP3	cal	66.6	19.5	23.4	−7.6
N05-28	499-L2-SEP4	cal	61.7	20.4	23.5	−7.4
N05-29	499-L3-SEP1	cal	57.4	31.8	22.6	−10.4
N05-30	499-L3-SEP2	cal	59.5	30.5	22.6	−10.3
N05-31	499-L3-SEP3	cal	59.2	29.6	22.6	−10.1
N05-32	499-L3-SEP4	cal	56.9	30.5	22.1	−10.3
N05-33	305-L1-SEP1	cal	60.9	31.9	23.6	−6.2
N05-34	305-L1-SEP2	cal	68.3	31.9	23.9	−6.1
N05-35	305-L1-SEP3	cal	70.6	32.2	23.7	−6.1
N05-37	305-L1-SEP4	cal	70.2	30.5	23.8	−6.0
N05-38	305-L2-SEP1	cal	64.5	32.0	23.2	−5.7
N05-39	305-L2-SEP2	cal	70.2	32.1	23.2	−5.7
N05-41	305-L2-SEP3	cal	72.3	31.2	23.5	−5.7
N05-42	305-L2-SEP4	cal	75.1	31.3	23.3	−5.7
N05-43	306-SEP1	cal	52.4	30.7	22.2	−7.8
N05-44	306-SEP2	cal	56.3	30.7	22.3	−7.8
N05-45	306-SEP3	cal	57.0	31.0	22.5	−7.8
N05-46	306-SEP4	cal	55.1	n.d.	22.5	−7.8

Table 6-14. Stable Isotope Data for Calcites and Caliches From Nopal I (continued)						
Sample	**NOPI Number***	**Type**	**Weight % Carbonate†**	**$\delta^{18}O$ Silicate‡**	**$\delta^{18}O$ Carbonate‡**	**$\delta^{13}C$ Carbonate§**
N05-47	434-SEP1	cal	84.3	18.7	23.5	1.1
N05-48	434-SEP2	cal	81.5	n.d.	23.4	1.1
N05-50	434-SEP3	cal	83.1	16.5	23.5	1.1
N05-51	434-SEP4	cal	81.3	n.d.	23.5	1.1
N05-52	501-W	cc	93.9	n.d.	17.3	1.2
N05-53	501-G-SEP1	cc	88.6	n.d.	21.1	−1.1
N05-54	501-G-SEP2	cc	92.8	17.6	21.3	−1.1
N05-55	501-G-SEP3	cc	83.1	n.d.	21.5	−1.3
N05-56	501-G-SEP4	cc	82.2	n.d.	21.2	−1.3
N05-57	458-SEP1	cal	0.5	21.4	20.5	−0.6
N05-58	458-SEP2	cal	n.d.	20.8	n.d.	n.d.
N05-59	458-SEP3	cal	n.d.	21.4	n.d.	n.d.
N05-61	458-SEP4	cal	n.d.	20.5	17.3	n.d.

*"L" indicates a layer within the sample indicated by the 3-digit NOPI number, and "SEP" indicates a grain-size fraction from the sample
†Based on mass change after orthophosphoric acid leach
‡Permil calculated against the SMOW standard
§Permil calculated against the PDB standard
cc = calcite, cal = caliche
n.d. = the value was not determined

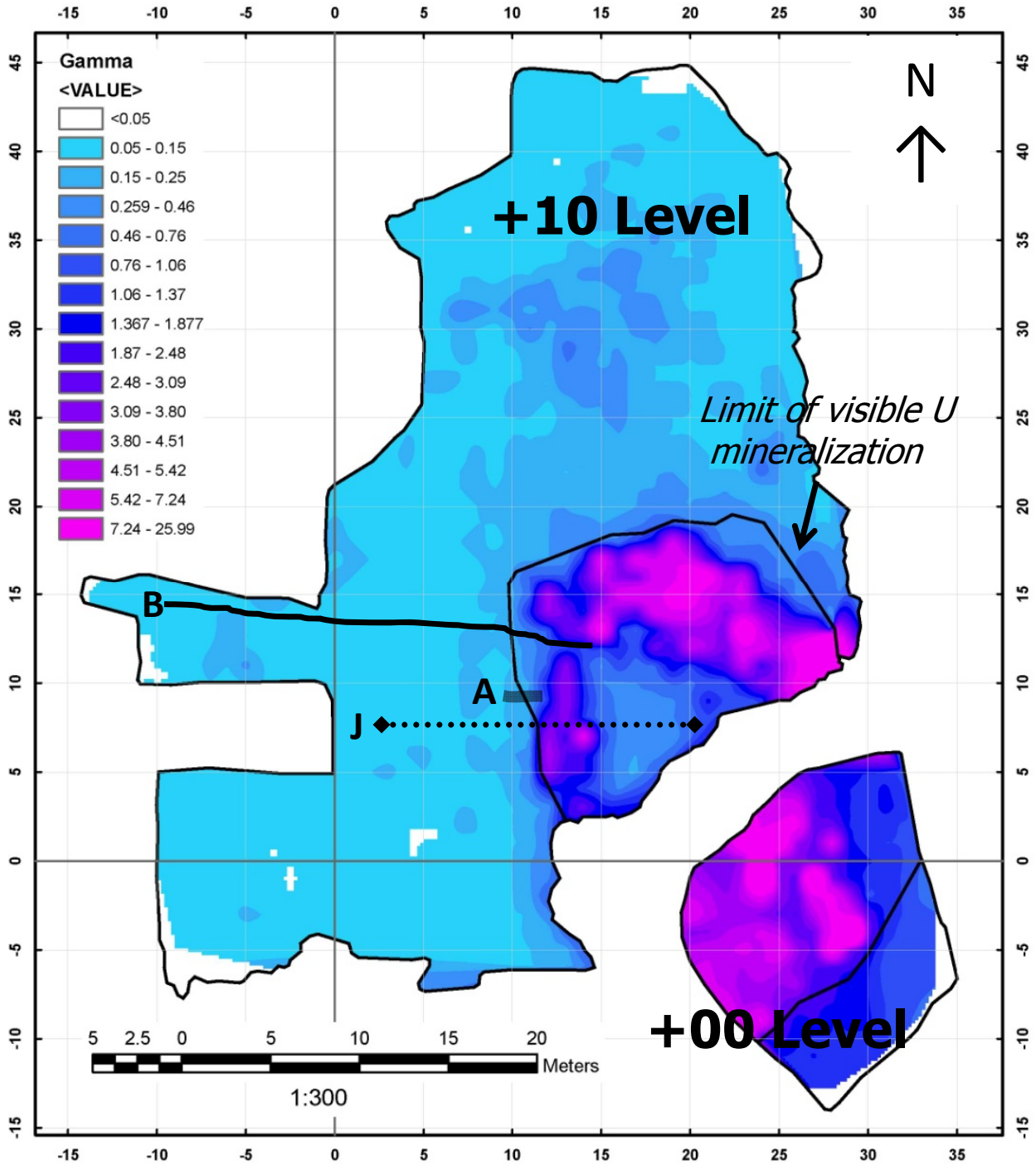

Figure 6-1. Gamma Intensity Map (After Pearcy, et al., 1995; Leslie and Pickett, 2006) of the Exposed Surface of Level +10 of the Nopal I Uranium Ore Deposit, Showing Locations of Whole-Rock Sampling Traverses A and J and Major East-West Fracture Set B. Contours Are in Units of mR/hour. Axis Numbers Correspond to Sampling Grid Locations in Meters [1 m = 3.28 ft].

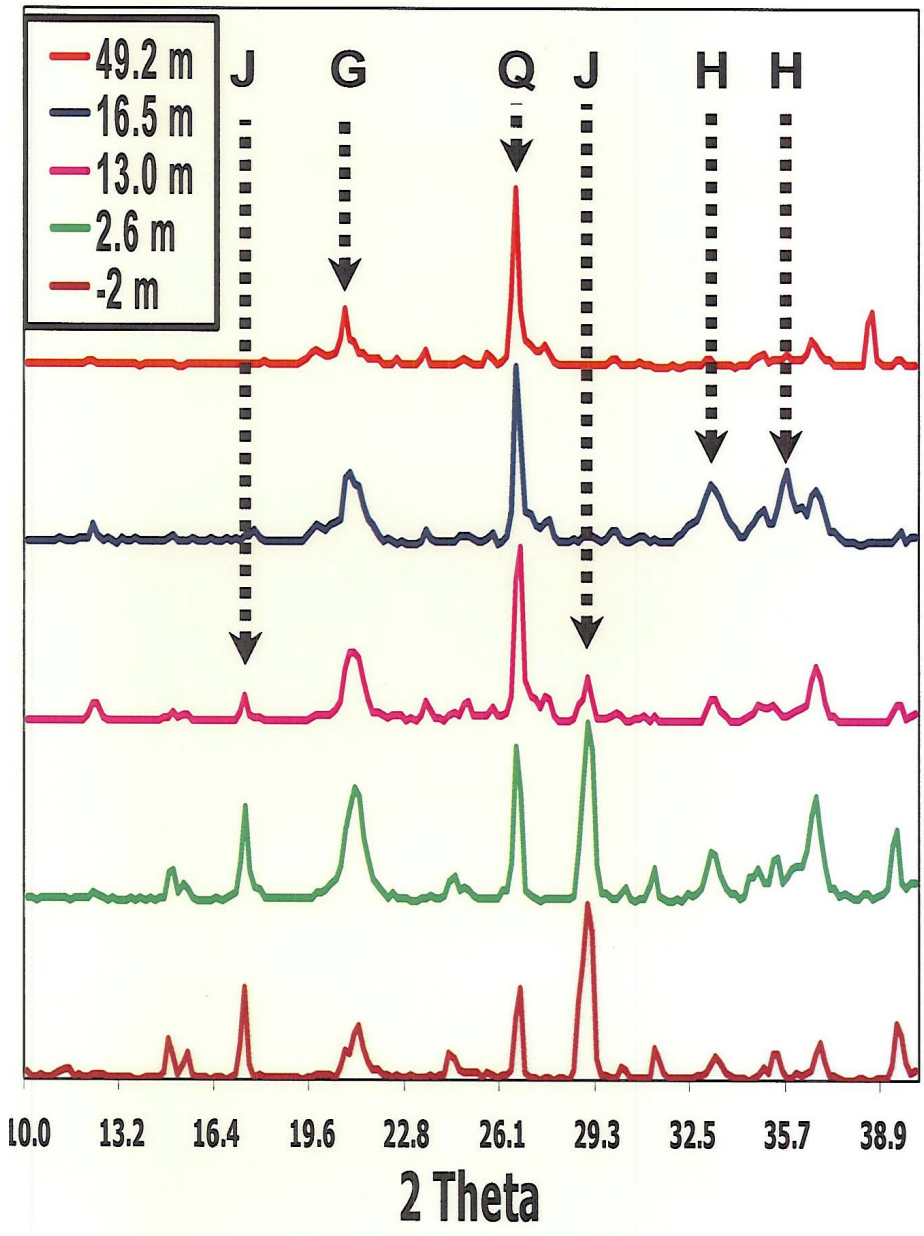

Figure 6-2. 2-Theta Angle Spectra (in Degrees), Measured by X-ray Diffraction, for Samples of Fracture-Filling Material Taken From Progressively Greater Distances in Meters [1 m = 3.28 ft] From the Edge of the Ore Body in Traverse B. {The 2-m Sample Is From Within the Ore Body Boundary}. Letters Indicate the Characteristic Lines Identifying Specific Minerals Jarosite (J), Goethite (G), Quartz (Q), and Hematite (H).

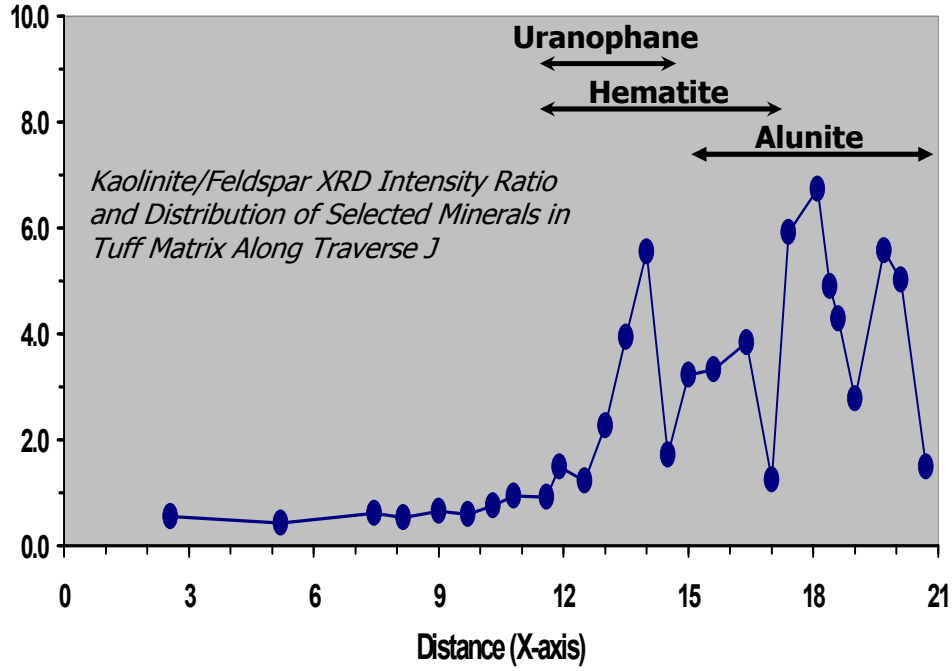

Figure 6-3. The Ratio of XRD Intensities for Characteristic Kaolinite and Alkali Feldspar Peaks in Bulk Tuff Samples Along Traverse J. Also Shown Are Linear Ranges of the Occurrences of Uranophane, Hematite, and Alunite. (Note That the Distances on the X Axis in Meters, Which Increase to the East, Correspond to the Field Sampling Grid and Do Not Coincide With Distances From the Edge of the Ore Body; 1 m = 3.28 ft.)

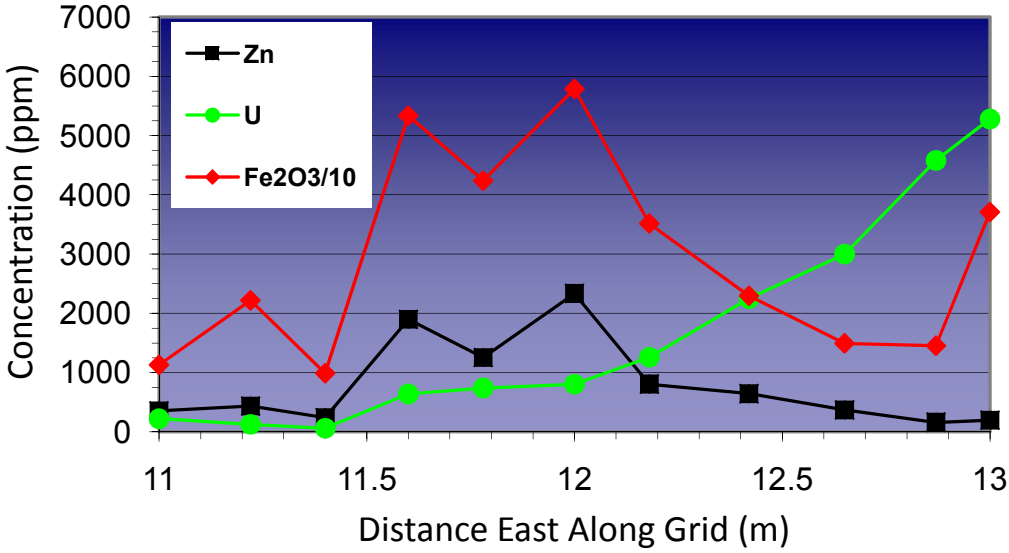

Figure 6-4. Zinc, Uranium, and Iron as Fe_2O_3 From Traverse A. The Fe_2O_3 Concentration Is Divided by 10 for Convenience of Plotting; the Patterns Are More Important Than the Actual Values. The Limit of Visible Uranium Mineralization Is at About the 11.6-m Mark. (Note That the Distances on the X Axis, Which Increase to the East, Correspond to the Field Sampling Grid and Do Not Coincide With Distances From the Edge of the Ore Body; 1 m = 3.28 ft.) Uranium Data Are From Pearcy, et al. (1995).

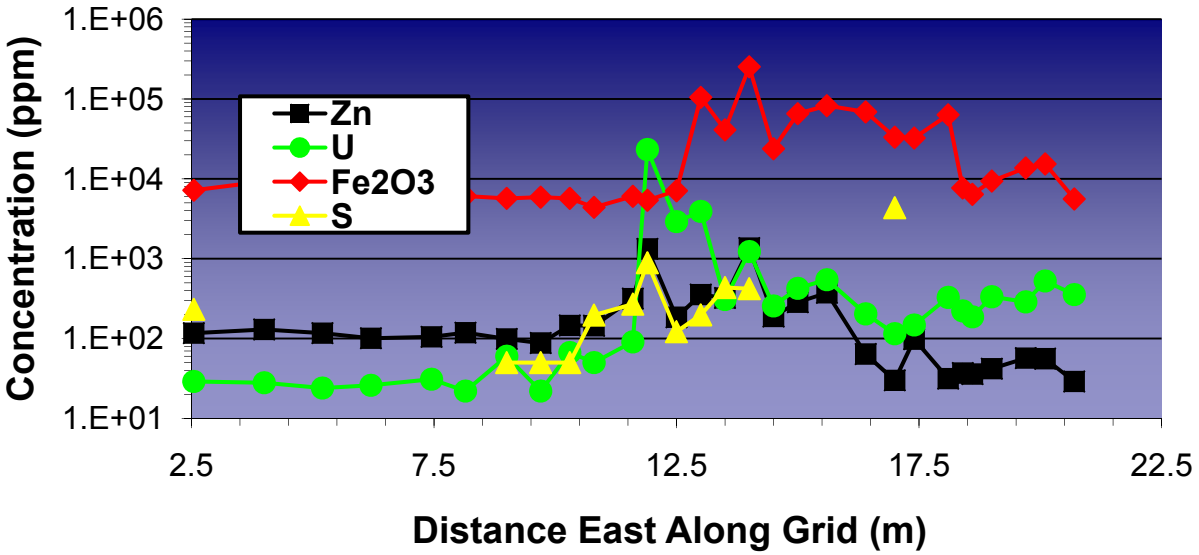

Figure 6-5. Zinc, Uranium, Iron as Fe_2O_3, and Sulfur Concentrations From Traverse J. The Limit of Visible Uranium Mineralization (On the Right) Is at About the 12-m Mark. (Note That the Distances on the X Axis, Which Increase to the East, Correspond to the Field Sampling Grid and Do Not Coincide With Distances From the Edge of the Ore Body; 1 m = 3.28 ft.) Uranium Data are From Leslie, et al. (1993).

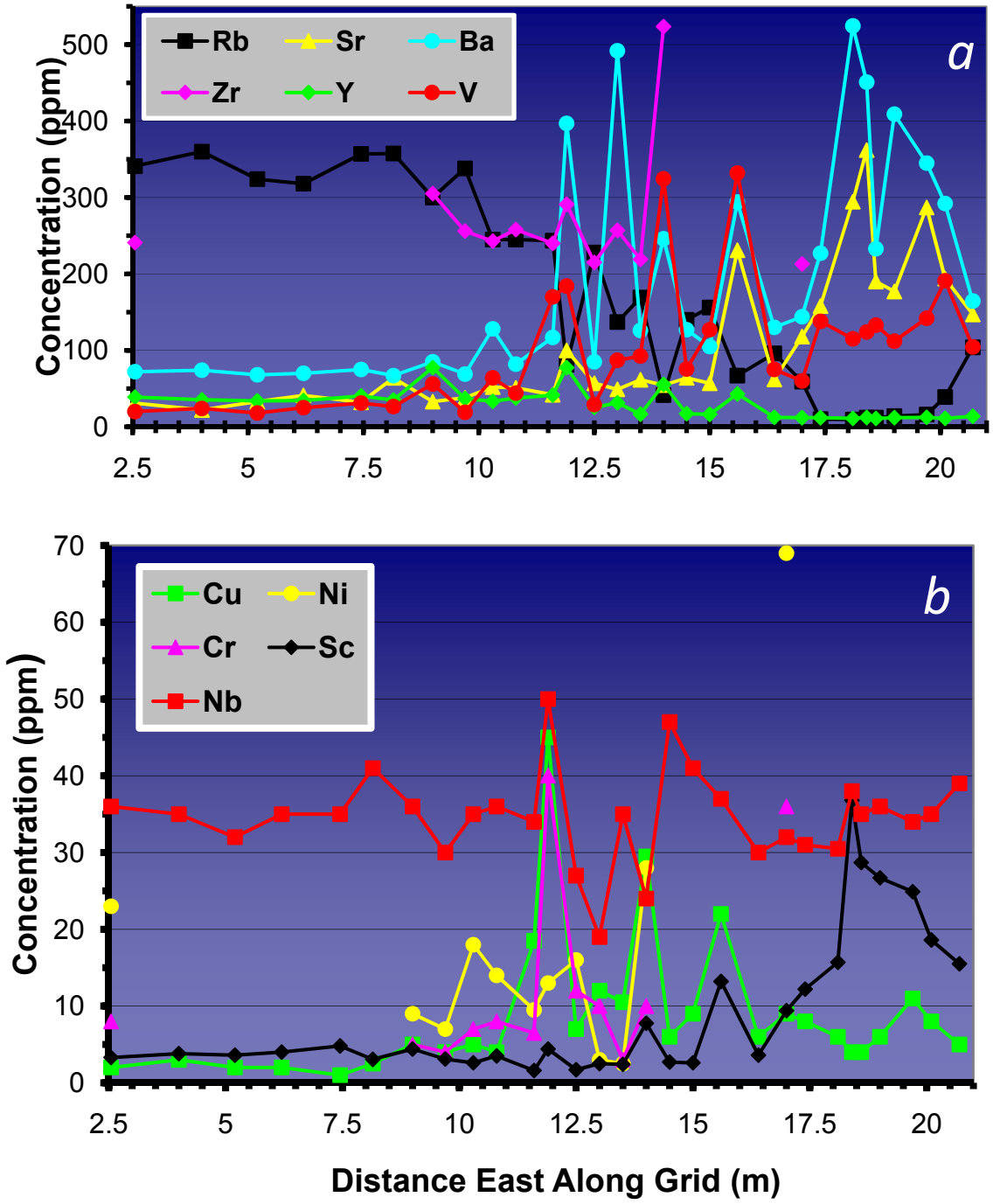

Figure 6-6. Trace Element Concentrations Along Traverse J in Matrix and Mineralized Tuff, Including Rubidium, Strontium, Barium, Zirconium, Yttrium, and Vanadium (a) and Copper, Nickel, Chromium, Scandium, and Niobium (b). The Limit of Visible Uranium Mineralization (On the Right) Is at About the 12-m Mark. (Note That the Distances on the X Axis, Which Increase to the East, Correspond to the Field Sampling Grid and Do Not Coincide With Distances From the Edge of the Ore Body; 1 m = 3.28 ft.)

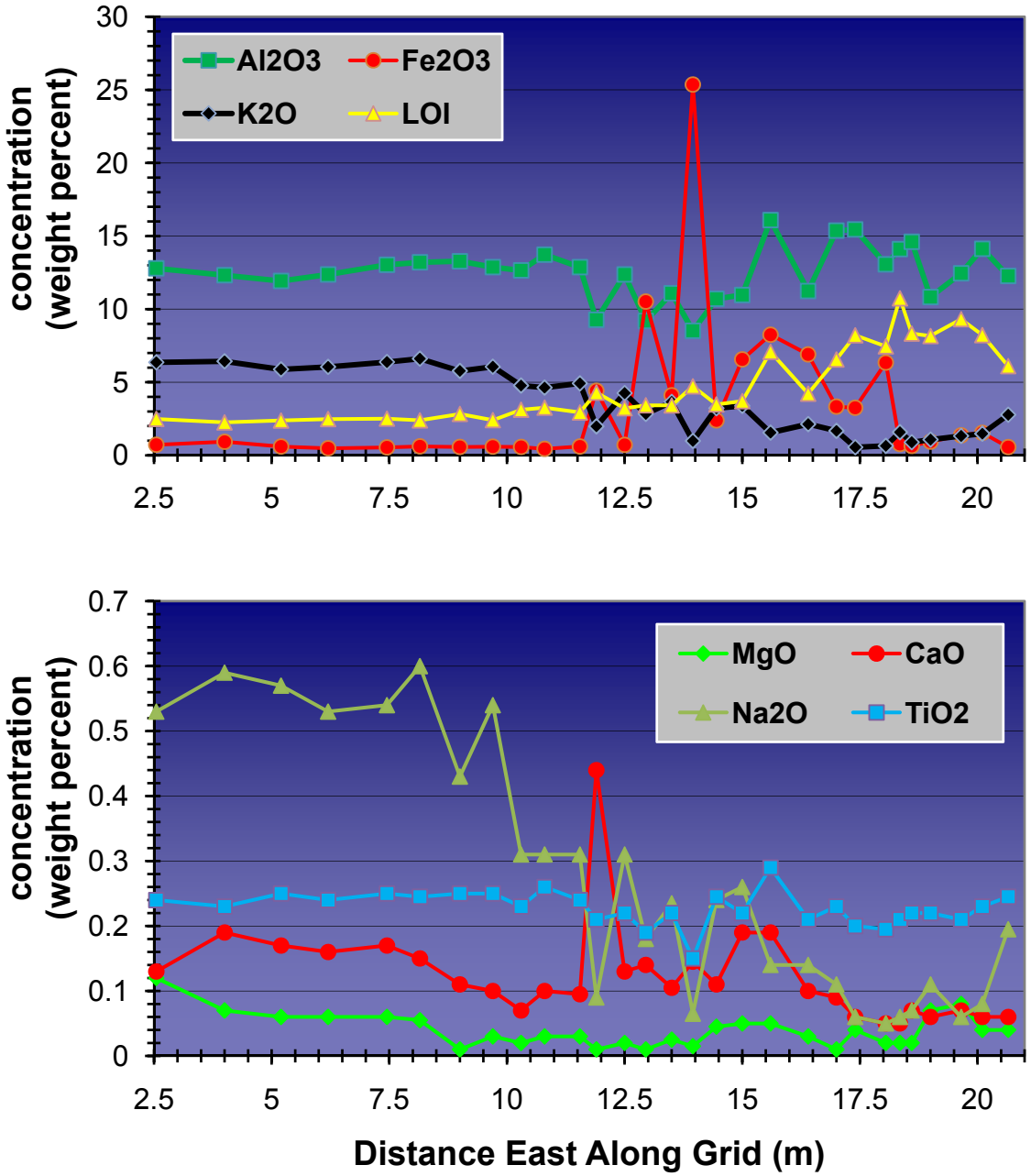

Figure 6-7. Major Element Oxide Concentrations Along Traverse J in Matrix and Mineralized Tuff. The Limit of Visible Uranium Mineralization (on the Right) Is at About the 12-m Mark. "LOI" Indicates the Weight Loss on Ignition and Reflects Concentrations of Volatile Species Such as H_2O and CO_2. (Note that the Distances on the X Axis, Which Increase to the East, Correspond to the Field Sampling Grid and Do Not Coincide With Distances From the Edge of the Ore Body; 1 m = 3.28 ft.)

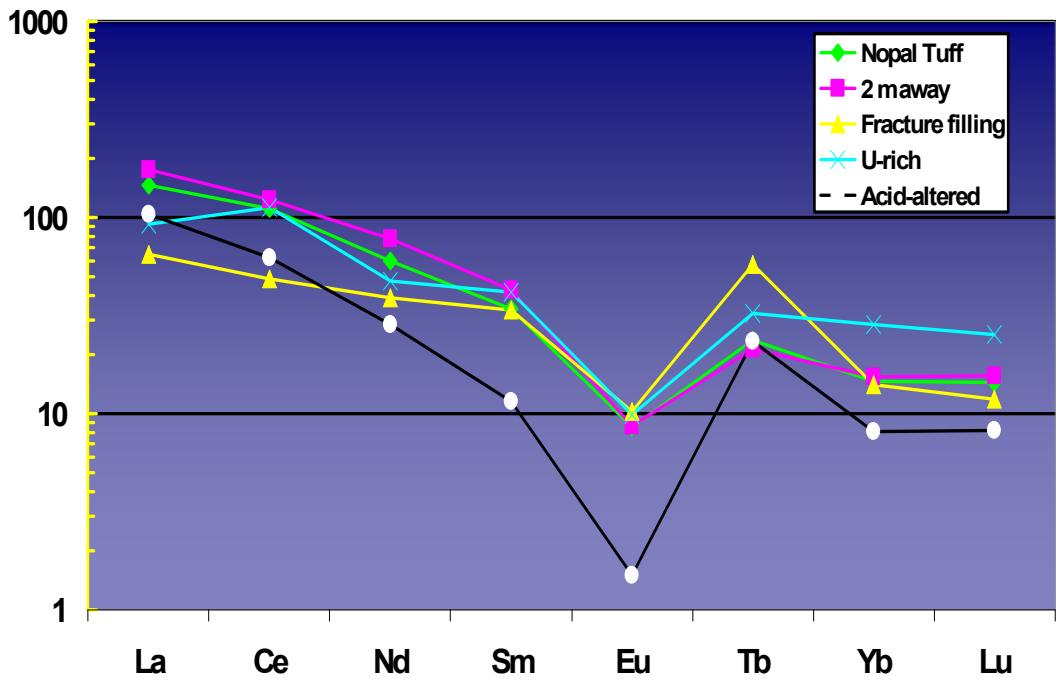

Figure 6-8. Rare-Earth Element Patterns of Selected Samples From Nopal I Level +10. Note that the X Axis Is Not Scaled by Atomic Number; Rather, Only the Measured REE Are Shown, in Order of Increasing Atomic Number. The Y Axis Shows the Sample Concentrations Normalized to the Chondritic Averages of Nakamura (1974).

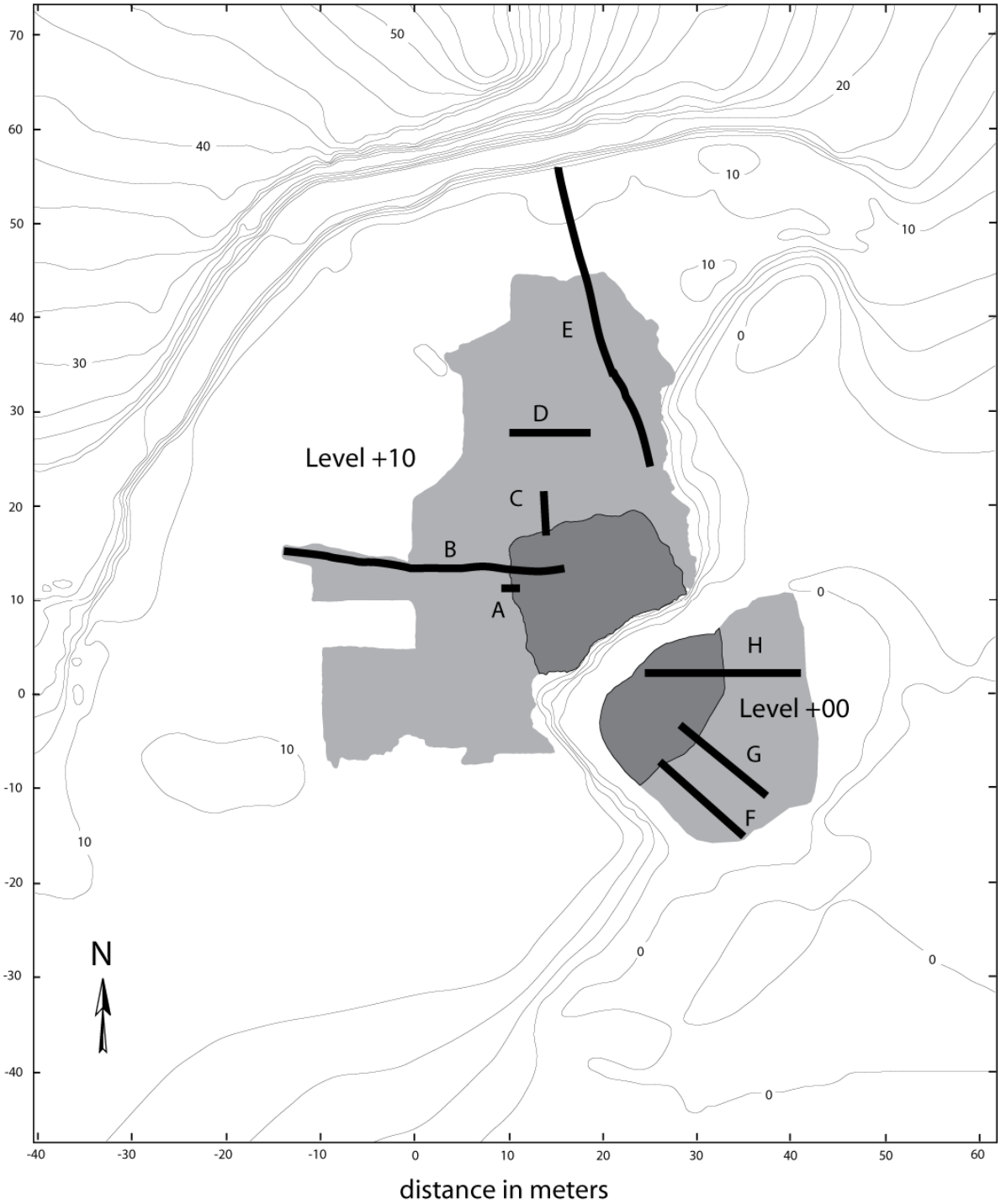

Figure 6-9. Map of the Level +00 and Level +10 Exposures at Nopal I, Showing Sampling Traverses (Heavy Lines A–H). Light Gray Denotes the Area Cleared of Debris for Detailed Study, and the Dark Gray Area Is the Zone of Visible Uranium Mineralization, or Ore Deposit. Contour Interval Is 2 m [6.56 ft], Referenced to Zero at Level +00; Axes (in Meters; 1 m = 3.28 ft) Correspond to the NS-EW Field Grid.

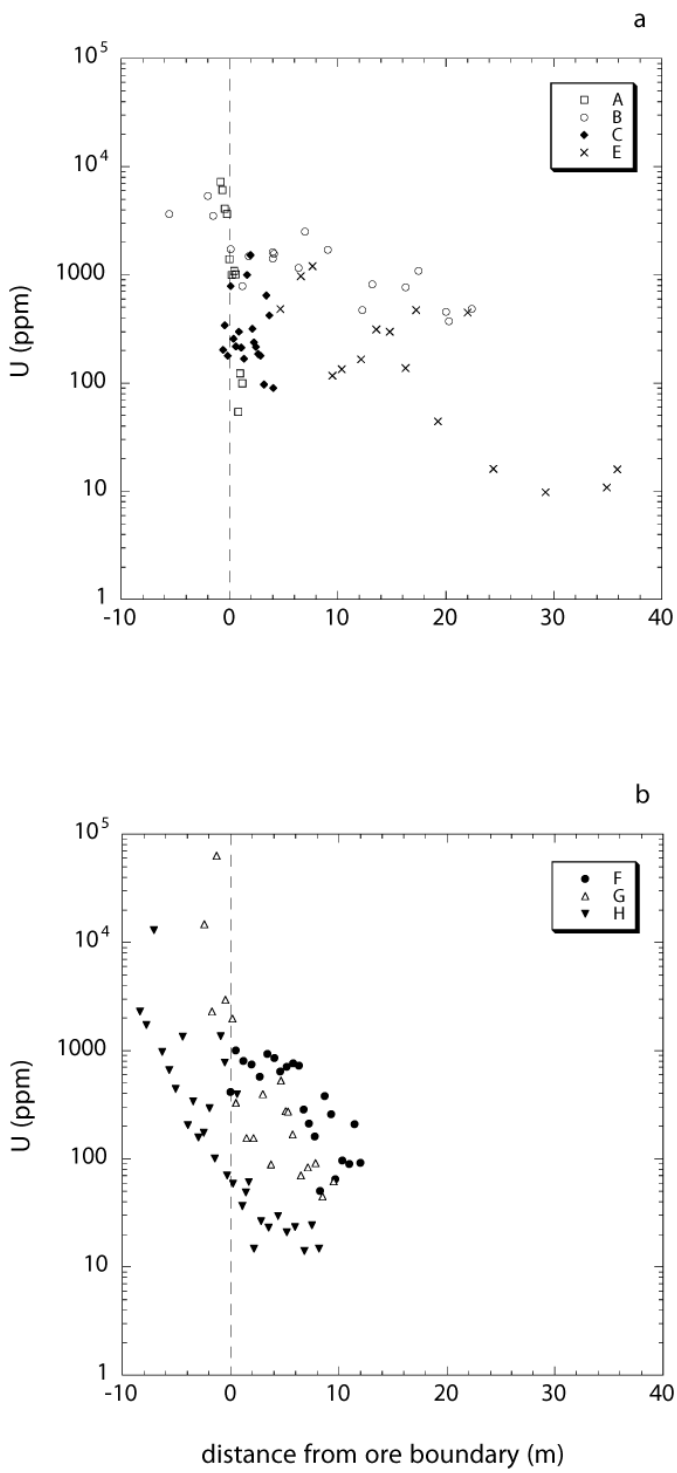

Figure 6-10. Uranium Concentrations in Bulk Samples Collected Along Traverses on Nopal I Levels +00 and +10 (Locations in Figure 6-9). Distance Is Measured From the Edge of the Uranium Ore Body, With Negative Values From Inside the Ore Body [1 m = 3.28 ft]. (a) Level +10 Data, Obtained by Alpha Spectrometry. (b) Level +00 Data, Obtained by Gamma Spectrometry. Samples From Traverses B and E Represent Fracture Infilling Material; the Other Traverses Sampled Generally Fractured Matrix Tuff.

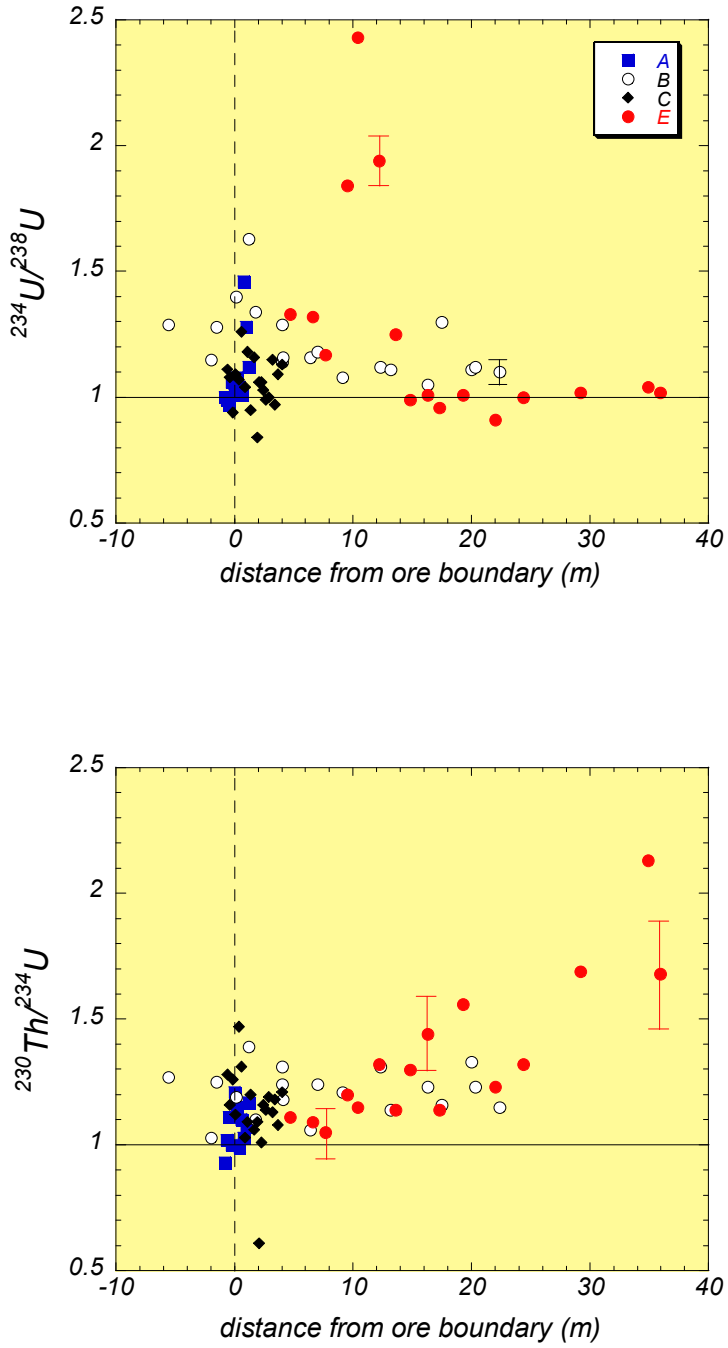

Figure 6-11. Uranium-Series Activity Ratios (a) $^{234}U/^{238}U$ and (b) $^{230}Th/^{234}U$ Along the Level +10 Traverses [1 m = 3.28 ft]. Included Are Example Conservative Uncertainty Bounds.

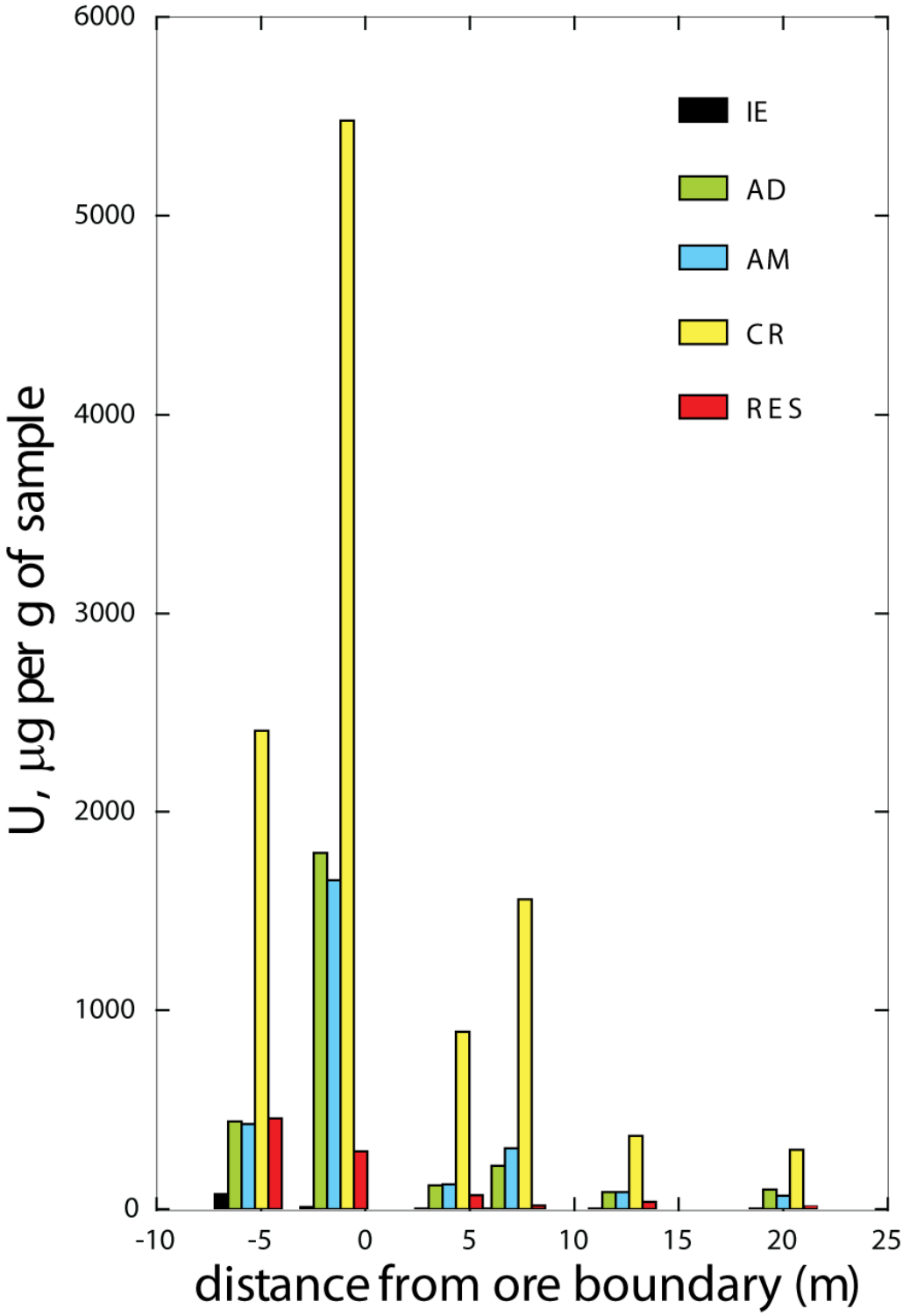

Figure 6-12. Sequential Extraction U Contents From Traverse B Samples [1 m = 3.28 ft], Represented as Micrograms of U in a Fraction Per Gram of Rock (Rather Than ppm in the Fraction).
IE = Ion Exchangeable Fractions, AD = Adsorbed Iron-Oxyhydroxide,
AM = Amorphous Iron-Oxyhydroxide, CR = Crystalline Oxides, RES = Resistates.

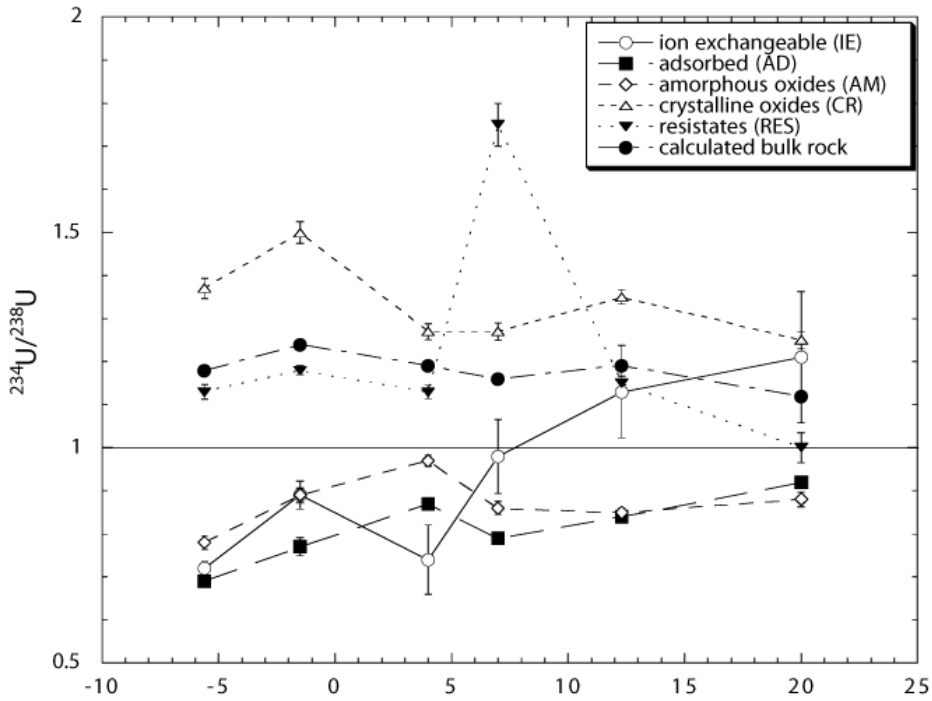

Figure 6-13. Uranium-Series Activity Ratio $^{234}U/^{238}U$ in Sequential Extraction Products From Traverse B, Plotted Against Distance From the Ore Body Boundary in Meters [1 m = 3.28 ft]. The Bulk Rock Values Are Calculated by Combining Ratios From the Five Fractions.

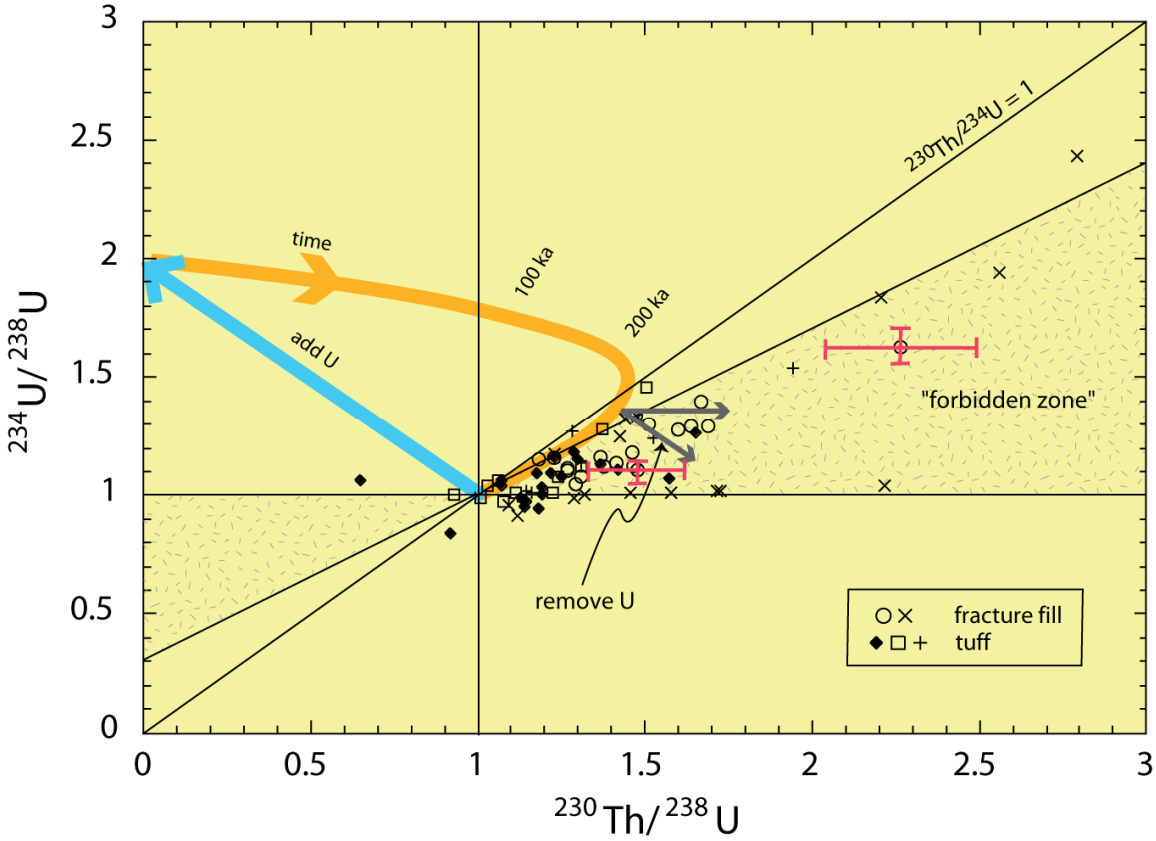

Figure 6-14. $^{234}U/^{238}U$ Versus $^{230}Th/^{238}U$ Plot of Traverse Bulk Rock Samples, With Preferred Model For Evolution (After Pickett and Murphy, 1997). Symbols as in Figure 6-11, With the Addition of Crosses (+) For Traverse D. Note the Different Axis Scales. The Model Assumes An Initial Rock at or Near Secular Equilibrium (i.e., Both Ratios Equal to 1) to Which High–$^{234}U/^{238}U$ Aqueous Uranium Is Added, Followed By Significant Time Evolution (Note Time Labels on Curve), and Finally By Partial Uranium Removal With or Without Uranium Isotope Fractionation. Typical Uncertainty Bars Are Shown in Red for Two Samples; Note Many Samples Are Within Uncertainty Outside the "Forbidden Zone." Clearly, Not All Rocks Would Have Followed the Same Path, and Uranium Addition and Removal Likely Occurred in a More Continuous or Episodic Manner. See Text for Explanation of "Forbidden Zone."

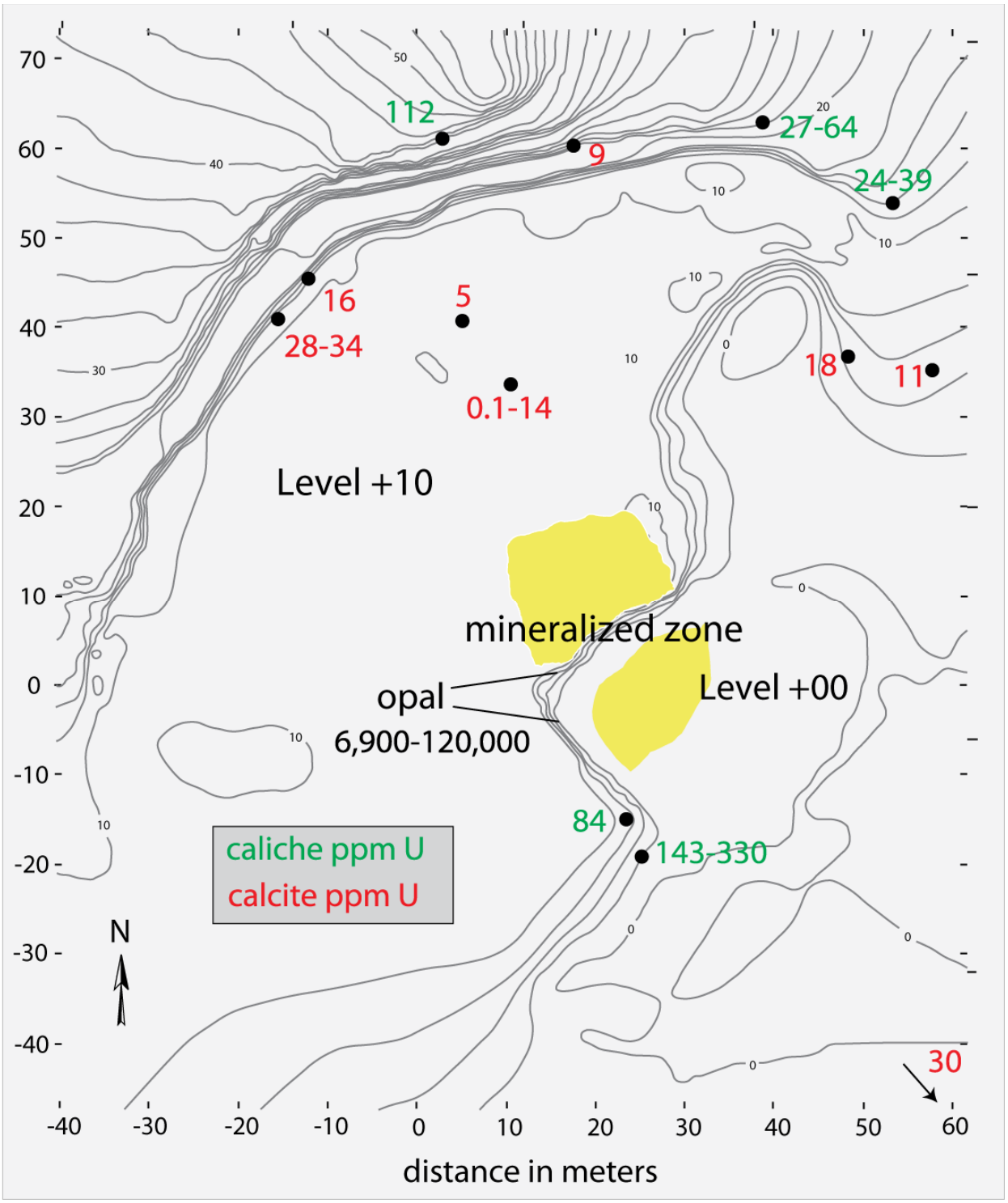

Figure 6-15. Map of the Nopal I Exposure With Sample Locations and Uranium Concentrations (ppm) for Crystalline Calcite, Caliches, and Opals [1 m = 3.28 ft]. The Zone of Visible Uranium Mineralization, or Ore Body, Is in Yellow. Contour Interval Is 2 m [6.56 ft]. The Calcite With 30 ppm Uranium Is From Off the Map.

Figure 6-16. Field Photograph of Crystalline Calcites From Level +10 of the Nopal I Exposure

Figure 6-17. Typical Fracture-Filling Caliche From Near the Nopal I Ore Body. Location Is Shown in Figure 6-18.

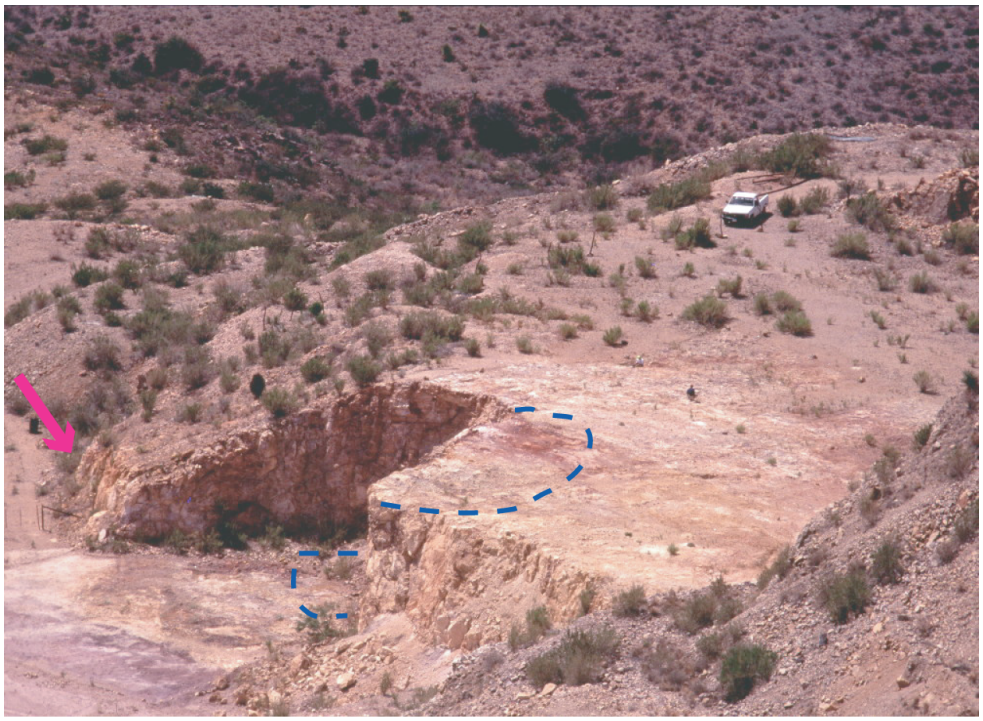

Figure 6-18. View From the Northeast of the Nopal I Uranium Deposit. Dashed Blue Line Is Approximate Outline of the Zone of Visible Uranium Ore on Both Levels +00 (Lower) and +10 (Upper). The Pink Arrow Points to a Road Cut Containing Some of the Caliche Samples.

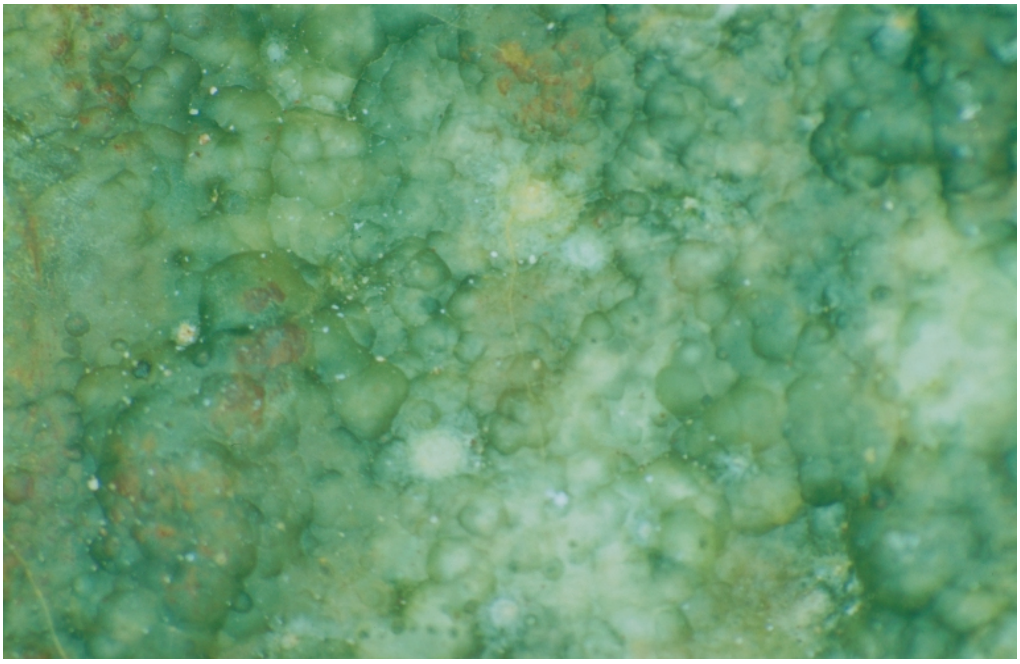

Figure 6-19. Photograph of a Typical Opal Sample, Showing Its Translucent to Transparent Color and Botryoidal Character. The Field of View Is 13 mm [0.51 in] Wide.

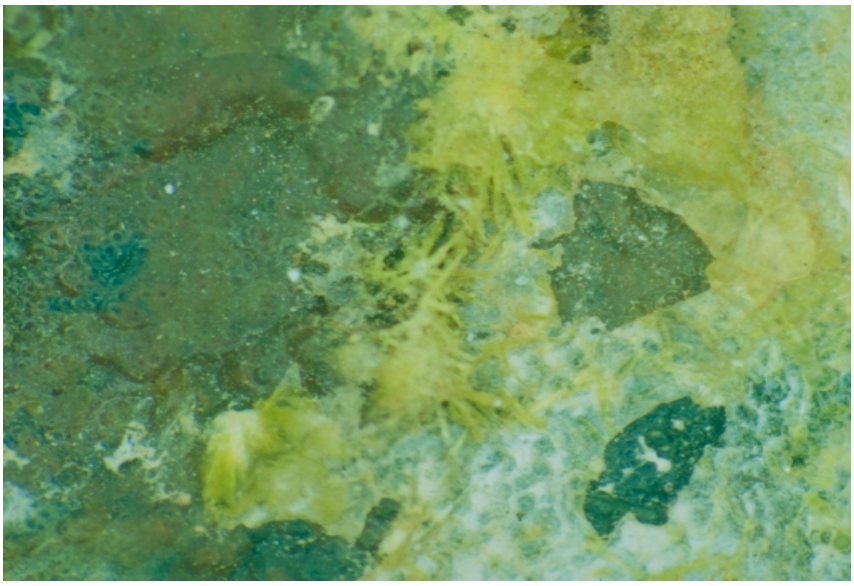

Figure 6-20. Photograph of an Association of Uranium-Rich Opals With Yellow Uranophane Needles. Field of View is 7 mm [0.28 in] Wide. In the Lower Right, Uranophane Needles Can Be Seen Covered by and Incorporated Into the Lighter Opal Coating, Whereas in the Center, Uranophane Needles Grow on Top of the Opal. The Lighter Opal Coating and the Uranophane Have Both Formed Atop the Base Opal Layer Seen on the Left (Which Is Clear but Appears Grayish-Brown) and in Windows Through the Younger Opal on the Right.

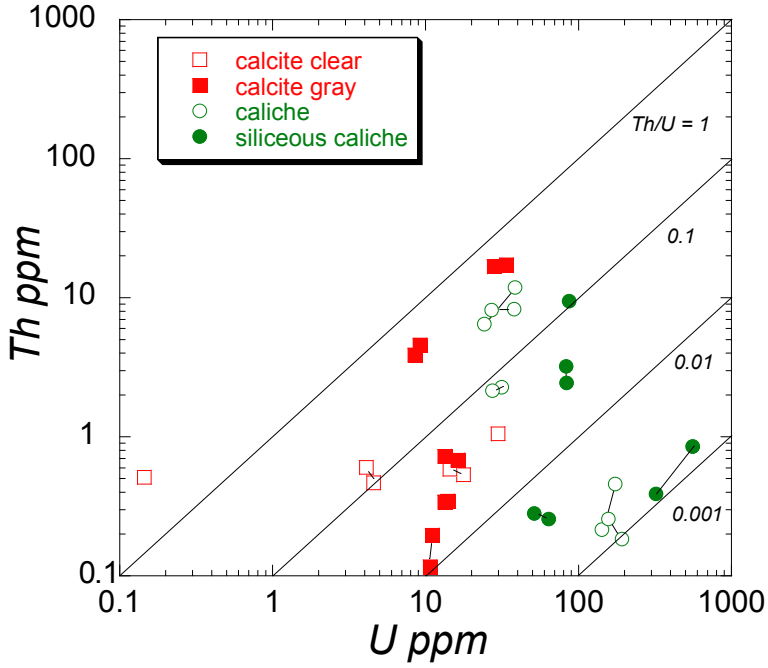

Figure 6-21. Uranium and Thorium Concentrations of Grain-Size Fraction Pairs of Calcite and Caliche Samples From Nopal I. The Line Connecting Pairs Is Not Visible if the Points Overlap. The Plot Shows That, for Each Sample, the Different Grain-Size Fractions Had Very Similar Concentrations and Th/U Ratios. (Grain-Size Fractions Were Not Prepared for the Sample Represented by the Single Point at Very Low Uranium.)

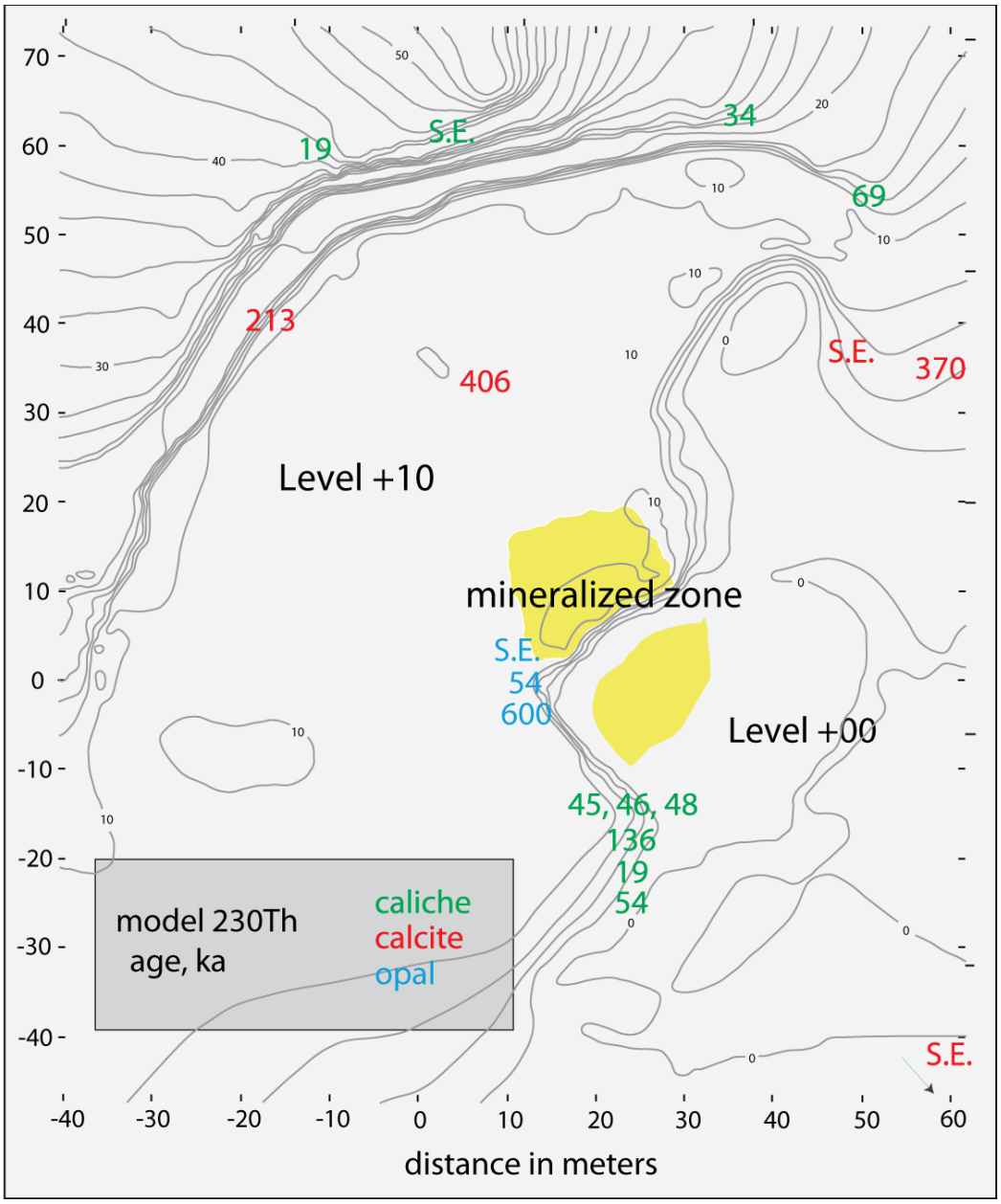

Figure 6-22. Total-Dissolution Th-230 Dates on Calcite, Caliche, and Opal From the Nopal I Exposure [1 m = 3.28 ft]. The Term "Model Age" Means That the Date Is Calculated Directly From the Isotopic Measurements, With No Corrections. "S.E." Indicates a Date Either Indistinguishable From Secular Equilibrium, or a Sample With Values Near Secular Equilibrium for Which a Date Cannot Be Calculated. In Either Case, the Rock Is Older Than about 600 ka. The S.E. "Caliche" From the Northern Portion of the Map Actually Consists of Quartz. The Map Includes Previously Reported Caliche Dates of 19 and 54 ka Pearcy, et al., 1994.[4]

[4]Unpublished data by B. Leslie

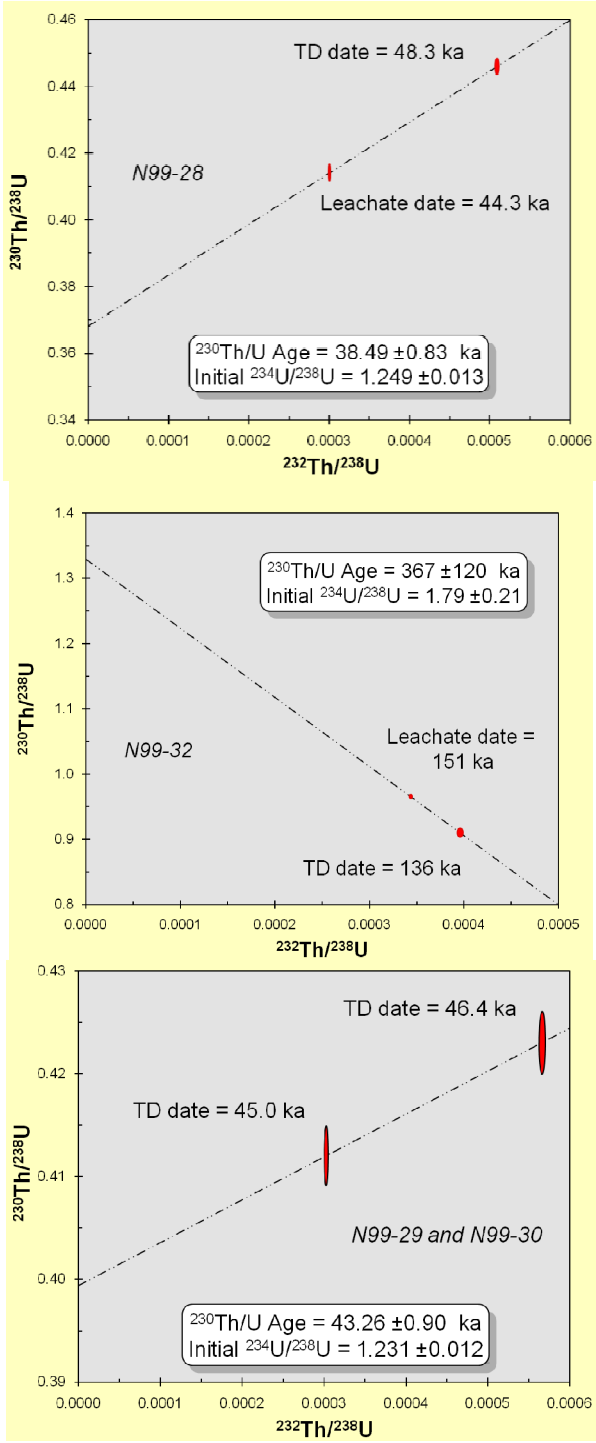

Figure 6-23. Isochron Plots Using Total Dissolution (TD) and Leachate Pairs for N99-28 and N99-32, and Two Total Dissolution Fractions From the Same Powder for N99-29 and N99-30. Isochron Dates Are Shown in the White Boxes. Data Points Are 2σ Error Ellipses. Uranium-Series Plots Produced Using K. Ludwig's Isoplot Add-In for Microsoft® Excel®.

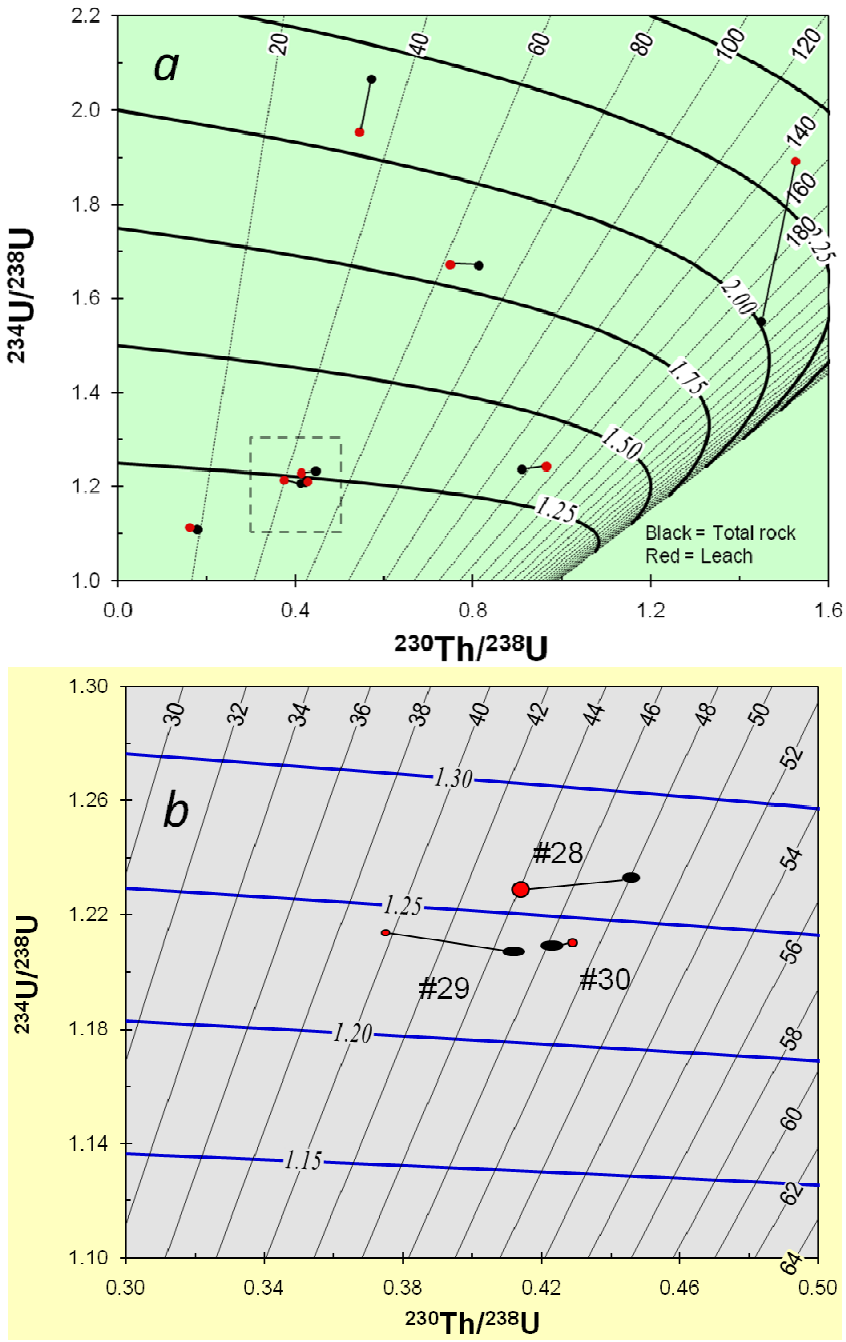

Figure 6-24. (a) Activity Ratios on Pairs of Total Dissolution and Leachate Measurements on One Calcite (Far Right of Plot) and Seven Caliches, Plotted on a Uranium-Series Evolution Diagram. The Dotted Lines Represent the ^{230}Th-^{234}U-^{238}U Age, Labeled in ka. The Thick Solid Lines Represent the Initial ^{234}U/^{238}U ratio. The Ages Assume No Initial ^{230}Th. Old Samples in Secular Equilibrium (i.e., Older Than About 600 ka, Depending on the Initial ^{234}U/^{238}U) Plot at the Point Where Both Ratios Equal 1. (b) Close-Up of the Portion of Figure "a" Enclosed in a Dashed Box.

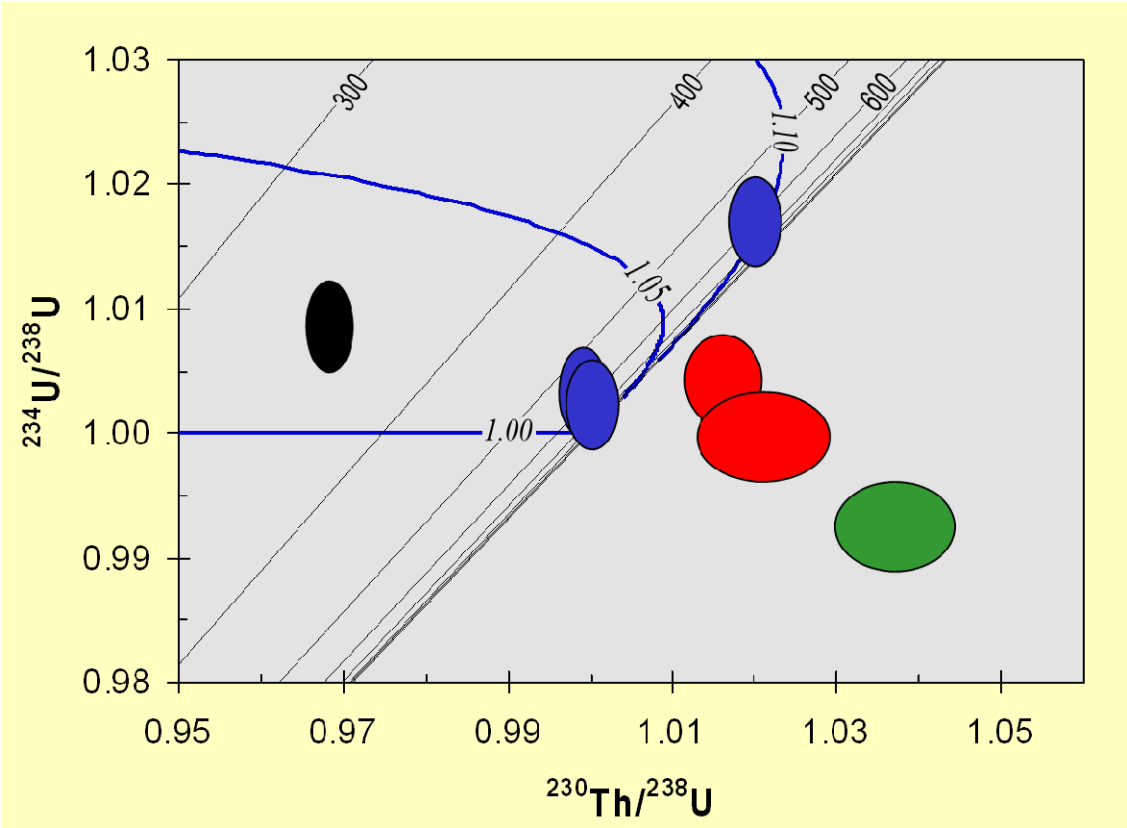

Figure 6-25. Uranium-Series Evolution Plots of Data From Opals (Blue), Uranophane (Black), Calcite (Red), and Quartz "Caliche" (Green) From Nopal I. The Figure 6-24 Caption Explains the Curves and Their Labels.

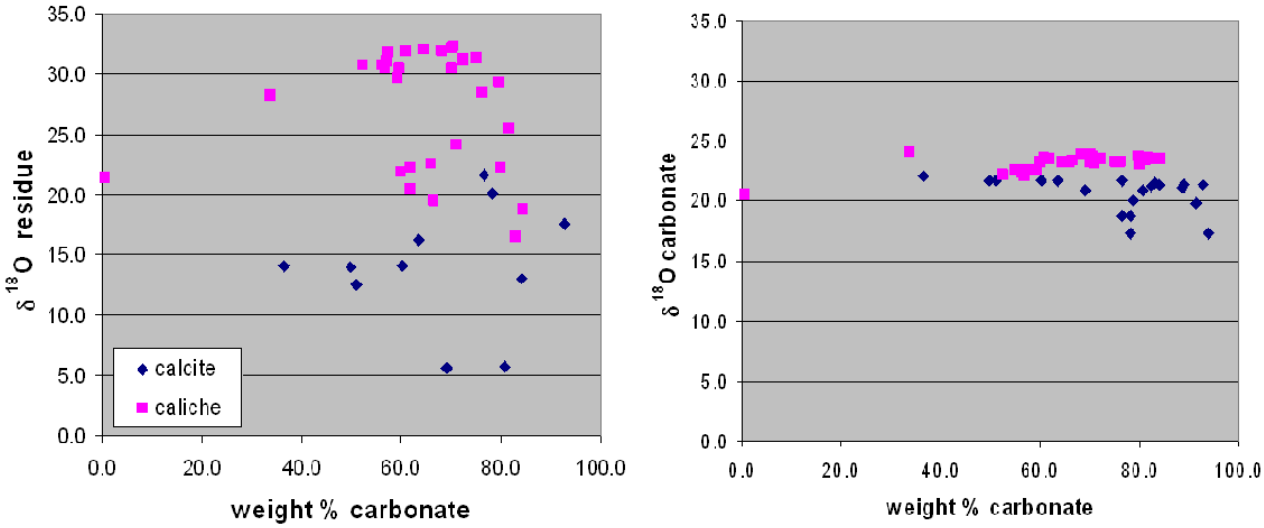

Figure 6-26. δ18O, Plotted as Permil Values Against SMOW, of the Carbonate and Silicate Components of Calcites and Caliches

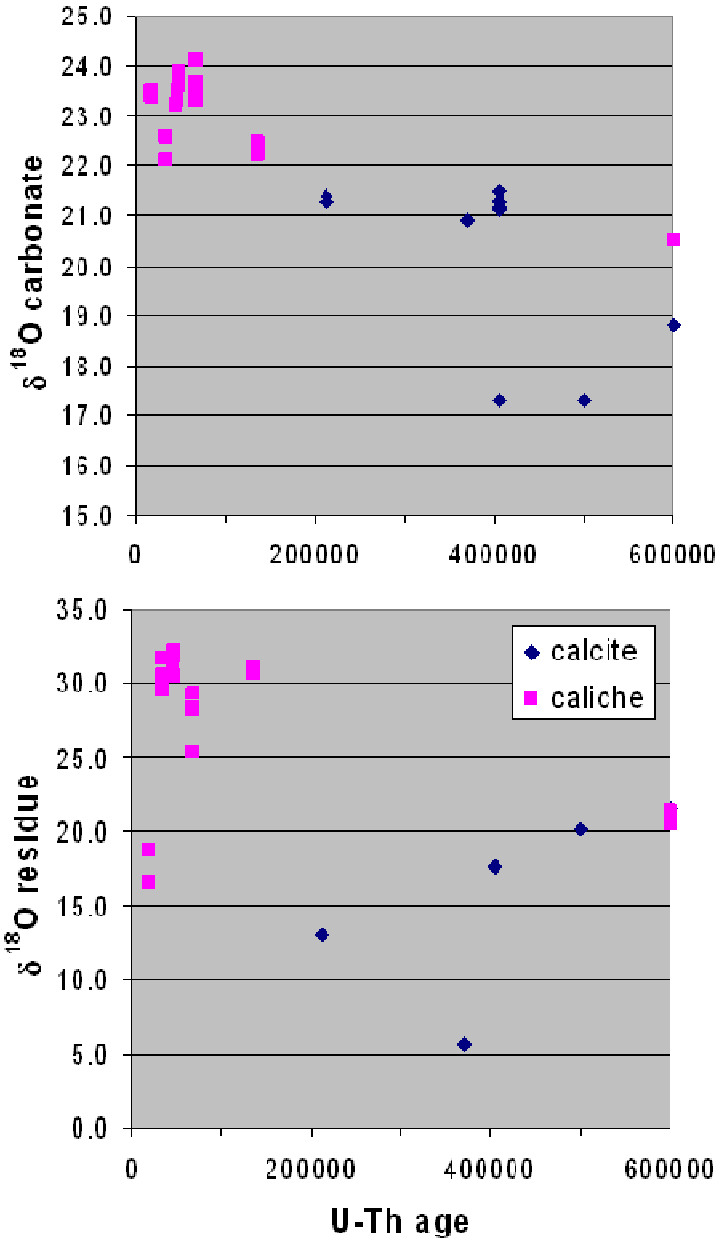

Figure 6-27. Oxygen Isotope Ratios (in Permil Against SMOW) for Calcites and Caliches Plotted Against the Interpreted ^{230}Th-^{234}U-^{238}U Age. Data for Carbonates and Silicate Residues Are Plotted Separately.

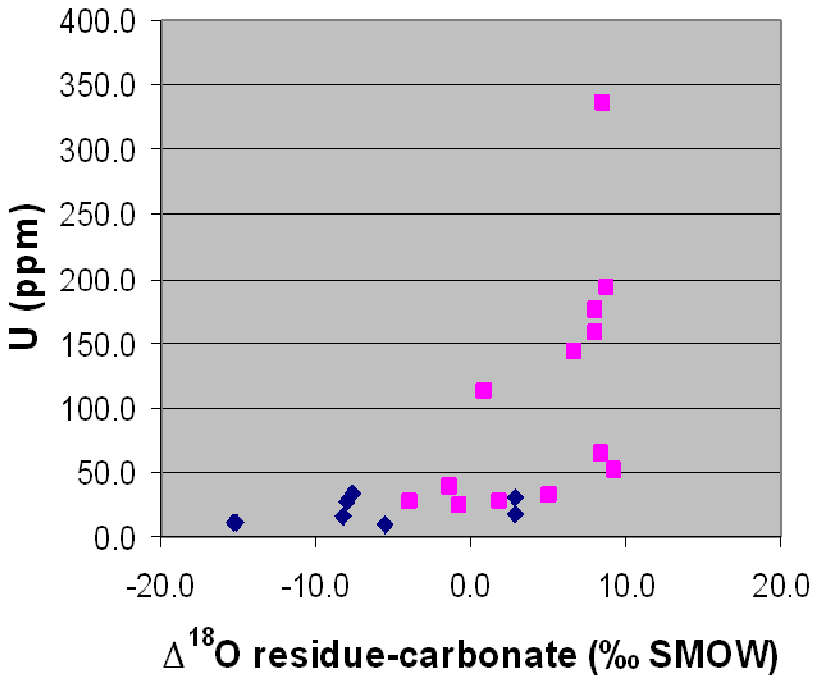

Figure 6-28. Uranium Concentrations in Nopal I Calcites and Caliches Plotted Against the Difference Between $\delta^{18}O$ Values in Residues and Carbonates. The Latter Value Is Termed Δ and Can Be Useful for Understanding Temperature Conditions.

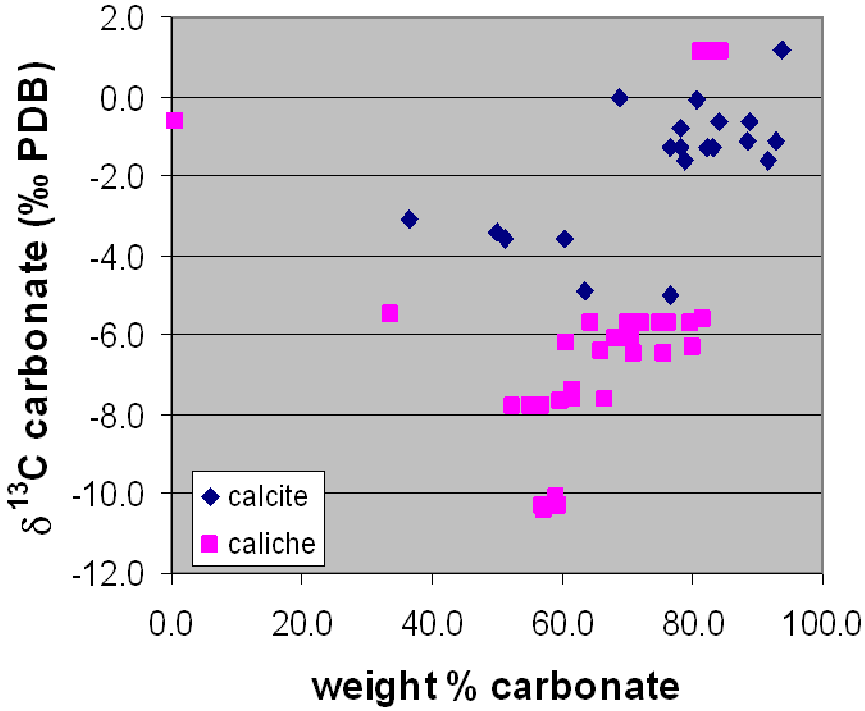

Figure 6-29. Carbon Isotope Ratios for Calcites and Caliches Around Nopal I

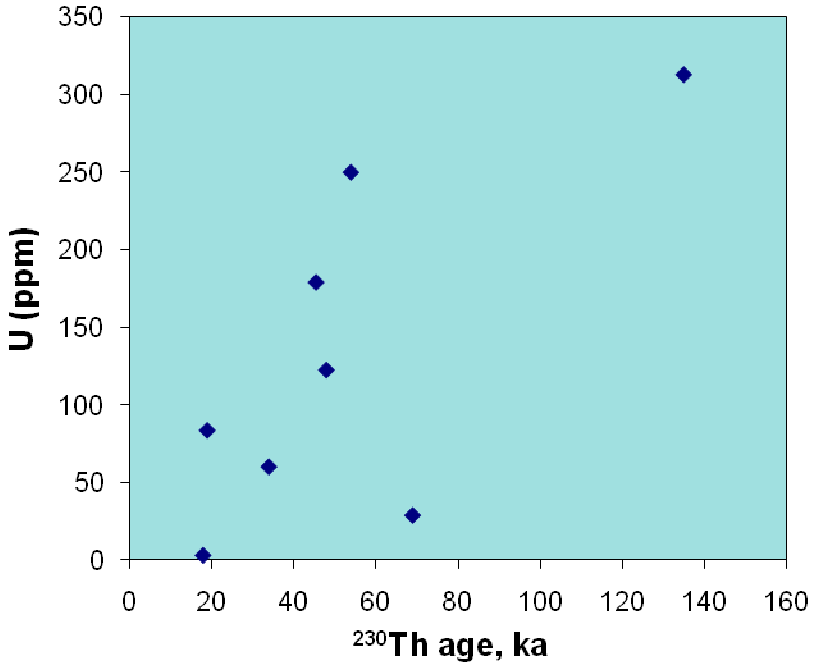

Figure 6-30. Nopal I Caliche Uranium Concentrations Plotted Against Uranium-Series Age. The Points Include Previously Reported Ages of 18 and 54 ka.

7 APPLICATIONS TO PERFORMANCE ASSESSMENT

U.S. Nuclear Regulatory Commission (NRC) and Center for Nuclear Waste Regulatory Analyses (CNWRA®) staffs have looked at ways information from Peña Blanca studies can inform performance assessments for geologic disposal, whether by providing data that can be used in calculations or in assessing different scenarios and processes. This chapter summarizes papers and presentations documenting those efforts. All CNWRA analog studies were conducted from the perspective of supporting regulation of deep geologic disposal, constraining conceptual models, and evaluating performance assessments. Perhaps the most prominent outcome of Peña Blanca studies is the confirmation of spent nuclear fuel analog laboratory observations supporting waste form conceptual models (Pearcy, et al., 1994). This chapter, however, is limited to products specifically focused on performance assessment applications and implications.

7.1 Source Term and Transport

The first CNWRA publication that directly related information from Peña Blanca to waste repository performance assessment was Murphy and Pearcy (1992). In this paper, the authors started with the observation that, at Nopal I, uranium mineral oxidation has been rapid relative to transport of uranium out of the ore body. They then calculated a maximum uranium oxidation rate for Nopal I, given estimates of the mass of uranium in the deposit, the water infiltration rate, uranophane solubility, and an oxidation time estimated from uplift rates. The paper concluded that further information on the real processes responsible for uranium release at Nopal I could inform release rate estimates for the proposed Yucca Mountain repository. Murphy and Pearcy (1993) more fully developed ideas about how analog information from Peña Blanca and from the Santorini archaeological site could support performance assessment. As they stated, "Natural analogs can contribute to nuclear waste repository performance assessment modeling both by providing qualitative identification of processes and by contributing to quantitative model validation" (Murphy and Pearcy, 1993, p. 223). The authors proposed anticipated and possible contributions from Peña Blanca in the areas of waste form/source term and flow and transport.

Murphy, et al. (1997) proposed expanding Peña Blanca studies from the Nopal I ore body, where intensive work was conducted, to the nearby site of temporary storage of high-grade uranium piles. The reasoning behind the proposed studies—which were not conducted—was that release and migration processes supporting performance assessment could be more tightly constrained than in the Nopal I exposure. The timing of the source was known from information on the piles, and data concerning potential transport processes (e.g., rainfall) were also relatively well known. It was expected that radionuclide release could be treated as essentially a pulse because of the limited duration of the piles.

Performance assessment application of Nopal I data moved from the theoretical to the actual as a result of the paper of Murphy and Codell (1999). The authors proposed alternate source term models that could be selected as options in the independent NRC Yucca Mountain performance assessment code Total-system Performance Assessment (TPA) (Leslie, et al., 2007). For one model, using the approach of Murphy and Pearcy (1992), a fixed spent nuclear fuel oxidation rate was scaled from Nopal I to the proposed Yucca Mountain repository. Radionuclides were calculated to be released congruently, subject to solubility limits. The other alternate model assumed radionuclide release was controlled by schoepite solubility. Murphy, et al. (2001) described these models again in a more general paper that also described the use of the Nopal I uranium paragenetic sequence in supporting performance assessments by U.S. Department of Energy (DOE) and the Electric Power Research Institute. Murphy, et al.

(2001) also discussed other, less direct contributions to performance assessment, including the transport role of fractures, evaluation of the effectiveness of matrix diffusion, and confirmation of the potential transport importance of iron oxyhydroxide minerals.

CNWRA experiences in attempting to apply Peña Blanca to waste repository performance assessment informed an analysis of analog applications by Murphy (2000). After general discussions on how analogs may be used to build confidence, support multiple lines of evidence, and validate models, Murphy (2000) summarized Peña Blanca applications in the areas of uranium mineral paragenesis, the alternate TPA source term models, and radionuclide transport (fracture processes and minor phase sorption). With respect to transport processes, the paper acknowledged the lack of direct performance assessment. Murphy (2000) emphasized that, because analogs are not perfect, their best applications are those that exploit very specific analogous features and processes.

7.2 Radioisotope Disequilibrium and Preferential Release

NRC and CNWRA investigators recognized that analog observations of uranium-series disequilibrium have potential implications for conceptual models of radionuclide release. A poster by Leslie and Pickett (2000) analyzed the potential performance assessment implications of observations of Ra-226 mobility and disequilibrium at Peña Blanca. The authors referred to observations of Ra-226 depletion in uranium ore and mobilization in vegetation (Leslie, et al., 1999; see Section 6.2) and DOE observations of ^{226}Ra/^{230}Th disequilibrium at Nopal I. The poster argued that the observations, notably by Los Alamos National Laboratory scientists, of apparently closed-system uranium-thorium behavior on 10^5 year time scales (see Section 6.6.3.1) do not necessarily extend to other decay-chain nuclides. Ra-226 depletion relative to Th-230 and U-238 is best explained, according to the poster, as a result of uranium mineral dissolution and reprecipitation within the last few thousand years. In other words, mobilization of shorter lived, higher solubility radionuclides such as Ra-226 could be greater than expected based on apparently closed-system uranium-thorium isotopic systematics. The authors raised the possibility of preferential release of such radionuclides during waste form degradation.

Murphy and Pickett (2002a,b) presented a different approach to applying decay-series disequilibrium concepts, based on Nopal I observations and common in nature, to understanding radionuclide release. The papers discussed how decay-series disequilibria can provide not only information on the geochemical characteristics of a site (e.g., openness or closedness based on ^{230}Th–^{234}U–^{238}U) and specific information on transport processes (see Chapter 6), but observations of disequilibrium also demonstrate the potential for preferential release of radionuclides relative to the major constituent element uranium. The chemical process potentially enhancing Ra-226 released addressed in the previous paragraph is one possible mechanism for preferential release. Murphy and Pickett (2002a,b) emphasized the nuclear processes (e.g., alpha recoil, lattice damage) that are responsible for natural system isotopic disequilibria such as observed for U-234 and U-238. Murphy and Pickett (2002b) tabulated actinide decay series nuclides present in spent nuclear fuel that may have the potential for preferential release by virtue of their substantial ingrowth over time from alpha decay.

Pickett and Murphy (2004) addressed the lack of performance assessment appreciation for these processes (Murphy and Pickett, 2002a,b) by performing TPA calculations based on assumptions about preferential release. The authors simulated an enhancement of release rate relative to waste form degradation based on a particular radionuclide's ingrowth history in spent nuclear fuel; notable calculated effects were observed for Np-237. While the precise

quantification of this process was exploratory, the study did suggest that preferential isotopic release analogous to natural system disequilibria is worth considering.

7.3 Episodic Behavior

The potential for episodic release and transport of uranium was recognized at Nopal I from uranium-series studies of tuff and fracture filling solids (Chapter 6). For example, Pickett, et al. (2001) noted, as discussed in Section 6.7.4, that an episode of elevated uranium release and migration was suggested by the apparent age clustering of high-uranium deposits at around 50 ka. There is a certain degree of ambiguity in this interpretation, because it could also be argued that the presence of uranium-rich fracture-filling deposits in that time period reflects more an environment conducive to uranium deposition, rather than conducive to uranium release and transport. The preferred interpretation is that elevated uranium in the fractures is reflective of enhanced mobility. It is not possible, however, to rule out a scenario in which uranium release is relatively unchanged and sequestration in fractures is episodically enhanced. In either case, the data suggest that uranium release may not have been continuous during the past 10^5 years or so. Pickett, et al. (2001) calculated a rough approximation for a lower limit on the rate of episodic uranium release at Nopal I using the circa 50-ka caliche deposition data. The following assumptions were made:

- 10,000-year episode duration
- 100 ppm uranium in caliche
- Caliche volume of 1,000 m^3 [35,000 ft^3], based on a 10-cm [4-in]-thick caliche covering 10,000 m^2 [108,000 ft^2]

The calculated lower limit rate of uranium deposition was 30 g/y [0.07 lb]. This estimate is highly uncertain, because it depends on extrapolations of field and laboratory observations.

Because much more uranium is transported than is actually captured in the caliches, this deposition rate provides a lower limit on release rate. The degree to which release rate exceeds deposition rate should far exceed any uncertainty in the calculated deposition rate. An upper limit on the long-term uranium release rate for the site based on solubility-limited uranium concentration and constant, modern-day water flux was also 30 g/y [0.07 lb/y] (Murphy and Pearcy, 1992). {For context, the original ore body was estimated to contain 2.8×10^8 g [6.2×10^5 lb] of uranium.} Although the exact match in results is coincidental, consistency between the independently estimated upper limit on the long-term release rate and lower limit on the episodic deposition rate lends credibility to the magnitude of these estimates. Furthermore, that the uranium episodic release rate likely greatly exceeds the calculated deposition rate suggests that the episodic release rate is much greater than the long-term maximum release rate estimate. Rapid episodic release could most simply be explained as resulting from greater water flux (compared to present) related to climate episodes. Pickett, et al. (2001) briefly addressed the potential role of episodic release in repository performance assessments. Episodic release and transport at Nopal I was further explored in a talk by Murphy and Pickett (2005).

In addition to the uranium-series evidence for episodic behavior at Nopal I discussed in Chapter 6, such behavior can be seen going back to the multiple histories of uranium mineral formation, both under reducing and oxidizing conditions (Chapter 5). More recently obtained uranium-lead and uranium-series ages in uranium minerals reveal a much more complex history

of significant uranium mobilization than previously recognized (see summary in Levy, et al., 2011). Murphy and Pickett (2005) speculated that some episodic behavior could be related to retrograde uranium mineral solubility. In total, these observations suggest that the notion of steady uranium solid phase evolution, release, and transport at the Nopal I analog is a simplistic view.

7.4 References

Leslie, B.W. and D. Pickett. "What Can U-series Measurements Tell Us About Radionuclide Mobilization and Migration in a Low-Water Flux, High-Uranium Concentration Setting?" *EOS Transactions of American Geophysical Union*. Vol. 81 (19 Supplement). pp. S442–S443. 2000.

Leslie, B., C. Grossman, and J. Durham. "Total-system Performance Assessment (TPA) Version 5.1 Module Descriptions and User Guide." Rev. 1. ML072710060. San Antonio, Texas: CNWRA. 2007.

Leslie, B.W., D.A. Pickett, and E.C. Pearcy, 1999, Vegetation-Derived Insights on the Mobilization and Potential Transport of Radionuclides from the Nopal I Natural Analog Site, Mexico, *Scientific Basis for Nuclear Waste Management XXII*, Materials Research Society, Warrendale, Pennsylvania, Symposium Proceedings 556, p. 833-842.

Levy, S., S. Goldstein, P.F. Dobson, P. Goodell, T.-L. Ku, A. Abdel-Fattah, G. Saulnier, M. Fayek, and R. de la Garza. "Peña Blanca Natural Analogue Project: Summary of Activities." Proceedings of the 13th International High-Level Radioactive Waste Management Conference. American Nuclear Society. Albuquerque, NM, April 10–14, 2011. pp. 330–341. 2011.

Murphy, W.M. "Natural Analogs and Performance Assessment for Geologic Disposal of Nuclear Waste." *Scientific Basis for Nuclear Waste Management XXIII.* Symposium Proceedings. R.W. Smith and D.W. Shoesmith, eds. Warrendale, Pennsylvania: Materials Research Society. Vol. 608. pp. 533–544. 2000.

Murphy, W.M. and R.B. Codell. "Alternate Source Term Models for Yucca Mountain Performance Assessment Based on Natural Analog Data and Secondary Mineral Solubility." *Scientific Basis for Nuclear Waste Management XXII.* Symposium Proceedings. D.J. Wronkiewicz and J.H. Lee, eds. Warrendale, Pennsylvania: Materials Research Society. Vol. 556. pp. 551–558. 1999.

Murphy, W.M., and E.C. Pearcy. "Source-term Constraints for the Proposed Repository at Yucca Mountain, Nevada, Derived from the Natural Analog at Peña Blanca, Mexico." *Scientific Basis for Nuclear Waste Management XV.* Symposium Proceedings 257. C.G. Sombret, ed. Pittsburgh, Pennsylvania: Materials Research Society. pp. 521–527. 1992.

Murphy, W.M. and E.C. Pearcy. "Performance Assessment Significance of Natural Analog Studies at Peña Blanca, Mexico, and at Santorini, Greece." *5th CEC Natural Analogue Working Group Meeting and Alligator River Analogue (ARAP) Final Workshop*. H. von Maravic and J. Smellie, eds. Toledo, Spain: CEC. pp. 219–224. 1993.

Murphy, W.M. and D.A. Pickett. "Isotope Fractionation Effects on Radionuclide Transport in Geologic Disposal of Nuclear Waste." *Radionuclide Retention in Geologic Media. Workshop Proceedings.* Paris, France: Nuclear Energy Agency. pp. 113–118. 2002a.

Murphy, W.M. and D.A. Pickett. "Radioisotope Fractionation and Secular Disequilibrium in Performance Assessment for Geologic Disposal of Nuclear Waste." *Scientific Basis for Nuclear Waste Management XXV.* Symposium Proceedings. B.P. McGrail and G.A. Cragnolino, eds. Warrendale, Pennsylvania: Materials Research Society. Vol. 713. pp. 867–874. 2002b.

Murphy, W.M. and D.A. Pickett. "Episodic Release and Transport at the Peña Blanca Repository Analog Site." 2005 Goldschmidt Conference Abstracts. *Geochimica Cosmochimica Acta.* Vol. 69, No. 10S. p. A408. 2005.

Murphy, W.M., E.C. Pearcy, and D.A. Pickett. "Radionuclide Transport from Mined Uranium Ore at Peña Blanca, Mexico." *Proceedings of the Fourth International Conference on Tailings and Mine Waste '97* Fort Collins, Colorado. Rotterdam, The Netherlands: A.A. Balkema. pp. 401–404. 1997.

Murphy, W.M., D.A. Pickett, E.C. Pearcy and D.R. Turner. "Peña Blanca Natural Analog Data in Recent Performance Assessment Models for the Proposed Geologic Repository at Yucca Mountain, Nevada." *Eighth EC Natural Analogue Working Group Meeting—Proceedings, EUR 19118.* H. von Maravic and W.R. Alexander, eds. city, Luxembourg. European Commission. pp. 365–375. 2001.

Pearcy, E.C., J.D. Prikryl, W.M. Murphy, and B.W. Leslie. "Alteration of Uraninite from the Nopal I Deposit, Peña Blanca District, Chihuahua, Mexico, Compared to Degradation of Spent Nuclear Fuel in the Proposed US High-Level Nuclear Waste Repository at Yucca Mountain, Nevada." *Journal of Applied Geochemistry.* Vol. 9. pp. 713–732. 1994.

Pickett, D.A. and W.M. Murphy. "Preferential Radionuclide Release Due to Alpha Decay: Effects on Repository Performance." *Scientific Basis for Nuclear Waste Management XXVIII.* Symposium Proceedings. J.M. Hanchar, S. Stroes-Gascoyne, and L. Browning, eds. Warrendale, Pennsylvania: Materials Research Society. Vol. 824. pp. 555–560. 2004.

Pickett, D.A., W.M. Murphy, and B.W. Leslie. "^{238}U-^{234}U-^{230}Th Ages of Secondary Deposits and Evidence on the Rate of Recent Radionuclide Migration at the Nopal I Natural Analog." *8th International Conference on the Behaviour of Actinides and Fission Products in the Geosphere. Migration '01, Abstracts,* Bregenz, Austria. p. 103. 2001.

8 SUMMARY

U.S. Nuclear Regulatory Commission (NRC)-sponsored natural analog studies at Peña Blanca have provided a great deal of useful information on the uranium mineral evolution, release behavior, and radionuclide transport characteristics of a geologic setting analogous to Yucca Mountain. In only one case—release rate—have site data been used directly in performance assessment, but this is a common limitation of natural analog studies. More significant have been the contributions to understanding specific processes and how they can help evaluate conceptual models used in performance assessment. Notable examples include oxidative uranium mineral alteration, radionuclide transport in fractured tuff, preferential release, and episodic system behavior—and the geochronologic context for these processes. The Peña Blanca work not only helped the NRC and Center for Nuclear Waste Regulatory Analyses staffs prepare to review natural analog information supporting a waste disposal performance assessment. More broadly, these efforts enriched staff understanding of processes that can affect repository performance—and related uncertainties and variability.

APPENDIX A

BIBLIOGRAPHY OF NRC-FUNDED PEÑA BLANCA-RELATED DOCUMENTS

BIBLIOGRAPHY OF NRC-FUNDED PEÑA BLANCA-RELATED DOCUMENTS

NRC ADAMS Accession numbers shown where applicable.

Green, R.T., and G. Rice. "Numerical Analysis of a proposed percolation experiment at the Peña Blanca natural analog site." Proceedings of the Sixth Annual International Conference on High-Level Radioactive Waste Management, American Nuclear Society, Las Vegas, Nevada. La Grange Park, Illinois: American Nuclear Society. pp. 226–228. 1995.

Green, R.T., G. Rice, and K. Meyer-James. NUREG/CR-6356, CNWRA 94-027, "Hydraulic Characterization of Hydrothermally Altered Nopal Tuff. ML040220209. Washington, DC: NRC. 1995.

Green R T and K. James. "Hydrogeologic Studies at the Peña Blanca Natural Analog Site." Abstract not submitted to or published by Scientific Basis for Nuclear Waste Management XIX Conference, Boston, Massachusetts. ML061370345. 1995.

Leslie, B.W. and E.C. Pearcy. "Uranium Migration at the Peña Blanca Natural Analog Site." *Geological Society of America Abstracts With Programs.* Vol. 25. p. A–184. 1993.

Leslie, B.W. and D. Pickett. "What C U-Series Measurements Tell us About Radionulicde Mobilization and Migration in a Low-Water Flux, High-Uranium Concentration Setting." AGU Spring 2000 Abstract. Vol. 81, Supplement 19. pp. S442–S443. 2000.

Leslie, B.W. and D. Pickett. "Chemical Alteration and Elemental Mobility at the Nopal I Mine, Peña Blanca District, Mexico." *Geological Society of America Abstracts With Programs.* , Vol. 38, No. 7. p. 14. 2006a**.**

Leslie, B.W. and D. Pickett, 2006b, Chemical Alteration and Elemental Mobility at the Nopal I Mine, Peña Blanca District, Mexico. *Geological Society of America Presentation Slides.* ML062910284. 2006b.

Leslie, B.W., E.C. Pearcy, W.M. Murphy, and J.D. Prikryl. "Fracture and Matrix Controlled Uranium Migration at the Peña Blanca Natural Analog Site. Fourth International Conference on the Chemistry and Migration Behavior of the Actinides and Fission Products in the Geosphere. Charleston, South Carolina: University of Georgia. p. 110. 1993.

Leslie, B.W., E.C. Pearcy, and J.D. Prikryl. "Oxidative Aalteration of Uraninite Under Hydrologically Unsaturated C at Peña Blanca, Chihuahua, Mexico: Contaminant Transport and Source Term Constraints for the Proposed Repository at Yucca Mountain, Nevada. *Scientific Basis for Nuclear Waste Management XVI.* C.G. Interrante and R.T. Pabalan, eds. Symposium Proceedings 294. Pittsburgh, Pennsylvania: Materials Research Society. pp. 505–512. 1993.

Leslie, B.W., E.C. Pearcy, and J.D. Prikryl. NUREG/CR–5817, CNWRA 92–01S, "Geochemical Natural Analogs." *NRC High-Level Radiactive Waste Research at CNWRA, January–June 1992*. W. Patrick, ed. Washington, DC: NRC. Vol 3, No. 1. 1993.

Leslie, B.W., D.A. Pickett, and E.C. Pearcy. "Vegetation-Derived Insights on the Mobilization and Potential Transport of Radionuclides From the Nopal I Natural Analog Site, Mexico. *Scientific Basis for Nuclear Waste Management XXII.* Warrendale, Pennsylvania: Materials Research Society. Symposium Proceedings 556. pp. 833–842. 1999.

Leslie, B.W., K.J. Smart, and E.C. Pearcy. "Characterization of Fractures at the Nopal I site and Comparison to Fracture Characteristics of Yucca Mountain, Nevada. *Geological Society of America Abstracts With Programs.* Vol. 37, No. 7. p. 196. ML051640113. 2005a.

Leslie, B.W., K.J. Smart, and E.C. Pearcy. "Characterization of Fractures at the Nopal I site and Comparison to Fracture Characteristics of Yucca Mountain, Nevada. *Geological Society of America Presentation Slides*. ML052800172. 2005b.

Murphy, W.M. "Natural Analog Studies for Geologic Disposal of Nuclear Waste." *Technology Today.* San Antonio, Texas: Southwest Research Institute®. pp.16–21. June 1992.

Murphy, W.M. "Natural Analogs for Yucca Mountain." *Radwaste Magazine.* Vol. 2, No. 6. pp. 44–50. 1995.

Murphy, W.M. "Retrograde Solubilities of Source Term Phases. *Scientific Basis for Nuclear Waste Management XX.* W.J. Gray and I.R. Triay, eds. Pittsburgh, Pennsylvania: Materials Research Society. Symposium Proceedings 465. pp. 713–720. 1997.

Murphy, W.M. "Natural Analogs and Performance Assessment for Geologic Disposal of Nuclear Waste." *Scientific Basis for Nuclear Waste Management XXIII.* R.W. Smith and D.W. Shoesmith, eds. Warrendale, Pennsylvania: Materials Research Society. Symposium Proceedings Vol. 608. pp. 533–544. 2000.

Murphy, W.M. "Hydrothermal Phase Relations Among Uranyl Minerals at the Nopal I Analog Site." Materials Research Society Symposium Proceedings. Pittsburgh, Pennsylvania: Materials Research Society. Vol. 985. pp. 53–58. 2007.

Murphy, W.M. and R.B. Codell. "Alternate Source Term Models for Yucca Mountain Performance Assessment Based on Natural Analog Data and Secondary Mineral Solubility." *Scientific Basis for Nuclear Waste Management XXII.* D.J. Wronkiewicz and J.H. Lee, eds. Warrendale, Pennsylvania: Materials Research Society. Symposium Proceedings Vol. 556. pp. 551–558. 1999.

Murphy, W.M. and L.A. Kovach, eds. "The Role of Natural Analogs in Geologic Disposal of High-Level Nuclear Waste." CNWRA 93–020. San Antonio, Texas: Center for Nuclear Waste Regulatory Analyses. ML040360540. 1993.

Murphy, W.M. and E.C. Pearcy. "Source-Term Constraints for the Proposed Repository at Yucca Mountain, Nevada, Derived From the Natural Analog at Peña Blanca, Mexico." *Scientific Basis for Nuclear Waste Management XV.* C.G. Sombret, ed. Pittsburgh, Pennsylvania: Materials Research Society. Symposium Proceedings 257. pp. 521–527. 1992.

Murphy, W.M. and E.C. Pearcy. "Performance Assessment Significance of Natural Analog Studies at Peña Blanca, Mexico, and at Santorini, Greece." *5th CEC Natural Analogue Working Group Meeting and Alligator River Analogue (ARAP) Final Workshop*. H. von Maravic and J. Smellie, eds. Toledo, Spain: CEC. pp. 219–224. 1993.

Murphy, W.M. and D.A. Pickett. "Isotope Fractionation Effects on Radionuclide Transport in Geologic Disposal of Nuclear Waste." *Radionuclide Retention in Geologic Media: Workshop Proceedings.* Paris, France: Nuclear Energy Agency. pp. 113–118. 2002a.

Murphy, W.M. and D.A. Pickett. "Radioisotope Fractionation and Secular Disequilibrium in Performance Assessment for Geologic Disposal of Nuclear Waste." *Scientific Basis for Nuclear Waste Management XXV.* B.P. McGrail and G.A. Cragnolino, eds. Warrendale, Pennsylvania: Materials Research Society. Symposium Proceedings Vol. 713. pp. 867–874. 2002b.

Murphy, W.M. and D.A. Pickett. "Episodic Release and Transport at the Peña Blanca Repository Analog Site." 2005 Goldschmidt Conference Abstracts. *Geochimica Cosmochimica Acta.* Vol. 69, No. 10S. p. A408. ML061370692. 2005.

Murphy, W.M., E.C. Pearcy, and P.C. Goodell. "Possible Analog Research Sites for the Proposed High-Level Nuclear Waste Repository in Hydrologically Unsaturated Tuff at Yucca Mountain, Nevada." *Fourth Natural Analogue Working Group Meeting and Poços de Caldas Project Final Workshop.* EUR 13014 EN. Brussels, Belgium: Commission of European Communities. pp. 267–276. 1991.

Murphy, W.M., E.C. Pearcy, and R.T. Green. "Nuclear Waste Technical Review Board (NWTRB) Meeting on Natural Analogs and Geochemical Analogs Research Project Field Trip to McDermitt Caldera and Virgin Valley." ML003746604. San Antonio, Texas: Center for Nuclear Waste Regulatory Analyses. 1991.

Murphy, W.M., E.C. Pearcy, and D.A. Pickett. "Natural Analog Studies at Peña Blanca and Santorini." *Seventh EC Natural Analogue Working Group Meeting.* H. Von Maravic and J. Smellie eds. EUR 17851 EN. Luxembourg. pp. 105–112. 1997.

Murphy, W.M., E.C. Pearcy, and D.A. Pickett. "Radionuclide Transport From Mined Uranium Ore at Peña Blanca, Mexico." Proceedings of the Fourth International Conference on Tailings and Mine Waste '97, Fort Collins, Colorado. Rotterdam, The Netherlands: A.A. Balkema. pp. 401–404. 1997.

Murphy, W.M., E.C. Pearcy, J.D. Prikryl, and I.A. Reyes. "Uranium Minerals at Peña Blanca, Mexico, Are an Analog of Nuclear Waste in a Geologic Disposal Site." *International Conference on Advanced Materials IV*. 1995.

Murphy, W.M., D.A. Pickett, E.C. Pearcy, and D.R. Turner. "Peña Blanca Natural Analog Data in Recent Performance Assessment Models for the Proposed Geologic Repository at Yucca Mountain, Nevada." *Eighth EC Natural Analogue Working Group Meeting: Proceedings, EUR 19118.* H. von Maravic and W.R. Alexander, eds. Luxembourg: European Commission. pp. 365–375. 2001.

Murphy, W.M., J. Prikryl, and D.A. Pickett. " Thermodynamics of Hydrothermal Uranyl Mineral Formation at Nopal I." *Geological Society of America Abstracts with Programs*, Vol. 37, No. 7, p. 197. 2005a.

Murphy, W.M., J. Prikryl, and D.A. Pickett. "Thermodynamics of Hydrothermal Uranyl Mineral Formation at Nopal I." *Geological Society of America Presentation Slides*. ML061700473. 2005b.

Pearcy, E.C. "Geochemical Natural Analogs." *Report on Research Activities for the Quarter April 1 Through June 30, 1990*. CNWRA 90–02Q. W. Patrick, ed. San Antonio, Texas: Center for Nuclear Waste Regulatory Analyses. ML040780271. 1990.

Pearcy, E.C. "Fracture Transport of Uranium at the Nopal I Natural Analog Site." CNWRA 94-011. San Antonio, Texas: Center for Nuclear Waste Regulatory Analyses. ML033630674. 1994.

Pearcy, E.C. "Geochemical Natural Analog Research." *NRC High-Level Radioactive Research at CNWRA, January Through June 1994.* CNWRA 94–01S. B. Sagar, ed. San Antonio, Texas: Center for Nuclear Waste Regulatory Analyses. ML040230547. 1994.

Pearcy, E.C. and B.W. Leslie. Geochemical Natural Analog Research. *NRC High-Level Radioactive Research at CNWRA, January Through June 1993.* CNWRA 93–01S. B. Sagar, ed. San Antonio, Texas: Center for Nuclear Waste Regulatory Analyses. ML033650178. 1993.

Pearcy, E.C. and W.M. Murphy. "Geochemical Natural Analogs Literature Review." CNWRA 90-008. San Antonio, Texas: Center for Nuclear Waste Regulatory Analyses. ML040330616. 1991.

Pearcy, E.C. and W.M. Murphy. "Oxidative Alteration of Uuraninite in a Silicic Tuffaceous Environment." *Geological Society of America Abstracts With Program.* Vol. 23. p. A419. 1991.

Pearcy, E.C. and W.M. Murphy. NUREG/CR–5817, CNWRA 90–01A "Geochemical Natural Analogs." *Report on Research Activities for Calendar Year, 1990*. W. Patrick, ed. ML040780247. 1991.

Pearcy, E.C. and W.M. Murphy. "Geochemical Natural Analogs." *Report on Research Activities for the Quarter July 1 Through September 30, 1991*. CNWRA 91–03Q. W. Patrick, ed. San Antonio, Texas: Center for Nuclear Waste Regulatory Analyses. ML040360622. 1991.

Pearcy, E.C., and W.M. Murphy. "Site Selection and Workplan Report for the Geochemical Natural Analog Research Project." CNWRA 92–014. San Antonio, Texas: Center for Nuclear Waste Regulatory Analyses. 1992.

Pearcy, E., W. Murphy, and P.C. Goodell. "Elemental Mobility in Uranium Deposits of the Sierra Peña Blanca as a Natural Analog of Radionuclide Migration in a High-Level Nuclear Waste Repository." *Energy Resources of the Chihuahua Desert Region.* P.C.C. Goodell, G. Garcia G., and I. Reyes, eds. El Paso, Texas: El Paso Geological Society. pp. 192–296. ML062430245. 1992.

Pearcy, E. C., J. D. Prikryl, and R. T. Green. "Trip Report of February 02 through March 04, 1994, Visit to Chihuahua New Mexico for Field Research at Peña Blanca Natural Analog Site." San Antonio, Texas: Center for Nuclear Waste Regulatory Analoyses. ML003744513. 1994.

Pearcy, E.C., B.W. Leslie, W.M. Murphy, and J.D. Prikryl. "Large-Scale Uranium Migration in Fractured, Silicic Tuff." Fourth International Conference on the Chemistry and Migration Behavior of the Actinides and Fission Products in the Geosphere, Charleston, South Carolina, Athens, Georgia: University of Georgia. p. 78. 1993.

Pearcy, E.C., W.M. Murphy, R.T. Green, B.W. Leslie, and J.D. Prikryl. NUREG/CR–5817, CNWRA 91-01A, "Geochemical Natural Analogs." *NRC High-Level Radioactive Waste Research at CNWRA, Calendar Year 1991*. Vol 2. W. Patrick, ed. Washington, DC: NRC. 1993.

Pearcy, E.C., W. M. Murphy, D. A. Pickett, and R. T. Green. "Trip Report of September 11–22, 1994, Visit to Santa Fe and Chihuahua New Mexico for Commission of European Communities Natural Analogue Working Group Meeting, Post-Meeting Field Trip to Peña Blanca Natural Analog Site and Field Research." San Antonio, Texas: Center for Nuclear Waste Regulatory Analyses. ML003751485. 1994.

Pearcy, E.C., W.M. Murphy, and J.D. Prikryl. "Geochemical Natural Analogs." *Report on Research Activities for the Quarter April 1 Through June 30, 1991*. CNWRA 91–02Q. W. Patrick, ed. San Antonio, Texas: Center for Nuclear Waste Regulatory Analyses. ML040360615. 1991.

Pearcy, E.C., J.D. Prikryl, and B.W. Leslie. "Uranium Transport Through Fractured Silicic Tuff and Relative Retention in Areas With Distinct Fracture Characteristics." *Journal of Applied Geochemistry.* Vol.10. pp. 685–704. 1995.

Pearcy, E.C., J.D. Prikryl, W.M. Murphy, and B.W. Leslie. "Uranium mineralogy of the Nopal I Natural Analog Site, Chihuahua, Mexico." CNWRA 93-012. San Antonio, Texas: Center for Nuclear Waste Regulatory Analyses. ML033650119. 1993.

Pearcy, E.C., J.D. Prikryl, W.M. Murphy, and B.W. Leslie. "Alteration of Uraninite From the Nopal I Deposit, Peña Blanca, District, Chihuahua, Mexico, Compared to Degradation of Spent Nuclear Fuel in the Proposed US High-Level Nuclear Waste Repository at Yucca Mountain, Nevada." *Journal of Applied Geochemistry.* Vol. 9. pp. 713–732. 1994.

Pearcy, E.C., J.D. Prikryl, and Y.-M. Pan. "Crystal Chemistry and Structures of Uraninite From the Nopal I Deposit, Peña Blanca District, Chihuahua, Mexico." *Geological Society of America Abstracts With Programs.* Vol. 25. p. A–382. 1993.

Pickett, D.A. "Natural Analogs and the Yucca Mountain Review Plan: NRC Perspective. *Applying Information from Analogue Systems to the Evaluation of Radioactive Waste Repositories: Proceedings of the EPRI Natural Analogues Workshop, Palo Alto, California, October 9–10, 2003.* Report 1007897. Palo Alto, California: Electric Power Research Institute. 2003.

Pickett, D.A. "Natural Analogs and the Yucca Mountain Review Plan: NRC Perspective." Presentation at the NAnet International Workshop on Natural Analogues: Their Application to Repository Safety Assessment and Stakeholder Communication, Château de Cadarache, France, May 2004. Meeting Summary Published in W. Miller, et al., 2006, "Network to Review Natural Analogue Studies and Their Applications to Repository Safety Assessment and Public Communication (NAnet): Synthesis Report." European Commission Research Report EUR 21919. Brussels, Belgium: European Commission. ML041900298. 2004.

Pickett, D.A. and B.W. Leslie. "Mobilization of Uranium From the Nopal I Analog and Implications for Nuclear Waste Repository Performance." *Geological Society of America Abstracts With Programs.* Vol. 37, No. 7. p. 268. 2005a.

Pickett, D.A. and B.W. Leslie. "Mobilization of Uranium From the Nopal I Analog and Implications for Nuclear Waste Repository Performance." *Geological Society of America Presentation Slides.* ML061700461. 2005b.

Pickett, D.A. and B.W. Leslie. "Use of Natural Analog Information by the Regulator: The U.S. Nuclear Regulatory Commission (NRC) Approach. *10th Natural Analogue Working Group Workshop,* Munich, Germany, August 2007. ML072060289. 2007.

Pickett, D.A. and W.M. Murphy. "Isotopic Constraints on Radionuclide Transport at Peña Blanca." *Seventh EC Natural Analogue Working Group Meeting.* H. Von Maravic and J. Smellie eds. EUR 17851 EN. Luxembourg. pp. 113–122. 1997.

Pickett, D.A. and W.M. Murphy. "Unsaturated Zone Waters From the Nopal I Natural Analog Chihuahua, Mexico—Implications for Radionuclide Mobility at Yucca Mountain." *Scientific Basis for Nuclear Waste Management XXII.* D.J. Wronkiewicz and J. Lee, eds. Warrendale, Pennsylvania: Materials Research Society. Symposium Proceedings Vol. 556. pp. 809–816. 1999.

Pickett, D.A. and W.M. Murphy. Uranium Chemistry and Isotopy in Waters and Rocks at Peña Blanca, Mexico." *Eighth EC Natural Analogue Working Group Meeting—Proceedings, EUR 19118.* H. von Maravic and W.R. Alexander, eds. Luxembourg"\: European Commission. pp. 333–337. 2001.

Pickett, D.A. and J.D. Prikyrl. "Trip Report: Observation of US Department of Energy Natural Analogue Field Work." San Antonio, Texas: Center for Nuclear Waste Regulatory Analyses. ML033600226. 2003.

Pickett, D.A., J.D. Prikryl, and E.C. Pearcy. "Geochemical Natural Analog Research." *NRC High-Level Radioactive Research at CNWRA, July Through December 1995*. CNWRA 95–02S. B. Sagar, ed. San Antonio, Texas: Center for Nuclear Waste Regulatory Analyses. ML040230584. 1996.

Pickett, D.A., B.W. Leslie, W.M. Murphy, and M. Nugent. "Estimating Radionuclide Release From a Uranium Deposit Through Uranium-Series Systematics in Carbonates and Opal." Goldschmidt 2000 Conference Abstracts. *Journal of Conference Abstracts.* Vol. 5. p. 797. 2000.

Pickett, D.A., W.M. Murphy and B.W. Leslie. "^{238}U-^{234}U-^{230}Th Ages of Secondary Deposits and Evidence on the Rate of Recent Radionuclide Migration at the Nopal I Natural Analog. *8th International Conference on the Behaviour of Actinides and Fission Products in the Geosphere. Migration '01, Abstracts.* Bregenz, Austria. p. 103. ML061370459. 2001.

Pickett, D.A., J.D. Prikryl, W.M. Murphy, and E.C. Pearcy. "Uranium-Series Disequilibrium at the Nopal I Uranium Deposit, Peña Blanca District, Chihuahua, Mexico: Implications for Radionuclide Transport at a Geologic Repository for High-level Nuclear Waste." *EOS, Transactions of the American Geophysical Union.* Vol 77, No. 17. p. 594. 1996.

Pickett, D.A., J.D. Prikryl, W.M. Murphy, and E.C. Pearcy. "Uranium-Series Disequilibrium Investigation of Radionuclide Mobility at the Nopal I Uranium Deposit, Peña Blanca District, Mexico. Submitted to *Applied Geochemistry*. 1999.

Prikryl, J.D. and E.C. Pearcy. "The Role of Secondary Mineral Formation on Uranium Retardation and Transport at the Nopal I Deposit, Peña Blanca District, Chihuahua, Mexico." *Geological Society of America Abstracts With Programs.* Vol. 26. p. A–441. 1994.

Prikryl, J.D., E.C. Pearcy, W.M. Murphy, and D.A. Pickett. "Migration Behavior of Naturally-Occurring Radionuclides at the Nopal I Uranium Deposit, Chihuahua, Mexico." *Chemistry and Migration Behaviour of Actinides and Fission Products in the Geosphere.* M. Del Nero and T. Fanghänel, eds. Saint-Malo, France: Institut de Physique Nucleaire and Forschungszentrum Karlsruhe. p. 47. 1995.

Prikryl, J.D., D.A. Pickett, and E.C. Pearcy. "Geochemical Natural Analog Research." *NRC High-Level Radioactive Research at CNWRA, January Through June 1995.* CNWRA. 95–01S. B. Sagar, ed. San Antonio, Texas: Center for Nuclear Waste Regulatory Analyses. ML040220368. 1995.

Prikryl, J.D., D.A. Pickett, W.M. Murphy, and E.C. Pearcy. "Migration Behavior of Naturally-Occurring Radionuclides at the Nopal I Uranium Deposit, Chihuahua, Mexico. *Journal of Contaminant Hydrology.* Vol. 26. pp. 61–69. 1997.

Prikryl, J.D., D.A. Pickett, and E.C. Pearcy. "Evidence for Uranium Mobilization and Retention on Fe-oxides/Hydroxides At the Nopal I Uranium Deposit, Chihuahua, Mexico." *Geological Society of America Abstracts With Programs.* Vol. 27. p. A–420. 1995.

Sandberg, S.K. "Analysis of Transient Electromagnetic Data Collected at the Nopal I Analog Site, Peña Blanca District, Chihuahua, Mexico." San Antonio, Texas: Center for Nuclear Waste Regulatory Analyses. 1995.

Veblen, L.A. and B.W. Leslie. "Retrospection of U.S. Nuclear Regulatory Commission Efforts on Natural Analogs and the Peña Blanca Uranium District." *Geological Society of America Abstracts With Programs.* Vol. 37, No. 7. p. 269. ML051610681. 2005.

APPENDIX B

SCIENTIFIC NOTEBOOKS ASSOCIATED WITH CNWRA NATURAL ANALOG WORK AT PEÑA BLANCA

SCIENTIFIC NOTEBOOKS ASSOCIATED WITH CNWRA NATURAL ANALOG WORK AT PEÑA BLANCA

NRC ADAMS accession numbers shown.

Green, R. "Hydrology Field Notes for the Peña Blanca and Akrotiri Natural Analog Sites." Scientific Notebook No. 023. San Antonio, Texas: Center for Nuclear Waste Regulatory Analyses. ML040640477. 1997.

Green, R.T. "Determination of the Hydrologic Properties of the Peña Blanca Nopal Tuff." Scientific Notebook No. 078. San Antonio, Texas: Center for Nuclear Waste Regulatory Analyses. ML040680572. 1997.

Green, R. "Hydrology Field Work at Peña Blanca, Mexico, and Akrotiri, Greece." Scientific Notebook No. 119. San Antonio, Texas: Center for Nuclear Waste Regulatory Analyses. ML040640483. 1997.

Leslie, B.W. "Mineralogic, Chemical, and Isotopic Analyses for the Geochemical Natural Analog Project." Supplemental Material for Scientific Notebook No. 080. San Antonio, Texas: Center for Nuclear Waste Regulatory Analyses. ML093270199. 1993.

Leslie, B. "Supplemental Scientific Notebook Material for Gamma Spectrometer Standards." San Antonio, Texas: Center for Nuclear Waste Regulatory Analyses. ML040490775. 1993.

Leslie, B.W. "Rare-Earth Element Analyses; Radioactive Plants from Peña Blanca; Alpha-Spectrometry of Solid Samples From Nopal I Uranium Deposit." Scientific Notebook No 084. San Antonio, Texas: Center for Nuclear Waste Regulatory Analyses. ML040650390. 1993.

Leslie, B. W. and E. C. Pearcy. "Rare-Earth Element Analyses; Radioactive Plants From Peña Blanca; Alpha-Spectrometry of Solid Samples From Nopal I Uranium Deposit." Supplemental Material for Scientific Notebook No. 084. San Antonio, Texas: Center for Nuclear Waste Regulatory Analyses. ML0932701930. 1993.

Leslie, B.W., and D. Pickett. "Descriptions of Field Sampling Activities at Peña Blanca in Support of Geochemical Natural Analog Research." San Antonio, Texas: Center for Nuclear Waste Regulatory Analyses. ML040680963. 1995.

Leslie, B. and J. Prikryl. Mineralogic, Chemical, and Isotopic Analyses for the Geochemical Natural Analog Project." Scientific Notebook No. 080. San Antonio, Texas: Center for Nuclear Waste Regulatory Analyses. ML040650749. 1996.

Murphy, W.M. "Natural Analogs Research Project Field Book Akrotiri and Nopal." Scientific Notebook No. 117 San Antonio, Texas: Center for Nuclear Waste Regulatory Analyses. ML040680784. 1997.

Murphy, W.M. "Geochemical Analogs Research Project Field Book." Scientific Notebook No. 022. San Antonio, Texas: Center for Nuclear Waste Regulatory Analyses. ML040490691. 1996.

Murphy, W.M. “Supplemental Scientific Notebook Material for Scanning Electron Microscopy and Energy Dispersive Spectrometry Analyses of Uranium Ore Samples, Peña Blanca, Chihuahua, Mexico.” San Antonio, Texas: Center for Nuclear Waste Regulatory Analyses. ML040490782. 1994.

Pearcy, E. “Peña Blanca, Nopal I-Geochemical Natural Analog Research Project.” Scientific Notebook No. 621. San Antonio, Texas: Center for Nuclear Waste Regulatory Analyses. ML040690088. 2003.

Pearcy, E.C. “Natural Analog Field Work at Nopal I, Mexico, and McDermitt, NV.” Scientific Notebook No. 21. San Antonio, Texas: Center for Nuclear Waste Regulatory Analyses. ML040650416. 1996.

Pearcy, E. “Numerical Experiments Using EQ3/6 for the Geochemical Natural Analog Project.” Scientific Notebook No. 041. San Antonio, Texas: Center for Nuclear Waste Regulatory Analyses. ML040650683. 1996.

Peary, E.C. “Development of Geological Maps for the Nopal I Site.” Scientific Notebook No. 044. San Antonio, Texas: Center for Nuclear Waste Regulatory Analyses. ML040650409. 1996.

Pearcy, E.C. “Natural Analog Field Work at Nopal I, Mexico, and Akrotiri, Greece.” Scientific Notebook No 036. San Antonio, Texas: Center for Nuclear Waste Regulatory Analyses. ML040650386. 1995.

Pearcy, E.C. “Natural Analog Field Work at Nopal I, Mexico, and Akrotiri, Greece.” Supplemental Material for Scientific Notebook No. 036 San Antonio, Texas: Center for Nuclear Waste Regulatory Analyses. ML093270195. 1994.

Pearcy, E.C. “Field Sampling of Peña Blanca Site Supporting Geochemical Analog of Contaminant Transport in Unsaturated Rock Research Project.” Part 1 of 2, Scientific Notebook No. 024. San Antonio, Texas: Center for Nuclear Waste Regulatory Analyses. ML040490655. 1993.

Pearcy, E.C. “Field Sampling of Peña Blanca Site Supporting Geochemical Analog of Contaminant Transport in Unsaturated Rock Research Project.” Part 2 of 2, Scientific Notebook No. 024. San Antonio, Texas: Center for Nuclear Waste Regulatory Analyses. ML040490656. 1993.

Pearcy, E. and Y. Pan. “Investigation on Microstructural Analysis and Phase Identification of Uranium-Containing Samples from the Nopal I Analog Site.” Scientific Notebook No. 050. San Antonio, Texas: Center for Nuclear Waste Regulatory Analyses. ML040650739. 1996.

Pickett, D. “Natural Analogs.” Scientific Notebook No. 121. San Antonio, Texas: Center for Nuclear Waste Regulatory Analyses. ML091610053. 2007.

Pickett, D. “Chemistry and Radiochemistry of Nopal I Waters--Analysis of Existing Data.” Scientific Notebook No. 276. San Antonio, Texas: Center for Nuclear Waste Regulatory Analyses. ML071800092. 2006.

Pickett, D. “Natural Analog Research Project and Radionuclide Transport Key Technical Issue Laboratory and Data Analyses Work.” Scientific Notebook No. 127. San Antonio, Texas: Center for Nuclear Waste Regulatory Analyses. ML040530088. 2000.

Pickett, D. “Radiochemical Laboratory Measurements Related to Natural Analog Investigations.” Scientific Notebook No. 031. San Antonio, Texas: Center for Nuclear Waste Regulatory Analyses. ML040530013. 2000.

Prikryl, J. “Radionuclide Transport (RT) Preparation for Field Trip to Nopal to Conduct Water Sampling.” Scientific Notebook No. 589. San Antonio, Texas: Center for Nuclear Waste Regulatory Analyses. ML073410408. 2003.

Prikryl, J. “Field Work at the Nopal I Uranium Deposit, Peña Blanca, Mexico.” Scientific Notebook No. 042. San Antonio, Texas: Center for Nuclear Waste Regulatory Analyses. ML040650733. 1996.

Prikryl, J. “Mineralogic and Chemical Analyses of Nopal I Samples.” Scientific Notebook No. 075. San Antonio, Texas: Center for Nuclear Waste Regulatory Analyses. ML040650746. 1996.

Prikryl, J. “Field Notes on Water Collection System in Nopal I Audits.” Scientific Notebook No. 151. San Antonio, Texas: Center for Nuclear Waste Regulatory Analyses. ML040650752. 1996.